Methods in Cell Biology • Volume 92

Cilia: Motors and Regulation

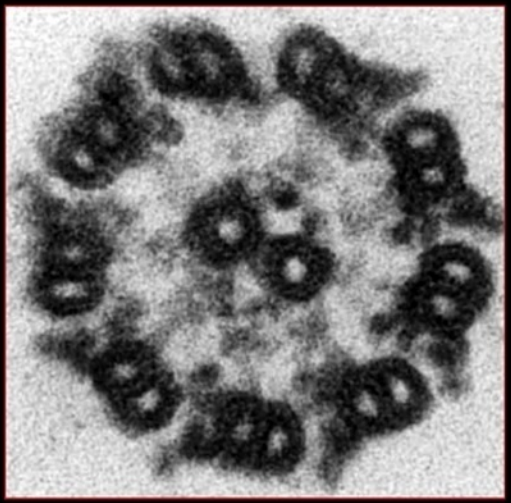

Edited by

Stephen King • Gregory Pazour

Methods in Cell Biology

VOLUME 92

Cilia: Motors and Regulation

Series Editors

Leslie Wilson
Department of Molecular, Cellular and Developmental Biology
University of California
Santa Barbara, California

Paul Matsudaira
Department of Biological Sciences
National University of Singapore
Singapore

Methods in Cell Biology

VOLUME 92

Cilia: Motors and Regulation

Edited by

Stephen M. King

Department of Molecular, Microbial and Structural Biology
University of Connecticut Health Center
Farmington, Connecticut

Gregory J. Pazour

Program in Molecular Medicine
University of Massachusetts Medical School
Worcester, Massachusetts

ELSEVIER

AMSTERDAM • BOSTON • HEIDELBERG • LONDON
NEW YORK • OXFORD • PARIS • SAN DIEGO
SAN FRANCISCO • SINGAPORE • SYDNEY • TOKYO
Academic Press is an imprint of Elsevier

Academic Press is an imprint of Elsevier
30 Corporate Drive, Suite 400, Burlington, MA 01803, USA
525 B Street, Suite 1900, San Diego, CA 92101-4495, USA
32, Jamestown Road, London NW1 7BY, UK
Linacre House, Jordan Hill, Oxford OX2 8DP, UK

First edition 2009

ISBN–13: 978-0-12-374974-1
ISSN: 0091-679X

For information on all Academic Press publications
visit our website at elsevierdirect.com

Printed and bound in USA
09 10 11 12 10 9 8 7 6 5 4 3 2 1

CONTENTS

CONTRIBUTORS

Numbers in parentheses indicate the pages on which the authors' contributions begin.

David J. Asai (11), Department of Biology, Harvey Mudd College, 301 Platt Blvd, Claremont California 91711, and Howard Hughes Medical Institute, 4000 Jones Bridge Road, Chevy Chase Maryland 20815

Nicole Bennardo (11), Department of Biology, Harvey Mudd College, 301 Platt Blvd, Claremont California 91711

Clarence W.C. Chan (11), Department of Biology, Harvey Mudd College, 301 Platt Blvd, Claremont California 91711

Yu-Loung Chang (11), Department of Biology, Harvey Mudd College, 301 Platt Blvd, Claremont California 91711

Elizabeth O. Corpuz (11), Department of Biology, Harvey Mudd College, 301 Platt Blvd, Claremont California 91711

Christen DiPetrillo (163), Department of Biological Sciences, Dartmouth College, Hanover, New Hampshire 03755

Jennifer DuMond (11), Department of Biology, Harvey Mudd College, 301 Platt Blvd, Claremont California 91711

Jordan A. Eboreime (11), Department of Biology, Harvey Mudd College, 301 Platt Blvd, Claremont California 91711

Candice A. Elam (133), Department of Cell Biology, Emory University School of Medicine, 465 Whitehead Biomedical Research Building, 615 Michael Street, Atlanta, Georgia 30322

Julianna Erickson (11), Department of Biology, Harvey Mudd College, 301 Platt Blvd, Claremont California 91711

Masahito Hayashi (107), Department of Biological Sciences, Graduate School of Science, University of Tokyo, 7-3-1 Hongo, Bunkyo-ku, Tokyo 113-0033, Japan

Jonathan Hetzel (11), Department of Biology, Harvey Mudd College, 301 Platt Blvd, Claremont California 91711

Erin E. Heyer (11), Department of Biology, Harvey Mudd College, 301 Platt Blvd, Claremont California 91711

Mark J. Hubenschmidt (11), Department of Biology, Harvey Mudd College, 301 Platt Blvd, Claremont California 91711

Kazuo Inaba (49), Shimoda Marine Research Center, University of Tsukuba, 5-10-1, Shimoda, Shizuoka 415-0025, Japan

Ritsu Kamiya (107), Department of Biological Sciences, Graduate School of Science, University of Tokyo, 7-3-1 Hongo, Bunkyo-ku, Tokyo 113-0033, Japan

Pooja Kelekar (181), Department of Biological Sciences, Marquette University, Milwaukee, Wisconsin 53201-1881

Stephen M. King (31), Department of Molecular, Microbial and Structural Biology, University of Connecticut Health Center, 263 Farmington Avenue, Farmington, Connecticut 06030-3305

Ekaterina Kniazeva (11), Department of Biology, Harvey Mudd College, 301 Platt Blvd, Claremont California 91711

Hiroaki Kojima (83), Kobe Advanced ICT Research Center, National Institute of Information and Communications Technology, 588-2 Iwaoka, Nishi-ku, Kobe 6512492, Japan

Takahide Kon (65), Department of Life Sciences, Graduate School of Arts and Sciences, University of Tokyo, Komaba 3-8-1, Tokyo 153-8902, Japan

Hallie Kuhn (11), Department of Biology, Harvey Mudd College, 301 Platt Blvd, Claremont California 91711

Michelle Lum (11), Department of Biology, Harvey Mudd College, 301 Platt Blvd, Claremont California 91711

David R. Mitchell (197), Department of Cell and Developmental Biology, SUNY Upstate Medical University, Syracuse, New York 13210

Katsutoshi Mizuno (49), Shimoda Marine Research Center, University of Tsukuba, 5-10-1, Shimoda, Shizuoka 415-0025, Japan

Kazuhiro Oiwa (83), Kobe Advanced ICT Research Center, National Institute of Information and Communications Technology, 588-2 Iwaoka, Nishi-ku, Kobe 6512492, Japan, and Graduate School of Life Science, University of Hyogo, Harima Science Park City, Hyogo 6781297, Japan

Vidyalakshmi Rajagopalan (11), Department of Biology, Harvey Mudd College, 301 Platt Blvd, Claremont California 91711

Liesl Van Ryswyk (11), Department of Biology, Harvey Mudd College, 301 Platt Blvd, Claremont California 91711

Hitoshi Sakakibara (83), Kobe Advanced ICT Research Center, National Institute of Information and Communications Technology, 588-2 Iwaoka, Nishi-ku, Kobe 6512492, Japan

Winfield S. Sale (133), Department of Cell Biology, Emory University School of Medicine, 465 Whitehead Biomedical Research Building, 615 Michael Street, Atlanta, Georgia 30322

Andrea Sand (11), Department of Biology, Harvey Mudd College, 301 Platt Blvd, Claremont California 91711

Alicia Schep (11), Department of Biology, Harvey Mudd College, 301 Platt Blvd, Claremont California 91711

Oksana Sergeeva (11), Department of Biology, Harvey Mudd College, 301 Platt Blvd, Claremont California 91711

Tomohiro Shima (65), Department of Life Sciences, Graduate School of Arts and Sciences, University of Tokyo, Komaba 3-8-1, Tokyo 153-8902, Japan

Chikako Shingyoji (113), Department of Biological Sciences, Graduate School of Science, University of Tokyo, Hongo, Tokyo 113-0033, Japan

Brandon Smith (197), Department of Cell and Developmental Biology, SUNY Upstate Medical University, Syracuse, New York 13210

Elizabeth Smith (163), Department of Biological Sciences, Dartmouth College, Hanover, New Hampshire 03755

Natt Supab (11), Department of Biology, Harvey Mudd College, 301 Platt Blvd, Claremont California 91711

Kazuo Sutoh (65), Department of Life Sciences, Graduate School of Arts and Sciences, University of Tokyo, Komaba 3-8-1, Tokyo 153-8902, Japan

Shiori Toba (83), Kobe Advanced ICT Research Center, National Institute of Information and Communications Technology, 588-2 Iwaoka, Nishi-ku, Kobe 6512492, Japan

Caroline R. Townsend (11), Department of Biology, Harvey Mudd College, 301 Platt Blvd, Claremont California 91711

Ken-ichi Wakabayashi (153), Department of Biological Sciences, Graduate School of Science, The University of Tokyo, Tokyo 113-0033, Japan

Hadley E. Watson (11), Department of Biology, Harvey Mudd College, 301 Platt Blvd, Claremont California 91711

Mei Wei (181), Department of Biological Sciences, Marquette University, Milwaukee, Wisconsin 53201-1881

Alice E. Wiedeman (11), Department of Biology, Harvey Mudd College, 301 Platt Blvd, Claremont California 91711

David E. Wilkes (11), Department of Biology, Harvey Mudd College, 301 Platt Blvd, Claremont California 91711

Maureen Wirschell (133), Department of Cell Biology, Emory University School of Medicine, 465 Whitehead Biomedical Research Building, 615 Michael Street, Atlanta, Georgia 30322

Toshiki Yagi (1), Structural Biology, Graduate School of Science, Kyoto University, Kyoto, 606-8502, Japan

Pinfen Yang (181), Department of Biological Sciences, Marquette University, Milwaukee, Wisconsin 53201-1881

This page intentionally left blank

PREFACE

Cilia and flagella have long been the subject of intense study and a previous volume of *Methods in Cell Biology* dedicated to this organelle was published in 1995. However, in the 15 years since that publication, interest in the organelle has dramatically increased as it has come to be appreciated that these tiny structures play fundamental roles in the development and health of mammals and are vital for vertebrates to perceive their environment and respond to it. In humans the list of ciliary diseases, or ciliopathies, has grown tremendously since the publication of the previous volume. In 1995 the field recognized that cilia and flagella played critical roles in male fertility and respiratory disease and were recognized as being important in the determination of left–right asymmetry of vertebrates but the mechanism was not known. In addition, it was known that the senses of vision and smell depended on receptors localized to modified cilia. It is now appreciated that ciliary defects underlie a wide range of human diseases. These include polycystic kidney disease (PKD), nephronophthisis, Bardet–Biedl syndrome (BBS), Meckel–Gruber syndrome, Joubert syndrome, Jeune syndrome, and short rib-polydactyly syndrome that are thought to result from defects in primary cilia. Other diseases such as male infertility, hydrocephaly, juvenile myoclonic epilepsy, primary ciliary dyskinesia, Kartagener's syndrome, and left-right asymmetry defects of the heart are thought to result from defects in motile cilia. In addition, anosmia and blindness can derive from dysfunction of the highly specialized sensory cilia of the olfactory epithelium and retina. It is clear from studies in mouse that this collection of diseases is just the tip of the iceberg for ciliary disorders of man.

Eukaryotic cilia and flagella are complex organelles composed of hundreds of different proteins. This complexity likely reflects the diverse motility and sensory roles played by these organelles. The motility functions of cilia have long been recognized and in mammals these are important for moving mucus in the lungs, moving cerebrospinal fluid in the brain, and propelling the male gametes. The sensory functions are less well known but include roles in olfaction in the nose and light detection in the eye. In addition, nearly every cell type in vertebrate organisms is ciliated by nonmotile primary cilia that are thought to sense the extracellular environment. The proteins of the cilium are organized around a microtubule-based cytoskeleton termed the axoneme and a specialized domain of the plasma membrane that covers the axoneme. The ciliary membrane is contiguous with the plasma membrane of the cell but is a separate domain containing a unique set of proteins, many of which play roles in sensory perception. The axonemes of motile cilia typically have a $9+2$ arrangement of microtubules while nonmotile sensory and primary cilia typically have a $9 + 0$ arrangement. These microtubules serve as scaffolding to bind and organize the multitude of proteins needed to carry out the motility and sensory functions of cilia. The microtubules of the axoneme are templated from a centriole at

the center of the centrosome. When the cell is ciliated, the centriole (which is now called a basal body) and centrosome remain at the base of the cilium. The centrosome is best known for its role in organizing the cytoskeleton and also is postulated to be an important control center of the cell, integrating signals that regulate morphology, migration, and proliferation.

With the explosion of interest in cilia, the model organisms available to study cilia and flagella have grown much more diverse, and the techniques available for assessing cilia structure and function have become more sophisticated. In these three volumes, we have asked top researchers in the field to provide methods used in their laboratories to study cilia and flagella. *Cilia: Structure and Motility,* Volume 91, focuses on general methods to study these organelles covering microscopic techniques for both structural analysis and detailing motility parameters, as well as biochemical approaches to define protein–protein associations and complexes. *Cilia: Motors and Regulation*, Volume 92, focuses on techniques for studying dynein structure and function and the varied mechanisms by which these motor complexes are regulated. *Cilia: Model Organisms and Intraflagellar Transport*, Volume 93, focuses on the methods for studying intraflagellar transport which is required for assembly of the organelle and provides general approaches for studying this and other cilia-related phenomena in all of the major model organisms that are currently being used to study cilia and flagella.

CHAPTER 1

Bioinformatic Approaches to Dynein Heavy Chain Classification

Toshiki Yagi
Structural Biology, Graduate School of Science, Kyoto University, Kyoto 606-8502, Japan

Abstract

Multiple dynein heavy chain (DHC) genes are found in the genomes of organisms with motile cilia and flagella. Phylogenetic analyses classify these into several groups, each of which may be associated with a specific function. The *Chlamydomonas* genome contains 16 *DHC* genes, of which 15 genes have been correlated with particular DHC proteins. The functional properties of *Chlamydomonas* DHCs have been extensively studied by biochemical and genetic methods. Therefore, the phylogenetic classification of *Chlamydomonas DHC* genes can serve as the standard for *DHC* gene classification in other organisms. Here, I classify *Chlamydomonas DHC* genes by phylogenetic analysis and then show how to use this information to classify dyneins from other species that lack biochemical and genetic characterization. As an example, I classify the 16 human *DHC* genes into functional groups using the *Chlamydomonas* genes as references. Many of the human *DHC* genes have a closely related counterpart in *Chlamydomonas*, suggesting that the human genes will have functional properties similar to what has been described in *Chlamydomonas*.

METHODS IN CELL BIOLOGY, VOL. 92

978-0-12-374974-1
DOI:10.1016/S0091-679X(08)92001-X

I. Introduction

Dynein complexes consist of one, two, or three dynein heavy chains (DHCs) and a variety of smaller subunits. The large DHC (4000–5000 amino acids) is organized into two domains: the N-terminal tail and the C-terminal motor domain. The tail domain binds most of the smaller subunits and mediates the tethering of the dynein complex to other cargos, while the conserved motor domain, containing six AAA+ domains and a C domain, transduces ATP hydrolysis energy into mechanical work. Thus, functional properties of each dynein complex are largely determined by the DHC motor domain. Recent determination of whole genome DNA sequences of a number of organisms revealed that 15 or more *DHC* genes are present in most organisms with motile cilia and flagella. Of these *DHC* gene products, two proteins are cytoplasmic and the others are axonemal (see Asai, 1995; Gibbons, 1995; Kamiya, 2002, for reviews). Phylogenetic analyses further classified the *DHC* genes into several distinct groups (Morris *et al*., 2006; Wickstead and Gull, 2007; Wilkes *et al.* 2008). Each group of DHCs may have specific functions in the cell.

Here, I show how we can classify *DHC* genes by phylogenetic analysis using the predicted amino acid sequence. First, as an example, analysis of the *DHC* genes of *Chlamydomonas* is shown. The *Chlamydomonas* genome contains 16 *DHC* genes (King and Kamiya, 2009; Pazour *et al*., 2006), of which 15 genes have been correlated to particular DHC proteins (Table I): one cytoplasmic DHC that functions in retrograde intraflagellar transport (IFT) (Pazour *et al*., 1999; Porter *et al*., 1999); three

Table I
***Chlamydomonas* Dynein Heavy Chains**

Class	Type	Name of gene	Name of protein
Cytoplasmic	IFT	*DHC1b*	DHC1b
Axonemal	Three-headed	OAD α (*ODA11*)	OAD α
		OAD β (*ODA4*)	OAD β
		OAD γ (*ODA2*)	OAD γ
	Two-headed IAD	*DHC1* (*PF9*)	Dynein f/I1 α
		DHC10 (*IDA2*)	Dynein f/I1 β
	Single-headed IAD	*DHC6*	Dynein a
		DHC5	Dynein b
		DHC9	Dynein c
		DHC2	Dynein d
		DHC8	Dynein e
		DHC7	Dynein g
		DHC3	DHC3
		DHC4	DHC4
		DHC11	DHC11
Uncharacterized		ID 5717029	ID 206178

IFT, intraflagellar transport; OAD outer-arm dynein; IAD inner-arm dynein.

DHCs of outer-arm dynein (Mitchell and Brown, 1994; Wilkerson *et al*., 1994); two DHCs of a two-headed inner-arm dynein (Myster *et al*, 1997; Perrone *et al*., 2000); and nine DHCs of a single-headed inner-arm dynein (Yagi *et al*., 2005, 2009). Second, 16 human *DHC* genes are compared with the *Chlamydomonas DHC* genes by phylogenetic analysis. The resulting phylogenetic tree reveals that many of the human *DHC* genes have a closely related counterpart in the *Chlamydomonas DHC* genes. Thus, these human *DHC* gene products may perform a function similar to their *Chlamydomonas* counterparts in axonemal motility.

II. Methods

1. Obtain the predicted DHC amino acid sequences at the NCBI Entrez site (http://www.ncbi.nlm.nih.gov/sites/entrez). To do this for *Chlamydomonas*, search the "Gene" database for "dynein heavy chain *Chlamydomonas.*" A list of the *DHC* genes will appear. Click the name of each gene to see information on that gene including a link to the predicted amino acid sequence. Save the predicted amino acid sequence of each DHC as a plain text file in the FASTA format. It will look as follows.

```
>XP_001696272
MAPFETRSGETPRKVLIQRRRRQFAAQDVAELVHGEGVAQPPQELPL
EVFDNTNFESRMHPEWSLHGERPQTPTTKPAGVPLTSGRALVAHDDG
TGHSVVDWVPCTVVDFDEA TNSYGVTLHQLAHSGNGSAEADAEDM.........
```

2. Protein sequences predicted from genomic sequence frequently contain significant errors so if cDNA sequences have been determined for any DHCs, replace the predicted sequences with the cDNA sequence. In the case of *Chlamydomonas*, search the NCBI Entrez "Protein" database for the name of each *DHC* gene, for example, "PF9 *Chlamydomonas*" or "DHC3 *Chlamydomonas*." As of April 2009, seven DHC cDNA sequences have been deposited: one for a cytoplasmic dynein (DHC1b); three for a outer-arm dynein α, β, and γ (OAD α, β, and γ); two for a two-headed inner-arm dynein [DHC1 (PF9) and DHC10 (IDA2)]; and one for a single-headed inner-arm dynein (DHC9). Comparing the predicted and determined DHC sequences, you will find that the predicted sequence of OAD γ is too short, and that of DHC9 is separated into two proteins: "DHC9" and the "CHLREDRAFT_133402." Copy the determined or predicted sequences of all the DHCs to a plain text file.
3. Multiple align the DHC sequences using the ClustalW program (Thompson *et al.*, 1994) and calculate the evolutionary distances by the neighbor-joining method

(Saitou and Nei, 1987) to construct a phylogenetic tree. The web-based ClustalW programs at (DNA Data Bank of Japan) DDBJ (http://clustalw.ddbj.nig.ac.jp/top-e.html) and (European Bioinformatics Institute) EBI (http://www.ebi.ac.uk/Tools/clustalw2/index.html) are convenient. I usually use the DDBJ site, which automatically calculates the evolutionary distances following multiple alignment. Upload the DHC sequence file and select "protein" as the "type" key. In this mode, many parameters, such as "a GAP open penalty" and "a GAP extend penalty" can be changed. However, the default parameters work well for DHC classification (for details of each parameter, see Thompson *et al*., 1994). Click the "submit" button. After some time (from a few to several tens of minutes, depending on the length and the number of sequences), the results of the multiple alignment will be obtained in a new window. In this window, you will find the multiple-alignment file (query.aln), the data files of a guide tree (query.dnd), and a phylogenetic tree (query.ph).

4. If necessary, edit the multiple alignment using an editor such as "Bioedit" (http://www.mbio.ncsu.edu/BioEdit/BioEdit.html). A common problem in phylogenetic analysis is that short (truncated) sequences will often inappropriately align with each other and this will result in an incorrect phylogenetic reconstruction. To correct this, either (1) delete the very short sequence data and reanalyze the remaining data or (2) select the common region in which all the DHC sequences are fully aligned and use only this region for analysis. To do this, copy the selected region from the alignment file to a new file and resubmit this file to ClustalW. In this case, select "off" at the "ALN" key to skip the process of multiple alignments. The reliability of the phylogenetic data can be estimated by bootstrap test. Select "on" at the "bootstrap" key.
5. Draw the phylogenetic tree of DHC sequences. The program "Treeview" (http://taxonomy.zoology.gla.ac.uk/rod/treeview.html) can be used. After installation of this program, a phylogenetic tree will be automatically drawn upon double-clicking the "query.ph" file. This program can draw (1) an unrooted tree, (2) a cladegram tree without evolutionary distance information, and (3) a phylogram tree with evolutionary distance information. The cladegram and phylogram are rooted trees. They can be drawn with a unique node corresponding to a hypothetical common ancestor. In the neighbor-joining method, the node is arbitrarily determined and is not related to the ancestor. Phylogenetic analysis of genes with an outgroup can give information on the evolutionary pathway of the family. Here, I select cytoplasmic DHCs as the outgroup. The cladegram is simple and it shows a clear classification of the genes, but it does not contain evolutionary distance information. In contrast, the phylogram contains information on both evolutionary distances and pathways. The unrooted tree shows the relatedness of genes of interest without the assumption of a common ancestor. Therefore, it clearly indicates clusters of related genes, but it contains no information on their evolutionary history.

A. Tips

1. The predicted amino acid sequences can be also obtained from organism-specific databases. For example, *Chlamydomonas* genome database (version 4.0) is available at the JGI site (http://genome.jgi-psf.org/cgi-bin/runAlignment?db=Chlre4&advanced=1). In the databases for some organisms, certain gene models may not be annotated or the annotation quality may be low. In these cases, each *DHC* gene can be found by searching translated nucleotide databases with protein sequence (tblastn search) using a DHC protein sequence. To obtain all *DHC* genes in the database, several searches with different DHC sequences are necessary.
2. The database contents are frequently updated. An update often causes a change in the predicted amino acid sequences in the database. The length of predicted sequences may increase or sometimes decrease. Therefore, you should check whether updated data is available in each database, and whether the quality of the predicted sequence is better than an older version. It is possible that, for some genes, an older database gives better information than a new one. For example, the DHC3 sequence registered in the *Chlamydomonas* genome database version 4.0 (protein ID 187119; 3751 amino acids) was shorter than that registered in the database version 2.0 (protein ID 161758 and 161759; 5354 amino acids). A recent study showed that the *DHC3* gene model registered in the database version 2.0 was better (Yagi *et al.*, 2009).
3. A stand-alone multiple-alignment program, ClustalX, is also available at the following FTP site (ftp://ftp.ebi.ac.uk/pub/software/clustalw2/).
4. GAP sequences are often found at many positions in DHC full-length multiple-alignment sequences. These GAPs are apparently inserted at the boundary positions between domains. More reliable phylogenetic analysis will be obtained with the parameter TOSSGAP (IGNORE GAP), ON.
5. After multiple alignment of full-length DHC sequences, the data can be reused for the phylogenetic analysis of a specific region of the DHC. Selected aligned sequences are cut out and pasted to a new file using an editor program. This file can be reanalyzed by the method described in step 4.
6. The guide tree data recorded in the file "query.dnd" can be used only for multiple alignment and cannot be used for drawing a phylogenetic tree.
7. To calculate evolutionary distances, several methods (e.g., maximum likelihood, maximum parsimony, and Bayesian methods) can be used as alternatives to the neighbor-joining method. For more accurate analysis, comparison among the phylogenetic trees constructed by different methods is recommended (Wickstead and Gull, 2007; Wilkes *et al.* 2008).

III. Materials

The predicted amino acid sequences used in this study are shown in Supplementary material on the companion web site (http://www.elsevierdirect.com/companions/9780123708731).

IV. Results and Discussion

To compare the relationships among *Chlamydomonas DHC* genes, a phylogenetic tree was constructed using the determined and predicted sequences of the DHCs (Fig. 1). This phylogenetic classification is consistent with prior classifications based on morphological, biochemical, and functional properties of DHCs. In both systems of classification, the dyneins were classified into four groups: cytoplasmic dynein, outer-arm dynein, two-headed inner-arm dynein, and single-headed inner-arm dynein. Single-headed DHCs can be further classified into three subgroups: IAD-3, IAD-4, and IAD-5, as observed previously (Hartman and Smith, 2009; Morris *et al*., 2006; Wickstead and Gull, 2007; Wilkes *et al.* 2008). This classification of single-headed dyneins may be related to functional differences (Yagi *et al*., 2009). For example, only dyneins belonging to IAD-4 (dynein d) and IAD-5 (dynein g) have

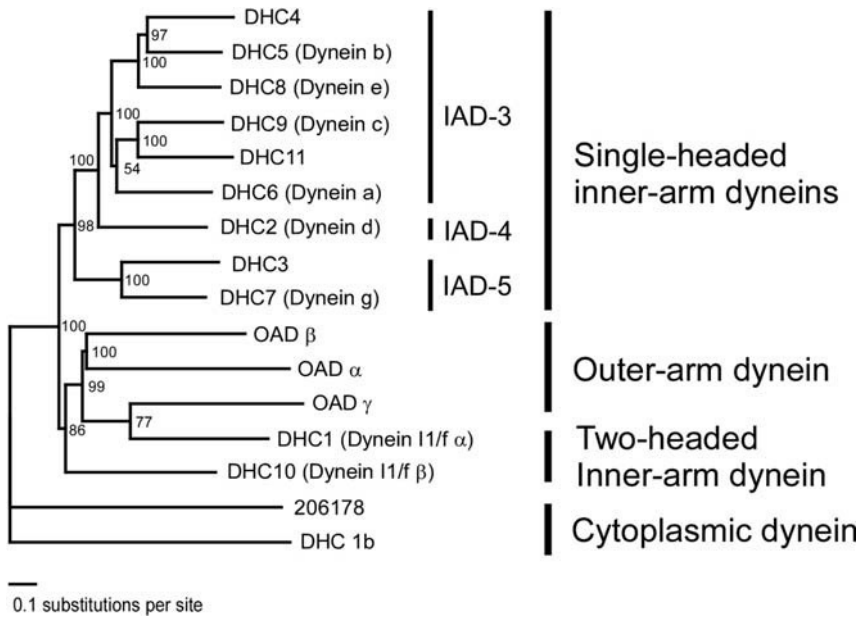

Fig. 1 Phylogenetic tree of *Chlamydomonas* dynein heavy chains (DHCs). A phylogenetic tree was constructed for cytoplasmic and flagellar DHCs in *Chlamydomona*s using the full-length sequences. For display, DHC1b, intraflagellar transport-type cytoplasmic dynein, was selected as the outgroup. For dyneins with cDNA sequences that have not yet been determined, the predicted sequences from the genome database were used. *Chlamydomonas* DHCs were largely classified into four groups: cytoplasmic dynein, outer-arm dynein, two-headed inner-arm dynein, and single-headed inner-arm dynein. The single-headed DHC type can be classified into three subgroups: IAD-3, IAD-4, and IAD-5 types, as reported previously (Morris *et al*., 2006; Wickstead and Gull, 2007). Bootstrap $>80\%$ (1000 iterations) are shown at branch points.

been shown to produce sufficient torque to cause microtubule bending (Kikushima and Kamiya, 2008).

To examine the relationship between the *Chlamydomonas* and human *DHC* genes, a second phylogenetic tree was constructed using the *DHC* genes of both organisms (Fig. 2). Previous phylogenetic analysis examined 31 *DHC* genes (16 *Chlamydomonas* and 15 human genes) (Pazour *et al*., 2006). This analysis examined 32 *DHC* genes,

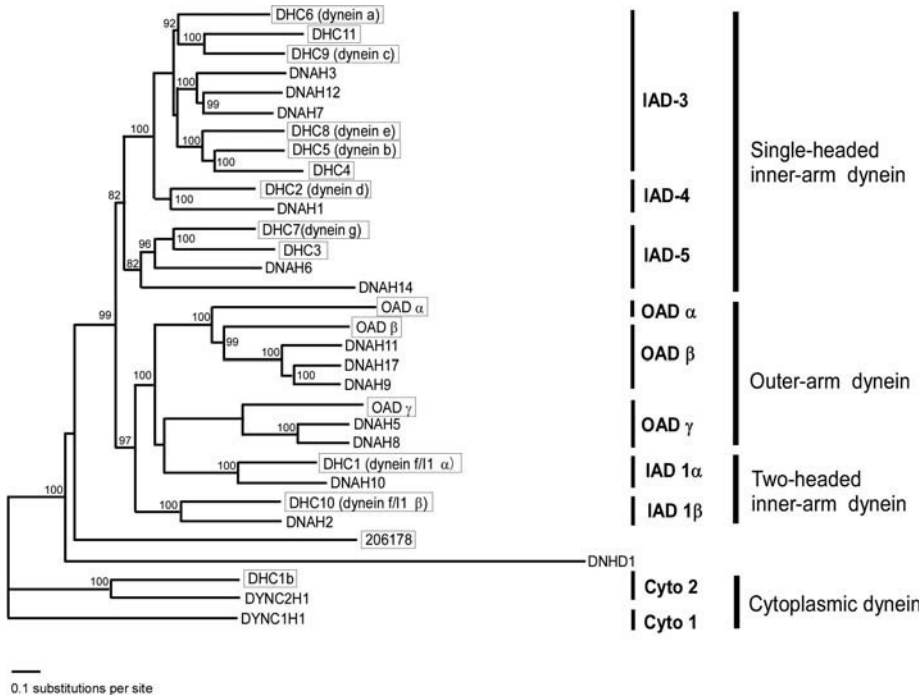

Fig. 2 Phylogenetic tree of *Chlamydomonas* and human dynein heavy chains (DHCs). A phylogenetic tree was constructed for *Chlamydomonas* and human DHCs using the full-length sequences. For display, DYNC1H1, human cytoplasmic dynein, was selected as the outgroup. *Chlamydomonas* DHCs are boxed. As described in Fig. 1, for dyneins with cDNA sequences that have not yet been determined, the predicted sequences from the genome database were used. A single counterpart to a specific *Chlamydomonas* DHC was found for some human DHCs, for example, human DYNC2H1 and *Chlamydomonas* DHC1b; human DNAH2 and *Chlamydomonas* DHC10. In contrast, multiple human *DHC* genes corresponding to *Chlamydomonas* OAD β and γ DHCs were found, suggesting gene duplication in humans. No human counterpart of *Chlamydomonas* OAD DHC α has been identified. The single-headed DHC types are more clearly classified into three subgroups when human and *Chlamydomonas* sequences are combined, than in the phylogenetic tree constructed with only *Chlamydomonas* DHC sequences. *Chlamydomonas* protein ID 206178, which had been previously assigned as a conventional cytoplasmic dynein (Porter *et al*., 1999), was classified into the cytoplasmic group in Fig. 1. However, it appears not to be the counterpart of human cytoplasmic DHC (DYNC1H1) in Fig. 2, rather it appears to be grouped with the flagellar dyneins, as suggested by Wickstead and Gull (2007). DNHD1, which is an uncharacterized protein containing a DHC domain, is located at the boundary position between the cytoplasmic and flagellar-type DHCs. Bootstrap >80% (1000 iterations) are shown at branch points.

because an additional *DHC* gene (*DNHD1*) has recently been found in the human genome database. The result is similar to that obtained in the previous study (Pazour *et al*., 2006) except for the classification of single-headed type DHCs. The disparity may result from differences in the analyzed sequence lengths; Pazour *et al*. (2006) used ~100 amino acids around the AAA1 domain, while I used nearly full-length sequences of the DHCs. As was observed with the *Chlamydomonas DHC* genes, the human *DHC* genes were also classified into four groups. For the cytoplasmic DHC that powers retrograde IFT and the DHCs of two-headed inner-arm dynein, a clear counterpart for each *Chlamydomonas DHC* is present in humans; the conventional cytoplasmic *DHC, DYNC1H1* in humans, is not found in *Chlamydomonas*. For OAD DHCs, no human counterpart to *Chlamydomonas* OAD α has been found, but multiple human genes corresponding to *Chlamydomonas* OAD β and γ are present. It is possible that a particular OAD DHC is expressed in a limited cell type and/or in a specific axonemal location, as is observed for human DNAH9; this DHC is located along the entire length of sperm axonemes, but is only in the distal portion of respiratory ciliary axonemes (Fliegauf *et al*., 2005). In single-headed inner-arm DHCs, the relationships among DHCs in IAD-3, IAD-4, and IAD-5 groups are different. In IAD-4, human *DNAH1* is clearly related to *Chlamydomonas DHC2*. In IAD-5, human *DNAH6* is similar to *Chlamydomonas DHC3* and *DHC7*, but no *Chlamydomonas* counterpart is found for human *DNAH14*. In IAD-3, *DHC* genes radiate into three distinct subfamilies. One family contains three human *DHC* genes, *DNAH3, DNAH7, and DNAH12*; and the other two families each contain three *Chlamydomonas DHC* genes: one consists of *DHC6, DHC9,* and *DHC11* and the other *DHC4, DHC5,* and *DHC8*. These results suggest that the single-headed DHCs may have diverged in an organism-specific manner, as proposed by Wickstead and Gull (2007).

These results indicate that the *Chlamydomonas DHC* genes can be used as the standard for comparative classification of *DHC* genes in other organisms to predict their cellular functions.

Acknowledgments

I thank Professor Ritsu Kamiya for critical reading of this manuscript.

References

Asai, D.J. (1995). Multi-dynein hypothesis. *Cell Motil. Cytoskeleton* **32**, 129–132.

Fliegauf, M., Olbrich, H., Horvath, J., Wildhaber, J.H., Zariwala, M.A., Kennedy, M., Knowles, M.R., and Omran, H. (2005). Mislocalization of DNAH5 and DNAH9 in respiratory cells from patients with primary ciliary dyskinesia. *Am. J. Respir. Crit. Care Med*. **171**, 1343–1349.

Gibbons, I.R. (1995). Dynein family of motor proteins: Present status and future questions. *Cell Motil. Cytoskeleton* **32**, 136–144.

Hartman, H., and Smith, T.F. (2009). The evolution of the cilium and the eukaryotic cell. *Cell Motil. Cytoskeleton* **66**, 215–219.

Kamiya, R. (2002). Functional diversity of axonemal dyneins as studied in *Chlamydomonas* mutants. *Int. Rev. Cytol*. **219**, 115–155.

Kikushima, K., and Kamiya, R. (2008). Clockwise translocation of microtubules by flagellar inner-arm dyneins in vitro. *Biophys. J*. **94**, 4014–4019.

King, S.M., and Kamiya, R. (2009). Axonemal dyneins; assembly, structure, and force generation. Cell motility and behavior. *In* "*Chlamydomonas* Sourcebook" (G.B. Witman, ed.), Vol. III, pp. 131–208. Elsevier Press, Amsterdam.

Mitchell, D.R., and Brown, K.S. (1994). Sequence analysis of the Chlamydomonas alpha and beta dynein heavy chain genes. *J. Cell Sci.* **107**, 635–644.

Morris, R.L., Hoffman, M.P., Obar, R.A., McCafferty, S.S., Gibbons, I.R., Leone, A.D., Cool, J., Allgood, E.L., Musante, A.M., Judkins, K.M., Rossetti, B.J., Rawson, A.P., et al., (2006). Analysis of cytoskeletal and motility proteins in the sea urchin genome assembly. *Dev. Biol.* **300**, 219–237.

Myster, S.H., Knott, J.A., O'Toole, E., and Porter, M.E. (1997). The *Chlamydomonas* DHC1 gene encodes a dynein heavy chain subunit required for assembly of the I1 inner arm complex. *Mol. Biol. Cell* **8**, 607–620.

Pazour G.J., Dickert B.L., Witman G.B. (1999). The DHC1b (DHC2) isoform of cytoplasmic dynein is required for flagellar assembly. *J Cell Biol*. **144**, 473–481.

Pazour, G.J., Agrin, N., Walker, B.L., and Witman, G.B. (2006). Identification of predicted human outer dynein arm genes: Candidates for primary ciliary dyskinesia genes. *J. Med. Genet.* **43**, 62–73.

Perrone, C.A., Myster, S.H., Bower, R., O'Toole, E.T., and Porter, M.E. (2000). Insights into the structural organization of the I1 inner arm dynein from a domain analysis of the 1beta dynein heavy chain. *Mol. Biol. Cell* **11**, 2297–2313.

Porter, M.E., Bower, R., Knott, J.A., Byrd, P., and Dentler, W. (1999). Cytoplasmic dynein heavy chain 1b is required for flagellar assembly in *Chlamydomonas. Mol. Biol. Cell* **10**, 693–712.

Saitou, N., and Nei, M. (1987). The neighbor-joining method: A new method for reconstructing phylogenetic trees. *Mol. Biol. Evol*. **4**, 406–425.

Thompson, J.D., Higgins, D.G., and Gibson, T.J. (1994). CLUSTAL W: Improving the sensitivity of progressive multiple sequence alignment through sequence weighting, position-specific gap penalties and weight matrix choice. *Nucleic Acids Res.* **22**, 4673–4680.

Wickstead, B., and Gull, K. (2007). Dyneins across eukaryotes: A comparative genomic analysis. *Traffic* **8**, 1708–1721.

Wilkerson, C.G., King, S.M., and Witman, G.B. (1994). Molecular analysis of the gamma heavy chain of Chlamydomonas flagellar outer-arm dynein. *J. Cell Sci.* **107**, 497–506.

Wilkes, D.E., Watson, H.E., Mitchell, D.R., and Asai, D.J. (2008). Twenty-five dyneins in Tetrahymena: A re-examination of the multidynein hypothesis. *Cell Motil. Cytoskeleton* **65**, 342–351.

Yagi, T., Minoura, I., Fujiwara, A., Saito, R., Yasunaga, T., Hirono, M., and Kamiya, R. (2005). An axonemal dynein particularly important for flagellar movement at high viscosity: Implication from a new *Chlamydomonas* mutant deficient in the dynein heavy chain gene *DHC9. J. Biol. Chem.* **280**, 41412–41420.

Yagi T., Uematsu K., Liu Z., Kamiya R. (2009). Identification of dyneins that localize exclusively to the proximal portion of *Chlamydomonas* flagella. *J Cell Sci*. **122**, 1306–1314.

This page intentionally left blank

CHAPTER 2

Identification and Characterization of Dynein Genes in *Tetrahymena*

David E. Wilkes[*], Nicole Bennardo[*], Clarence W.C. Chan[*], Yu-Loung Chang[*], Elizabeth O. Corpuz[*], Jennifer DuMond[*], Jordan A. Eboreime[*], Julianna Erickson[*], Jonathan Hetzel[*], Erin E. Heyer[*], Mark J. Hubenschmidt[*], Ekaterina Kniazeva[*], Hallie Kuhn[*], Michelle Lum[*], Andrea Sand[*], Alicia Schep[*], Oksana Sergeeva[*], Natt Supab[*], Caroline R. Townsend[*], Liesl Van Ryswyk[*], Hadley E. Watson[*], Alice E. Wiedeman[*], Vidyalakshmi Rajagopalan[*], *and* David J. Asai[*,†]

[*]Department of Biology, Harvey Mudd College, 301 Platt Blvd, Claremont California 91711

[†]Howard Hughes Medical Institute, 4000 Jones Bridge Road, Chevy Chase Maryland 20815

Abstract

We describe the protocol through which we identify and characterize dynein subunit genes in the ciliated protozoan *Tetrahymena thermophila*. The gene(s) of interest is found by searching the *Tetrahymena* genome, and it is characterized *in silico* including the prediction of the open reading frame and identification of likely introns. The gene

METHODS IN CELL BIOLOGY, VOL. 92

978-0-12-374974-1
DOI: 10.1016/S0091-679X(08)92002-1

is then characterized experimentally, including the confirmation of the exon–intron organization of the gene and the measurement of the expression of the gene in nondeciliated and reciliating cells. In order to understand the function of the gene product, the gene is modified—for example, deleted, overexpressed, or epitope-tagged—using the straightforward gene replacement strategies available with *Tetrahymena*. The effect(s) of the dynein gene modification is evaluated by examining transformants for ciliary traits including cell motility, ciliogenesis, cell division, and the engulfment of particles through the oral apparatus. The multistepped protocol enables undergraduate students to engage in short- and long-term experiments. In our laboratory during the last 6 years, more than two dozen undergraduate students have used these methods to investigate dynein subunit genes.

I. Introduction

Dyneins, first discovered in *Tetrahymena* (Gibbons and Rowe, 1965), are a large family of microtubule-based molecular motors that are required for a wide variety of essential cellular and intracellular movements. Except for higher plants, eukaryotes have at least one type of dynein, while species with motile cilia or flagella express more than a dozen different dyneins. There are two functional classes of dynein: axonemal dyneins produce the movement of cilia and flagella (reviewed in Porter, 1996); nonaxonemal or "cytoplasmic" dyneins transport various cargoes through the cytoplasm along tracks of microtubules (reviewed in Vale, 2003). The two subclasses of axonemal dyneins are defined by their locations in the axoneme. The several different two-headed and one-headed inner arm dyneins (IADs) are distributed in a precise pattern along the axoneme (Piperno and Ramanis, 1991) where they generate shear between adjacent outer doublet microtubules (reviewed in Asai and Brokaw, 1993). The multiheaded outer arm dynein (OAD; two-headed in metazoans, three-headed in protozoans) is present along the entire length of the axoneme where it contributes to the sliding velocity of the outer doublet microtubules (Nicastro *et al*., 2006). The nonaxonemal dyneins are also divided into two subclasses defined, in part, by their subcellular locations. Cytoplasmic dynein-1 is nearly ubiquitous among eukaryotes (an exception is *Chlamydomonas* which has no dynein-1) and is implicated in many cellular movements including mitosis, endocytosis, and retrograde axonal transport (e.g., Burkhardt *et al*., 1997; Echeverri *et al*., 1996; Harada *et al*., 1998; Hirokawa *et al*., 1990; Lee *et al*., 1999; Ma *et al*., 1999; Schnapp and Reese, 1989). Cytoplasmic dynein-2 occurs only in organisms with cilia or flagella and is the motor for retrograde intraflagellar transport (Gibbons *et al*., 1994; Pazour *et al*., 1999; Porter *et al*., 1999; Signor *et al*., 1999; Wicks *et al*., 2000).

At the core of each dynein is its one, two, or three heavy chains (HCs); the HC motor domain transduces the free energy obtained from ATP hydrolysis into mechanical work (Burgess *et al*., 2003; Kon *et al*., 2009; Roberts *et al*., 2009). Because every dynein has at least one HC, the number of HC genes is a measure of the complexity of the dyneins in an organism. For example, *Tetrahymena* expresses 25 different dynein heavy chain

(DYH) genes that form 22 separate dynein complexes (Wilkes *et al*., 2008). Assembled onto the HC core is a specific combination of smaller dynein subunit proteins, including the intermediate (IC), light intermediate (LIC), and light (LC) chains (reviewed in Pfister *et al*., 2006; Sakato and King, 2004). These smaller subunits are the important dynein control elements, regulating dynein motor activity and specifying cargo binding. Thus, understanding the biology of dynein requires knowing the subunit composition of each dynein complex and how each subunit contributes to the way that dynein functions in the cell.

We have learned a great deal about dynein and axonemes from the study of the green alga *Chlamydomonas reinhardtii*, which enjoys a rich history of the application of genetics, biochemistry, and ultrastructural studies to the study of flagellar motility (e.g., Luck, 1984; Randall *et al*., 1964). The ciliated protozoan *Tetrahymena thermophila* also is a powerful experimental system (see Asai and Forney, 2000), offering approaches that complement the "forward genetics" approach available in organisms such as *Chlamydomonas*. In particular, *Tetrahymena* presents the opportunity for straightforward "reverse genetics" in which any gene can be modified exclusively by homologous recombination and the effect of the disruption of even an essential gene can be evaluated in a living cell.

T. thermophila has two nuclei in one cytoplasm (see Karrer, 2000). The germline micronucleus is diploid and is transcriptionally silent, and the somatic macronucleus contains about 45 copies of each expressed gene and determines the phenotype of the cell. During vegetative growth, the micronucleus is faithfully divided by mitosis, but the macronucleus is amitotic, being pinched apart during cytokinesis. Phenotypic assortment allows for a selectable allele to replace the wild-type versions of the gene in the macronucleus; all of the wild-type copies can be replaced if the gene is not essential, or some of the wild-type copies can be replaced if the gene is essential for vegetative growth. In either case, the resulting phenotype can be evaluated in a living cell.

Unlike many experimental systems, the modification of genes in *Tetrahymena* can be readily achieved by homologous recombination. A DNA construct that contains the modification (or "mutation")—for example, the complete replacement of the gene with a selectable marker, the insertion of an inducible promoter, or the addition of an epitope tag—flanked by chromosomal DNA is introduced into cells by one of several methods including microinjection, electroporation, or biolistic transformation (Bruns and Cassidy-Hanley, 2000; Chalker *et al*., 2000; Gaertig and Kapler, 2000). A complete replacement is assured by inserting the mutated gene into the micronucleus. Through a series of matings, the micronucleus can be made homozygous for the mutated allele in a cell whose macronucleus is completely wild type (Hai *et al*., 2000). When two of these heterokaryons mate, their progeny will have only the mutant allele in their macronuclei, thus these progeny will lack altogether the wild-type version of the targeted gene. A simpler approach and one that guarantees viable transformants is to introduce the construct in the macronucleus. Through phenotypic assortment, the copy number of the mutant allele is enriched. The germline disruption of the targeted gene results in the knockout of

the gene; the macronuclear disruption of the gene results in a knockdown of the gene.

In addition to the ease in which reverse genetics can be pursued, *Tetrahymena* also offers other practical advantages. It is easy and inexpensive to culture in the laboratory. Wild-type cells divide every 3 h at 30°C and achieve densities exceeding 10^6 cells/ml. The cells are large (60×30 μm) and photogenic. Each cell has >1000 cilia and simple assays can measure swimming velocity and behavior; the rate of ciliogenesis; and the number, density, and lengths of cilia (e.g., Rajagopalan *et al*., 2009). The 104 Mb macronuclear genome has been sequenced, assembled, and annotated (Eisen *et al*., 2006).

Finally, an important advantage of *Tetrahymena* is that it is an accessible experimental system for undergraduate research students. A central objective of our work is to provide opportunities for students to be meaningfully engaged in research. All of the methods described in this chapter were developed for and are routinely used by undergraduate students in our laboratory.

II. Methods and Results

A. Identification and Sequence Analysis of *Tetrahymena* Dynein Subunit Genes

1. Rationale

An important strength of *Tetrahymena* is that it is an experimental system in which one is able to precisely target any gene in order to study the contribution of that gene's product to the phenotype of a living cell. However, *Tetrahymena* lags behind other systems—an exemplar being *Chlamydomonas*—for the discovery of genes involved in axonemal motility. A powerful strategy is to use the two systems in a complementary fashion: gene discovery in one organism and the direct test of the function of the gene product in *Tetrahymena*. Thus, the first objective is to identify dynein subunit genes in *Tetrahymena*.

2. Methods and Materials

a. Finding Open Reading Frames. Finding open reading frames of *Tetrahymena* genes tBLASTn (Altschul *et al*., 1997) is used to search the *T. thermophila* macronuclear genome (Eisen *et al*., 2006; tigrblast.tigr.org/er-blast/index.cgi?project=ttg) using known dynein subunits identified in other systems as the query sequences. The fragments identified from the BLAST are extended to include start and stop codons (always TGA in *Tetrahymena*).

b. Prediction of Introns. The criteria for predicting introns are based on our experience with the 64 introns that we experimentally confirmed in our studies of the *Tetrahymena* cytoplasmic dynein heavy chains 1 and 2 and the axonemal dynein β heavy chain (Lee *et al*., 1999; Lincoln *et al*., 1998). The introns are 50–332 bp in

length (average = 80 bp) and have 78.0–95.3% A+T content (average = 87.7%). All *Tetrahymena* introns have the canonical consensus splice sites of GT at the 5′ end and AG at the 3′ end (Karrer, 2000). Mapping of introns is an iterative approach in which the conceptual translation from likely exons is aligned with published sequences.

c. Phylogenetic Analyses. The *Tetrahymena* sequences obtained are compared to orthologous sequences from other organisms. Alignments are performed by ClustalW (ebi.ac.uk/clustalw/index.html). Comparisons are also made with predicted protein sequences from the human and *Drosophila* genomes and expressed sequence tags (EST) databases (NCBI BLAST; www.ncbi.nlm.nih.gov/BLAST) and the *Chlamydomonas* genome (Department of Energy Joint Genome Institute; genome.jgi-psf.org/chlre2/chlre2.home.html). Phylogenetic and molecular evolutionary analyses are performed using MEGA version 2.1 (Kumar *et al*., 2001). Trees are constructed by the unweighted pair group method using arithmetic average (Sokal and Michener, 1958), neighbor-joining (Saitou and Nei, 1987), and maximum parsimony (Eck and Dayhoff, 1966) methods. Robustness is tested by bootstrap resampling 500 times. In all of our analyses, all three types of trees have yielded similar results. Neighbor-joining trees are usually presented as a representative example.

d. Reevaluation of Genes. After the initial identification, each gene is reevaluated. We examine how well the predicted protein sequence aligns with known dynein subunit sequences paying attention to the predicted intron splice sites. Predicted introns that result in poor alignments are experimentally determined by sequencing the PCR (polymerase chain reaction) products (see later). Although the sequences originally obtained are the best hits from a BLAST search, they are not necessarily orthologs of the query sequence. To characterize the sequence more stringently, we perform a reciprocal best BLAST. If the *Tetrahymena* sequence and the query sequence (or other known sequences of that dynein subunit) are best BLAST results for each other, then this is strong evidence that the *Tetrahymena* sequence is a true ortholog. An example in which we did not obtain a convincing reciprocal best BLAST result is dynein light chain 3, LC3, of OAD. *Chlamydomonas* LC3 is a member of the thioredoxin family (Patel-King *et al*., 1996). The closest *Tetrahymena* sequences to LC3 were not better matches to LC3 than other thioredoxin proteins (Wilkes *et al*., 2007b). Therefore, we have named the *Tetrahymena* genes "LC3-like."

3. Results

Our searches have identified 25 genes encoding dynein heavy chains, 22 genes encoding other dynein subunits, and 7 genes encoding possible dynein subunits (Table I; Wilkes *et al*., 2007b, 2008). The open reading frames and introns have been determined for 14 LC, 2 LIC, and 6 IC genes. There are eight different classes of *Tetrahymena* LC genes (Fig. 1; Wilkes *et al*., 2007b). One isoform each was found for the two LICs (Fig. 2). *Tetrahymena* expresses one isoform of each of the ICs except

Table I
Dynein Small Subunit Genes Identified and Characterized by Undergraduates

Gene	Query sequence[a]	ORF (bp)	# AA	# Introns	Induction vs DYH4[b]	Disruption in *Tetrahymena*[c]
LC1	*Chlamy*	609	202	0	2.7	KD
LC2A	*Chlamy*	628	132	2	1.7	–
LC2B	*Chlamy*	384	127	0	2.7	–
LC3-likeA	*Chlamy*	330	109	0	1.0	–
LC3-likeB	*Chlamy*	407	110	1	0.4	–
LC4A	*Chlamy*	730	160	1	0.7	KD
LC4B	*Chlamy*	679	155	3	2.9	KD
LC7A	*Chlamy*	318	105	0	2.5	–
LC7B	*Chlamy*	312	103	0	3.2	–
LC8	*Chlamy*	276	91	0	4.1	–
LC8-likeA	*Chlamy*	285	94	0	6.1	–
LC8-likeB	*Chlamy*	279	92	0	5.5	–
LC8-likeC	*Chlamy*	291	96	0	4.3	–
LC8-likeD	*Chlamy*	264	87	0	14.1	–
LC8-likeE	*Chlamy*	482	93	2	0.9	–
LC10	Urchin	655	110	3	12.2	KD
Tctex1A	*Chlamy*	330	109	0	7.1	–
Tctex1B	*Chlamy*	372	123	0	3.3	–
p28A	*Chlamy*	919	246	1	2.5	–
p28B	*Chlamy*	1235	240	3	1.8	–
p28C	*Chlamy*	969	254	2	1.9	–
D1LIC	Chicken	2078	457	10	ND	RNAi
D2LIC[d]	*Chlamy*	1607	474	1	1.2	KO, RNAi
IC2	*Chlamy*	3147	724	8	1.2	–
IC3	*Chlamy*	3014	670	8	1.2	–
IC4	*Dicty*	2676	594	11	0.2	–
IC5	*Chlamy*	2964	717	7	0.1	–
IC6	*Chlamy*	3965	919	11	0.5	–
D2IC	*Chlamy*	2397	594	8	2.1	–

[a] Organism with known dynein gene sequence used for original query.
[b] Change in transcript level relative to known axonemal positive control gene, DYH4, after double deciliation.
[c] Types of gene disruptions created in *Tetrahymena* to date. KD, knockdown; KO, knockout; RNAi, short hairpin RNA interference.
[d] Undergraduates did not identify the D2LIC gene but have worked with the sequence.

IC1 which has no *Tetrahymena* ortholog (Fig. 3). The absence of IC1 in *Tetrahymena* is consistent with the model that it is a metazoan-specific component of the axonemal outer arm (Ogawa *et al*., 1995). In addition to the dynein subunit genes, we have used the same methods to identify genes encoding *Tetrahymena* intraflagellar transport complex A and complex B genes.

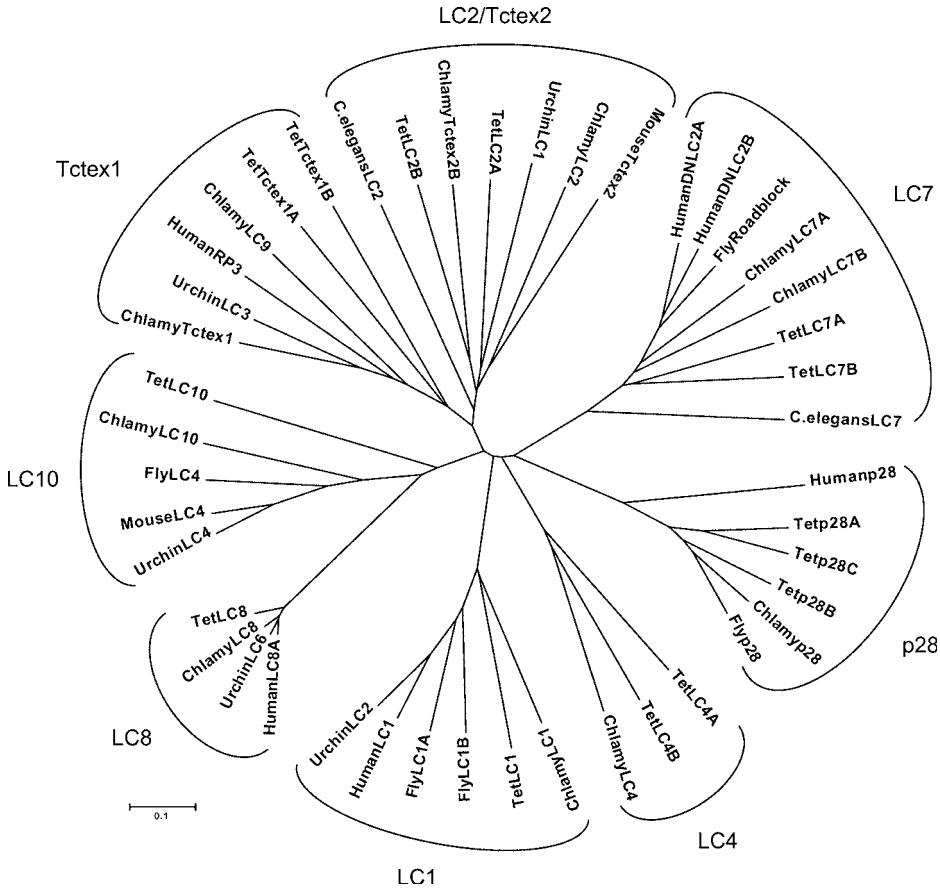

Fig. 1 Dynein light chains (LCs). Phylogenetic comparison of the LC genes found in *Tetrahymena* demonstrates that each groups with similar sequences in other organisms. Although diagrammed as a rooted tree, we do not expect that the different LCs originated from a common sequence. Each *Tetrahymena* sequence is used as an outlier for the other groups. Bar = 0.1 amino acid substitution/site. Chlamy, *Chlamydomonas reinhardtii*; fly, *Drosophila melanogaster*; human, *Homo sapiens*; mouse, *Mus musculus*; Tet, *Tetrahymena thermophila*; urchin, *Strongylocentrotus purpuratus*.

B. Gene Expression

1. Rationale

Once a dynein gene has been identified, it is important to confirm that it is expressed and to determine its pattern of expression in reciliating cells. If the transcript level of a gene increases in response to deciliation, then this is strong evidence that the gene product either is a component of the cilium or is involved in ciliogenesis (Lefebvre *et al*., 1980; Schloss *et al*., 1984; Soares *et al*., 1993). We often are also interested in the relative expression of different isoforms of the same dynein subunit.

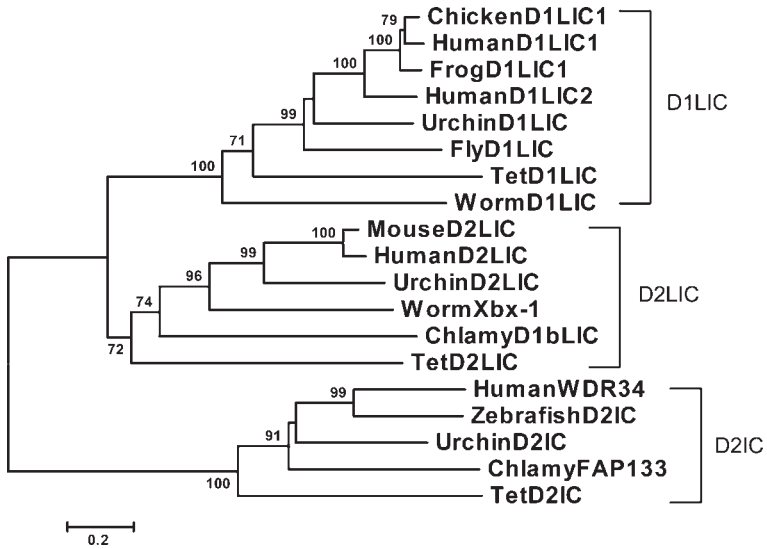

Fig. 2 Dynein light intermediate chains (LICs). There are two classes of LICs: D1LIC is a component of cytoplasmic dynein-1 and D2LIC is a component of cytoplasmic dynein-2. In this analysis, D2IC was used as the outlier. Bootstrap percentages >70% (500 iterations) are shown at branch points. Bar = 0.2 amino acid substitution/site. Species as noted in Fig. 1 and, in addition chicken, *Gallus gallus*; frog, *Xenopus laevis*; worm, *Caenorhabditis elegans*; zebrafish, *Danio rerio*.

2. Methods and Materials

a. Test for Gene Expression. RNA-directed PCR is performed to determine if the *Tetrahymena* genes are expressed and to test the accuracy of intron predictions. RNA is isolated from *Tetrahymena* wild-type strain B2086 by the method of Chirgwin *et al*. (1979). To remove remaining genomic DNA from the RNA, samples are treated with DNaseI (Invitrogen, Carlsbad, CA). Reverse transcription is performed with Superscript III Reverse Transcriptase (Invitrogen) using primers comprising random hexamers. The negative control is a PCR reaction of mock reverse-transcribed RNA in which no Superscript III is added to the reaction.

b. Deciliation and Quantitative "Real-Time" RT-PCR. Wild-type cells are twice deciliated and allowed to reciliate by the method of Calzone and Gorovsky (1982). Prior to deciliation, the cells are starved in 10 mM Tris (pH 7.5) for 24 h at 30°C. The starved cells are pelleted at 1500 rpm for 2 min in a clinical centrifuge, the supernatant decanted, and the volume of the cell pellet noted. The cells are suspended in 10 pellet volumes of deciliation solution (10% Ficoll, 10 mM sodium acetate, 10 mM EDTA, pH 4.2), and cilia sheared off the cells by three to five gentle passes through an 18 gauge hypodermic needle. Immediately after deciliation, 5 volumes of regeneration buffer (15 mM Tris, 2 mM $CaCl_2$, pH 7.9) are added to the cells and the cells are transferred to a sterile flask. Cilia are allowed to regrow for 2 h and then deciliated for

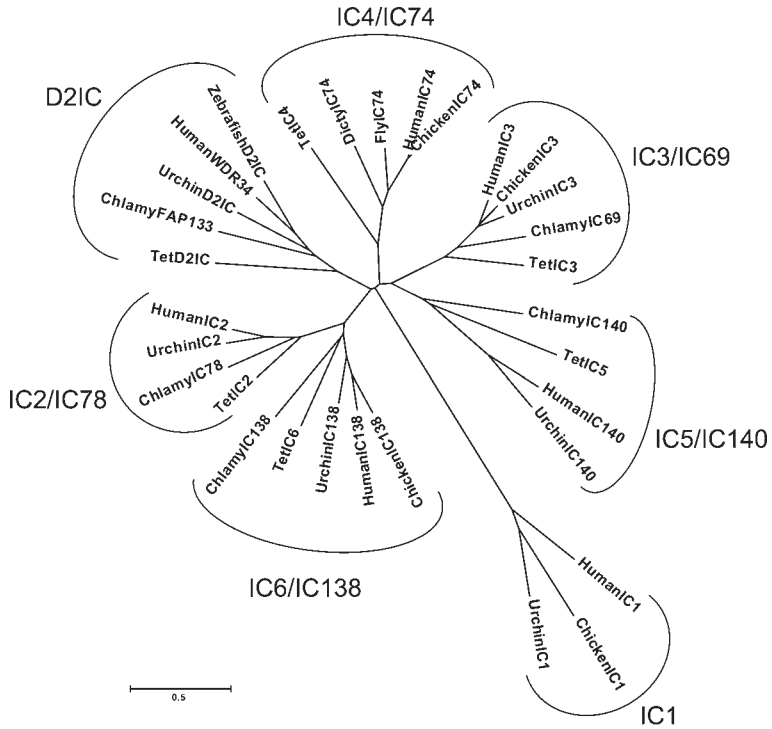

Fig. 3 Dynein intermediate chains (ICs). The (ICs) divide into seven clades. IC1, IC2/IC78, and IC3/IC69 are components of axonemal outer arm dynein. IC1 appears to be only in metazoans. IC4/IC74 and D2IC are components of cytoplasmic dyneins-1 and -2, respectively. IC5/IC140 and IC6/IC138 are axonemal inner arm dynein I1 subunits. Although diagrammed as a rooted tree, we do not expect the different ICs to have originated from a common sequence. Bar = 0.5 substitution/site. Species as noted in Figs. 1 and 2 and, in addition dicty, *Dictyostelium discoideum*.

a second time. RNA is isolated 45 min after the second deciliation. To remove remaining genomic DNA from the RNA, samples are treated with DNaseI (Invitrogen). RNAs from deciliated and untreated control cells are reverse transcribed with the Superscript III Reverse Transcriptase (Invitrogen) using random hexamer primers. Quantitative real time RT-PCR is performed with the Platinum SYBR Green qPCR SuperMix-UDG kit following the protocol of the supplier (Invitrogen). Relative transcript levels are determined by the method of Pfaffl (2001). Three dilutions of each cDNA are made over a 100-fold range. PCR efficiency is calculated for each gene from the relationship between the C_t value and the log of the cDNA concentration. R^2 is the correlation coefficient, where 1.0 means a perfect fit to the theoretical line. The results are used for calculations only if the curve fit has an $R^2 > 0.95$. Dynein heavy chain 1 (*DYH1*) expression is assumed to be insensitive to deciliation and the amount of its transcript after deciliation relative

to the level of transcript before deciliation is used to compensate for differences in the quantity of total cDNA used as template (Gibbons *et al.*, 1994). Outer arm dynein heavy chain β (*DYH4*), whose transcript level increases during reciliation (Gibbons *et al.*, 1994; Wilkes *et al.*, 2007b), is used as the positive control. The expression of the gene being examined is reported as relative to the change seen with *DYH4* expression.

c. Quantification of Transcript Levels. We use the following strategy to quantify the amount of a specific transcript represented in a mixture of cDNAs. This method can be used to compare the expression levels of different genes in the same sample. RNA is isolated and reverse transcribed into cDNA as described above. Because the primer pairs used for each gene will have different efficiencies even under the same conditions, we produce a standard curve for each gene. Known quantities of plasmid (over a 10,000-fold range) containing the gene of interest are used as templates for quantitative real-time PCR. The C_t value is plotted against quantity of template (Fig. 4). This strategy allows for the same cDNA sample to be queried for the amount of cDNA corresponding to each gene of interest.

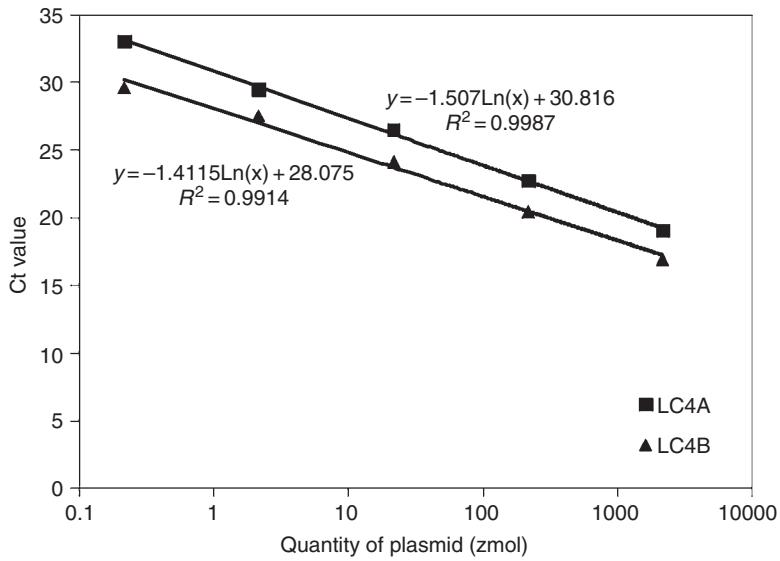

Fig. 4 Quantification of LC4 cDNAs. Standard curves were produced by "real-time" quantitative PCR using known quantities of plasmids containing the gene of interest as template. A standard curve was generated for each gene. The quantity of each sequence in a cDNA sample is obtained from the equation of the line and the experimentally determined C_t value (*LC4A* $C_t = 22.70$; *LC4B* $C_t = 22.78$). Squares, *LC4A*; triangles, *LC4B*.

3. Results

Most of the axonemal dynein subunit genes were found to have transcript levels that increased more than *DYH4*, the positive control, after double deciliation (Table I). This increase supports the conclusion that these are axonemal components or are involved in ciliogenesis. However, some genes such as *IC5*, which is predicted to be a component of IAD I1, did not show an increase. Our assay only determines transcript level relative to that present before deciliation. We do not measure absolute concentrations. It is possible that *IC5*, for example, already has high transcript levels before deciliation and therefore does not require an increase after the deciliation. Additionally, we only examine a single time point after deciliation. The timing of expression regulation may vary among genes. We have used the standard curve method to compare the expression levels of the two *LC4* genes. In nonreciliating cells, the cDNA contained 219 zmol (zepto- $= 10^{-21}$) of *LC4A* and 42.5 zmol of *LC4B*. Thus, *LC4A* is expressed approximately fivefold more than *LC4B* in vegetatively growing cells. Interestingly, in reciliating cells, *LC4B* expression increases approximately fourfold more than that of *LC4A*.

C. Gene Disruption

1. Rationale

After finding and characterizing the gene of interest, we can begin to understand the function of the gene product in *Tetrahymena*. Usually, our strategy is to disrupt the targeted gene by deleting the coding region of the gene and inserting in its place a selectable marker. Targeted replacement can also be used to truncate, epitope-tag, and overexpress genes using the inducible metallothionein promoter (Shang *et al*., 2002). The modification of macronuclear genes is straightforward and is the strategy typically pursued by our undergraduates.

2. Methods and Materials

a. Building the Disruption Construct. A gene of interest can be specifically targeted for disruption in *Tetrahymena* by homologous recombination. Disruption constructs are built by adding chromosomal sequences taken from either side of the targeted gene to flank a drug-resistance cassette. Three plasmids serve as the starting point in building the disruption constructs. Each plasmid includes a drug-resistance cassette with multicloning sites on either side. We use the *neo2* (neomycin-resistance) and *bsr1* (blasticidin-resistance) cassettes for macronuclear knockdowns and *neo3* for micronuclear knockouts (the plasmids were gifts from Dr. Marty Gorovsky, University of Rochester, Rochester, NY, and Dr. Jacek Gaertig, University of Georgia, Athens, GA).

For many genes, we delete the entire coding region. However, if the gene is significantly longer than 2 kb, we create a partial deletion because we have found that larger deletions often result in inefficient transformation. In the case of partial

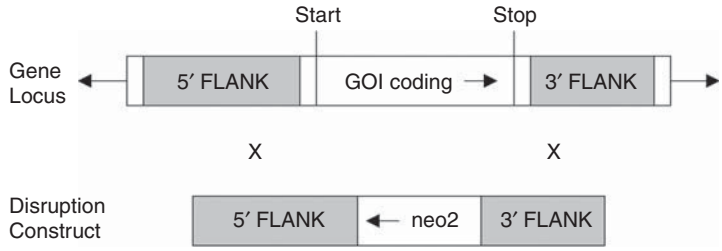

Fig. 5 Gene disruption strategy. The disruption construct (lower drawing) is built with a drug-resistance cassette (e.g., *neo2*) flanked by sequences (gray) identical to the chromosomal DNA sequences flanking the region to be deleted. After introduction of the construct into the nucleus, integration occurs by homologous recombination. In this example, the entire coding region of the gene of interest is deleted. Arrows indicate directions of transcription.

deletions we make sure to remove the start codon as well as a large portion of the coding region. Each of the drug-resistance cassettes has its own 5′ promoter and 3′ terminator sequences. The upstream and downstream flanks of the gene of interest are ligated sequentially into the plasmid such that they are oriented opposite of the direction of transcription of the resistance cassette (Fig. 5). The flanking regions allow for targeted integration by homologous recombination into the host chromosome. Chromosomal sequences between the two flanks are deleted. We have found that recombination is efficient if the large flank is >1000 bp and the small flank is >500 bp.

b. Transformation. We use biolistic bombardment to create our transformants. Excellent protocols for macronuclear and micronuclear transformations of *Tetrahymena* can be found in Bruns and Cassidy-Hanley (2000) and Hai *et al*. (2000). For the simultaneous knockdown of two genes in the same cell we build one knockdown construct with *neo2* and one with *bsr1*. Cells are then transformed sequentially.

c. Verification of Targeted Replacement. Once drug-resistant cell lines have been obtained, proper integration of the disruption cassette must be verified. We design PCR experiments to confirm proper integration of the drug-resistance gene. Genomic DNA is isolated from the putative knockdown cell line by the method of Gaertig *et al*. (1994). PCR primers are then designed with one in *neo2* and one within the chromosome outside of either the 5′ or 3′ flank. PCR products of the expected sizes verify that the *neo2* cassette is inserted in the correct locus.

In addition to determining the intended integration, the degree of gene replacement can be examined for knockdown cell lines. The *Tetrahymena* macronucleus contains ~45 copies of each gene. Transformants initially have only a few of the wild-type copies replaced. Because the macronucleus undergoes amitotic division, increases in the concentration of the selection drug result in phenotypic assortment in which the

ratio of disrupted copies to wild-type copies increases. To estimate the extent of gene replacement we use a PCR-based test. In this assay, PCR primers are designed to anneal to both regions flanking the deleted portion of the gene. Because these regions are not deleted in the disruption, PCR products should be obtained from both the wild type and disrupted versions of the gene. As long as the deleted region is not the same size as the resistance cassette, the PCR products will be of different sizes. The ratio of the two products can be estimated by comparing the brightness of the two bands and adjusting for their sizes.

3. Results

Undergraduates in our lab have successfully produced several cell lines with knockdowns of dynein LC genes (Table I). The *LC1* and *LC10* knockdowns have been verified for their integration but have not been characterized further. Single knockdowns of *LC4A* and *LC4B* and a double knockdown of both *LC4A* and *LC4B* have been created and verified. The single *LC4A* and *LC4B* knockdowns have approximately 70 and 60% of the gene copies disrupted, respectively. The double knockdown of *LC4A* and *LC4B* has about 80 and 50% of the copies disrupted, respectively.

D. Phenotypic Characterization

1. Rationale

Most of the dynein small subunits are predicted to be part of the axoneme. Therefore, we use a variety of assays that examine ciliary function. Each of these methods is accessible to undergraduate students. *Tetrahymena* cells use rotokinesis to effect cell division, and motility defects inhibit the rate of growth of a culture (Brown *et al*., 1999a,b, 2003; Williams *et al*., 2006). To quantify ciliary function, we determine swimming speed and the swimming linearity of individual cells. The function of oral cilia can be examined with a simple test in which cells are incubated with fluorescent beads. We use immunofluorescence microscopy to measure the lengths and density of cilia on a cell. When analyzing knockdown cell lines, we maintain the cultures at a specific concentration of selection drug. To control for nonspecific effects of the selection drug, dynein transformants are compared to drug-resistant control cell lines whose ciliary phenotypes are not affected by the mutation. The control lines are a histone H1:*neo2* disruption (Shen *et al*., 1995) and a β-tubulin1:*bsr1* disruption (Xia *et al*., 2000).

2. Methods and Materials

a. Cell Division. The culture of cells begins with a single cell. We isolate single cells by removing 1 μl from a diluted culture, examining the drop in a 24-well plate at low magnification so that the entire drop is in the field of view, and determining the number of cells present. Depending on the number of cells in the drop, the original culture is either diluted or concentrated by brief centrifugation. When a drop with one

cell is obtained, 1 ml of modified Neffs medium is added to the well. For each cell type, triplicate cultures are analyzed by measuring the cell density at least once per day. Cells are fixed with formaldehyde (1% final concentration) and counted using a hemacytometer. After 6 days, a single cell from each of the initial cultures is picked and placed in fresh media and a second round of cell growth measurements is determined. After 6 days, single cells are again picked and a third round of cell densities is determined. The generation times of the different cell types are calculated from the initial slopes of their growth curves.

b. Cell Motility. Stock cultures of transformants and control cells are grown to about 5×10^4 cells/ml. Cells are then further diluted in modified Neffs medium so that the microscope field contains only a few cells. We use dark-field microscopy with a 2.5X objective and obtain time-lapsed images over either 3 s or 6 s using a CCD camera. A micrometer scale is also photographed and the lengths of the tracks are measured from the digital images. The swimming path linearity coefficient is defined as the ratio of the shortest distance from the starting point to the end point divided by the actual path length swum by the cell (perfect linearity = 1.00). P values are determined by unpaired one-tailed t-tests. A dark-field image of swimming cells is shown in Fig. 6.

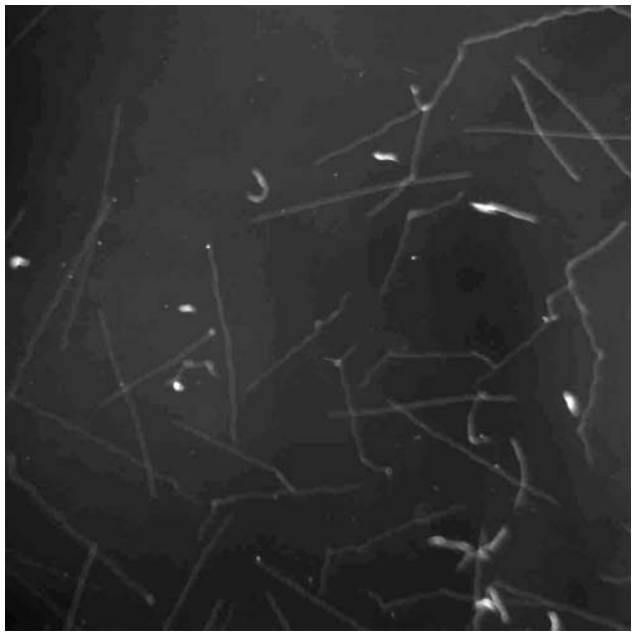

Fig. 6 *Tetrahymena* swimming assay. Time-lapsed images of cells photographed with dark-field microscopy and a 3 s exposure. Wild-type cells are shown in this example. Path lengths are measured using ImageJ software.

c. Phagocytosis. Freshly seeded cultures of cells at ~1.2×10^5 cells/ml are used. Red fluorescent latex beads of 2 μm diameter (Sigma-Aldrich) are added to cultures and the cells incubated at 30°C with gentle shaking at 100 rpm. At 1.5 and 24 h, the cells are washed three times in 10 mM Tris (pH 7.5) and then fixed with 2% paraformaldehyde, 0.4% Triton X-100 in 1X PHEM buffer (60 mM PIPES, 25 mM HEPES, 10 mM EGTA, 2 mM $MgCl_2$, pH 6.9). The percentage of cells that contain beads is determined by viewing the cells using epi-illumination fluorescence microscopy and brightfield microscopy ($N = 100$). Because the beads sometimes adhere to the surface of the cells, we count as active phagocytosis cells with >5 beads.

d. Cilia Density and Length. Cells are grown to approximately 5×10^4 cells/ml, washed once in 1X PHEM buffer and fixed with 2% paraformaldehyde, 0.4% Triton X-100 in 1X PHEM buffer. Cells are stained with mAb 1-6.1, an antibody specific for acetylated α-tubulin (Asai *et al*., 1982), at 1:50 dilution in 0.1% bovine serum albumin in phosphate-buffered saline. Rhodamine-conjugated goat anti-mouse IgG is used as the secondary antibody (Kirkegaard and Perry Laboratories, Gaithersburg, MD). The stained cells are examined by confocal fluorescence microscopy, using a Zeiss LSM510 system. An image of the widest optical section (i.e., its "equator") of each cell is captured and the ciliary densities and lengths are determined using the LSM510 software. At least 25 cells for each of the cell lines are evaluated. The density of cilia is defined as the number of measurable cilia per micrometer of the cell circumference. *P* values are determined by unpaired, one-tailed *t*-tests.

e. Ciliary Reversal. Depolarization-induced backward swimming is examined after the method of Hennessey *et al*. (2002). Cells are grown to 4×10^5 cells/ml, washed with control solution (10 mM Tris, 0.5 mM MOPS, 50 μM $CaCl_2$, pH 7.2), and resuspended in control solution. The increase in intraciliary Ca^{2+} is induced by depolarizing the cells with the addition of KCl to a final concentration of 30 mM. Cells are recorded at 30 frames/s with a CCD camera attached to a Nikon DIC microscope and MetaMorph software (Molecular Devices, Downingtown, PA). Images are typically recorded over a 5 min time span. At 30 s intervals cells are scored as swimming forward or backward, or immotile. An example of normal reversal and recovery is shown in Fig. 7.

3. Results

We have evaluated the ciliary phenotypes of several cell lines carrying disruptions of genes encoding dynein subunits as well as other proteins. The germline knockouts of dynein-2 heavy chain, *DYH2*, and dynein-2 LIC, *D2LIC*, resulted in a misregulation of ciliary lengths which caused the cells to swim poorly (Rajagopalan *et al*., 2009). The knockdown of *LC4A* but not *LC4B* resulted in cells that exhibited a pronounced delay in their recovery from depolarization-induced ciliary reversal, and epitope-tagged *LC4A* was detected to accumulate in the axoneme (Wilkes *et al*., 2007a). The knockdown of the retrograde complex A *IFT140* gene resulted in only a mild ciliary

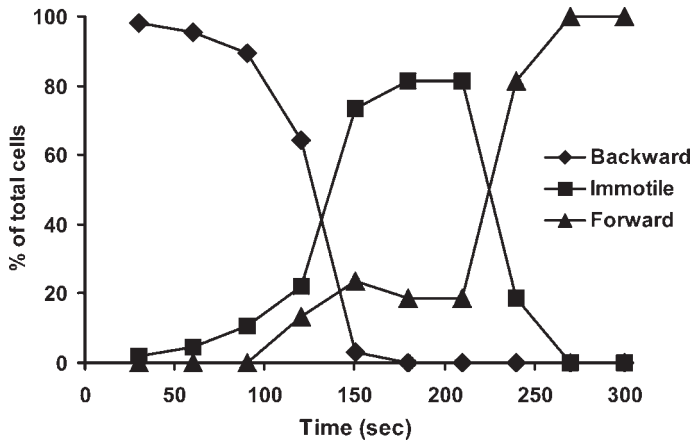

Fig. 7 Ciliary reversal assay. The swimming reversal behavior of wild-type cells is shown. After stimulation with 30 mM KCl, cells are scored at 30 s intervals as swimming forward, immotile, or swimming backward. After stimulation all of the cells swim backward and then they pause for a short time. After about 2 min, the cells recover and resume forward swimming. Diamonds, backward swimming; squares, immotile; triangles, forward swimming.

phenotype. And the double knockdown of two isoforms of the microtubule end-binding protein, *EB1A* and *EB1B*, resulted in a significant slowdown of cell growth and division (Sergeeva *et al*., 2008).

III. Discussion

Tetrahymena presents the opportunity to study the function of dynein subunit genes. The cells are easy to grow in the laboratory, any gene can be modified by targeted replacement, and the phenotypes of the resulting transformants can be measured with simple methods. *Tetrahymena* also has limitations, including the following two. One limitation is that *Tetrahymena* lags behind other model organisms in the discovery of new dynein subunits, and so our approach currently depends on having sequences of orthologs from other organisms. The second limitation is the need to carefully interpret knockdown phenotypes. Sometimes, there is a lack of noticeable effect of the gene knockdown because of the remaining wild-type copies of the gene. More commonly, there is a noticeable effect when the culture is viewed as a whole (e.g., growth curves). Because a culture of cells with macronuclear knockdowns is likely not homogeneous in terms of the extent of gene replacement, it is often challenging to directly correlate the phenotype and genotype of a single cell in the culture. If the gene is not essential for viability, the complete replacement of a gene can be achieved through phenotypic assortment or the production of knockout heterokaryons, but these methods require

significantly more time, effort, and luck, and are more difficult for busy undergraduates to achieve. As an alternative, we have successfully employed RNAi (Howard-Till and Yao, 2006) to suppress gene expression of the cytoplasmic dynein LICs.

An important objective of our studies is that they involve undergraduate students in meaningful, hypothesis-driven experiments. The procedures summarized here enable students to undertake shorter term (e.g., one semester) experiments as well as leading a longer term (e.g., summer or senior thesis) project. This flexibility is especially important with undergraduates whose schedules and class loads vary from semester to semester. The protocol is also flexible in terms of the types of experiments available to the students, with experimental strategies varying from gene annotation and molecular biology to cell biology and microscopy.

Acknowledgments

Our laboratory is supported by grants from the National Science Foundation. Several students were provided summer research stipends from grants awarded to Harvey Mudd College from the Howard Hughes Medical Institute and AAAS-Merck.

References

Altschul, S.F., Madden, T.L., Schaffer, A.A., Zhang, J., Zhang, Z., Miller, W., and Lipman, D.J. (1997). Gapped BLAST and PSI-BLAST: A new generation of protein database search programs.*Nucleic Acids Res*. **25**, 3389–3402.

Asai, D.J., and Brokaw, C.J. (1993). Dynein heavy chain isoforms and axonemal motility. *Trends Cell Biol*. **3**, 398–402.

Asai, D.J., and Forney, J.D. (2000). *Tetrahymena thermophila*. "Methods in Cell Biology." Vol. 62. Academic Press, San Diego, CA.

Asai, D.J., Brokaw, C.J., Thompson, W.C., and Wilson, L. (1982). Two different monoclonal antibodies to alpha-tubulin inhibit the bending of reactivated sea urchin spermatozoa. *Cell Motil*. **2**, 599–614.

Brown, J.M., Fin, N.A., Pandiyan, G., Thazhath, R., and Gaertig, J. (2003). Hypoxia regulates assembly of cilia in suppressors of *Tetrahymena* lacking an intraflagellar transport subunit gene. *Mol. Biol. Cell* **14**, 3192–3207.

Brown, J.M., Hardin, C., and Gaertig, J. (1999a). Rotokinesis, a novel phenomenon of cell locomotion-assisted cytokinesis in the ciliate *Tetrahymena thermophila*. *Cell Biol. Int.* **23**, 841–848.

Brown, J.M., Marsala, C., Kosoy, R., and Gaertig, J. (1999b). Kinesin-II is preferentially targeted to assembling cilia and is required for ciliogenesis and normal cytokinesis in *Tetrahymena*. *Mol. Biol. Cell* **10**, 3081–3096.

Bruns, P.J., and Cassidy-Hanley, D. (2000). Biolistic transformation of macro- and micronuclei. *Methods Cell Biol*. **62**, 501–512.

Burgess, S.A., Walker, M.L., Sakakibara, H., Knight, P.J., and Oiwa, K. (2003). Dynein structure and power stroke. *Nature* **421**, 715–718.

Burkhardt, J.K., Echeverri, C.J., Nilsson, T., and Vallee, R.B. (1997). Overexpression of the dynamitin (p50) subunit of the dynactin complex disrupts dynein-dependent maintenance of membrane organelle distribution. *J. Cell Biol*. **139**, 469–484.

Calzone, F.J., and Gorovsky, M.A. (1982). Cilia regeneration in *Tetrahymena*. A simple reproducible method for producing large numbers of regenerating cells. *Exp. Cell Res*. **140**, 471–476.

Chalker, D.L., Ward, J.G., Randolph, C., and Yao, M.-C. (2000). Microinjection of *Tetrahymena thermophila*. *Methods Cell Biol.* **62**, 469–484.

Chirgwin, J.M., Przybyla, A.E., MacDonald, R.J., and Rutter, W.J. (1979). Isolation of biologically active ribonucleic acid from sources enriched in ribonuclease. *Biochemistry* **18**, 5294–5299.

Echeverri, C.J., Paschal, B.M., Vaughan, K.T., and Vallee, R.B. (1996). Molecular characterization of the 50-kD subunit of dynactin reveals function for the complex in chromosome alignment and spindle organization during mitosis. *J. Cell Biol*. **132**, 617–633.

Eck, R.V., and Dayhoff, M.O. (1966). "Atlas of Protein Sequence and Structure." National Biomedical Research Foundation, Silver Springs, MD.

Eisen, J.A., Coyne, R.S., Wu, M., Wu, D., Thiagarajan, M., Wortman, J.R., Badger, J.H., Ren, Q., Amedeo, P., Jones, K.M., Tallon, L.J., Delcher, A.L. et al., (2006). Macronuclear genome sequence of the ciliate *Tetrahymena thermophila*, a model eukaryote. *PLoS Biol.* **4**, e286.

Gaertig, J., and Kapler, G. (2000). Transient and stable DNA transformation of *Tetrahymena thermophila* by electroporation. *Methods Cell Biol*. **62**, 485–500.

Gaertig, J., Thatcher, T.H., Gu, L., and Gorovsky, M.A. (1994). Electroporation-mediated replacement of a positively and negatively selectable beta-tubulin gene in *Tetrahymena thermophila*. *Proc. Natl. Acad. Sci. USA* **91**, 4549–4553.

Gibbons, B.H., Asai, D.J., Tang, W.J.Y., Hays, T.S., and Gibbons, I.R. (1994). Phylogeny and expression of axonemal and cytoplasmic dynein genes in sea urchins. *Mol. Biol. Cell* **5**, 57–70.

Gibbons, I.R., and Rowe, A.J. (1965). Dynein: A protein with adenosine triphosphatase activity from cilia. *Science* **149**, 424–426.

Hai, B., Gaertig, J., and Gorovsky, M.A. (2000). Knockout heterokaryons enable facile mutagenic analysis of essential genes in *Tetrahymena*. *Methods Cell Biol*. **62**, 513–531.

Harada, A., Takei, Y., Kanai, Y., Nonaka, S., and Hirokawa, N. (1998). Golgi vesiculation and lysosome dispersion in cells lacking cytoplasmic dynein. *J. Cell Biol.* **141**, 51–59.

Hennessey, T.M., Kim, D.Y., Oberski, D.J., Hard, R., Rankin, S.A., and Pennock, D.G. (2002). Inner arm dynein 1 is essential for Ca++-dependent ciliary reversals in *Tetrahymena thermophila*. *Cell Motil. Cytoskeleton* **53**, 281–288.

Hirokawa, N., Sato-Yoshitake, R., Yoshida, T., and Kawashima, T. (1990). Brain dynein (MAP1C) localizes on both anterogradely and retrogradely transported membranous organelles *in vivo*. *J. Cell Biol.* **111**, 1027–1037.

Howard-Till, R.A., and Yao, M.-C. (2006). Induction of gene silencing by hairpin RNA expression in *Tetrahymena thermophila* reveals a second small RNA pathway. *Mol. Cell Biol*. **26**, 8731–8742.

Karrer, K.M. (2000). *Tetrahymena* genetics: Two nuclei are better than one. *Methods Cell Biol*. **62**, 127–186.

Kon, T., Imamula, K., Roberts, A.J., Ohkura, R., Knight, P.J., Gibbons, I.R., Burgess, S.A., and Sutoh, K. (2009). Helix sliding in the stalk coiled coil of dynein couples ATPase and microtubule binding. *Nature Struct. Mol. Biol.* **16**, 325–333.

Kumar, S., Tamura, K., Jakobsen, I.B., and Nei, M. (2001). "*MEGA2*: Molecular Evolutionary Genetics Analysis Software." Arizona State University, Tempe, AZ.

Lee, S.W., Wisniewski, J.C., Dentler, W.L., and Asai, D.J. (1999). Gene knockouts reveal separate functions for two cytoplasmic dyneins in *Tetrahymena thermophila*. *Mol. Biol. Cell* **10**, 771–784.

Lefebvre, P.A., Silflow, C.D., Wieben, E.D., and Rosenbaum, J. (1980). Increased levels of mRNAs for tubulin and other flagellar proteins after amputation or shortening of *Chlamydomonas* flagella. *Cell* **20**, 469–477.

Lincoln, L.M., Gibson, T.M., Lee, S.W., Forney, J.D., and Asai, D.J. (1998). The characterization and targeted disruption of the dynein beta heavy chain in *Tetrahymena thermophila*. *Mol. Biol. Cell* **9**(S), 899.

Luck, D.J.L. (1984). Genetic and biochemical dissection of the eucaryotic flagellum. *J. Cell Biol.* **98**, 789–794.

Ma, S., Trivinos-Lagos, L., Graf, R., and Chisholm, R.L. (1999). Dynein intermediate chain mediated dynein-dynactin interaction is required for interphase microtubule organization and centrosome replication and separation in *Dictyostelium*. *J. Cell Biol*. **147**, 1261–1274.

Nicastro, D., Schwartz, C., Pierson, J., Gaudette, R., Porter, M.E., and McIntosh, J.R. (2006). The molecular architecture of axonemes revealed by cryoelectron tomography. *Science* **313**, 944–948.

Ogawa, K., Kamiya, R., Wilkerson, C.G., and Witman, G.B. (1995). Interspecies conservation of outer arm dynein intermediate chain sequences defines two intermediate chain subclasses. *Mol. Biol. Cell* **6**, 685–696.

Patel-King, R.S., Benashski, S.E., Harrison, A., and King, S.M. (1996). Two functional thioredoxins containing redox-sensitive vicinal dithiols from the *Chlamydomonas* outer dynein arm. *J. Biol. Chem*. **271**, 6283–6291.

Pazour, G.J., Dickert, B.L., and Witman, G.B. (1999). The DHC1b (DHC2) isoform of cytoplasmic dynein is required for flagellar assembly. *J. Cell Biol*. **144**, 473–481.

Pfaffl, M.W. (2001). A new mathematical model for relative quantification in real-time RT-PCR. *Nucleic Acids Res*. **29**, e45.

Pfister, K.K., Shah, P.R., Hummerich, H., Russ, A., Cotton, J., Annuar, A.A., King, S.M., and Fisher, E.M.C. (2006). Genetic analysis of the cytoplasmic dynein subunit families. *PLoS Genet.* **2**, e1.

Piperno, G., and Ramanis, Z. (1991). The proximal portion of *Chlamydomonas* flagella contains a distinct set of inner dynein arms. *J. Cell Biol*. **112**, 701–709.

Porter, M.E. (1996). Axonemal dyneins: Assembly, organization, and regulation. *Curr. Opin*. *Cell Biol*. **8**, 10–17.

Porter, M.E., Bower, R., Knott, J.A., Byrd, P., and Dentler, W. (1999). Cytoplasmic dynein heavy chain 1b is required for flagellar assembly in *Chlamydomonas*. *Mol. Biol. Cell* **10**, 693–712.

Rajagopalan, V., Subramanian, A., Wilkes, D.E., Pennock, D.G., and Asai, D.J. (2009). Dynein-2 affects the regulation of ciliary length but is not required for ciliogenesis in *Tetrahymena thermophila*. *Mol. Biol. Cell* **20**, 708–720.

Randall, J., Warr, J.R., Hopkins, J.M., and McVittie, A. (1964). A single gene mutation of *Chlamydomonas reinhardii* affecting motility: A genetic and electron microscope study. *Nature* **203**, 912–914.

Roberts, A.J., Numata, N., Walker, M.L., Kato, Y.S., Malkova, B., Kon, T., Ohkura, R., Arisaka, F., Knight, P.J., Sutoh, K., and Burgess, S.A. (2009). AAA+ ring and linker swing mechanism in the dynein motor. *Cell* **136**, 485–495.

Sakato, M., and King, S.M. (2004). Design and regulation of the AAA+ microtubule motor dynein. *J. Struct. Biol.* **146**, 58–71.

Saitou, N., and Nei, M. (1987). The neighbor-joining method: A new method for reconstructing phylogenetic trees. *Mol. Biol. Evol*. **4**, 406–425.

Schloss, J.A., Silflow, C.D., and Rosenbaum, J.L. (1984). mRNA abundance changes during flagellar regeneration in *Chlamydomonas reinhardtii*. *Mol. Biol. Cell* **4**, 424–434.

Schnapp, B.J., and Reese, T.S. (1989). Dynein is the motor for retrograde axonal transport of organelles. *Proc. Natl. Acad. Sci. USA* **86**, 1548–1552.

Sergeeva, O.A., Wilkes, D.E., and Asai, D.J. (2008). Multiple isoforms of EB1 in *Tetrahymena thermophila*. *Mol. Biol. Cell* **19**(S), 280.

Shang, Y., Song, X., Bowen, J., Corstanje, R., Gao, Y., Gaertig, J., and Gorovsky, M.A. (2002). A robust inducible-repressible promoter greatly facilitates gene knockouts, conditional expression, and overexpression of homologous and heterologous genes in *Tetrahymena thermophila*. *Proc. Natl. Acad. Sci. USA* **99**, 3734–3739.

Shen, X., Yu, L., Weir, J.W., and Gorovsky, M.A. (1995). Linker histones are not essential and affect chromatin condensation *in vivo*. *Cell* **82**, 47–56.

Signor, D., Wedaman, K.P., Orozco, J.T., Dwyer, N.D., Bargmann, C.I., Rose, L.S., and Scholey, J.M. (1999). Role of a class DHC1b dynein in retrograde transport of IFT motors and IFT raft particles along cilia, but not dendrites, in chemosensory neurons of living *Caenorhabditis elegans*. *J. Cell Biol*. **147**, 519–530.

Soares, H., Galego, L., Cóias, R., and Rodrigues-Pousada, C. (1993). The mechanisms of tubulin messenger regulation during *Tetrahymena pyriformis* reciliation. *J. Biol. Chem*. **268**, 16623–16630.

Sokal, R.R., and Michener, C.D. (1958). A statistical method for evaluating systematic relationships. *Univ. KS Sci. Bull*. **28**, 1409–1438.

Vale, R.D. (2003). The molecular motor toolbox for intracellular transport. *Cell* **112**, 467–480.

Wicks, S.R., de Vries, C.J., van Luenen, H.G.A.M, and Plasterk, R.H.A. (2000). CHE-3, a cytosolic dynein heavy chain, is required for sensory cilia structure and function in *Caenorhabditis elegans*. *Dev. Biol*. **221**, 295–307.

Wilkes, D.E., Heyer, E., Hubenschmidt, M., Kuhn, H., Wiedeman, A., Rajagopalan, V., and Asai, D.J. (2007a) Dynein light chain 4 (LC4) regulates the recovery from ciliary reversal in *Tetrahymena thermophila*. *Mol. Biol. Cell* **18**(S), 490.

Wilkes, D.E., Rajagopalan, V., Chan, C.W., Kniazeva, E., Wiedeman, A.E., and Asai, D.J. (2007b). Dynein light chain family in *Tetrahymena thermophila*. *Cell Motil. Cytoskeleton* **64**, 82–96.

Wilkes, D.E., Watson, H.E., Mitchell, D.R., and Asai, D.J. (2008). Twenty-five dyneins in *Tetrahymena*: A re-examination of the multidynein hypothesis. *Cell Motil. Cytoskeleton* **65**, 342–351.

Williams, N.E., Tsao, C.C., Bowen, J., Hehman, G.L., Williams, R.J., and Frankel, J. (2006). The actin gene ACT1 is required for phagocytosis, motility, and cell separation of *Tetrahymena thermophila. Eukaryot*. *Cell* **5**, 555–567.

Xia, L., Hai, B., Gao, Y., Burnette, D., Thazhath, R., Duan, J., Bré, M.H., Levilliers, N., Gorovsky, M.A., and Gaertig, J. (2000). Polyglycylation of tubulin is essential and affects cell motility and division in *Tetrahymena thermophila*. *J. Cell Biol*. **149**, 1097–1106.

CHAPTER 3

Purification of Axonemal Dyneins and Dynein-Associated Components from *Chlamydomonas*

Stephen M. King

Department of Molecular, Microbial and Structural Biology, University of Connecticut Health Center, 263 Farmington Avenue, Farmington, Connecticut 06030-3305

Abstract

Axonemal dyneins are responsible for generating the force required to power ciliary and flagellar motility. These highly complex enzymes form the inner and outer arms associated with the outer doublet microtubules. They are built around one or more ~520 kD heavy chains that exhibit motor activity and also include additional components that are required for assembly within the axonemal superstructure and/or regulation of motor function in response to a broad range of signaling inputs. The

METHODS IN CELL BIOLOGY, VOL. 92

978-0-12-374974-1
DOI: 10.1016/S0091-679X(08)92003-3

dyneins from flagella of *Chlamydomonas* have been extensively studied as this organism is amenable to genetic, biochemical, and physiological approaches. In this chapter, I describe methods that have been devised by a number of laboratories to extract and purify individual dyneins from *Chlamydomonas*. When combined with the wide range of available mutants, these methods allow for the analysis of dyneins lacking individual components or motor units.

I. Introduction

Axonemal dyneins are permanently associated with the A-tubule of the outer doublet microtubules of the ciliary/flagellar axoneme. These motors interact in an ATP-dependent manner with the B-tubule of the adjacent doublet to generate the sliding force that is ultimately responsible for powering ciliary/flagellar beating. In order to generate a functional ciliary/flagellar bend, dynein function must be precisely controlled. A wide variety of regulatory signals are known or predicted to exist, including responses to cAMP, Ca^{2+}, redox poise, and phosphorylation, as well as signals that derive from the dynein regulatory complex and the radial spoke/central pair microtubule complex (Bessen *et al*., 1980; Hasegawa *et al*., 1987; Hyams and Borisy, 1978; Piperno *et al*., 1992; Smith and Yang, 2004; Wakabayashi and King, 2006). Furthermore, both theoretical models [discussed in Brokaw (2009)] and mechanical activation experiments, for example, Hayashibe *et al*. (1997), suggest that mechanisms exist to detect alterations in flagellar curvature allowing for the propagation of waves of activity along the length of the organelle. There is also evidence that certain axonemal dyneins are necessary for motility under specific solution conditions such as increases in viscosity (Yagi *et al*., 2005). The complexity of the axonemal dynein system in large part appears to reflect the requirement for responding to this myriad of cues.

The flagellum of the biflagellate green alga *Chlamydomonas* has proven to be a highly useful model system in which to study axonemal dyneins. This has been due to several factors including the ease of genetic manipulation which has lead to the generation of many mutants that are defective in dynein and other axonemal components, and the existence of assays to assess various motility parameters. In addition, it is simple to grow large quantities of cells and to readily detach the flagella from the cell bodies. Thus, biochemically tractable quantities of dyneins and other components can be obtained.

Currently, it is thought that the *Chlamydomonas* flagellar axoneme contains 15 different dynein heavy chains (HCs) that comprise three distinct groupings of motors [see Table I and King and Kamiya (2008) for recent in-depth review]. These are arranged in a 96-nm axonemal repeat that contains four outer arms, one copy of inner arm I1/f, and two additional inner arms that vary depending on the location within the axoneme. The outer arm consists of 3 HCs associated with 2 WD-repeat intermediate chains (ICs) and at least 11 distinct light chains (LCs); LCs 1, 3, 4, and 5 interact directly with the HCs, whereas the others associate with IC1 and/or IC2. *In situ*, this motor also interacts with a trimeric docking complex (DC)

Table I
Composition of *Chlamydomonas* Axonemal Inner and Outer Arm Dyneins

Dynein[a]	Heavy chains	Intermediate chains	Light chains	Additional components[b]
Outer arm	α	IC1	LC1	DC1
	β	IC2	LC2	DC2
	γ		LC3	DC3
			LC4	ODA5
			LC5	Lis1
			LC6	ODA7
			LC7a	
			LC7b	
			LC8	
			LC9	
			LC10	
Inner arm I1/f	1α (DHC1)	IC140	Tctex1	ODA7
	1β (DHC10)	IC138	Tctex2b	
		IC97	LC7a	
			LC7b	
			LC8	
Inner arms a, c, d	DHC6 (a)	none	Actin	p44 (d only)
	DHC9 (c)		p28	p38 (d only)
	DHC2 (d)			
Inner arms b, e, g	DHC5 (b)	none	Actin	
	DHC8 (e)		Centrin	
	DHC7 (g)			

[a] Inner arms containing DHC3, DHC4, and DHC11 have been identified but only obtained in very small amounts making their analysis difficult. In addition, a fourth apparently axonemal HC of unknown function is present in the genome and is expressed (see *Chlamydomonas* genome version 3; gene model 206178).

[b] Although these additional components associate with various dyneins, some (e.g., Lis1 and ODA5) do not copurify with the motors as the interactions are disrupted during extraction from the axoneme.

(Takada and Kamiya, 1994) and several other components [such as ODA5 (Wirschell *et al*., 2004)] that are all essential for assembly. There are also several components that have a more transient association with the outer arm, including ODA16 that is involved in dynein transport into the flagellum (Ahmed *et al*., 2008) and the lissencephaly protein Lis1 that interacts with the outer arm in a manner regulated by other axonemal substructures (Pedersen *et al*., 2007; Rompolas and King, 2008). The classic view has been that there is one type of outer dynein arm within the *Chlamydomonas* flagellum. However, given that cryoEM tomography has revealed a linker connecting every fourth outer arm to inner arm I1/f (Nicastro *et al*., 2006), there must be something distinct about one outer arm in every 96-nm axonemal repeat.

The inner dynein arm system may be divided into two groupings. Each 96-nm repeat contains one copy of inner arm I1/f which is built around two distinct HCs and has a composition related to that of the outer arms in that it contains two WD-repeat ICs and members of the Tctex1, Tctex2, LC7, and LC8 light chain families (Wirschell *et al*., 2007). The other inner arm dyneins (termed dyneins a, b, c, d, e, g) consist of

monomeric HCs that each associate with one actin molecule and either the Ca^{2+}-binding protein centrin (dyneins b, e, g) or a dimer of the essential LC-termed p28 (dyneins a, c, d) (see Table I) (Kagami and Kamiya, 1992).

In this chapter, I describe the various methods that have been devised to purify axonemal dyneins based on their physical and chemical properties. Each extraction/purification method has both advantages and disadvantages that become manifest as alterations in composition and/or assembly state of the motor. Thus, it is essential to carefully consider the ultimate goal of the experiment prior to deciding on a particular preparative methodology. In addition, I briefly review methods for detaching and isolating flagella; for additional details of these procedures and for culturing and harvesting large quantities of *Chlamydomonas*, the reader is referred to King (1995) and Witman (1986).

II. Detachment and Isolation of Flagella

There are two methods that are currently routinely employed to detach flagella from *Chlamydomonas* cell bodies. The first involves resuspending cells in ice-cold 10 mM Hepes, pH 7.4, 5 mM $MgSO_4$, 1 mM dithiothreitol (DTT), 4% (w/v) sucrose (HMDS) and then treating them with the anesthetic dibucaine (final concentration of 1 mM; diluted from a 25 mM stock solution in water) in the presence of a small amount (a few micromolar) of free Ca^{2+}. Note that buffers made using distilled water (unlike deionized water) usually contain sufficient contaminating Ca^{2+} that supplementation is not necessary. Dibucaine permeabilizes the flagellar membrane and the consequent inrush of Ca^{2+} activates the flagellar excision machinery. The other consequence of dibucaine treatment is that it leads directly to cell death so that this method cannot be used if flagellar regeneration is required. The second standard approach to deflagellation involves exposing the cells to a brief period of pH shock. Cells are concentrated to ~1/10 the original culture volume, placed in a beaker or other container with constant stirring, and the pH continually monitored. The medium pH is then rapidly dropped to ~pH 4.5 by addition of 0.5 M acetic acid. After approximately 20–30 s, the pH is then increased above pH 7 by addition of 1 M $NaHCO_3$. Although both approaches are highly effective, this latter method is to be preferred if subsequent flagellar regeneration is required.

Irrespective of which method is used for deflagellation, the resulting cell bodies are first pelleted by low-speed centrifugation. The flagella-containing supernatant is then layered on top of a 25% sucrose cushion made in HMD buffer and the sample centrifuged for 10–20 min at 1100 × *g* at 4°C. Any contaminating cell bodies will pellet through the sucrose cushion whereas flagella remain in the upper 4% sucrose layer and concentrate as a white broadband at the 4%/25% sucrose interface. These regions are collected using a pipette and the flagella harvested by centrifugation at 10,000 rpm using a Sorvall SS34 rotor. From this point on, all buffers should contain 1 mM phenylmethylsulfonyl fluoride (made as a 200 mM stock in methanol) or a more comprehensive protease inhibitor cocktail (e.g., P8849, Sigma Chemical Co., St Louis, MO).

III. Flagellar Demembranation

Purified flagella pellets are resuspended in 30 mM Hepes, pH 7.4, 5 mM $MgSO_4$, 1 mM DTT, 0.5 mM EDTA, 25 mM KCl (HMDEK) buffer that has been supplemented with detergent to a final concentration of 1% (v/v). Previous descriptions of this procedure recommended the use of Nonidet P-40. However, that formulation is no longer commercially available and we have found that Igepal CA-630 (Sigma Chemical Co., St Louis, MO) is an acceptable substitute (Fig. 1). Demembranated flagellar axonemes are harvested by centrifugation at 10,000 rpm using a Sorvall SS34 rotor.

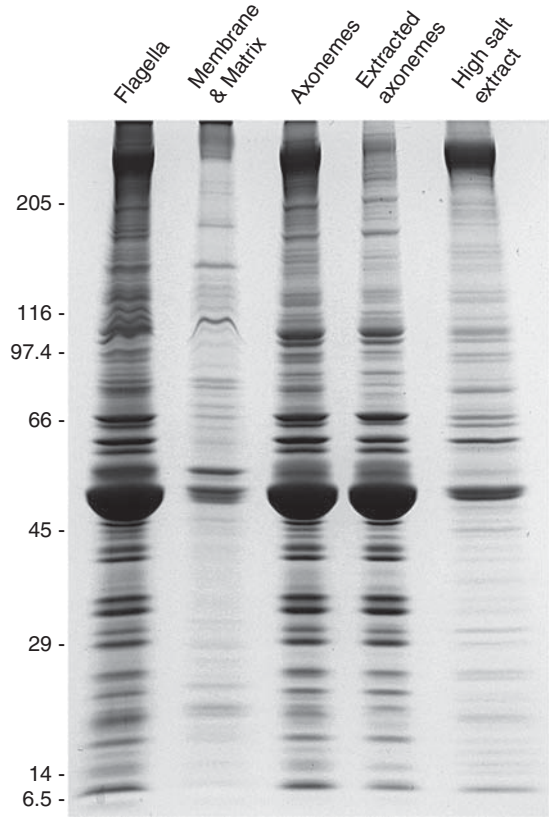

Fig. 1 Fractionation of *Chlamydomonas* flagella. Flagella were demembranated with Igepal CA-630 to solubilize the membrane and flagellar matrix. The resulting axonemes were subsequently treated with 0.6 M NaCl to extract dyneins and other components whose axonemal association is mediated through ionic interactions. Flagellar fractions (based on an initial ~150 μg of flagella) were separated in a 5–15% polyacrylamide SDS gel and stained with Coomassie blue. The position at which the M_r standards migrated is shown at left. Modified from Pedersen *et al*. (2007).

For large-scale dynein preparations, we routinely treat flagella with detergent twice to ensure that all membrane has been removed.

An alternative here is to break the flagellar membrane by three rounds of freeze–thaw in which the samples are frozen rapidly in dry ice and then warmed either on the bench or in a water bath. Although not routinely employed for axonemal dynein purifications, this method may be useful in attempting to stabilize associations (such as that between the outer arm and Lis1) that are disrupted during detergent treatment.

IV. Dynein Extraction from Flagellar Axonemes

The standard approach to removing dyneins from the axonemal superstructure has been to treat axonemes with high concentrations of salt. Most procedures have employed either 0.6 M NaCl or 0.6 M KCl in 30 mM Hepes or Tris-Cl, pH 7.5, 5 mM $MgSO_4$, 0.5–1 mM EDTA, 1 mM DTT, for example, DiBella *et al*. (2005) and Pfister *et al*. (1982) (Fig. 1). These salts appear equally effective at solubilizing the dynein arms. However, it is important to remember that if the subsequent purification step involves sedimentation through a 5–20% sucrose density gradient, it will be necessary to reduce the density of the 0.6 M KCl (but not NaCl) extract by dialysis into an appropriate buffer as otherwise the extract will sink when applied to the top of the gradient (and see later). A very useful addendum to this procedure was introduced by Nakamura *et al*. (1997) and involves pretreating the axonemes with 0.6 M CH_3COOK as this removes many salt-sensitive components that would otherwise contaminate the dynein-containing 0.6 M NaCl or KCl extracts.

Two alternative methods have been described that may be useful for certain experiments. One involves the treatment of axonemes with high levels (5 mM) of ATP. This results in release of an outer arm dynein particle containing all three HCs (Goodenough and Heuser, 1984); it is uncertain what other axonemal components are released using this method. The final extraction procedure that has been employed with success (initially in sea urchins) is dialysis of the axonemal sample against a buffer of very low ionic strength which leads to the disruption of hydrophobic interactions. A 24-h dialysis against 1 mM Tris-Cl, pH 8.0, 0.1 mM EDTA, 5 mM KCl, 0.1 mM DTT has been found to solubilize most dynein arms from *Chlamydomonas* axonemes (Freshour *et al*., 2007).

V. Fractionation of Flagellar Extracts

A. Sucrose Density Gradient Centrifugation

Dyneins containing a single HC sediment in sucrose density gradients at ~10–12 S whereas HC dimers are found at 18–20 S and the three-headed outer arm at ~23 S; the relationship between various outer arm species is shown in Fig. 2A. Consequently, this method provides a very reliable and easy approach by which to fractionate dynein-

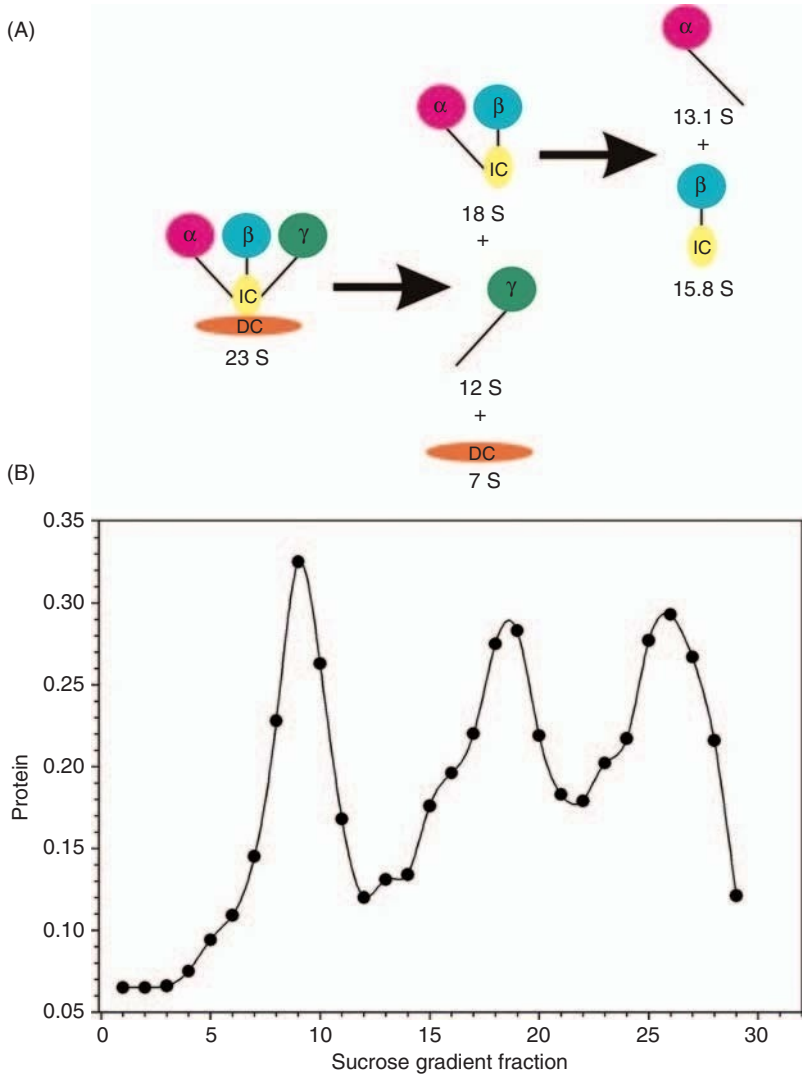

Fig. 2 Outer arm dynein subspecies and sucrose density gradient profile of axonemal salt extracts. (A) Diagram illustrating the relationship between intact outer arm dynein and various subparticles and their S values determined from sucrose gradient centrifugation. (B) Protein profile of an axonemal high salt extract sedimented in a 5–20% sucrose density gradient under conditions that cause the outer αβ and γ heavy chain subunits to dissociate. The bottom of the gradient is at *left*. (See Plate no. 1 in the Color Plate Section.)

containing extracts and obtain either the intact particles or various subparticles. However, there are a number of parameters that must be considered in order to obtain the desired particle; notably, rotor diameter, centrifugation speed, tube size, and buffer composition. This is most dramatically evidenced by the outer dynein arm, as the

oligomeric state of this motor is altered by changes in the imposed hydrostatic pressure and by the presence/absence of Mg^{2+}. These parameters have not been reported to affect the oligomeric state or composition of either the inner arm I1/f or the monomeric inner arm dyneins.

The basic method employs a ~12.5 ml 5–20% sucrose gradient made in 30 mM Tris-Cl, pH 7.5, 0.5 mM EDTA, 1 mM DTT, 25 mM KCl buffer upon which ~0.5 ml of the salt extract is layered (Pfister *et al*., 1982). Note that if 0.6 M KCl is used, the extract must first be dialyzed to reduce the salt concentration otherwise it will sink into the upper region of the sucrose gradient; this step is not necessary if NaCl is utilized instead. The sample is then subjected to ultracentrifugation in a SW-41 rotor at 36,000 rpm for ~13.5 h at 4°C (total angular momentum $\omega^2 t = 6.4 \times 10^{11}$ rad^2/s). A typical protein profile of a fractionated wild-type extract is shown in Fig. 2B. Three major peaks of protein are obtained: these contain (1) the αβ HC dimer subunit from the outer arm and inner arm I1/f, (2) the outer arm γ HC subunit and monomeric inner dynein arms, and (3) other salt-extracted axonemal proteins including the outer arm DC, Lis1 and ODA5; this third peak also contains considerable amounts of tubulin.

Several useful modifications to this basic procedure have been introduced. In the first, the amount of nondynein axonemal proteins present in the high salt extract can be dramatically reduced by employing a pretreatment with 0.6 M K acetate. This step disrupts many salt-sensitive interactions within the axoneme but does not solubilize dyneins. Consequently, fractionation of the subsequent NaCl extracts yields dyneins that are significantly less contaminated (Nakamura *et al*., 1997).

A second advance came with the realization that an outer arm dynein particle containing all the HCs and the associated DC can be obtained by adding Mg^{2+} to the buffer in combination with a reduction in hydrostatic pressure (Takada *et al*., 1992); this is achieved simply by using a smaller tube; we routinely employ an SW55Ti rotor which holds ~5 ml tubes. Dyneins are well separated in this system by ultracentrifugation for ~10 h at 30,000 rpm at 4°C (Fig. 3). If necessary, outer arm dynein components obtained by sucrose density gradient centrifugation can be further purified by additional chromatographic steps (see below). Utilization of various mutants that lack entire dyneins, individual components or HC motor domains can be used to great advantage to prepare specific dynein particles that are not contaminated by copurifying proteins and/or dyneins that contain any desired subset of motor units. A list of mutants that may be useful here is given in Table II.

In order to dissociate the ~20 S particle containing the outer arm α and β HCs and IC/LC complex, the purified sample is dialyzed extensively against a buffer of very low ionic strength (5 mM Tris-Cl, pH 8.3, 0.2 mM EDTA, 0.1% (v/v) 2-mercaptoethanol). Subsequent sedimentation of the dialysate through a 5–20% sucrose gradient made in 5 mM Tris-Cl, pH 8.3, 0.2 mM EDTA, 1 mM DTT (~12.5 h, Beckman SW-41 rotor at $160{,}000 \times g$) results in two overlapping peaks. One sediments at 13.1 S and contains the α HC with LC5, whereas the second consisting of the β HC associated with the IC/LC complex is found at 15.8 S (Pfister and Witman, 1984). As both peak fractions are contaminated by minor amounts of the other HC, it is then necessary to exchange the proteins into a buffer of higher ionic strength such as 10

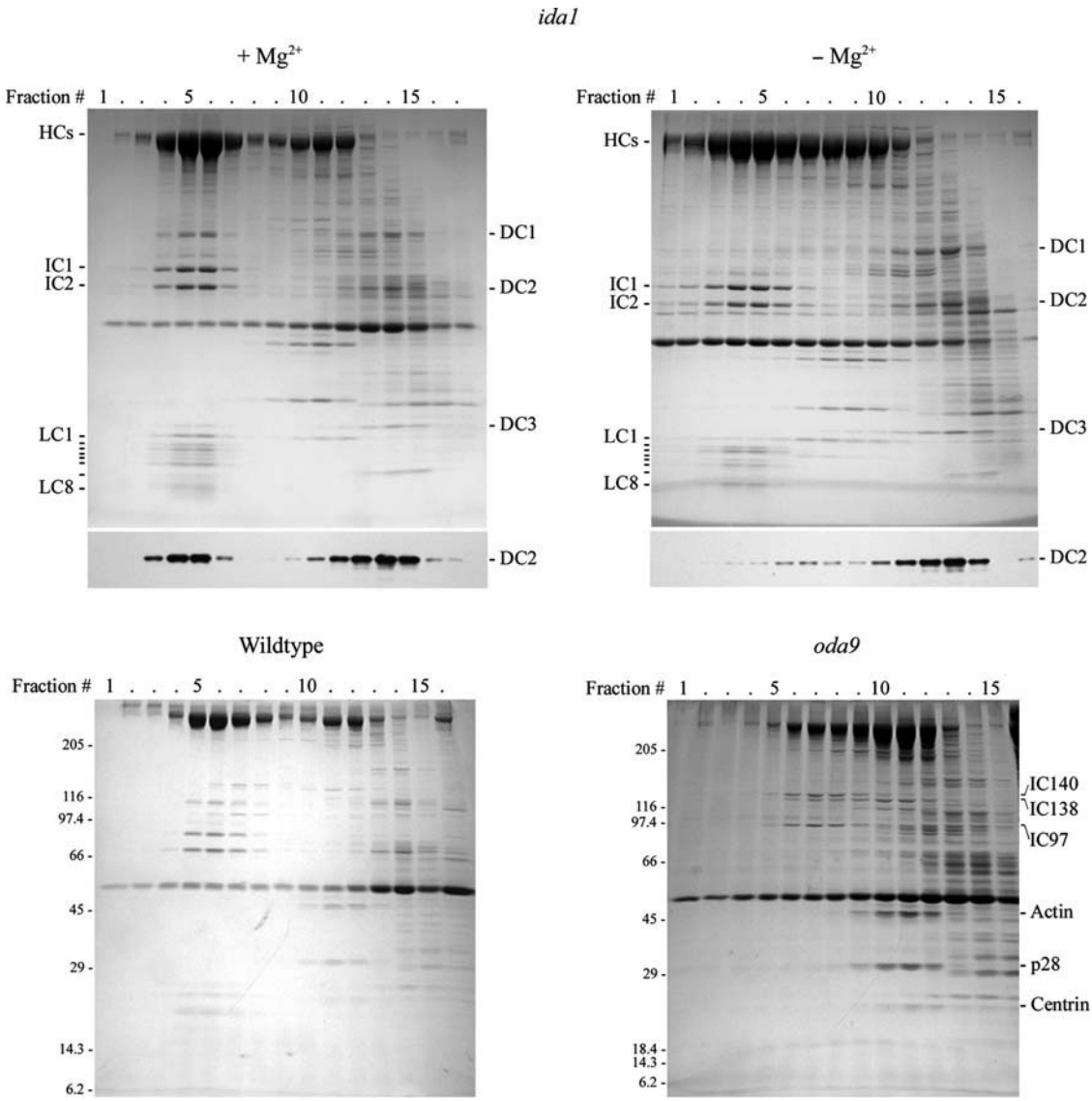

Fig. 3 Sucrose gradient purification of outer arm dynein and associated docking complex (DC). In the upper two panels, dyneins were extracted from the *ida*1 strain which lacks inner arm I1/f and then sedimented in 5–20% sucrose gradients either at low hydrostatic pressure in the presence of Mg^{2+} (upper left panel) or at high hydrostatic pressure in the absence of divalent cations (upper right panel). An immunoblot probed for the DC2 component of the DC is shown beneath the Coomassie blue-stained 5–15% polyacrylamide gradient gel. This figure was modified from DiBella *et al*. (2004a) © 2004 by the *American Society for Cell Biology.* The inner arm I1/f migrates at ~17 S and is clearly observed following fractionation of an *oda9* extract that lacks the outer dynein arms (bottom right panel; modified from DiBella *et al*. (2004a) © 2004 by the *American Society for Cell Biology*). For comparison a similar gradient loaded with a wild-type high salt extract is shown at bottom left and illustrates the partial overlap of the outer arm and I1/f inner arm peaks. This panel was modified from DiBella *et al*. (2005) © 2005 by the *American Society for Cell Biology.*

Table II
Mutant Strains Useful for Generating Dyneins Lacking Specific Components

Dynein	Mutant	Defective gene	Missing component(s)	References
Outer arm	*oda11*	α HC	α HC + LC5 thioredoxin + Lis1	Pedersen *et al*. (2007); Sakakibara *et al*. (1991)
	oda4-s7	β HC	β HC motor domain	Sakakibara *et al*., (1993)
	oda2-t	γ HC	γ HC motor domain	Liu *et al*. (2008)
	oda6-r88	IC2	Altered region of IC2 lacks LC2 + LC6 + LC9	DiBella *et al*. (2005); Mitchell and Kang (1993)
	oda12-2	LC2	LC2 (assembly is reduced compared to wild type)	Pazour *et al*. (1999)
	oda12-1	LC2, LC10	LC2 and LC10 (assembly is reduced compared to wild type)	DiBella *et al*. (2005); Pazour *et al*. (1999); Tanner *et al.* (2008)
	oda13	LC6	LC6	DiBella *et al*. (2005); Pazour and Witman (2000)
	oda14	DC3	DC3 (assembly is reduced compared to wild type)	Casey *et al*. (2003)
	oda15	LC7a	LC7a (assembly is reduced compared to wild type)	(DiBella *et al*., 2004a; Pazour and Witman (2000)
Inner arm I1/f	*pf9::cW1*	1α HC (Dhc1)	1α HC null rescued for N-terminal domain. Lacks motor unit	Myster *et al*. (1999)
	ida2-6::λC	1β HC(Dhc10)	1β HC null rescued for N-terminal domain. Lacks motor unit	Perrone *et al*. (2000)
	bop5	IC138	Truncated IC138. Lacks IC97 + LC7b	Hendrickson *et al*. (2004); Wirschell *et al*. (2005)
	pf16-D2	Tctex2	Tctex2. Dynein is unstable	DiBella *et al*. (2004b); Smith and Lefebvre (1996)
	oda15	LC7a	LC7a	DiBella *et al*. (2004a); Pazour and Witman (2000)
Monomeric inner arms	*ida5*	Actin	Actin. Dyneins b and g incorporate a novel actin-related protein (NAP)	Kato-Minoura *et al*. (1997)

mM Tris-Cl, pH 7.5, 0.5 mM EDTA, 1 mM DTT, 25 mM KCl. This allows for reformation of the αβ HC complex and so when these samples are again sedimented in a 5–20% sucrose gradient in the same buffer, two peaks are obtained: the purified α or β HC subunit and a smaller amount of the ~20 S αβ dimer (Pfister and Witman, 1984).

B. Ion Exchange Chromatography

Use of an anion exchange column attached to a high-pressure liquid chromatography system allows for the separation of at least six monomeric inner arm species, the inner arm I1/f, and the γ and αβ HC subunits of the outer arm (Goodenough *et al*., 1987; Kagami and Kamiya, 1992) (Fig. 4). If the goal is to obtain inner arm species, it is best to employ an outer arm-less mutant as this removes the possibility of outer arm contamination. Most published separations have employed a MonoQ column (GE Healthcare, Chalfont St Giles, UK), for example, Kagami and Kamiya (1992); however, a recent report suggests that improved separations of monomeric inner arm d may be obtained by using an even stronger anion exchange column such as Uno-Q (Bio-Rad, Hercules, CA) (Yamamoto *et al*., 2006).

The high salt axonemal extracts are passed through a 0.2 μm filter and then diluted ~10-fold to reduce the salt concentration. This dynein-containing solution is then loaded onto the column and the various species eluted using a 0.2–0.5 M gradient of KCl. For a HR5/5 MonoQ column a flow rate of 0.5 ml/min with a 50 ml gradient has proven highly effective (Kagami and Kamiya, 1992). This methodology has the distinct advantages over sucrose gradient centrifugation in that it is rapid and allows for the clear separation of multiple inner arm species. The major disadvantage is that the outer arm is obtained as two HC-containing subparticles rather than as the intact enzyme with associated DC.

C. Gel Filtration Chromatography

Although gel filtration chromatography has not routinely been used to isolate *Chlamydomonas* axonemal dyneins, it has proven useful in several other systems; for example, the purification of outer arm dynein from trout sperm flagella using a Sepharose CL-6B column (Gatti *et al*., 1989; Moss *et al*., 1991). When fractionating freeze–thaw extracts of *Chlamydomonas* flagella to obtain fractions enriched in a multimeric complex containing both the Fla10 kinesin and the cytoplasmic dynein 1b or 2 that power anterograde and retrograde intraflagellar transport, respectively, we found that the LC2 light chain of outer arm dynein was obtained as a sharp peak (Rompolas *et al*., 2007). In this procedure, the extract in 30 mM Hepes, pH 7.4, 5 mM $MgSO_4$, 0.5 mM EDTA, 25 mM KCl was concentrated to ~250 μl using an Amicon Ultra-4 ultrafiltration filter unit, passed through a 0.2 μm filter and then applied to a Superose 6 HR10/30 column; this column is especially suited to dynein fractionation as it has an exclusion limit of ~40 MDa and thus even the intact outer arm can enter the matrix. The column was run at 0.4 ml/min using a Biologics II chromatography work

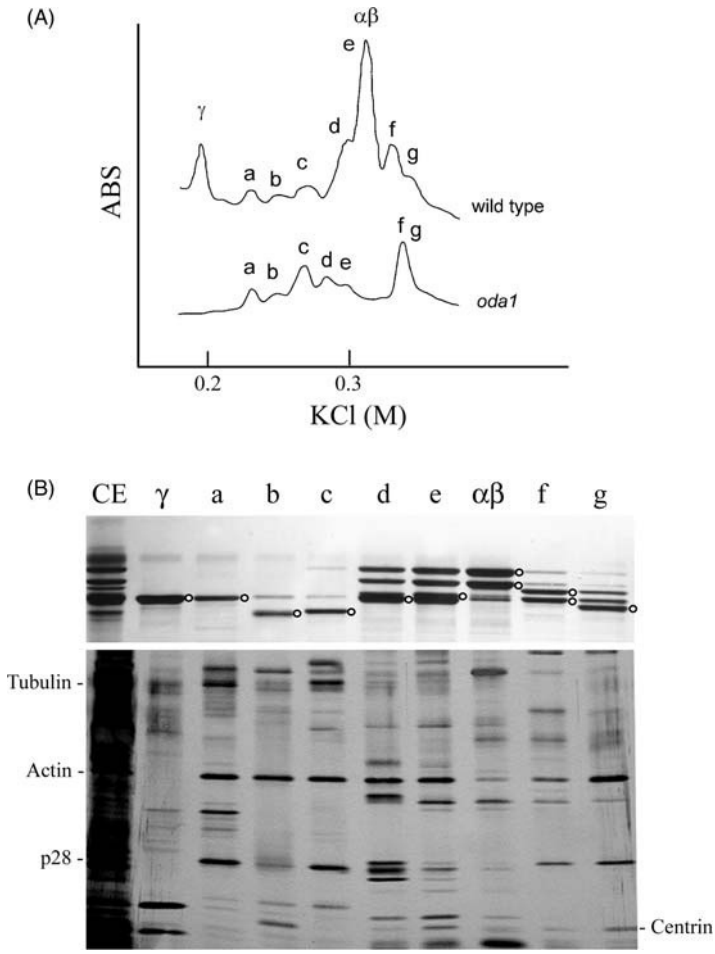

Fig. 4 Fractionation of inner and outer arm dyneins by ion exchange chromatography. (A) Chromatograms of 0.6 M KCl extracts of wild-type and *oda*1 axonemes separated by ion exchange chromatography on a MonoQ column. The outer arm is obtained as two distinct peaks: the γ heavy chain (HC) elutes at ~0.2 M salt whereas the αβ HC complex requires in excess of 0.3 M salt. Inner arm I1/f elutes near the αβ HC complex and consequently, it is most easily purified from an *oda* strain. The monomeric inner arms are fractionated into six distinct peaks. (B) The *upper panel* shows the HC region of a silver-stained 3–5% acrylamide gel loaded with the peak fractions indicated in (A). The major HC constituents of each fraction are indicated by small circles. The *lower panel* shows a portion of a 5–20% acrylamide gel in which similar samples were electrophoresed. This silver-stained gel reveals the lower molecular weight species (actin, p28, and centrin) associated with the various monomeric inner arm species. This figure was modified from originals provided by Drs. Yagi and Kamiya (University of Tokyo).

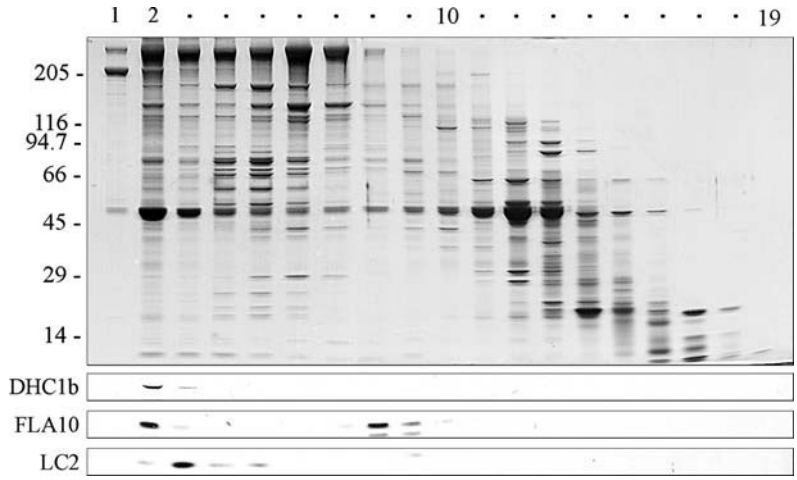

Fig. 5 Gel filtration chromatography of dynein-containing extracts. A freeze–thaw extract of *Chlamydomonas* flagella was separated in Superose 6 HR10/30 gel filtration column. Samples were electrophoresed in two 5–15% acrylamide gradient gels and stained with Coomassie blue. Similar samples were blotted to nitrocellulose and probed for the intraflagellar transport motors FLA10 and DHC1b and also for the outer arm dynein light chain LC2. The outer arm was found mainly in fraction 3; an additional peak containing dynein HCs is present in fractions 6–7. This figure was modified from Rompolas *et al*. (2007).

station (Bio-Rad) and a total of 30×0.75 ml fractions were collected (Fig. 5). This method holds particular promise as a final purification step for various dyneins obtained by sucrose density gradient centrifugation or ion exchange chromatography.

D. Affinity Chromatography on Phenylarsine Oxide

Outer arm dynein contains two thioredoxin-like proteins (LC3 and LC5) that are associated with the β and α HCs, respectively (Patel-King *et al*., 1996). The key feature of this protein class is a redox-active center containing a pair of vicinal dithiols that can be oxidized to form an intramolecular disulfide bond; a molecular model of LC5 illustrating the active site is shown in Fig. 6A. Such vicinal dithiols show a high affinity for trivalent metals such as arsenic as they can react to form a covalent dithioarsine ring structure (Kalef and Gitler, 1994). Consequently, phenylarsine oxide (PAO) can be used as an affinity matrix as the dithioarsine ring can be disrupted by treatment with DTT (Fig. 6B). When recombinant LC5 protein is expressed as a fusion with maltose-binding protein (MBP) both the intact fusion protein and the LC separated by Factor Xa digestion can be specifically eluted with 0.5 M 2-mercaptoethanol (Fig. 6C). In contrast, MBP alone shows no affinity for the matrix. This observation provided direct evidence that the dynein thioredoxin LCs are indeed redox active. When a high salt extract of *Chlamydomonas* axonemes is applied to the PAO resin, inner arm dyneins and a major membrane protein show no affinity and are found in the flow-through. In contrast, the

Fig. 6 Purification of outer arm dynein by affinity chromatography on PAO resin. (A) Ribbon diagram of a molecular model (Harrison *et al*., 2002) of dynein LC5 which contains a perfect copy of the thioredoxin active site motif (WCGPCK). The vicinal Cys residues that comprise the redox-active site are indicated. (B) Scheme illustrating the covalent association of a vicinal dithiol-containing protein (a dynein LC thioredoxin) with phenylarsine oxide (PAO) to form a dithioarsine ring structure. Bound proteins can be eluted from the arsenic column using a reducing agent. (C) A maltose-binding protein (MBP) fusion with the LC5 outer arm dynein LC was incubated with Factor Xa to cleave the LC from MBP. The digest was passed over PAO resin and bound proteins eluted with 0.5 M β-mercaptoethanol. The uncut fusion protein and released LC5 both bound to the column whereas free MBP did not. (D)A high salt extract of *Chlamydomonas* axonemes was passed over the PAO resin, washed, and bound proteins eluted with 2-mercaptoethanol. Samples were separated in a 4% acrylamide 4 M urea gel and stained with silver. The regions between lanes were excised to illustrate the band alignment more clearly. Neither the inner arm dynein HCs (IA) nor a prominent membrane protein bound to the column whereas the outer dynein arm HCs (α, β, and γ) did. For further details, see Patel-King *et al*. (1996). (See Plate no. 2 in the Color Plate Section.)

three outer arm HCs interact with the column and are eluted by 2-mercaptoethanol (Fig. 6D). The buffer for chromatography on PAO resin contains 50 mM Tris-Cl, pH 7.5, 1 mM EDTA, 100 mM NaCl; it is also necessary to add 0.5% Tween 20 to all buffers to reduce nonspecific interactions with the resin matrix (Patel-King *et al*., 1996). Unfortunately, prepared PAO resin is no longer commercially available; however, it can be readily synthesized from an agarose or other resin, derivatized with an amine-reactive side chain, and 4-aminophenylarsine oxide (Hoffman and Lane, 1992).

VI. Immunoprecipitation from Cell Body Extracts

A procedure for obtaining dynein subparticles preassembled in the cell body was originally devised by Fowkes and Mitchell (1998) and modified by Sakato *et al*. (2007). A 500 ml culture of *Chlamydomonas* is grown to a cell density of

~1.0×10^6 cells/ml and treated with autolysin as necessary to remove cell walls (Qin *et al*., 2004). Cells are harvested by centrifugation and resuspended in IP buffer consisting of 30 mM Hepes, pH 7.4, 5 mM $MgSO_4$, 0.5 mM EDTA, 25 mM KCl, 1 mM DTT and protease inhibitor cocktail (1/100 volume; P8849, Sigma Chemical Co., St Louis, MO). An equal volume of acid-washed 1-mm diameter glass beads is then added and the sample vortexed for 1 min. The homogenate is then removed from the beads and spun in a TLA100.2 rotor (Beckman, Fullerton, CA) at 33,000 rpm for 2 h. NaCl and Triton X-100 are then added to the clarified extract to final concentrations of 75 mM and 0.05% (v/v), respectively, and the specific antibody then added. Following a 1 h incubation at 4°C, 10 μl of ImmunoPure immobilized protein G beads (Pierce Biotechnology, Rockford, IL) is added. After a further incubation, the beads are collected by centrifugation and washed three times with IP buffer. For electrophoretic analysis, immunoprecipitated proteins are released by treatment with $2 \times$ gel loading buffer (0.1 M Tris-Cl, pH 6.8, 0.2 M DTT, 4% sodium dodecyl sulfate, 0.2% bromophenol blue) and heating at > 90°C. The coimmunoprecipitation of the γ HC and LC4 light chain using an antibody raised against residues 1-442 of the γ HC is shown in Fig. 7.

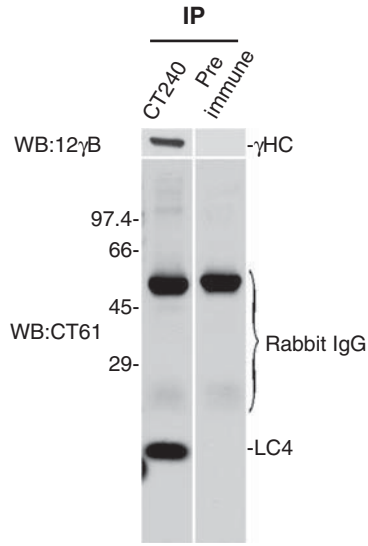

Fig. 7 Immunoprecipitation of dynein from cell body extract. The CT240 antibody against the N-terminal region of the outer arm γ HC was added to a cell body homogenate and immunoprecipitated using immobilized protein G beads; the preimmune serum was used as a control. The upper panels were probed with CT240 to detect the γ HC and the lower panels with CT61 to identify the Ca^{2+}-binding LC4 light chain. From Sakato *et al*. (2007) © 2007 by the *American Society for Cell Biology.*

VII. Conclusions

There are available a variety of procedures that allow for the purification of specific dynein particles and subcomponents. When combined with the large number of mutants available in the *Chlamydomonas* model system, it is now possible to prepare dyneins that lack individual motor units or other polypeptides. These methods should prove highly useful in defining the properties of individual proteins within these massive molecular motors.

Acknowledgments

I thank Drs Toshiki Yagi (University of Kyoto) and Ritsu Kamiya (University of Tokyo) for providing the ion exchange chromatography figure. My laboratory is supported by grant GM51293 from the National Institutes of Health.

References

Ahmed, N., Gao, C., Lucker, B., Cole, D., and Mitchell, D. (2008). ODA16 aids axonemal outer row dynein assembly through an interaction with the intraflagellar transport machinery. *J. Cell Biol*. **183**, 313–322.

Bessen, M., Fay, R.B., and Witman, G.B. (1980). Calcium control of waveform in isolated flagellar axonemes of *Chlamydomonas*. *J. Cell Biol*. **86**, 446–455.

Brokaw, C. 2009. Thinking about flagellar oscillation. *Cell Motil. Cytoskeleton*. **66**, 425–436.

Casey, D., Inaba, K., Pazour, G., Takada, S., Wakabayashi, K., Wilkerson, C., Kamiya, R., and Witman, G. (2003). DC3, the 21-kD subunit of the outer dynein arm-docking complex (ODA-DC), is a novel EF-hand protein important for assembly of both the outer arm and the ODA-DC. *Mol. Biol. Cell*. **14**, 3650–3663.

DiBella, L.M., Gorbatyuk, O., Sakato, M., Wakabayashi, K., Patel-King, R.S., Pazour, G.J., Witman, G.B., and King, S.M. (2005). Differential light chain assembly influences outer arm dynein motor function. *Mol. Biol. Cell*. **16**, 5661–5674.

DiBella, L.M., Sakato, M., Patel-King, R.S., Pazour, G.J., and King, S.M. (2004a). The LC7 light chains of *Chlamydomonas* flagellar dyneins interact with components required for both motor assembly and regulation. *Mol. Biol. Cell* **15**, 4633–4646.

DiBella, L.M., Smith, E.F., Patel-King, R.S., Wakabayashi, K., and King, S.M. (2004b). A novel Tctex2-related light chain is required for stability of inner dynein arm I1 and motor function in the *Chlamydomonas* flagellum. *J. Biol. Chem.* **279**, 21666–21676.

Fowkes, M.E., and Mitchell, D.R. (1998). The role of preassembled cytoplasmic complexes in assembly of flagellar dynein subunits. *Mol. Biol. Cell*. **9**, 2337–2347.

Freshour, J., Yokoyama, R., and Mitchell, D.R. (2007). *Chlamydomonas* flagellar outer row dynein assembly protein Oda7 interacts with both outer row and I1 inner row dyneins. *J. Biol. Chem.* **282**, 5404–5412.

Gatti, J.L., King, S.M., Moss, A.G., and Witman, G.B. (1989). Outer arm dynein from trout spermatozoa. Purification, polypeptide composition, and enzymatic properties. *J. Biol. Chem*. **264**, 11450–11457.

Goodenough, U., and Heuser, J. (1984). Structural comparison of purified dynein proteins with *in situ* dynein arms. *J. Mol. Biol*. **180**, 1083–1118.

Goodenough, U.W., Gebhart, B., Mermall, V., Mitchell, D.R., and Heuser, J.E. (1987). High-pressure liquid chromatography fractionation of *Chlamydomonas* dynein extracts and characterization of inner-arm dynein subunits. *J. Mol. Biol*. **194**, 481–494.

Harrison, A., Sakato, M., Tedford, H.W., Benashski, S.E., Patel-King, R.S., and King, S.M. (2002). Redox-based control of the γ heavy chain ATPase from *Chlamydomonas* outer arm dynein. *Cell Motil. Cytoskeleton* **52**, 131–143.

Hasegawa, E., Hayashi, H., Asakura, S., and Kamiya, R. (1987). Stimulation of in vitro motility of *Chlamydomonas* axonemes by inhibition of cAMP-dependent phosphorylation. *Cell Motil*. **8**, 302–311.

Hayashibe, K., Shingyoji, C., and Kamiya, R. (1997). Induction of temporary beating in paralyzed flagella of *Chlamydomonas* mutants by application of external force. *Cell Motil. Cytoskeleton* **37**, 232–239.

Hendrickson, T.W., Perrone, C.A., Griffin, P., Wuichet, K., Mueller, J., Yang, P., Porter, M.E., and Sale, W.S. (2004). IC138 Is a WD-repeat dynein intermediate chain required for light chain assembly and regulation of flagellar bending. *Mol. Biol. Cell* **15**, 5431–5442.

Hoffman, R., and Lane, M. (1992). Iodophenylarsine oxide and arsenical affinity chromatography: New probes for dithiol proteins. Application to tubulins and to components of the insulin receptor-glucose transporter signal transduction pathway. *J. Biol. Chem.* **267**, 14005–14011.

Hyams, J., and Borisy, G. (1978). Isolated flagellar apparatus of *Chlamydomonas*: Characterization of forward swimming and alteration of waveform and reversal of motion by calcium ions *in vitro*. *J. Cell Sci*. **33**, 235–253.

Kagami, O., and Kamiya, R. (1992). Translocation and rotation of microtubules caused by multiple species of *Chlamydomonas* inner-arm dynein. *J. Cell Sci.* **103**, 653–664.

Kalef, E., and Gitler, C. (1994). Purification of vicinal dithiol-containing proteins by arsenical-based affinity chromatography. *Methods Enzymol*. **233**, 395–403.

Kato-Minoura, T., Hirono, M., and Kamiya, R. (1997). *Chlamydomonas* inner-arm dynein mutant, *ida5*, has a mutation in an actin-encoding gene. *J. Cell Biol*. **137**, 649–656.

King, S.M. (1995). Large-scale isolation of *Chlamydomonas* flagella. *Methods Cell Biol*. **47**, 9–12.

King, S.M., and Kamiya, R. (2008). Axonemal dyneins: Assembly, structure and force generation. *In* "The *Chlamydomonas* Source Book" (G. B. Witman, ed.), 2nd edn., Volume 3: Cell Motility and Behavior Vol. III, pp. 131–208. Elsevier, San Diego.

Liu, Z., Takazaki, H., Nakazawa, Y., Sakato, M., Yagi, T., Yasunaga, T., King, S.M., and Kamiya, R. (2008). Partially functional outer arm dynein in a novel *Chlamydomonas* mutant expressing a truncated γ heavy chain. *Eukaryotic Cell* **7**, 1136–1145.

Mitchell, D.R., and Kang, Y. (1993). Reversion analysis of dynein intermediate chain function. *J. Cell Sci*. **105**, 1069–1078.

Moss, A.G., Gatti, J.L., King, S.M., and Witman, G.B. (1991). Purification and characterization of *Salmo gairdneri* outer arm dynein. *Methods Enzymol*. **196**, 201–222.

Myster, S.H., Knott, J.A., Wysocki, K.M., O'Toole, E., and Porter, M.E. (1999). Domains in the 1a dynein heavy chain required for inner arm assembly and flagellar motility in *Chlamydomonas*. *J. Cell Biol*. **146**, 801–818.

Nakamura, K., Wilkerson, C.G., and Witman, G.B. (1997). Functional interaction between *Chlamydomonas* outer arm dynein subunits: The γ subunit suppresses the ATPase activity of the αβ dimer. *Cell Motil. Cytoskeleton* **37**, 338–345.

Nicastro, D., Schwartz, C., Pierson, J., Gaudette, R., Porter, M.E., and McIntosh, J.R. (2006). The molecular architecture of axonemes revealed by cryoelectron tomography. *Science* **313**, 944–948.

Patel-King, R.S., Benashki, S.E., Harrison, A., and King, S.M. (1996). Two functional thioredoxins containing redox-sensitive vicinal dithiols from the *Chlamydomonas* outer dynein arm. *J. Biol. Chem*. **271**, 6283–6291.

Pazour, G.J., Koutoulis, A., Benashski, S.E., Dickert, B.L., Sheng, H., Patel-King, R.S., King, S.M., and Witman, G.B. (1999). LC2, the *Chlamydomonas* homologue of the *t* complex-encoded protein Tctex2, is essential for outer dynein arm assembly. *Mol. Biol. Cell* **10**, 3507–3520.

Pazour, G.J., and Witman, G.B. (2000). Forward and reverse genetic analysis of microtubule motors in *Chlamydomonas*. *Methods* **22**, 285–298.

Pedersen, L., Rompolas, P., Christensen, S., Rosenbaum, J.L., and King, S.M. (2007). The lissencephaly protein Lis1 is present in motile mammalian cilia and requires outer dynein arm for targeting to *Chlamydomonas* flagella. *J. Cell Sci*. **120**, 858–867.

Perrone, C.A., Myster, S.H., Bower, R., O'Toole, E.T., and Porter, M.E. (2000). Insights into the structural organization of the I1 inner arm dynein from a domain analysis of the 1b dynein heavy chain. *Mol. Biol. Cell* **11**, 2297–2313.

Pfister, K.K., Fay, R.B., and Witman, G.B.. (1982). Purification and polypeptide composition of dynein ATPases from *Chlamydomonas* flagella. *Cell Motil*. **2**, 525–547.

Pfister, K.K., and Witman, G.B. (1984). Subfractionation of *Chlamydomonas* 18 S dynein into two unique subunits containing ATPase activity. *J. Biol. Chem*. **259**, 12072–12080.

Piperno, G., Mead, K., and Shestak, W. (1992). The inner dynein arms I2 interact with a "dynein regulatory complex" in Chlamydomonas flagella. *J. Cell Biol*. **118**, 1455–1463.

Qin, H., Diener, D.R., Geimer, S., Cole, D.G., and Rosenbaum, J.L. (2004). Intraflagellar transport (IFT) cargo: IFT transports flagellar precursors to the tip and turnover products to the cell body. *J. Cell Biol.* **164**, 255–266.

Rompolas, P., and King, S.M. (2008). Regulated association of CrLis1 with the outer dynein arm. *Mol. Biol. Cell* **19**, CD-ROM (abstr.).

Rompolas, P., Pedersen, L., Patel-King, R.S., and King, S.M. (2007). *Chlamydomonas* FAP133 is a dynein intermediate chain associated with the retrograde intraflagellar transport motor. *J. Cell Sci*., **120**, 3653–3665.

Sakakibara, H., Mitchell, D.R., and Kamiya, R. (1991). A *Chlamydomonas* outer arm dynein mutant missing the α heavy chain. *J. Cell Biol*. **113**, 615–622.

Sakakibara, H., Takada, S., King, S.M., Witman, G.B., and Kamiya, R. (1993). A *Chlamydomonas* outer arm dynein mutant with a truncated β heavy chain. *J. Cell Biol*. **122**, 653–661.

Sakato, M., Sakakibara, H., and King, S.M. (2007). *Chlamydomonas* outer arm dynein alters conformation in response to Ca^{2+}. *Mol. Biol. Cell* **18**, 3620–3634.

Smith, E., and Lefebvre, P. (1996). PF16 encodes a protein with armadillo repeats and localizes to a single microtubule of the central apparatus in Chlamydomonas flagella. *J. Cell Biol.* **132**, 359–370.

Smith, E., and Yang, P. (2004). The radial spokes and central apparatus: Mechanochemical transducers that regulate flagellar motility. *Cell Motil. Cytoskeleton* **57**, 8–17.

Takada, S., and Kamiya, R. (1994). Functional reconstitution of Chlamydomonas outer dynein arms from α-β and γ subunits: Requirement of a third factor. *J. Cell Biol*. **126**, 737–745.

Takada, S., Sakakibara, H., and Kamiya, R. (1992). Three-headed outer arm dynein from *Chlamydomonas* that can functionally combine with outer-arm-missing axonemes. *J Biochem* (*Tokyo*). 111, 758–762.

Tanner, C.A., Rompolas, P., Patel-King, R.S., Gorbatyuk, O., Wakabayashi, K., Pazour, G.J., and King, S.M. (2008). Three members of the LC8/DYNLL family are required for outer arm dynein motor function. *Mol. Biol. Cell* **19**, 3724–3734.

Wakabayashi, K., and King, S.M. (2006). Modulation of *Chlamydomonas reinhardtii* flagellar motility by redox poise. *J. Cell Biol*. **173**, 743–754.

Wirschell, M., Hendrickson, T., Fox, L., Haas, N., Silflow, C., Witman, G.B., and Sale, W. (2005). IC97, a novel dynein intermediate chain from flagellar inner arm dynein I1, interacts with tubulin *in situ*. *Mol. Biol. Cell* **16**, Abstract #1023 (CD-ROM).

Wirschell, M., Hendrickson, T., and Sale, W. (2007). Keeping an eye on I1: I1 dynein as a model for flagellar dynein assembly and regulation. *Cell Motil. Cytoskeleton* **64**, 569–579.

Wirschell, M., Pazour, G., Yoda, A., Hirono, M., Kamiya, R., and Witman, G. (2004). Oda5p, a novel axonemal protein required for assembly of the outer dynein arm and an associated adenylate kinase. *Mol. Biol. Cell* **15**, 2729–2741.

Witman, G.B. 1986. Isolation of *Chlamydomonas* flagella and flagellar axonemes. *Methods Enzymol*. **134**, 280–290.

Yagi, T., Minoura, I., Fujiwara, A., Saito, R., Yasunaga, T., Hirono, M., and Kamiya, R. (2005). An axonemal dynein particularly important for flagellar movement at high viscosity: Implications from a new *Chlamydomonas* mutant deficient in the dynein heavy chain gene DHC9. *J. Biol. Chem.* **280**, 41412–41420.

Yamamoto, R., Yanagisawa, H., Yagi, T., and Kamiya, R. (2006). A novel subunit of axonemal dynein conserved among lower and higher eukaryotes. *FEBS Lett*. **580**, 6357–6360.

CHAPTER 4

Purification of Dyneins from Sperm Flagella

Kazuo Inaba *and* Katsutoshi Mizuno
Shimoda Marine Research Center, University of Tsukuba, 5-10-1, Shimoda, Shizuoka 415-0025, Japan

METHODS IN CELL BIOLOGY, VOL. 92

978-0-12-374974-1
DOI: 10.1016/S0091-679X(08)92004-5

Abstract

Metazoan spermatozoa, especially those from marine invertebrates and fish, are excellent sources for isolating axonemal dyneins because of their cellular homogeneity and the large amounts that can be collected. Sperm flagella can be easily isolated by homogenization and subsequent centrifugation. Axonemes are obtained by demembranation of flagella with the nonionic detergent Triton X-100. The outer arm dyneins have been most widely studied because they are specifically extracted by a high-salt solution and can be isolated as a relatively pure fraction of ~20 S two-headed dynein by sucrose density gradient centrifugation. Only a few reports have described the isolation of inner arm dyneins from sperm and the protocol has room for improvement. Sperm show clear changes in motility at fertilization, which are exerted through the regulation of axonemal dyneins by protein phosphorylation and Ca^{2+} binding. Therefore dyneins from sperm flagella are an excellent biochemically tractable source for studying the regulation of axonemal dyneins. Here we describe protocols used for purification of flagellar dyneins from sperm of tunicates, sea urchins, and fish. The techniques described here could be applied to other species with appropriate modifications.

I. Introduction

Metazoan sperm typically bear long flagella as their motile machinery for fertilizing eggs. These sperm, as well as *Chlamydomonas* and other protozoan cilia/flagella, have been used for studying dyneins for nearly a half century. Marine invertebrates and fish have been the main sources of sperm because a large amount of sperm can be obtained without contamination by other cells. Another advantage to using sperm flagella is in examining the regulation of axonemal dyneins, as sperm motility shows dynamic changes at fertilization and hence the axonemal dyneins are strictly regulated.

Isolation of sperm dyneins starts with collection of sperm. The methods to collect sperm differ among animal species, but sperm collected from externally fertilizing animals during their breeding season usually show high cellular homogeneity. Dyneins are huge protein complexes, so that they are efficiently separated from other proteins by size, such as by sucrose density gradient centrifugation or gel filtration. In this sense, whole sperm could be used for extraction of dyneins. However, sperm are usually fractionated to isolate flagella to increase the purity of dyneins and to prevent degradation by acrosomal proteases. Here we discuss protocols to isolate and purify axonemal dyneins, mostly the outer arm dyneins, from sperm of the ascidian *Ciona intestinalis*, several sea urchins, and fish. These methods are applicable or serve as a good reference to establish protocols to isolate dynein from sperm of other animals.

II. Short Protocol for Isolation of Sperm Outer Arm Dynein from the Ascidian *C. intestinalis*

Outer arm dyneins from metazoan sperm are usually composed of two heavy chains, five or six intermediate chains (ICs), and six light chains (LCs) (Inaba, 2003, 2007). Here is the short protocol that we usually employ for isolating outer arm dynein from sperm of *C. intestinalis* (e.g., Mizuno *et al*., 2009). The principles behind the protocol and tips for its successful completion, as well as methods for other species, are described in detail in later sections.

A. Short Protocol

1. Collect 2 ml of undiluted sperm.
2. Dilute with artificial seawater (ASW) (filtered seawater, FSW, or artificial calcium-free seawater, CaFSW can be substituted) to 10 ml and centrifuge at 5000 × *g* at 4°C for 10 min.
3. Suspend the sperm pellet with 5 ml of ASW.
4. Homogenize in a glass/Teflon Potter–Elvehjem-type homogenizer at 500–1000 rpm for five strokes on ice.
5. Check the homogenate under a phase contrast or differential interference contrast microscope to ensure that the head and flagella are completely detached. If the detachment is not complete enough, repeat step 4.
6. Dilute the homogenate with another 5 ml of ASW and centrifuge at 2000 × *g* at 4°C for 10 min.
7. Carefully collect the white turbid supernatant from the top of the tubes and pool them. Do not collect all the supernatant, but leave a small volume to avoid the sperm heads. Check for contamination by heads under a microscope.
8. Centrifuge the pooled supernatant at 12,000 × *g* at 4°C for 10 min.
9. Remove the supernatant and add 3 ml of demembranation buffer (DM) to the pellet and resuspend well.
10. Centrifuge at 12,000 × *g* at 4°C for 10 min.
11. Remove the supernatant and add 3 ml of axoneme buffer (AXB) and resuspend the pellet well. Centrifuge at 12,000 × *g* at 4°C for 10 min.
12. Repeat step 11 twice.
13. Remove the supernatant and add 3 ml of high-salt buffer (HSB) and resuspend the pellet. Keep the tube on ice for 30 min.
14. Centrifuge at 12,000 × *g* at 4°C for 10 min.
15. Collect the supernatant and spin in an ultracentrifuge at 100,000 × *g* at 4°C for 30 min.
16. Collect the supernatant (HSB extract) and place in a prewashed dialysis bag.
17. Put the dialysis bag in a small plastic tray and cover it with powdered Aquacide I (Calbiochem).

18. Place in a refrigerator and check occasionally to prevent overconcentration.
19. Prepare 5–20% sucrose density gradients in centrifuge tubes with a gradient maker and a peristaltic pump.
20. Remove the concentrated HSB extract from the dialysis bag and centrifuge at 12,000 × *g* at 4°C for 10 min.
21. Remove the supernatant and carefully layer onto the sucrose gradients.
22. Centrifuge in an ultracentrifuge swing-out rotor at 94,000 × *g* for 15–20 h at 4°C.
23. Fractionate the gradient from the bottom of the tube (set the fraction size so that the total number of fractions will be 20–25).
24. Measure protein concentration by absorbance at 280 nm or by using the dye-binding method (Bradford, 1976). ATPase activity may be measured by any standard protocol (e.g., Taussky and Shorr, 1953). Check the protein components in each fraction by SDS-PAGE.

B. Solution Used

ASW: 460 mM NaCl, 10 mM KCl, 9 mM $CaCl_2$, 36 mM $MgCl_2$, 17 mM $MgSO_4$, 10 mM HEPES-NaOH (pH 8.2)

CaFSW: 469 mM NaCl, 10 mM KCl, 36 mM $MgCl_2$, 17 mM $MgSO_4$, 10 mM HEPES-NaOH (pH 8.2), 10 mM EGTA

DM: 0.1% Triton X-100, 0.15 M KCl, 2 mM $MgCl_2$, 0.5 mM EGTA, 10 mM Tris-HCl, pH 8.0, 0.2 mM DTT

AXB: 0.15 M KCl, 2 mM $MgCl_2$, 0.5 mM EGTA, 10 mM Tris-HCl, pH 8.0, 0.2 mM DTT

HSB: 0.6 M KCl, 2 mM $MgCl_2$, 0.5 mM EGTA, 10 mM Tris-HCl, pH 8.0, 0.2 mM DTT

III. Collection of Sperm

A. Sea Urchins

Sea urchins (Echinodermata) have been used in the study of gametes and fertilization for a long time. Large amounts of sperm can be collected. Gametes are artificially spawned by injection of 0.5 M KCl or 100 mM acetylcholine into the body cavity (Fig. 1A). Alternatively, it can be placed in the body cavity after removal of the mouthparts (Aristotle's lantern), but injection by syringe needle is highly recommended because it does not kill the animals and they can survive the collection of gametes (Fig. 1A). After injection, the males are put on a large Petri dish or tray with the gonopores facing down (Fig. 2A). After half an hour, the sperm attached to the body surface near the gonopore are isolated by washing with seawater and the urchin is removed. Although the volume of sperm depends on species, 0.5–2 ml of dry sperm (undiluted sperm) can be usually obtained from one male.

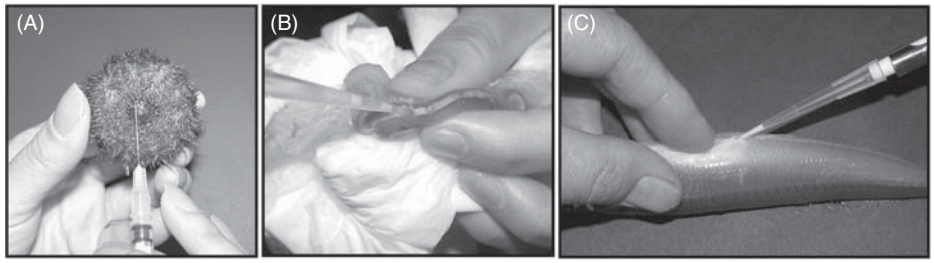

Fig. 1 Collection of sperm. (A) Injection of acetylcholine using a syringe into the body cavity of a sea urchin. (B) Collection of sperm from the sperm duct of *Ciona*. After opening the tunic and body wall, the animal is held with tissue paper. Sperm are collected using a micropipette with a tip after piercing the sperm duct with a needle. (C) Collection of sperm from the whiting *Sillago japonica*. Sperm are squeezed out of the cloaca and collected using a micropipette with a tip.

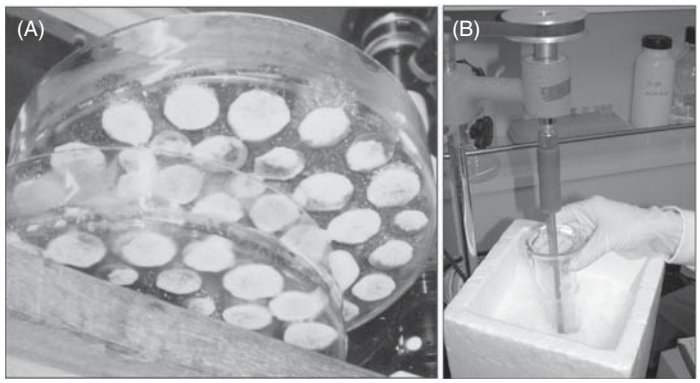

Fig. 2 (A) Multiple sea urchins are put in a large petri dish after injection of acetylcholine. Sperm are then recovered by a pipette. (B) Homogenization of sperm in a glass/Teflon Potter–Elvehjem-type homogenizer on ice. The homogenizer is connected to a motor-drive unit.

B. Tunicates

Marine invertebrates, ascidians (Chordata), are sessile and filter feeders. They are hermaphroditic and each individual possesses both ovary and testis. *Ciona*, a family member of the Enterogona, is one of the solitary ascidians. Both sperm duct and oviduct are attached along the intestine in parallel and it is easy to collect gametes by simple dissection. We describe here the method to collect sperm from *C. intertinalis* or *Ciona savygni*. Sexually mature animals usually contain significant amounts of sperm in the sperm duct, but keeping animals collected from the wild under constant light to prevent natural spawning is effective for accumulating more sperm in the sperm duct. After opening the tunic, the body wall on the atrial siphon side is further cut open and both sperm duct and oviduct are exposed. Sperm are extracted by piercing the sperm

duct with a 25-gauge needle, followed by gently squeezing them out. The sperm are collected using a micropipette with a tip (Fig. 1B). As the sperm duct and oviduct are attached along the intestine in parallel, much attention should be paid to ensure that the oviduct is not broken, as it is best to collect sperm without contamination from eggs. Alternatively, the eggs can be washed out in advance by cutting the oviduct followed by rinsing with seawater. The volume of sperm obtained depends on both the body size of *Ciona* and on the extent of sexual maturation, but usually 0.02–0.2 ml of sperm can be obtained from one individual.

C. Fish

The amount of sperm that can be collected varies among fish species. Sperm used for experiments are usually obtained from fish during their normal breeding season, but it is also possible to collect sperm from artificially matured males by injection of hormones. Semen can be obtained from large salmonid fish by inserting a pipette through the cloaca into the sperm duct and gently sucking while squeezing the abdomen. However, it is highly recommended to collect semen by just squeezing the abdomen and collecting the outflow semen using a micropipette since this approach is much easier (Fig. 1C). In this case, one should wipe clean the area near the cloaca in advance so as not to contaminate the sample with urine or bodily fluids. Concentrations and volumes of sperm in semen differ depending on body size and species. For example, 2–20 ml semen can be collected from rainbow trout; 10–100 ml from chum salmon; 0.5–2.0 ml from the puffer fish *Takifugu niphobles*; 1–5 ml from the flounder *Limanda yokohamae*; and 0.02–0.1 ml from the whiting *Sillago japonica*.

D. Other Animals

When it is necessary to collect sperm from other species, determine the best method for collecting mature sperm. For example, sperm storage organs are often a good source of material. However, the amount of sperm stored in these organs is sometimes not sufficient and so testes can be harvested and minced in an appropriate buffer. The material is then passed through nylon mesh and the filtrate used as the starting material for isolation of dyneins. Examples of dynein isolations from sperm obtained by mincing testes have been reported for oyster (Wada *et al*., 1992), mussels (Stephens and Prior, 1992), and sea anemone (Mohri *et al*., 1999).

IV. Isolation of Sperm Flagella

A. Dissociation of Sperm Head and Flagella

When a large enough quantity of sperm has been obtained, sperm flagella are usually isolated by homogenization, followed by centrifugation. Before homogenization, semen or dry sperm is normally washed with an appropriate buffer by dilution and centrifugation. The buffers used for washing are typically isotonic to body fluid, which means, seawater for sperm of sea urchins and tunicates and a buffer containing 0.15 M

KCl (or NaCl) for marine and freshwater fish. In the case of salmonid fish, a K^+-containing solution (0.15 M KCl and 10 mM Tris-HCl pH 8.0) is often used as K^+ suppresses sperm motility (Inaba *et al*., 1998). Sperm are suspended in an appropriate buffer, placed on ice, and homogenized in a motor-driven glass/Teflon Potter–Elvehjem-type homogenizer (Fig. 2B). Conditions for homogenization vary with the clearance in the homogenizer and the concentration of sperm. Suspensions with high sperm concentration need less speed and fewer strokes to dissociate flagella. Usually 5–10 volumes of buffer are added to 1 volume of sperm pellet and the suspension is homogenized at 500–1000 rpm for 10 strokes on ice.

B. Centrifugation to Isolate Flagella

After homogenization, it is important to check the homogenate by phase-contrast or differential interference contrast microscopy to ensure complete deflagellation (Fig. 3). After dissociation of head and flagella, the homogenate is centrifuged at a low speed ($2000 \times g$, 10 min, 4°C) to sediment the sperm heads. Under these conditions, some long flagella (these appear as a white layer) are also layered on top of the pellet of head (appears as a yellowish layer). The supernatants are carefully removed without contamination from the head layer, pooled, and then checked by microscopy (Fig. 3). If too many heads are observed, the conditions for centrifugation should be changed. The pooled supernatant is further centrifuged at higher speed ($12{,}000 \times g$, 10 min, 4°C) to sediment the flagella.

V. Purification of Outer Arm Dyneins

A. Isolation of Flagellar Axonemes

The flagellar pellet is demembranated in a buffer containing Triton X-100. The concentration of Triton X-100 is in the range of 0.1–0.25% and the volume of the buffer is 10–20 times that of the flagellar pellet. Other components in the buffer include

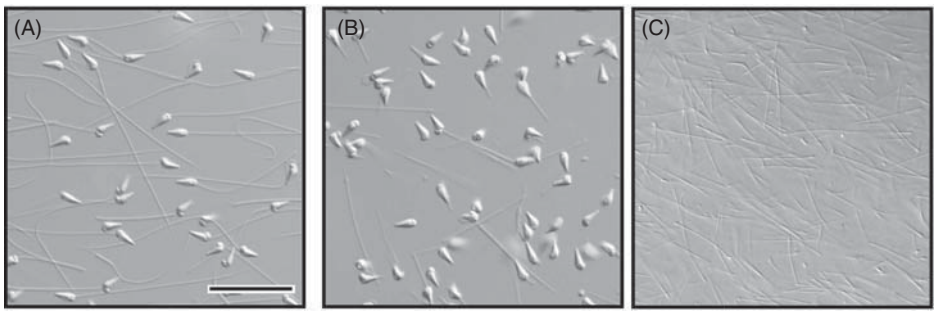

Fig. 3 Isolation of sperm flagella from the sea urchin *Hemicentrotus pulcherrimus*. Images taken using a differential interference contrast microscope are shown. (A) Sperm. (B) Sperm after homogenization. (C) Isolated flagella. Bar, 20 μm.

10–20 mM Tris-HCl, pH 8.0 (or HEPES–NaOH), 0.15 M salt (KCl, NaCl, or K-acetate), 1–2 mM Mg^{2+}, and a reducing reagent such as 0.2–1 mM DTT. Ca^{2+} is kept at low concentration by inclusion of EGTA at 0.2–0.5 mM. To prevent proteolysis, protease inhibitors, such as 1 mM PMSF and 1 μM leupeptin, should be included in the buffer. After demembranation, the pellet (axonemes) is washed two to three times with Triton-free DB (AXB). The final pellet is used for isolation of dyneins.

B. Extraction of Outer Arm Dynein

In several animals, it has been confirmed by electron microscopy that outer arm dynein is extracted by a buffer containing 0.5–0.6 M KCl or NaCl (Gatti *et al*., 1989; Gibbons and Fronk, 1972). The other components of the buffer are the same as those in the AXB. The axonemal pellet is resuspended in 5–10 volumes of the HSB and kept on ice for 30 min. The efficiency of outer arm dynein extraction appears to depend on species: for example, 10 min is enough for the sea urchin *Hemicentrotus pulcherrimus*, but a 1 h incubation is not sufficient to extract all the outer arm dynein from sperm of another sea urchin *Anthocidaris crassispina*. The conditions needed to extract outer arm dynein should be investigated by electron microscopy when it is carried out in a species for the first time.

C. Concentration of the Extract

The high-salt extract is further clarified by ultracentrifugation to remove any debris such as short axoneme fragments or partially disintegrated microtubules and then concentrated to a small volume prior to sucrose density gradient centrifugation or gel filtration chromatography. Dyneins easily aggregate or become denatured when they are exposed to vigorous mixing, such as pipetting or vortexing, all of which should be avoided. Salting-out or solvent precipitation results in less recovery of dynein. High recovery is obtained by ultrafiltration under N_2 pressure (Amicon) with a stirred cell or by placing the sample in a dialysis bag which is then covered in polyethylene glycol or Aquacide (Calbiochem) (Inaba and Mohri, 1989; Yokota and Mabuchi, 1994). The concentrated high-salt extract is subject to ultracentrifugation to remove aggregates before loading onto a sucrose density gradient or gel filtration column.

Another way to prepare the high-salt extract with a high protein concentration is to use a small volume of extraction buffer. In this case a somewhat higher salt concentration (0.65–0.7 M KCl) is used to adjust the final concentration of salt in the sample to 0.6 M. This method avoids protein loss during the concentration process, but extraction is less efficient due to the low buffer/axoneme ratio.

D. Sucrose Density Gradient Centrifugation

Sucrose density gradients are made in the buffer used for extraction of outer arm dynein but with a lower salt concentration. Usually AXB is used. Buffers containing

two concentrations (5 and 20%) of sucrose are made, and a linear sucrose gradient is prepared in a centrifuge tube using a gradient maker and peristaltic pump (Fig. 4A). A capillary is connected to a tube from peristaltic pump and put at the bottom of the centrifuge tube. The gradient is continuously made from the bottom to the top of the tube. Concentrated salt extract is carefully loaded onto the gradient without disturbing the interface and centrifuged at 100,000 × *g* for 16–20 h. A mixture of markers, such as thyroglobulin (19 S), catalase (11.4 S) and bovine serum albumin (4.6 S), can be

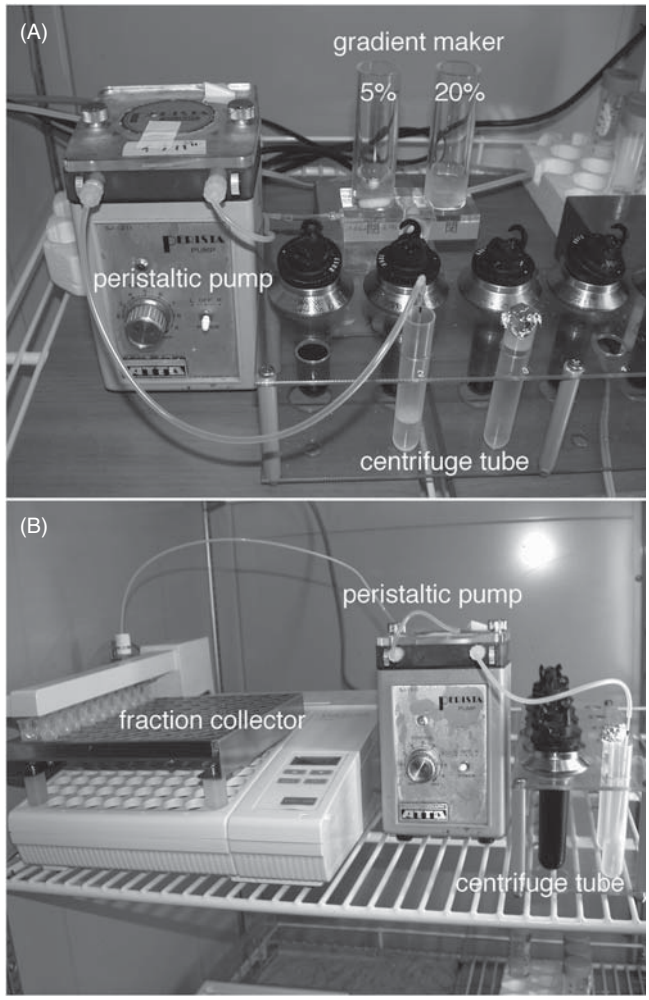

Fig. 4 Sucrose density gradient centrifugation. (A) Preparation of a 5–20% sucrose gradient. A gradient maker with 5 and 20% sucrose solutions is connected to a peristaltic pump and a linear sucrose gradient is made in a centrifuge tube. (B) After ultracentrifugation, the sucrose gradient is fractionated by a peristaltic pump and a fraction collector.

centrifuged in another tube for estimation of sedimentation coefficients. The gradient is fractionated from the bottom of the tube using a peristaltic pump and fraction collector (Fig. 4B). Protein concentration and ATPase activity of each fraction are measured to determine the position of the outer arm dynein. SDS-PAGE is necessary to check the purity of the outer arm dynein fractions (Fig. 5). Figure 6 shows a comparison of the ICs and LCs of the outer arm dyneins purified by sucrose density gradient centrifugation from *Ciona*, the sea urchin *A. crassispina* and chum salmon *Oncorhynchus keta*.

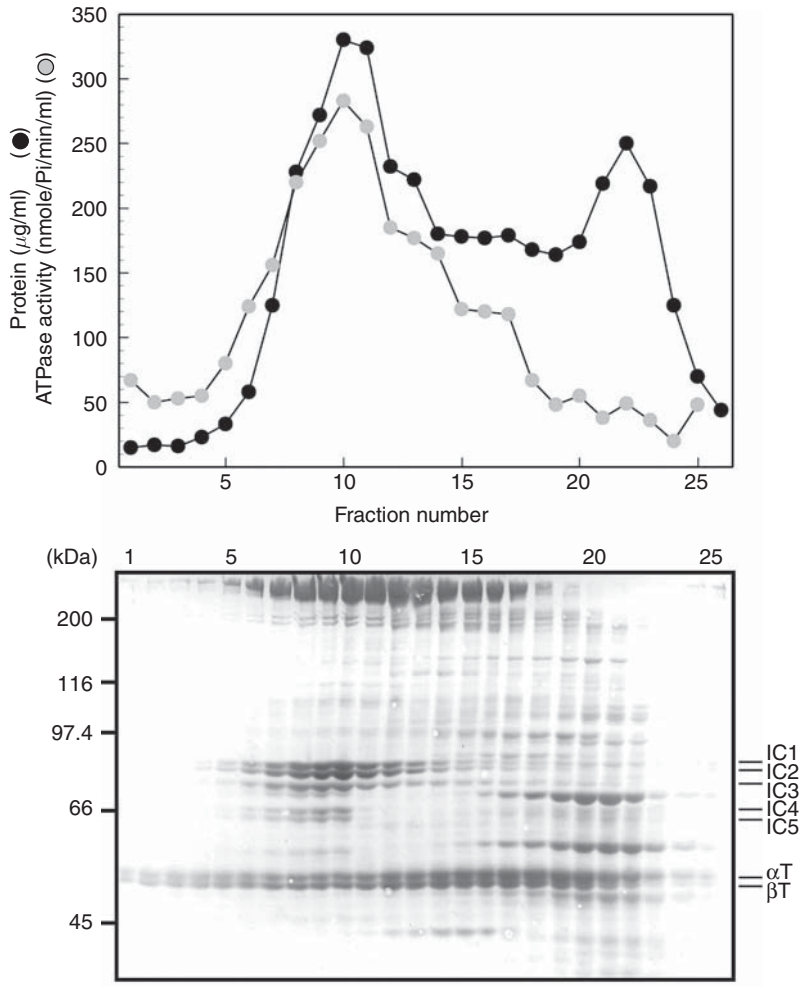

Fig. 5 Isolation of outer arm dynein from *Ciona* sperm flagella by sucrose density gradient centrifugation. The upper profile shows protein concentration and ATPase activity in each fraction. The lower figure shows 6% SDS-PAGE of each fraction. The outer arm dynein is present in fractions 6–10. The positions of the dynein ICs and tubulins are indicated.

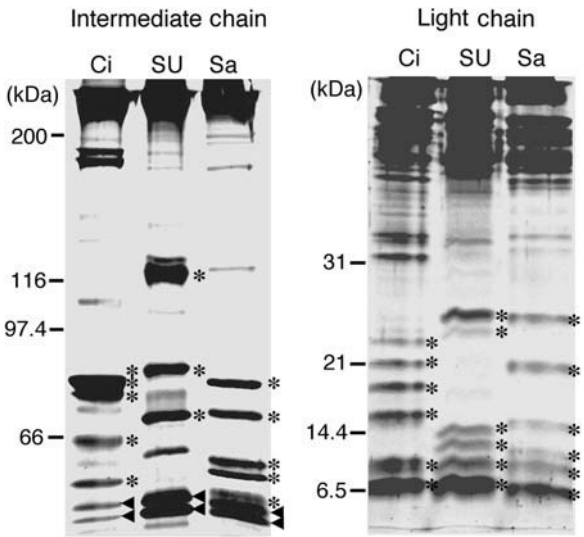

Fig. 6 Comparison of intermediate chains (ICs) and light chains (LCs) in the outer arm dyneins from *Ciona intestinalis* (Ci), sea urchin *Anthocidaris crassispina* (SU), and chum salmon *Oncohrynchus keta* (Sa). The left panel shows 6% SDS-PAGE for separation of ICs. The right panel shows 15% SDS-PAGE for separation of LCs. Asterisks indicate the positions of ICs and LCs in the three organisms. Arrowheads show the position of α- and β-tubulin. Molecular mass of each subunit is: *Ciona* ICs (IC1, 80 kDa; IC2, 78 kDa; IC3, 75 kDa; IC4, 65 kDa; IC5, 64 kDa); sea urchin ICs (IC1, 128 kDa; IC2, 98 kDa; IC3, 74 kDa); chum salmon ICs (IC1, 80 kDa; IC2, 71 kDa; IC3, 62 kDa; IC4, 60 kDa; IC5, 56 kDa); *Ciona* LCs (LC1, 23 kDa; LC2, 20 kDa; LC3, 16 kDa; LC4, 11 kDa; LC5, 8.5 kDa; LC6, 7.5 kDa); sea urchin LCs (LC1, 23 kDa; LC2, 22 kDa; LC3, 15.5 kDa; LC4, 9 kDa; LC5, 8.5 kDa; LC6, 7.5 kDa); chum salmon LCs (LC1, 24 kDa; LC2, 20 kDa; LC3, 15 kDa; LC4, 9.5 kDa; LC5, 8.5 kDa; LC6, 7.5 kDa).

Gel filtration can also be used to isolate outer arm dyneins. To date, we have tested both Superdex 200 and Superose 6 (Pharmacia Biotech Inc.) gel filtration columns connected to a liquid chromatography workstation. Both columns work well to purify outer arm dyneins (Hozumi *et al*., 2006; Padma *et al*., 2001).

E. Dissociation of Two-Headed Dynein

Removal of divalent cations under low-salt conditions induces dissociation of two-headed outer arm dynein into single head species. To induce the dissociation, the dynein fractions from the sucrose gradients are pooled and placed in a dialysis bag. They are then dialyzed against a large excess of buffer containing 5 mM Tris-HCl (pH 8.0) and 1 mM EDTA overnight with two changes of the buffer. The outer arm dynein from sea urchin dissociates into three main subcomplexes: the α heavy chain fraction, the β heavy chain/IC 1 fraction, and the IC2/IC3 fraction (Tang *et al*., 1982). The subunits of outer arm dynein from rainbow trout were also isolated in a similar way (King *et al*., 1990).

F. Further Purification by Ion Exchange Column Chromatography

The outer arm dynein fractions isolated by sucrose density gradient centrifugation still contain other axonemal components. The dynein from the sucrose density gradients can be further purified by anion exchange column chromatography, using MonoQ or Poros HQ columns (Fig. 7). Outer arm dyneins elute from the column with relatively low salt concentrations, whereas α- and β-tubulins and other contaminants in the sucrose density gradient fractions require higher salt concentrations for elution.

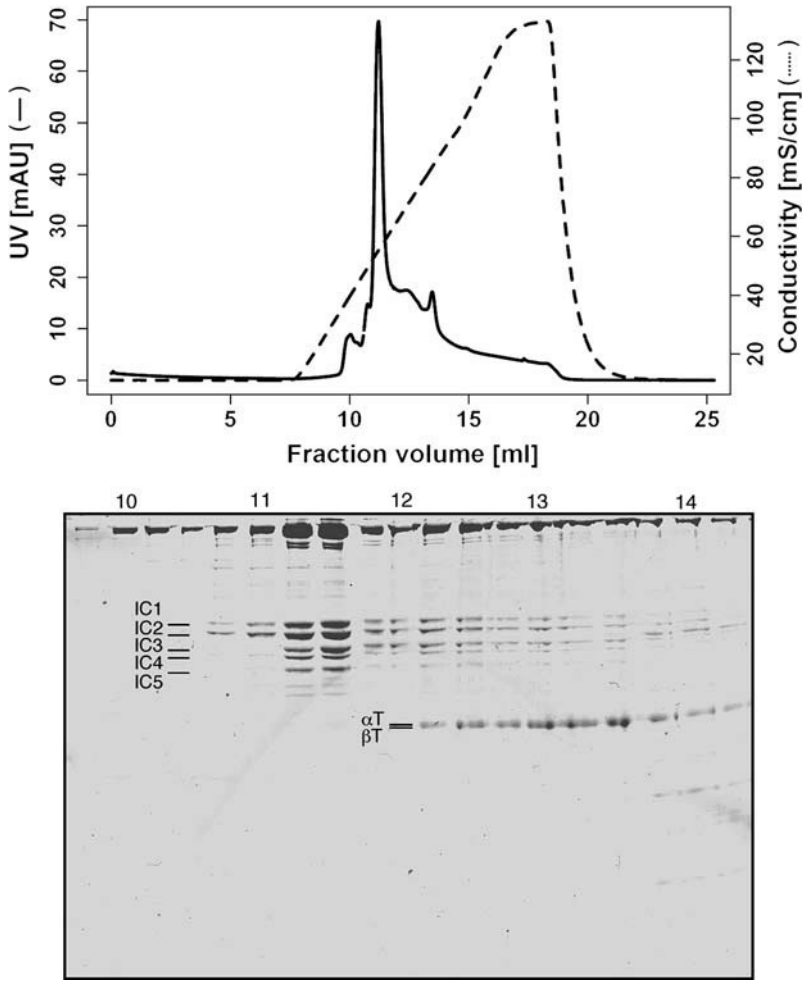

Fig. 7 MonoQ anion exchange column chromatography of *Ciona* outer arm dynein. Outer arm dynein from the sucrose density gradient is further purified. The upper panel shows the protein elution profile. The lower panel shows SDS-PAGE (10% gel) of each fraction. Note that nonsubunit components such as tubulins are separated from outer arm dynein.

G. Storage

There have been a few reports on the storage of purified axonemal dyneins. Mocz and Gibbons (1990) reported the precipitation of dynein by 60% ammonium sulfate. We recently developed a method to store purified outer arm dynein from *Ciona* sperm flagella by quick liquid N_2 freezing of sucrose density gradient fractions in polypropylene tubes. After thawing the dynein samples at room temperature or in one's hand, the previously frozen dynein displayed apparently normal activity as measured by *in vitro* gliding of singlet microtubules (K. Mizuno and K. Inaba, unpublished data).

VI. Regulation of Outer Arm Dynein

Once sea urchin sperm are exposed to seawater, Na^+ triggers the activation of motility. By using choline chloride instead of NaCl, nonactivated sperm can be obtained (Nishioka and Cross, 1978). In *C. intestinalis*, the sperm are typically immotile in seawater but can show motility depending on season. They are naturally activated by an egg-derived substance, called SAAF (sperm-activating and -attracting factor) (Yoshida *et al*., 2002). Fish sperm are completely immotile in a solution isotonic to body fluid, but are activated by the salt conditions for spawning: hypoosmotic conditions for freshwater fish and hyperosmotic conditions for seawater fish (Morisawa and Suzuki, 1980).

Activation of sperm motility is accompanied by phosphorylation or dephosphorylation of axonemal proteins. It is possible that depletion of ATP during the preparation of dynein results in the isolation of dynein with partly dephosphorylated subunits. To identify the phosphorylated subunits, 10 μM cAMP, 1 mM ATP, and an inhibitor of protein phosphatases (1 μM okadaic acid), can be added to the DB, AXB, and the high-salt solution for extraction of outer arm dynein (Inaba *et al*., 1998, 1999).

Ca^{2+}-binding proteins are also important for the modulation of dynein activity. We usually use an EGTA-containing buffer for extraction of dynein. However, inclusion of Ca^{2+} in the purification buffers results in the isolation of outer arm dynein with an associated Ca^{2+}-binding protein (Mizuno *et al*., 2009).

VII. Purification of Inner Arm Dyneins

There have been only a few studies aimed at isolating inner arm dyneins from sperm flagella. In one case, a two-headed inner arm dynein (equivalent to the I1 or f inner arm dynein in *Chlamydomonas*) was isolated along with the outer arm dynein from *Ciona* sperm. This dynein, even though it was a two-headed species, exhibited a low sedimentation coefficient (11 S), indicating dissociation into single-headed subcomplexes (unpublished data). In another study, a low ionic strength solution was used to isolate single-headed inner arm dynein from sea urchin sperm flagella (Wada *et al*., 1991). Also, apparent single-headed dynein was isolated from Antarctic rockcod sperm

(King *et al*., 1997) and a two-headed inner arm dynein was obtained from sea urchin sperm flagella by KCl-extracted axonemes with 0.7 M NaCl and 5 mM ATP (Yokota and Mabuchi, 1994).

VIII. Conclusion

Sperm flagella are a good system for studying axonemal dyneins because large amounts of flagella can be collected for studies on the molecular composition of axonemal dyneins in metazoans. In addition, the fact that the motility is regulated by external factors allows for studies of the regulatory mechanisms that control axonemal dyneins. Here we describe general protocols for purification of outer arm dynein from sperm flagella of several species. For characterization of axonemal dyneins from other organisms, the protocols described here should be a good starting point that can be modified as needed to obtain the best recovery and purity of dyneins.

References

Bradford, M.M. (1976). A rapid and sensitive method for the quantitation of microgram quantities of protein utilizing the principle of protein-dye binding. *Anal. Biochem*. **72**, 248–254.

Gatti, J.L., King, S.M., Moss, A.G., and Witman, G.B. (1989). Outer arm dynein from trout spermatozoa: Purification, polypeptide composition, and enzymatic properties. *J. Biol. Chem*. **264**, 11450–11457.

Gibbons, I.R., and Fronk, E. (1972). Some properties of bound and soluble dynein from sea urchin sperm flagella. *J. Cell Biol*. **54**, 365–381.

Hozumi, A., Satouh, Y., Makino, Y., Toda, T., Ide, H., Ogawa, K., King, S.M., and Inaba, K. (2006). Molecular characterization of *Ciona* sperm outer arm dynein reveals multiple components related to outer arm docking complex protein 2. *Cell Motil. Cytoskeleton* **63**, 591–603.

Inaba, K. (2003). Molecular architecture of the sperm flagella: Molecules for motility and signaling. *Zool. Sci*. **20**, 1043–1056.

Inaba, K. (2007). Molecular basis of sperm flagellar axonemes: Structural and evolutionary aspects. *Ann. NY. Acad. Sci*. **1101**, 506–526.

Inaba, K., Kagami, O., and Ogawa, K. (1999). Tctex2-related outer arm dynein light chain is phosphorylated at activation of sperm motility. *Biochem. Biophys. Res. Commun*. **256**, 177–183.

Inaba, K. and Mohri, H. (1989). Dynamic conformational changes of 21S dynein ATPase coupled with ATP hydrolysis revealed by proteolytic digestion. *J. Biol. Chem*. **264**, 8384–8388.

Inaba, K., Morisawa, S., and Morisawa, M. (1998). Proteasomes regulate the motility of salmonid fish sperm through modulation of cAMP-dependent phosphorylation of an outer arm dynein light chain. *J. Cell Sci*. **111**, 1105–1115.

King, S.M., Gatti, J.L., Moss, A.G., and Witman, G.B. (1990). Outer-arm dynein from trout spermatozoa: Substructural organization. *Cell Motil. Cytoskeleton* **16**, 266–278.

King, S.M., Marchese-Ragona, S.P., Parker, S.K.H., and Detrich, H.W., III. (1997). Inner and outer arm axonemal dyneins from the Antarctic rockcod *Notothenia coriiceps. Biochemistry* **36**, 1306–1314.

Mizuno, K., Padma, P., Konno, A., Satouh, Y., Ogawa, K., and Inaba, K. (2009). A novel neuronal calcium sensor family protein, calaxin, is a potential Ca^{2+}-dependent regulator for the outer arm dynein of metazoan cilia and flagella. *Biol. Cell* **101**, 91–103.

Mocz, G., and Gibbons, I.R. (1990). A circular dichroic study of helical structure in flagellar dynein. *Biochemistry* **29**, 4839–4843.

Mohri, H., Inaba, K., Kubo-Irie, M., Takai, H., and Toyoshima, Y.Y. (1999). Characterization of outer arm dynein in sea anemone, *Anthopleum midori*. *Cell Motil. Cytoskeleton* **44**, 202–208.

Morisawa, M., and Suzuki, K. (1980). Osmolality and potassium ion: Their roles in initiation of sperm motility in teleosts. *Science* **210**, 1145–1147.

Nishioka, D., and Cross, N. (1978). The role of external sodium in sea urchin fertilization. *In* "Cell Reproduction" (E.R. Dirsken, D. Prescott, and D.F. Fox, eds.), pp. 403–413. Academic Press, New York.

Padma, P., Hozumi, A., Ogawa, K., and Inaba, K. (2001). Molecular cloning and characterization of a thioredoxin/nucleoside diphosphate kinase related dynein intermediate chain from the ascidian, *Ciona intestinalis*. *Gene* **275**, 177–183.

Stephens, R.E., and Prior, G. (1992). Dynein from serotonin-activated cilia and flagella: Extraction characteristics and distinct sites for cAMP-dependent protein phosphorylation. *J. Cell Sci.* **103**, 999–1012.

Tang, W.J.Y., Bell, C.W., Sale, W.S., and Gibbons, I.R. (1982). Structure of the dynein-1 outer arm in sea urchin sperm flagella. I. Analysis by separation of subunits. *J. Biol. Chem*. **257**, 508–515.

Taussky, H.H., and Shorr, E. (1953). A microcolorimetric method for the determination of inorganic phosphorus. *J. Biol. Chem*. **202**, 675–685.

Wada, S., Okuno, M., and Mohri, H. (1991). Inner arm dynein ATPase fraction of sea urchin sperm flagella causes active sliding of axonemal outer doublet microtubule. *Biochem. Biophys. Res. Commun*. **175**, 173–178.

Wada, S., Okuno, M., Nakamura, K.-I., and Mohri, H. (1992). Dynein of sperm flagella of oyster belonging to Protostomia also has a 2-headed structure. *Biol. Cell*. **76**, 311–317.

Yokota, E., and Mabuchi, I. (1994). Isolation and characterization of a novel dynein that contains C and A heavy chains from sea urchin sperm flagellar axonemes. *J. Cell Sci*. **107**, 345–351.

Yoshida, M., Murata, M., Inaba, K., and Morisawa, M. (2002). A chemoattractant for ascidian spermatozoa is a sulfated steroid. *Proc. Natl. Acad. Sci. USA* **99**, 14831–14836.

This page intentionally left blank

CHAPTER 5

Protein Engineering Approaches to Study the Dynein Mechanism using a *Dictyostelium* Expression System

Takahide Kon, Tomohiro Shima, *and* Kazuo Sutoh

Department of Life Sciences, Graduate School of Arts and Sciences, University of Tokyo, Komaba 3-8-1, Tokyo 153-8902, Japan

Abstract

Dyneins are microtubule-based motor complexes that power a wide variety of motile processes within eukaryotic cells, including the beating of cilia and flagella and intracellular trafficking along microtubules. Mechanistic studies on dynein have been hampered by their enormous size (molecular masses of 0.5–3 MDa) and molecular complexity. However, the

METHODS IN CELL BIOLOGY, VOL. 92

978-0-12-374974-1
DOI: 10.1016/S0091-679X(08)92005-7

recent establishment of recombinant expression systems for cytoplasmic dynein, together with structural and functional analyses, has advanced our understanding of the molecular mechanisms of dynein motility. Here, we describe several protocols for protein engineering approaches to the dynein mechanism using a *Dictyostelium discoideum* expression system. We first describe the design and preparation of recombinant dynein suitable for mechanistic studies. We then discuss two distinct functional assays that take advantage of the recombinant dynein. One is for detection of dynein's conformational changes during the ATPase cycle. Another is an *in vitro* motility assay at multiple- and single-molecule levels for examination of the dynamic behavior of dynein moving on a microtubule.

I. Introduction

Dyneins are enormous motor complexes that utilize ATP as an energy source to move toward the minus ends of microtubules (Gibbons and Rowe, 1965; Paschal and Vallee, 1987). This motor activity is critical to diverse cellular processes within eukaryotic cells, including the beating of cilia and flagella, mitosis, cell migration, and the intracellular trafficking of various vesicles and organelles along microtubules (DiBella and King, 2001; Karki and Holzbaur, 1999; Vale, 2003; Vallee *et al.*, 2004).

Dyneins generate a broad range of cellular motile activities by the coordinated actions of a number of subunits that comprise the dynein complex (Pfister *et al.*, 2006; Sakato and King, 2004). Among them, the dynein heavy chain, belonging to the AAA^+ superfamily of mechanochemical enzymes (Neuwald *et al.*, 1999), is solely responsible for the fundamental motor activity (Koonce and Samso, 1996; Nishiura *et al.*, 2004). The heavy chain is composed of three structurally and functionally distinct domains referred to as head, tail, and stalk (Fig. 1). The head contains six tandemly linked AAA^+ modules (AAA1–AAA6) arranged in a ring-shaped structure (Samso *et al.*, 1998) and acts as an ATPase unit (Gibbons *et al.*, 1987; Kon *et al.*, 2004;

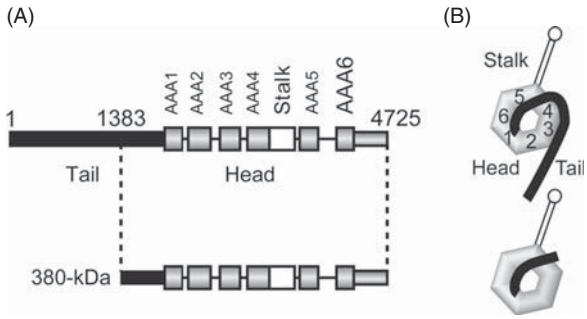

Fig. 1 Structural organization of the *Dictyostelium* dynein heavy chain. (A) Schematic diagram of the primary sequence of the dynein heavy chain. The heavy chain is composed of the tail, the head containing six AAA^+ modules (AAA1–AAA6), and the stalk. (B) A structural model of the heavy chain illustrating the ring-shaped structure of the head and the elongated stalk and tail domains.

Reck-Peterson and Vale, 2004; Silvanovich *et al.*, 2003). The tail and stalk domains emerge from the head as long, slender structures (Burgess *et al.*, 2003; Goodenough and Heuser, 1984). The tail is responsible for multimerization of the heavy chains and binding to cargo (King, 2000), whereas the stalk functions as an ATP-sensitive microtubule-binding site of dynein (Gee *et al.*, 1997; Koonce, 1997).

The molecular mechanism of action of dynein is still poorly understood when compared to that of other AAA^+ machines and cytoskeletal molecular motors. This is partly because the establishment of an expression and purification system for recombinant dynein retaining full motor activity has been hampered because of the huge size (molecular mass of >500 kDa) and the molecular complexity of the dynein heavy chain. However, this drawback has recently been overcome by using either insect cells, budding yeast, or the cellular slime mold *Dictyostelium discoideum* as expression hosts for the production of cytoplasmic dyneins (Mazumdar *et al.*, 1996; Nishiura *et al.*, 2004; Reck-Peterson *et al.*, 2006). The genetically engineered dyneins produced using these expression systems, together with biochemical, structural, and single-molecule analyses, have opened new avenues to investigate how dynein works (e.g., Carter *et al.*, 2008; Gennerich *et al.*, 2007; Hook *et al.*, 2005; Kon *et al.*, 2009; Shima *et al.*, 2006).

In this chapter, we describe several protocols for protein engineering approaches to the dynein mechanism using the *Dictyostelium* expression system. We begin with the design and preparation of recombinant dynein suitable for mechanistic studies. We then discuss two distinct functional assays that take advantage of the produced recombinant dynein. One is for detection of dynein's conformational changes during the ATPase cycle. Another is an *in vitro* motility assay at multiple- and single-molecule levels for examination of the dynamic behavior of dynein moving on a microtubule.

II. Preparation of Recombinant Dynein

We have used the *Dictyostelium* dynein heavy chain gene to produce recombinant dynein in *Dictyostelium* cells (Kon *et al.*, 2004; Nishiura *et al.*, 2004). Very useful and comprehensive information about *Dictyostelium* techniques can be found in books (e.g., see Eichinger and Rivero, 2006; Spudich, 1987) and on the dictyBase/the Dicty Stock Center web site (http://dictybase.org/). Here, we first mention several features of the heavy chain gene and expression system that should be helpful in the design and construction of expression plasmids. We then focus on particular methods for the expression and purification of recombinant dynein from *Dictyostelium* cells.

A. Materials

1. For Cultivation of *Dictyostelium* Cells

HL5 medium: Add 14.3 g proteose peptone No. 3 (Becton Dickinson 211693), 7.15 g yeast extract (Becton Dickinson 212750), 15.4 g glucose, 0.49 g KH_2PO_4 and 1.28 g $Na_2HPO_4 \cdot 12H_2O$ to 1 l of deionized water, autoclave at 121°C for 15 min,

remove from the autoclave immediately to avoid overcaramelization and store at room temperature. For regular use, add 6 ml of a penicillin–streptomycin mixture (Invitrogen 15140-148) to 1 l of the HL5 medium to avoid bacterial contamination and growth. We usually test the quality of the proteose peptone before purchasing in large quantities because this may influence the growth rate of *Dictyostelium* cells significantly. Premixed medium powder can be purchased from ForMedium (HL5 medium including glucose; HLG0102).

10 mg/ml G418: dissolve in water, filter-sterilize, and store at –30°C.

10 mg/ml blasticidin S (Funakoshi KK-400): dissolve in water, filter-sterilize, and store at –30°C.

10 mg/ml tetracycline: dissolve in 50% ethanol and store in the dark at –30°C.

H-50 electroporation buffer (Pang *et al*., 1999): 20 mM HEPES, 50 mM KCl, 10 mM NaCl, 1 mM $MgSO_4$, 5 mM $NaHCO_3$ and 1 mM NaH_2PO_4, pH 7.0. Autoclave and store at 4°C.

2. For Purification of Recombinant Dynein

100 mM ATP (Sigma A2383): dissolve in water, adjust pH to 7.0, and store at –30°C.

2 mg/ml chymostatin/pepstatin (Peptide Institute 4063 and 4397): dissolve in DMSO and store at −30°C.

10 mg/ml leupeptin (Peptide Institute 4041): dissolve in water and store at –30°C.

100 mM PMSF: dissolve in DMF and store at −30°C.

Ni-NTA agarose (Qiagen 30230)

AntiFLAG M2 affinity gel (Sigma A2220)

5 mg/ml FLAG peptide (Sigma F3290): dissolve in the PMEG30 buffer and store at –30°C.

Lysis buffer: 100 mM PIPES, 4 mM $MgCl_2$, 0.1 mM EGTA, 0.9 M glycerol, and 10 mM imidazole, pH 7.0; filter through a 0.22 μm nitrocellulose membrane and store at 4°C. Prior to immediate use, add 10 μg/ml chymostatin/pepstatin, 50 μg/ml leupeptin, 0.5 mM PMSF, 1 mM 2-mercaptoethanol, and 0.1 mM ATP.

Wash buffer: 100 mM PIPES, 4 mM $MgCl_2$, 0.1 mM EGTA, 0.9 M glycerol, and 20 mM imidazole, pH 7.0; filter through a 0.22 μm nitrocellulose membrane and store at 4°C. Prior to immediate use, add 10 μg/ml chymostatin/pepstatin, 50/μg ml leupeptin, 0.5 mM PMSF, 1 mM 2-mercaptoethanol, and 0.1 mM ATP.

Elution buffer: 100 mM PIPES, 4 mM $MgCl_2$, 0.1 mM EGTA, 0.9 M glycerol, and 250 mM imidazole, pH 7.0; filter through a 0.22 μm nitrocellulose membrane and store at 4°C. Prior to immediate use, add 10 μg/ml chymostatin/pepstatin, 50 μg/ml leupeptin, 0.5 mM PMSF, 1 mM 2-mercaptoethanol, and 0.1 mM ATP.

PMEGS buffer: 100 mM PIPES, 4 mM $MgCl_2$, 5 mM EGTA, 0.1 mM EDTA, 0.9 M glycerol, and 150 mM NaCl, pH 7.0. Store at 4°C and prior to immediate use add 10 μg/ml chymostatin/pepstatin, 50 μg/ml leupeptin, 0.5 mM PMSF, 1 mM DTT, and 0.1 mM ATP.

PMEG30 buffer: 30 mM PIPES, 4 mM $MgCl_2$, 5 mM EGTA, 0.1 mM EDTA, and 0.9 M glycerol, pH 7.0. Store at 4°C and prior to immediate use, add 10 μg/ml

chymostatin/pepstatin, 50 μg/ml leupeptin, 0.5 mM PMSF, 1 mM DTT, and 0.1 mM ATP.

Cryostorage buffer: 2.5 M sucrose (nuclease and protease tested, Nacalai 30406-25), 35 mM Tris-HCl and 5 mM $MgSO_4$, pH 7.2.

B. Construction of Plasmids for Expression of Recombinant Dynein

The *Dictyostelium* dynein heavy chain is a protein of 4725 residues encoded by a 14-kbp cDNA fragment (Fig. 1; Koonce *et al.*, 1992). The nucleotide sequence of our cDNA for the heavy chain is slightly different from the originally reported sequence, but is identical to DDB0185096 in the dictyBase. We primarily use the C-terminal 380-kDa portion of the heavy chain (hereafter referred to as the 380-kDa dynein) for mechanistic studies. This portion forms a monomeric motor that contains the N-terminal truncated tail and the entire head and stalk domains (Fig. 1; Koonce and Samso, 1996) while retaining dynein's motor activity (Nishiura *et al.*, 2004). The 380-kDa dynein region (10-kbp DNA encoding V1383–I4725) of the heavy chain gene does not include any introns and can therefore be easily cloned using genomic PCR methods. The heavy chain gene may be unstable in standard *Escherichia coli* strains such as JM109 and DH5α because of its large size and high A+T content. We thus use *E. coli* strains designed for cloning of unstable DNA fragments, such as Stbl2 (Invitrogen 10268-019) and SURE (Stratagene 200227), for the genetic manipulations. Point mutations, insertions, and deletions within the dynein gene are created using PCR-based methods (e.g., QuikChange mutagenesis kit, Stratagene) according to the manufacturer's instructions.

To facilitate purification, we genetically add affinity tags, such as His_6 and FLAG (DYKDDDDK), at the N-terminus of the 380-kDa dynein. In addition, we frequently use several N-terminal tags such as EGFP, BioEase (Invitrogen), and glutathione *S*-transferase (GST) for *in vivo* fluorescent labeling, biotinylation, and dimerization of the dynein heavy chain, respectively. The resulting DNA fragment encoding the dynein heavy chain fused with appropriate tags is subcloned into the unique MluI site of the expression vector MB38 (ID 45 in the Dicty Stock Center).

To overexpress the recombinant heavy chain in *Dictyostelium* cells, we have employed a tetracycline-regulated (Tet-off) expression system (Blaauw *et al.*, 2000). In this system, the MB35 plasmid (ID 44 in the Dicty Stock Center) encoding a tetracycline-controlled transcriptional activator is first introduced into *Dictyostelium* cells by multicopy genomic integration. The cells are subsequently transformed by an MB38-based plasmid harboring the dynein gene preceded by an inducible promoter. The resulting cells inducibly express the recombinant dynein when tetracycline is removed from the culture medium. This system has allowed us to express various dynein mutants, even when overexpression of the mutants was potentially harmful to the cells (Kon *et al.*, 2004).

C. Transformation and Cultivation of *Dictyostelium* Cells

To overexpress recombinant dynein, the MB35-integrated *Dictyostelium* cells are transformed by an expression plasmid, selected, and cultivated as follows:

1. Cultivate the cells at 22°C in 10-cm culture dishes containing 10 ml of HL5 medium supplemented with 10 μg/ml G418 and 12 μg/ml tetracycline until the cells reach confluence.
2. Pellet the cells harvested from the 10-cm dish by centrifugation at 500×*g* for 5 min at 4°C.
3. Wash the cells by resuspending in 10 ml of ice-cold H-50 electroporation buffer and pelleting them again at 500×*g* for 5 min at 4°C.
4. Resuspend the cell pellet in 100 μl of H-50 buffer and mix the suspension with 1–5 μg of the dynein expression plasmid.
5. Transfer the cell suspension into an ice-cold electroporation cuvette with a 1-mm gap.
6. Electroporate the cells using the Bio-Rad Gene Pulser at 0.85 kV/25 μF and incubate the cuvette on ice for 5 min.
7. Transfer the cells to a 10-cm culture dish containing 10 ml of HL5 medium supplemented with 10 μg/ml G418 and 12 μg/ml tetracycline.
8. Add 10 μg/ml blasticidin S the following day.
9. Incubate the cells for ~7 days at 22°C until colonies of the transformants are clearly visible and replace the medium with fresh HL5 supplemented with the three drugs.
10. After additional 2–3 days incubation at 22°C, the transformed cells reach confluence. For routine maintenance, dilute the cell culture to ~1/50 in fresh medium every 3–4 days.
11. To start a culture for recombinant dynein preparation, inoculate ~3×10^7 cells harvested from a confluent culture in a 10-cm dish into 800 ml of HL5 supplemented with the three drugs in two 1-l flasks and incubate at 22°C with shaking at 150 rpm.
12. To induce the expression of dynein, harvest the cells at a density of ~1×10^7 cells/ml (after ~5–6 days of cultivation) by centrifugation at 1320 g for 5 min. After removal of the medium, resuspend the cell pellets in 2 l of HL5 supplemented only with 10 μg/ml G418 in four 1-l flasks and incubate at 22°C with shaking at 150 rpm for ~24 h. In the case of constructs containing biotin tags, add 30 μM of d-biotin to the medium at the time of the induction to increase the efficiency of *in vivo* biotinylation.

D. Purification of Recombinant Dynein

Purification methods for native cytoplasmic and axonemal dyneins have been established for various biological sources. However, our preliminary results suggest that they are not readily applicable to the preparation of the *Dictyostelium* recombinant dynein with retained reproducible motor activity. We have therefore developed a

simple and rapid procedure that employs two sequential affinity purification steps using genetically introduced His_6 and FLAG tags. This procedure with the tetracycline-regulated expression in *Dictyostelium* cells of a 2–6-l culture yields relatively large quantities of purified recombinant dynein (up to 1–6 mg) with high motor activity (~90% of the dynein molecules in our preparations have been found to be active as judged by a microtubule-binding assay), which would be suitable for many biochemical and biophysical studies. The following protocol refers to a 2-l culture, grown in HL5 medium in four 1-l flasks, which we use for routine examination of various mutant dyneins. The culture will yield 30–40 g of wet cells, which in turn will yield 1.0–1.5 mg of the purified 380-kDa dynein.

1. All solutions are ice-cold and all operations are performed at 0–4°C because *Dictyostelium* cells contain relatively large amounts of proteases.
2. Harvest cultured cells by centrifugation at 1320×g for 5 min and wash the cells by resuspending in ~250 ml of 17 mM KPi buffer (pH 6.8) and pelleting them again at 1320×g for 7 min.
3. Resuspend the cell pellets in an equal volume of lysis buffer (~30–40 ml).
4. Disrupt the suspended cells by sonication in 6×10-s bursts at the maximum power on a TOMY UR-20P, with a 30-s cooling period between each sonication burst. Under these conditions, typically >95% of the cells are lysed as judged by microscopic observations.
5. Sediment cell debris by centrifugation at 24,000×*g* for 20 min, collect the supernatant, and clarify further by centrifugation at 187,000×*g* (45,000 rpm in a Hitachi RP-50T rotor) for 60 min.
6. Transfer the resulting high-speed supernatant to a conical tube with 2.5 ml of Ni-NTA agarose preequilibrated with lysis buffer and mix gently for ~1 h using a rotating wheel.
7. Load the mixture into an empty column and discard the column flow-through.
8. Wash the Ni-NTA agarose with 5 column volumes (CV; ~13 ml) of wash buffer.
9. Elute slowly (~0.4 ml/min) the bound proteins with 2 CV (5 ml) of elution buffer.
10. Mix the eluate with 150 mM NaCl, 5 mM EGTA, and 0.1 mM EDTA.
11. Transfer the mixture to a conical tube with 0.5 ml of antiFLAG M2 affinity gel preequilibrated with the PMEGS buffer and mix gently for 1.5–2 h using a rotating wheel.
12. Load the mixture into an empty column and discard the column flow-through.
13. Wash the antiFLAG gel with 8 CV (~4 ml) of PMEGS buffer.
14. Wash the antiFLAG gel with 16 CV (~8 ml) of PMEG30 buffer.
15. Elute slowly (<0.4 ml/min) the bound recombinant dynein with 6 CV (3 ml) of PMEG30 buffer containing 0.2 mg/ml FLAG peptide.
16. To remove aggregated proteins, centrifuge the eluate at 100,000×*g* (43,000 rpm in a Beckman TLA 100.3 rotor) for 10 min and collect the supernatant for mechanistic studies.
17. Examine the purity of the recombinant dynein by 5% or 4–20% SDS-PAGE with Coomassie blue staining.

For biochemical assays such as microtubule binding, ATPase, and fluorescence resonance energy transfer (FRET) measurements, the purified proteins are stored on ice and used within 3 days. For *in vitro* microtubule-gliding and single-molecule motility assays, the preparations can be stored in liquid nitrogen after mixing at a ratio of 10:4 with a cryostorage buffer. The protein can be used after thawing and centrifugation at 88,000×*g* (45,000 rpm in a Beckman TLA 120.2 rotor) for 10 min at 2°C.

Purified 380-kDa dynein (HFG380) shows a basal ATPase rate of 5.7/s, and the addition of microtubules activates the rate with estimated k_{cat} and K_m (MT) values of 120.3/s and 31 μM, respectively (Kon *et al.*, 2004). Contaminating ATPase/motor proteins in our preparations are below the levels of detection, as evaluated by measuring ATPase and microtubule-gliding activities of preparations from *Dictyostelium* cells transformed with an empty vector.

III. FRET-Based Detection of Dynein's Conformational Changes

A crucial mechanism underlying the motor activity of dynein is the conformational changes that generate unidirectional movements along a microtubule. EM studies have suggested that swinging or docking/undocking motions of the tail domain relative to the head domain are major contributors to the movements of dynein (Burgess *et al.*, 2003; Ueno *et al.*, 2008). This section describes a FRET-based method to detect and monitor directly the tail motions under physiologically relevant conditions using a genetically engineered dynein that contains EGFP and EBFP as FRET sensors (Kon *et al.*, 2005).

A. Materials

Dynein assay buffer: 10 mM K-PIPES, 50 mM potassium acetate, 4 mM $MgSO_4$, and 1 mM EGTA, pH 7.0. Store at 4°C and add 1 mM DTT immediately before use.
100 mM ADP (Sigma A5285): dissolve in water, adjust pH to 7.0, and store at –30°C.
Desalting columns: NAP-5, NAP-10, or PD-10 (GE Healthcare).
Perkin–Elmer LS50B fluorophotometer equipped with a circulating water bath.

B. Design of FRET-Based Sensors for Dynein's Tail Motions

FRET has been widely used for detection of the intra- or intermolecular dynamics of proteins. Based on the FRET efficiency between a pair of fluorescent moieties (donor and acceptor), we can estimate the distance between them and thus can monitor conformational changes occurring in a fluorescently labeled protein. We have used EGFP and EBFP as FRET acceptor and donor, respectively, to detect and monitor directly the tail motions of dynein by means of intramolecular FRET analysis. To achieve this, EGFP was fused to the tail and EBFP was inserted into the head domain

of the 380-kDa dynein by genetic manipulations. To facilitate independent folding of the three portions of the fusion protein, that is, EGFP, EBFP, and dynein, flexible spacers have been inserted between them: for the fusion of EGFP (Val2−Lys238) to the N-terminus of the 380-kDa dynein, Gly-Gly-Gly-Lys was used as a spacer; for the insertion of EBFP (Val2−Lys238), Thr-Gly-Gly-Gly and Gly-Gly-Gly-Thr-Gly were attached at the N-terminus and C-terminus of EBFP, respectively, as spacers.

Selection of insertion sites for EBFP within the head domain would be critical for the success of the FRET analysis. By inserting at nonconserved regions of cytoplasmic dynein heavy chains, we have created seven types of 380-kDa dynein, each of which contains EBFP at different locations (Roberts *et al.*, 2009). Although EGFP/EBFP are relatively large tags (27 kDa), these insertions have little effect on either the motor activity or the overall fold of the 380-kDa dynein. Among them, HG380B1, HG380B2, and HG380B7 were used for FRET-based detection of the tail motions (Fig. 2A). They have His_6-EGFP at the N-terminus of the tail and EBFP inserted either into a junction region between the AAA1 and AAA2 modules (site 1; between Ala2172 and Glu2173), into the AAA2 module (site 2; between Ser2471 and Ser2472) or into the C-terminal region (site 7; between Ser4450 and Ser4451) of the head domain. Indeed, all three constructs show ATP-dependent reciprocal changes in EGFP/EBFP emissions (Fig. 2B), a hallmark of FRET, which would probably reflect the expected tail motions relative to the head domain. We routinely use HG380B2 (or HFG380B2) for monitoring the tail motions because this construct exhibits the largest changes in the FRET signal.

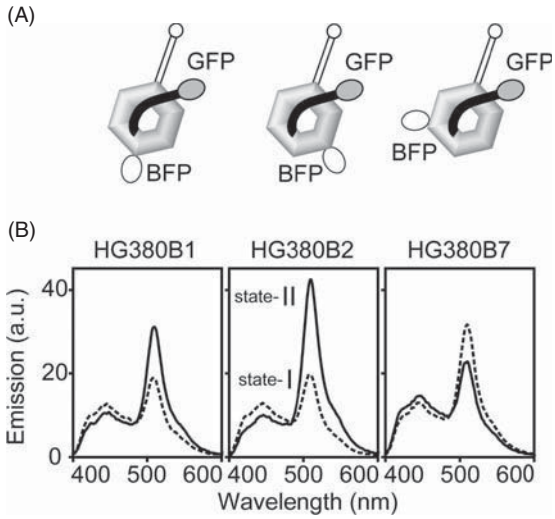

Fig. 2 Fluorescence resonance energy transfer (FRET)-based detection of the tail motions of dynein. (A) Design of the 380-kDa dynein containing FRET sensors for detection of the tail motions. In these constructs, EGFP and EBFP were genetically fused into the tail and head domains, respectively. (B) Emission spectra of the EGFP/EBFP-labeled 380-kDa dyneins excited at 380 nm in the presence of 200 μM ADP (dotted lines) or ATP (solid lines). The fluorescence measurements detected two FRET states, state I and state II. Reproduced from Kon *et al.* (2005).

C. Fluorescence and FRET Measurements

Steady-state fluorescence of the 380-kDa dyneins fused with EGFP and EBFP is measured and FRET efficiency is estimated as follows:

1. On the day of the experiment, replace the solvent of the purified dynein with dynein assay buffer supplemented with 0.1 mM ADP using a desalting column. We usually add ~0.1 mM ADP to the dynein preparations since the 380-kDa dynein may be unstable in the absence of adenine nucleotides. For examination of the apo (no nucleotide) state of dynein, ADP is omitted from the buffer and the experiments should be performed within ~6 h following buffer replacement.
2. Equilibrate the dynein solution at 25°C for 2 min and mix with the selected nucleotide. The final concentrations of dynein and the nucleotides are typically 125 nM and 0–1000 μM, respectively.
3. Record the emission from 400–600 nm with excitation at a wavelength of 380 nm (EBFP excitation) and then measure that from 500–600 nm with excitation at 488 nm (EGFP excitation). Background fluorescence from the buffer solution should be determined and subtracted from the spectral data. The measurements are performed in a total volume of 400 μl at 25°C using a Perkin–Elmer LS50B fluorophotometer.
4. Calculate FRET efficiency (E) from the sensitized emission of the acceptor (EGFP) according to the method of Clegg (1992) as previously applied to myosin (Suzuki *et al.*, 1998) using Eq. (1):

$$E = \{F^{a}{}_{\mathrm{FRET}}/F^{a}{}_{\mathrm{DIR}} - \varepsilon^{a}(380)/\varepsilon^{a}(488)\}\varepsilon^{a}(488)/\varepsilon^{d}(380) \quad (1)$$

where the superscripts d and a refer to donor (BFP) and acceptor (GFP), respectively; $\varepsilon^{a}(380)$, $\varepsilon^{a}(488)$, and $\varepsilon^{d}(380)$ are the molar extinction coefficients of the acceptor and donor at the designated wavelength; $F^{a}{}_{\mathrm{FRET}}$ is the fluorescence intensity of the acceptor at 510 nm when the donor is excited at 380 nm; $F^{a}{}_{\mathrm{DIR}}$ is the fluorescence intensity of the acceptor at 510 nm when it is directly excited at 488 nm. We have used 55,000/31,000/M/cm as the $\varepsilon^{a}(488)/\varepsilon^{d}(380)$ value and 0.08 as the $\varepsilon^{a}(380)/\varepsilon^{a}(488)$ value for HFG380B2.

FRET analysis of HFG380B2 has shown that, depending on the bound nucleotide, dynein adopts either of two FRET states, termed state I and state II that exhibit low FRET (E, ~5%) and high FRET (E, 20–35%), respectively. The states probably correspond to the two conformations with distinct tail positions detected by EM analyses (Roberts *et al.*, 2009). Thus, the FRET analysis together with nucleotide and/or mutation trapping can be used to determine the relationships between the tail positions and the ATPase steps of dynein (Kon *et al.*, 2005). Furthermore, the FRET signal can also be utilized to monitor directly the tail motions using stopped flow methods (Imamula *et al.*, 2007; Mogami *et al.*, 2007).

IV. Motility Assays

This section describes *in vitro* assays that use darkfield or fluorescence microscopy to visualize directly the dynein motility along a microtubule track. The methods can be used to examine motile properties of mutant dyneins. Furthermore, in combination with recombinant dynein that contains site-specific probes such as biotin moieties, fluorescent dyes and quantum dots (Qdot), the motility assays allow us to examine the motions of the labeled domain (Reck-Peterson *et al.*, 2006) and their contributions to the motor activity of dynein (Shima *et al.*, 2006). Here we present basic protocols for two types of the methods, microtubule-gliding and single-molecule fluorescence assays.

A. Materials

1 mg/ml streptavidin (Wako 192-11644): dissolve in dynein assay buffer, freeze in liquid nitrogen, and store at –80°C. After thawing, filter using a 0.22 μm membrane (Millipore Millex-GV 4 mm).

2 mg/ml biotinamidocaproyl BSA (Sigma A-6043): dissolve in dynein assay buffer, freeze in liquid nitrogen, and store at –80°C.

Casein: dissolve 10 mg of casein powder (Hammarsten, Merck) in 1 ml of casein buffer (10 mM Tris-HCl and 200 mM NaCl, pH 8.8), rotate for 2 h at 4°C, centrifuge at 541,000×*g* (100,000 rpm in a Beckman TLA 100.3 rotor) for 10 min at 4°C, and collect the supernatant.

Tubulin: isolated from porcine brain by two cycles of assembly and disassembly and separated from microtubule-associated proteins (MAPs) by phosphocellulose chromatography according to the procedure of Williams and Lee (1982). Store in liquid nitrogen.

Microtubules: assembled from MAP-depleted tubulin at 37°C for 30 min and stabilized with 40 μM paclitaxel (Sigma T1912).

Oregon Green 488-labeled microtubules: assembled from Oregon Green 488-labeled tubulin prepared according to the procedure of Hyman *et al.* (1991) at 37°C for 30 min and stabilized with 40 μM paclitaxel.

Anti-α-tubulin antibody DM1A (Millipore 05-829).

Qdot 605 streptavidin conjugate (Invitrogen Q10101MP).

Cover glass (Iwaki 2918, 18×18 mm thickness No. 1 and Matsunami 24×32 mm, thickness No. 1).

Slide glass (Matsunami S7213).

Double-sided transparent tape (Scotch 3M W-18, thickness 80 μm).

Single-molecule assay buffer (S buffer): 20 mM K-PIPES, 10 mM potassium acetate, 4 mM $MgSO_4$, and 1 mM EGTA, pH 7.0; store at room temperature and add 10 μM paclitaxel immediately before use.

Final solution: add 10 mM glucose, 85 U/ml glucose oxidase (Sigma G6641), 1300 U/ml catalase (Roche 106810), 1% 2-mercaptoethanol, 0.4 mg/ml casein, and 1 mM ATP to the S buffer immediately before use.

B. Microtubule-Gliding Assay

In the microtubule-gliding assay, dynein molecules are fixed to a glass surface, and microtubules are observed to attach to and glide over the dynein-coated surface. To achieve this, a flow chamber is sequentially coated with biotinylated BSA, streptavidin, and the biotinylated 380-kDa dynein. After the addition of microtubules and ATP, the movements of microtubules are visualized with a dark-field microscope and analyzed, as detailed below.

1. Darkfield Microscopy Setup

An inverted optical microscope (Olympus IX51) is equipped with a dark field condenser (Olympus U-DCW) and 10×/0.30 and 40×/0.75 object lenses (Olympus UPlan FL). Objectives are illuminated with a mercury lamp (Osram 1×HBO 103W/2) through three UV filters (Olympus C5060), two yellow filters (Olympus GG455), a green filter (Olympus IF550), and ND filters (Olympus 45NDRef). Images are magnified by a 3.3× relay lens (Olympus PE 3.3×), acquired with an image-intensified charge-coupled device (CCD) camera (Ikegami ICD6100), averaged and contrast-enhanced with an image processor (Hamamatsu Photonics ARGUS-20), and recorded onto a hard disk via an analog/digital video converter (Canopus ADVC-300).

2. Construction of a Flow Chamber

1. To make a flow chamber, put two slices of the double-sided transparent tape on a slide glass in parallel with a distance of ~4 mm apart and place a cover glass on the tapes. The chamber volume is typically ~6 µl.
2. Coat the chamber with biotinamidocaproyl BSA by infusing one chamber volume of the protein (2 mg/ml) into the chamber, incubating for 3 min, and washing with 3 volumes of the dynein assay buffer.
3. Coat the chamber with streptavidin by infusing 1 volume of the protein (1 mg/ml), incubating for 3 min and washing with 3 volumes of the assay buffer.
4. To avoid nonspecific binding of dynein and microtubules to the glass surface, block the chamber with casein by infusing 2 volumes of the protein (8 mg/ml), incubating for 3 min, and washing with 3 volumes of the assay buffer.
5. Add 2 volumes of ~7 nM biotinylated dynein to the chamber twice at 5-min intervals and then wash out unattached dynein with 3 volumes of the assay buffer. The microtubule-gliding velocity is highly dependent on the surface dynein density. Consequently, introducing the dynein solution at an appropriate density to the chamber is important in evaluating the motility.
6. Add 1 volume of ~400 nM microtubules to the chamber, incubate for 2 min, and wash out unattached microtubules with 3 volumes of the assay buffer.

Notes. Instead of a biotin tag, purified dynein can be attached to a glass surface using other tags such as His_6 and EGFP combined with the corresponding antibodies.

In this case, a chamber is sequentially coated with streptavidin, protein G-biotin, antipenta-His or antiGFP antibodies, and finally dynein (Kon *et al.*, 2004).

3. Observation and Analysis

7. Examine the chamber using the dark-field microscope. At first, roughly focus on the upper side of the slide glass by adjusting the position of the 10× objective lens and the dark-field condenser. Subsequently focus precisely by using the 40× objective lens.
8. Add 2 volumes of ATP to the chamber and record the gliding of microtubules for 10–180 s such that the microtubules move $\geq 5\mu m$.
9. Measure the gliding velocity of a microtubule by following the leading end of the microtubule using a tracking program (Mark2; courtesy of K. Furuta, National Institute of Information and Communications Technology, Japan).

The microtubule-gliding velocity is highly sensitive to the anchoring position of the 380-kDa dynein onto the glass surface (Fig. 3). By inserting a biotinylated tag into eight different locations of the 380-kDa dynein and fixing these molecules onto the glass surface via the biotin–streptavidin linkage, we have found that high-speed

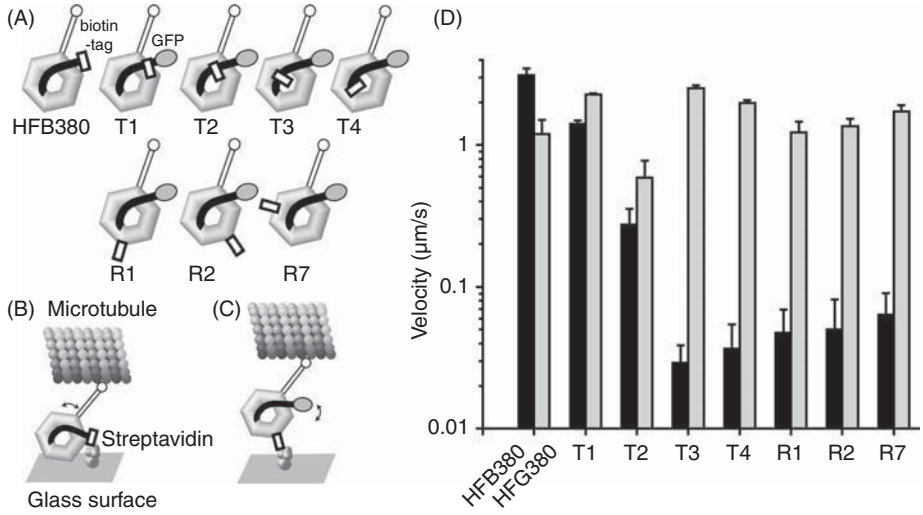

Fig. 3 Microtubule-gliding assay using genetically biotin-inserted dyneins. (A) Diagrams of the biotin-inserted dyneins. A biotin tag (white box) was inserted into the tail (HFB380, T1-4) or the AAA modules (R1, R2, R7) of the 380-kDa dynein. (B, C) Schematic drawings of the assay. The expected orientation of the 380-kDa dynein fixed on the glass surface at its tail (B) and AAA module (C). (D) Log-scale histograms of microtubule-gliding velocities. When the dyneins were fixed on a surface via their biotin tag (black bars), the microtubule gliding velocity significantly depended on the fixing positions. In contrast, when the dyneins were fixed on a surface via the N-terminal GFP tag (gray bars), the dyneins drove robust microtubule gliding independently of the biotin tag positions. Error bars indicate the standard deviation. Reproduced from Shima *et al.* (2006) with permission. Copyright (2006) the National Academy of Sciences, USA.

microtubule gliding (1–3 μm/s) requires the contribution of the distal end of the truncated tail domain (Shima *et al.*, 2006). The results have provided evidence that the tail motions detected by EM and FRET studies are primarily responsible for the motile activity of dynein.

C. Single-Molecule Fluorescence Assay

In the single-molecule assay, fluorescently labeled microtubules are fixed on a glass surface via an antibody, and Qdot-labeled dynein molecules moving along the microtubules are visualized under a total internal reflection fluorescence (TIRF) microscope as follows.

1. TIRF Microscopy Setup

An inverted optical microscope (Olympus IX71) equipped with 100×objective lens (Olympus PlanApo, NA 1.45) is set on a vibration-isolated table (Newport optics VS-4-I2000) connected with an air pump (Jun-air Minor) and the microscope stage is replaced with a stable one (G-angstrom GAS01) to reduce vibrations. A 488-nm excitation line from an argon ion laser (Melles Griot IMA101) is introduced into the microscope through a TIRFM illuminator (Olympus IX2-RFAEVA-2) and a 505-nm dichroic mirror (Olympus DM505). Fluorescence images are passed through a band-pass filter (Omega 530WB20 for Oregon Green 488 or Omega 605WB20 for Qdot 605), magnified by a 2×relay lens, and captured by a back-illuminated electron multiplier CCD camera (Andor iXon^{EM} + DV887DCS-BV) that is connected to a circulating cooling pump (Tokyo Rikakikai CCA-1111).

2. Construction of a Flow Chamber

1. Mix 1.1× the amount of Qdot 605 to HFB-GST-380 (biotinylated and dimerized 380-kDa dynein; see later) for streptavidin-mediated conjugation, incubate for 15 min, and store on ice.
2. To make a flow chamber, put two slices of the double-sided transparent tape on a cover glass (24×32 mm) in parallel with a distance of ~3 mm and place a cover glass (18×18 mm) onto the tapes. The chamber volume is typically ~5 μl.
3. Coat the chamber with anti-α-tubulin antibody by infusing one chamber volume of the protein (0.17 mg/ml) twice at 5-min intervals and then washing with 2 volumes of the S buffer.
4. Add 1 volume of Oregon Green 488-labeled microtubules, incubate for 2 min, wash out unattached microtubules with 2 volumes of the S buffer, and equilibrate and block the chamber with 1 volume of the final solution.

3. Observation and Analysis

5. Examine the chamber using the TIRF microscope with the 488-nm laser. Focus on microtubules on the glass surface.

6. Dilute the Qdot-labeled dynein to 30–300 pM with the final solution and introduce this solution into the chamber.
7. Record one still image of the microtubules.
8. Record the images of Qdot-labeled dynein for 30–200 s at 10–200 frame rates and save as an uncompressed avi file.
9. Quantify the movement of Qdot-labeled dynein by kymograph analysis or by calculating the center position of the point spread function of the image using the tracking program (Mark2). The latter method provides more detailed information of the movement if enough photons are collected.

4. Analysis using Kymograph

Make a kymograph of the movements of Qdot-labeled dynein by using the reslice plug-in of the Image J software (NIH). The x and y axes of the generated kymograph correspond to the distance along the microtubule and time points, respectively. In the kymograph, the movement of a Qdot-labeled dynein along the microtubule appears as a sloped trajectory (Fig. 4). Motility parameters such as velocity, run length, duration time on a microtubule, and directionality of the movement can be obtained by measuring the x and y coordinates of the start and the end points of the trajectory.

5. Analysis using Tracking Software

To determine the position of the Qdot-labeled dynein with high precision, fit the intensity distribution from 11×11 pixels to the two-dimensional Gaussian function at every frame (Yildiz *et al.*, 2003). Using 100-ms exposure times, the localization accuracy of the Qdot estimated by the standard deviation in 500 frames is typically ~3.5 nm in this assay system. In addition to the motility parameters described earlier,

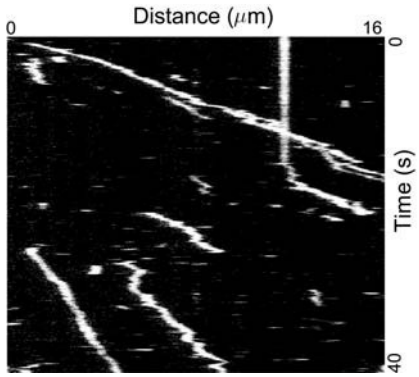

Fig. 4 Kymograph showing the movements of single molecules of the GST–dynein conjugated with Qdot 605. Images were recorded at 30 frames/s for 40 s.

the diffusion constant (D) of the dynein movements can be determined by calculating the mean square displacement (ρ) and fitting with Eq. (2):

$$\rho(\tau) = 2D\tau + v^2\tau^2 \quad (2)$$

where τ represents the nonoverlapping time intervals and v is a drift velocity (Qian *et al.*, 1991). By reducing ATP concentrations, step-wise movements of the Qdot-labeled dynein can be observed.

Like most of the other cytoskeletal motors, dimerization of two heavy chains is required for processive movements of cytoplasmic dynein along a microtubule. A recent single-molecule study using yeast cytoplasmic dynein has shown that artificial dimerization of N-terminal truncated heavy chains (corresponding to the *Dictyostelium* 380-kDa dynein) via N-terminal GST tags produces a fully functional processive motor (Reck-Peterson *et al.*, 2006). We thus use HFB-GST-380 (380-kDa dynein fused at the N terminus with His_6-FLAG-BioEase-GST tags)-based constructs for routine examination of various mutant dyneins using the single-molecule fluorescence assay.

Acknowledgments

This work was supported by a Grant-in-Aid for Young Scientists (A) from the Ministry of Education, Culture Sports, Science, and Technology of Japan, a Grant-in-Aid for Scientific Research (S) from the Japan Society of the Promotion of Science, and a grant from the Human Frontier Science Program.

References

Blaauw, M., Linskens, M.H., and van Haastert, P.J. (2000). Efficient control of gene expression by a tetracycline-dependent transactivator in single Dictyostelium discoideum cells. *Gene* **252**, 71–82.

Burgess, S.A., Walker, M.L., Sakakibara, H., Knight, P.J., and Oiwa, K. (2003). Dynein structure and power stroke. *Nature* **421**, 715–718.

Carter, A.P., Garbarino, J.E., Wilson-Kubalek, E.M., Shipley, W.E., Cho, C., Milligan, R.A., Vale, R.D., and Gibbons, I.R. (2008). Structure and functional role of dynein's microtubule-binding domain. *Science* **322**, 1691–1695.

Clegg, R.M. (1992). Fluorescence resonance energy transfer and nucleic acids. *Methods Enzymol*. **211**, 353–388.

DiBella, L.M., and King, S.M. (2001). Dynein motors of the Chlamydomonas flagellum. *Int. Rev. Cytol*. **210**, 227–268.

Eichinger, L., and Rivero, F. (eds.), (2006). "Dictyostelium discoideum Protocols." Humana Press, Inc., Totowa.

Gee, M.A., Heuser, J.E., and Vallee, R.B. (1997). An extended microtubule-binding structure within the dynein motor domain. *Nature* **390**, 636–639.

Gennerich, A., Carter, A.P., Reck-Peterson, S.L., and Vale, R.D. (2007). Force-induced bidirectional stepping of cytoplasmic dynein. *Cell* **131**, 952–965.

Gibbons, I.R., Lee-Eiford, A., Mocz, G., Phillipson, C.A., Tang, W.J., and Gibbons, B.H. (1987). Photosensitized cleavage of dynein heavy chains. Cleavage at the "V1 site" by irradiation at 365 nm in the presence of ATP and vanadate. *J. Biol. Chem*. **262**, 2780–2786.

Gibbons, I.R., and Rowe, A.J. (1965). Dynein: A protein with adenosine triphosphatase activity from cilia. *Science* **149**, 424–426.

Goodenough, U., and Heuser, J. (1984). Structural comparison of purified dynein proteins with in situ dynein arms. *J. Mol. Biol*. **180**, 1083–1118.

Hook, P., Mikami, A., Shafer, B., Chait, B.T., Rosenfeld, S.S., and Vallee, R.B. (2005). Long range allosteric control of cytoplasmic dynein ATPase activity by the stalk and C-terminal domains. *J. Biol. Chem*. **280**, 33045–33054.

Hyman, A., Drechsel, D., Kellogg, D., Salser, S., Sawin, K., Steffen, P., Wordeman, L., and Mitchison, T. (1991). Preparation of modified tubulins. *Methods Enzymol*. **196**, 478–485.

Imamula, K., Kon, T., Ohkura, R., and Sutoh, K. (2007). The coordination of cyclic microtubule association/dissociation and tail swing of cytoplasmic dynein. *Proc. Natl. Acad. Sci. USA* **104**, 16134–16139.

Karki, S., and Holzbaur, E.L. (1999). Cytoplasmic dynein and dynactin in cell division and intracellular transport. *Curr. Opin. Cell Biol*. **11**, 45–53.

King, S.M. (2000). The dynein microtubule motor. *Biochim. Biophys. Acta*. **1496**, 60–75.

Kon, T., Imamula, K., Roberts, A.J., Ohkura, R., Knight, P.J., Gibbons, I.R., Burgess, S.A., and Sutoh, K. (2009). Helix sliding in the stalk coiled coil of dynein couples ATPase and microtubule binding. *Nat. Struct. Mol. Biol*. **16**, 325–333.

Kon, T., Mogami, T., Ohkura, R., Nishiura, M., and Sutoh, K. (2005). ATP hydrolysis cycle-dependent tail motions in cytoplasmic dynein. *Nat. Struct. Mol. Biol*. **12**, 513–519.

Kon, T., Nishiura, M., Ohkura, R., Toyoshima, Y.Y., and Sutoh, K. (2004). Distinct functions of nucleotide-binding/hydrolysis sites in the four AAA modules of cytoplasmic dynein. *Biochemistry* **43**, 11266–11274.

Koonce, M.P. (1997). Identification of a microtubule-binding domain in a cytoplasmic dynein heavy chain. *J. Biol. Chem*. **272**, 19714–19718.

Koonce, M.P., Grissom, P.M., and McIntosh, J.R. (1992). Dynein from Dictyostelium: Primary structure comparisons between a cytoplasmic motor enzyme and flagellar dynein. *J. Cell Biol*. **119**, 1597–1604.

Koonce, M.P., and Samso, M. (1996). Overexpression of cytoplasmic dynein's globular head causes a collapse of the interphase microtubule network in Dictyostelium. *Mol. Biol. Cell* **7**, 935–948.

Mazumdar, M., Mikami, A., Gee, M.A., and Vallee, R.B. (1996). In vitro motility from recombinant dynein heavy chain. *Proc. Natl. Acad. Sci. USA* **93**, 6552–6556.

Mogami, T., Kon, T., Ito, K., and Sutoh, K. (2007). Kinetic characterization of tail swing steps in the ATPase cycle of Dictyostelium cytoplasmic dynein. *J. Biol. Chem*. **282**, 21639–21644.

Neuwald, A.F., Aravind, L., Spouge, J.L., and Koonin, E.V. (1999). AAA+: A class of chaperone-like ATPases associated with the assembly, operation, and disassembly of protein complexes. *Genome Res*. **9**, 27–43.

Nishiura, M., Kon, T., Shiroguchi, K., Ohkura, R., Shima, T., Toyoshima, Y.Y., and Sutoh, K. (2004). A single-headed recombinant fragment of Dictyostelium cytoplasmic dynein can drive the robust sliding of microtubules. *J. Biol. Chem*. **279**, 22799–22802.

Pang, K.M., Lynes, M.A., and Knecht, D.A. (1999). Variables controlling the expression level of exogenous genes in Dictyostelium. *Plasmid* **41**, 187–197.

Paschal, B.M., and Vallee, R.B. (1987). Retrograde transport by the microtubule-associated protein MAP 1C. *Nature* **330**, 181–183.

Pfister, K.K., Shah, P.R., Hummerich, H., Russ, A., Cotton, J., Annuar, A.A., King, S.M., and Fisher, E.M. (2006). Genetic analysis of the cytoplasmic dynein subunit families. *PLoS Genet*. **2**, e1.

Qian, H., Sheetz, M.P., and Elson, E.L. (1991). Single particle tracking. Analysis of diffusion and flow in two-dimensional systems. *Biophys. J*. **60**, 910–921.

Reck-Peterson, S.L., and Vale, R.D. (2004). Molecular dissection of the roles of nucleotide binding and hydrolysis in dynein's AAA domains in Saccharomyces cerevisiae. *Proc. Natl. Acad. Sci. USA* **101**, 1491–1495.

Reck-Peterson, S.L., Yildiz, A., Carter, A.P., Gennerich, A., Zhang, N., and Vale, R.D. (2006). Single-molecule analysis of dynein processivity and stepping behavior. *Cell* **126**, 335–348.

Roberts, A.J., Numata, N., Walker, M.L., Kato, Y.S., Malkova, B., Kon, T., Ohkura, R., Arisaka, F., Knight, P.J., Sutoh, K., and Burgess, S.A. (2009). AAA+ ring and linker swing mechanism in the dynein motor. *Cell* **136**, 485–495.

Sakato, M., and King, S.M. (2004). Design and regulation of the AAA+ microtubule motor dynein. *J. Struct. Biol*. **146**, 58–71.

Samso, M., Radermacher, M., Frank, J., and Koonce, M.P. (1998). Structural characterization of a dynein motor domain. *J. Mol. Biol*. **276**, 927–937.

Shima, T., Kon, T., Imamula, K., Ohkura, R., and Sutoh, K. (2006). Two modes of microtubule sliding driven by cytoplasmic dynein. *Proc. Natl. Acad. Sci. USA* **103**, 17736–17740.

Silvanovich, A., Li, M.G., Serr, M., Mische, S., and Hays, T.S. (2003). The third P-loop domain in cytoplasmic dynein heavy chain is essential for dynein motor function and ATP-sensitive microtubule binding. *Mol. Biol. Cell* **14**, 1355–1365.

Spudich, J.A. (ed.) (1987). "Dictyostelium discoideum: Molecular Approaches to Cell Biology." Academic Press, INC., Orlando.

Suzuki, Y., Yasunaga, T., Ohkura, R., Wakabayashi, T., and Sutoh, K. (1998). Swing of the lever arm of a myosin motor at the isomerization and phosphate-release steps. *Nature* **396**, 380–383.

Ueno, H., Yasunaga, T., Shingyoji, C., and Hirose, K. (2008). Dynein pulls microtubules without rotating its stalk. *Proc. Natl. Acad. Sci. USA* **105**, 19702–19707.

Vale, R.D. (2003). The molecular motor toolbox for intracellular transport. *Cell* **112**, 467–480.

Vallee, R.B., Williams, J.C., Varma, D., and Barnhart, L.E. (2004). Dynein: An ancient motor protein involved in multiple modes of transport. *J. Neurobiol*. **58**, 189–200.

Williams, R.C., Jr., and Lee, J.C. (1982). Preparation of tubulin from brain. *Methods Enzymol*. **85(**Pt. B), 376–385.

Yildiz, A., Forkey, J.N., McKinney, S.A., Ha, T., Goldman, Y.E., and Selvin, P.R. (2003). Myosin V walks hand-over-hand: Single fluorophore imaging with 1.5-nm localization. *Science* **300**, 2061–2065.

CHAPTER 6

Biophysical Measurements on Axonemal Dyneins

Hiroaki Kojima[*], Shiori Toba[*], Hitoshi Sakakibara[*], *and* Kazuhiro Oiwa[*,†]

[*]Kobe Advanced ICT Research Center, National Institute of Information and Communications Technology, 588-2 Iwaoka, Nishi-ku, Kobe 6512492, Japan

[†]Graduate School of Life Science, University of Hyogo, Harima Science Park City, Hyogo 6781297, Japan

Abstract

In recent decades, the development of technologies such as optical trap nanometry and advanced fluorescence microscopy have provided tools for studying the dynamics of single protein molecules *in vitro* and *in vivo* with nanometer precision over time-scales from milliseconds to seconds. The single-molecule sensitivities of these

METHODS IN CELL BIOLOGY, VOL. 92

978-0-12-374974-1
DOI: 10.1016/S0091-679X(08)92006-9

methods permit studies to be made on conformational changes and dynamics of protein molecules that are masked in ensemble-averaged experiments. For protein motors, force generation, processivity, step size, transitions among mechanical states, and mechanochemical coupling are among the properties that can be directly measured by single-molecule techniques. Our understanding of the functions of protein motors has thus benefited considerably from the application of single-molecule techniques. This chapter will focus on single-molecule techniques applicable to axonemal dyneins, the principles upon which they work and how they are constructed and conducted.

I. Introduction

The various heavy chains of axonemal dyneins so far studied have distinct properties and specific functions in flagellar motility (Asai and Lee, 1995; Kagami and Kamiya, 1992; Yagi *et al*., 2005; reviewed in Kamiya, 2002). Furthermore, biophysical studies on axonemal dyneins have also shown that some heavy chains of axonemal dyneins permit the generation of torque (Kagami and Kamiya, 1992; Kikushima and Kamiya, 2008; Vale and Toyoshima, 1988) and/or oscillations (Shingyoji *et al*., 1998). Since coordinated beating and bend propagation of cilia and flagella are generated by ensembles of these various types of axonemal dyneins, characterization of the mechanical properties of each type of dynein organized as single molecules and in ensembles is important to understanding the mechanism of ciliary and flagellar motility.

Early progress in electron microscopic observations provided many insights into the force-generating action of axonemal dyneins, especially outer-arm dyneins in flagellar axonemes (Avolio *et al.*, 1984, 1986; Burgess, 1995; Goodenough and Heuser, 1982, 1984; Johnson and Wall, 1983; Sale *et al.*, 1985). The next breakthrough in studies on dynein motility used systems in which dynein heavy chain genes can be mutated or engineered and produced in large quantities suitable for biochemical and biophysical analyses. For instance, recent success in expressing active cytoplasmic dyneins in *Dictyostelium* cells (Nishiura *et al.*, 2004), yeast (Reck-Peterson and Vale, 2004), and insect cells (Höök *et al.*, 2005) has ushered in a new era of dynein research.

Combined with protein engineering of cytoplasmic dyneins, single-molecule measurements are now well established as indispensable tools for studying dynein motility and these advanced biophysical measurements shed light on key unsolved questions concerning how the dynein molecule is organized, what conformational changes accompany ATP hydrolysis, and whether two or three motor domains are coordinated in their motions (Gennerich *et al.*, 2007; Reck-Peterson *et al.,* 2006; Toba *et al.*, 2006; reviewed in Oiwa and Sakakibara, 2005).

On the other hand, difficulties in expressing and purifying large quantities of mutant axonemal dyneins have hampered progress in mechanistic studies on axonemal dyneins. However, powerful single-molecule techniques have provided a hint of the force-generating mechanism of axonemal dyneins. In this chapter, we provide a concise practical guide to the biophysical measurement tools of optical trap nanometry and high-accuracy fluorophore localization methods, so-called fluorescence imaging

with one-nanometer accuracy (FIONA; Yildiz *et al.*, 2003), for axonemal dyneins purified from *Chlamydomonas* flagella.

II. Materials and Methods

A. Protein Preparations

1. Inner-Arm Dynein Subspecies

Although expression systems for cytoplasmic dyneins have been established in *Dictyostelium* and *Saccharomyces*, none have been reported for axonemal dyneins. In the absence of a suitable expression system, axonemal dyneins can be purified from organisms (*Chlamydomonas, Tetrahymena*, sea urchin sperm flagella, and so on) that provide biochemical quantities of dyneins. In this chapter, focus is on the inner-arm dyneins of *Chlamydomonas* flagella. For alternative forms of dynein, other chapters in this volume may be consulted.

Chlamydomonas flagella contain at least seven subspecies of inner-arm dyneins. These subspecies of inner-arm dyneins are isolated from flagella of an outer-armless mutant (*oda1*) of *Chlamydomonas reinhardtii* (strain 137c) as described (Kagami and Kamiya, 1992; Sakakibara *et al.*, 1999). Since single-molecule sensitivity can unintentionally pick up the property of contaminating molecules if they are more highly active than the target molecule, attention should be paid to the purity of the samples. To avoid contamination by outer-arm dyneins, the use of an outer-armless mutant is recommended.

Flagellar axonemes of *Chlamydomonas* are prepared according to the method described by King (1995). Sixty liters of *Chlamydomonas* culture in TAP medium are grown as described by Gorman and Levine (1965) or Witman (1986). The cultures reach $\sim 2 \times 10^6$ cells/ml. To harvest these large cultures, a centrifuge with a high-capacity rotor that can process 12 L of sample in a single run (Sorvall RC12BP with H-12000 rotor, 750 g for 9 min, Kendro Laboratory Products, Newton, Connecticut, USA) is used in our laboratory, rather than a tangential flow filtration system used by others. Once the cells are harvested and washed, they are deflagellated with dibucaine HCl. Resultant flagella are purified through a series of centrifugations and demembranated with HMKE solution (10 mM HEPES, 5 mM $MgSO_4$, 25 mM KCl, 1 mM EGTA, pH 7.4) containing 0.2% (w/v) Nonidet P40 (NP40) and proteinase inhibitors (0.5 mM phenylmethylsulfonyl fluoride (PMSF), 10 μg/ml aprotinin, and 10 μg/ml leupeptin). The axonemes are precipitated by centrifugation, resuspended in 2 ml of HMDE (30 mM HEPES, 5 mM $MgSO_4$, 1 mM dithiothreitol, 1 mM EGTA, pH 7.4) containing 0.6 M KCl and the same proteinase inhibitors as those used in demembranation, left at 0°C for 15 min, and then precipitated by centrifugation. The supernatant containing dynein is retained. The pellet is re-extracted and centrifuged in the same manner once more. The two supernatant fractions containing dynein are combined and diluted up to 20 ml with the sample solution containing 30 mM HEPES, 5 mM $MgSO_4$, 1 mM dithiothreitol, 1 mM EGTA, 0.1 mM PMSF, 10 μg/ml aprotinin, and 10 μg/ml leupeptin, pH 7.4 to yield 20 ml of the extract with a final KCl concentration of

120 mM. The solution is centrifuged at 27,000 × *g* for 30 min at 4°C before it is loaded onto a column.

The crude dynein extract described above is fractionated by high-performance liquid chromatography with a Mono Q 5/50 GL anion exchange column (GE Healthcare Japan, Tokyo, Japan) by elution with a linear gradient from 120 to 500 mM KCl in 30 mM HEPES, 5 mM $MgSO_4$, 1 mM dithiothreitol, 1 mM EGTA, and 0.5 mM PMSF (pH 7.4). The pooled fractions of each subspecies are purified by a second HPLC fractionation (Mini Q PC 3.2/3 column, GE Healthcare Japan). Purity and aggregation of subspecies can be examined by 3% SDS-PAGE with silver staining and by sucrose density gradient centrifugation. No significant contamination of other subspecies and no aggregation should be observed. Sixty liters of the *Chlamydomonas* culture provides ca. 200 μg/ml × 50 μl of dynein-c and 300 μg/ml × 100 μl of dynein-f. Although some purified dyneins can be stored in liquid nitrogen in the presence of 10% glycerol (dynein-c) or 20% sucrose (dynein-f) for a few weeks or a month without loss of their motility, freshly purified samples are recommended for the best results in single-molecule measurements.

2. Preparation of Dynein-Coated Beads

To grasp dynein molecules by an optical trap (Fig. 1D), polystyrene beads are used as a handle for the trap. The beads can be coated with different types of dynein molecules in many ways including direct covalent linkage, noncovalent adsorption, or indirect linkage through an antibody or avidin–biotin interactions. The following is a protocol that we have used to coat beads of 0.2- or 1-μm diameter with dynein-c or dynein-f. Note that salt and protein concentrations should be modified for other dynein subspecies and different types of beads used.

For dynein-c, polystyrene carboxylated beads (Polybead Carboxylate Microspheres or Fluoresbrite Bright Blue (excitation maxima 365 nm, emission maxima 435 nm), Polysciences Inc, Warrington, PA) with a 1-μm diameter are washed and activated according to the instruction supplied by the manufacturer. They are preincubated in buffer (100 mM NaCl, 10 mM Tris, pH 10) supplemented with 1 mg/ml casein. Beads are then incubated in assay buffer (5 mM $MgSO_4$, 1 mM EGTA, 30 mM HEPES/KOH, pH 7.4) for 10 min with varying concentrations of dynein-c. For optical trap nanometry, dynein-coated beads are then added into a flow cell described below and are captured by an optical trap and brought into contact with taxol-stabilized rhodamine-labeled microtubules (10 μM taxol) adsorbed onto a coverslip. The dynein-c-coated beads can survive only for a day on ice.

For dynein-f, the beads are coated via indirect linkage through anti-IC140 antibody. Polystyrene carboxylated beads (Polybead Carboxylate Microspheres, Polysciences Inc, Warrington, PA) with 0.2-μm diameter are washed and activated according to the instruction supplied from the manufacturer.

First, protein-G is covalently coupled with the carboxylated beads. The Carbodiimide Kit (#19539, Polysciences Inc, Warrington, PA) is useful for this coupling. Follow the instructions supplied by the manufacturer except avoid the usage of bovine serum albumin (BSA) as a blocking agent. This is because BSA facilitates attachment

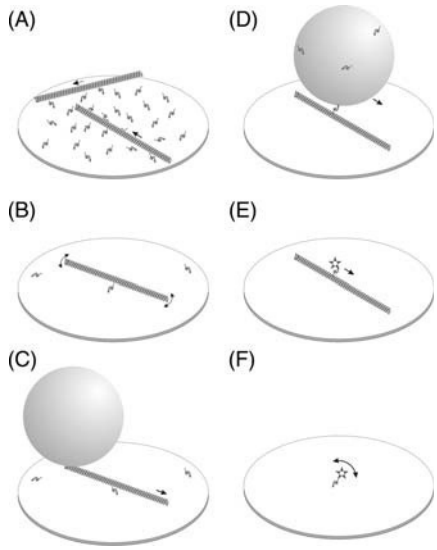

Fig. 1 Various versions of the *in vitro* motility assay. (A) Surface assay with multiple motor proteins. (B) Surface assay with a single motor protein. The pivoting motion of the filament can be observed. (C) Bead assay derived from the surface assay. A filament is tagged with a micrometer-sized bead, and the bead can be trapped by the optical trap for measurements of force generated by the protein motor. (D) Bead assay. A micrometer-sized bead is coated with the motor protein, and the movement of the bead along a filament fixed on the coverslip is observed. (E, F) Single-molecule assay. The behaviors of single motor proteins are traced by labeling them with a fluorophore or with quantum dots (Q-dots). Their movement along a filament (E) and their movements or conformational changes (F) can be monitored using this assay.

of beads to the glass surface when they are coated with dynein-f. After rigorous wash of the beads, they are then incubated in buffer containing 5 mM $MgSO_4$, 1 mM EGTA, and 30 mM HEPES/KOH (pH 7.4) for 30 min with anti-IC140 antibody. Antibody-coated beads can survive for a week on ice. Just before the experiment, the beads are mixed with dynein-f at various mixing ratios. The resultant solution is diluted 10 to 50 times before use or washed twice with the binding buffer. If washing, gentle centrifugations are recommended to avoid formation of bead aggregates.

3. Preparation of Microtubules and Their Fluorescent Labeling

Porcine brain tubulin, purified according to Vallee (1986), is polymerized into microtubules in assembly buffer (1 mM $MgCl_2$, 1 mM EGTA, 1 mM GTP, 10% (v/v) dimethylsulfoxide, 80 mM PIPES/KOH, pH 6.9) at 37°C and stabilized by adding 10 μM taxol. Fluorescent microtubules are prepared by mixing the fluorescent tubulin and the nonlabeled tubulin. Tubulin is labeled with fluorescent dyes according to the method of Hyman *et al.* (1991). For single-molecule measurements, the choice of fluorescent dye is important. To simplify the optical layout, it is recommended that a single beam of the laser is used for excitation of both fluorophores on dyneins and

microtubules. Since Cy5 dye has a long tail in its excitation spectrum, the dye can be excited by a 532-nm frequency-doubled Nd-YAG laser, which also is a suitable light source for excitation of the Cy3 dye often used for single-molecule imaging experiments. For single-molecule measurements, the brightness of the microtubules can be adjusted by altering the ratios of fluorescent and nonfluorescent tubulin.

B. Preparation of a Flow Cell

A flow cell with a volume of 10 µl is made from two different sized coverslips (#1, 24 mm × 36 mm and #1, 18 mm × 18 mm, Matsunami Glass Ind. Ltd., Osaka, Japan) that have been cleaned by soaking overnight in a solution of 0.1 M HCl and 70% ethanol, rinsed with distilled water, and dried. For detection of single fluorescent molecules under aqueous conditions, a flow cell made of clean coverslips is indispensable. Two slivers of polycarbonate film (2 mm wide and 50 µm thick) are placed about 5 mm apart on the larger glass coverslip (24 mm × 36 mm), which is fixed to the stage of an inverted microscope. The smaller coverslip is then placed carefully on the polycarbonate spacers. The space between the two coverslips is used as a chamber (volume ca. 5–10 µl) for observation of microtubule movements or optical trap experiments. To avoid movement of the meniscus by vaporization, which may cause slow drift, accidental flow, or change in salt concentrations, the side openings of the flow cell should be sealed with vaseline or nail enamel after completion of the experimental buffer perfusions.

C. *In Vitro* Motility Assays

1. General

In general, *in vitro* motility assays enable motility of protein motors (myosin, kinesin, dynein) along protein filaments (actin filaments or microtubules) to be reconstituted from purified and characterized component molecules. Since experimental conditions such as temperature, buffer composition, ionic strength, and ATP concentrations are readily controlled, these assays permit precise observation of a motor's mechanical properties. Basically, *in vitro* motility assays have two types of geometries: surface assays (Fig. 1A) and bead assays (Fig. 1D). In surface assays, motors are attached onto a glass surface using specific or nonspecific interactions. Upon addition of actin filaments/microtubules and ATP, the action of motors is observed as the gliding of the actin filaments/microtubules over the surface (Supplementary movie 1). The movement of the protein filaments is observed using dark-field microscopy or conventional epifluorescence microscopy when fluorescent-labeled filaments are used.

In the bead assay (Fig. 1D), filaments are fixed on the glass surface through antibodies, filament-associated proteins, silane couplers, or nonspecific interactions. A glass or carboxylated polystyrene bead with a size of the order of a micrometer is coated with motors, using either specific or nonspecific interactions as described in the previous section. When these beads are introduced into a flow cell in the presence of ATP, they bind to filaments fixed on the surface and move along the filaments.

Their movement is observed using bright-field microscopy or dark-field microscopy (Supplementary movie 2). When fluorescent beads or fluorescently labeled beads are used, the movement of the beads is observed with a fluorescence microscope.

These two motility assays are often used to characterize ensemble properties of motors. To study the mechanical properties of individual motors, these *in vitro* motility assays are extended to the single-molecule level. In the surface assay, this is done by decreasing the number of motors attached to surface. Even at very low surface density of motors, filaments will still land and show movement. At these low motor densities, filaments are typically attached to the surface at only one point, around which they swivel while moving forward (Figs. 1B and 2C, inset). The property that

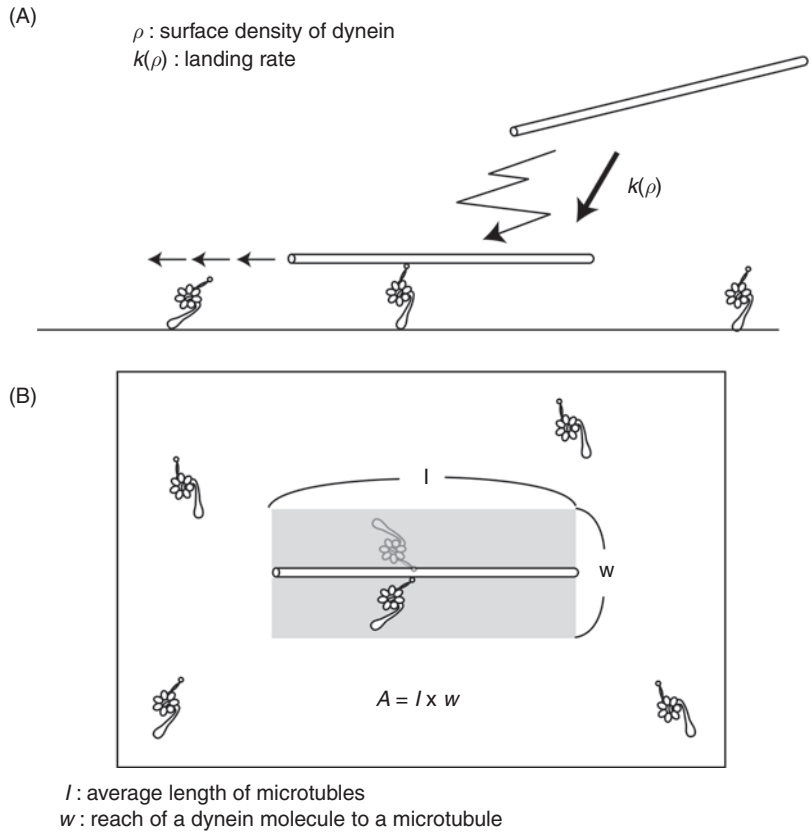

Fig. 2 Schematic illustration of the landing rate assay. (A) To assess the processivity of the dynein molecule, we determined the relationship between the microtubule-landing rate k (ρ) and the density of the dynein-coated glass surface (ρ). This relationship is expressed as $k(\rho) = C_0[1 - \exp(-A \times \rho)]$; this expression is based on the assumption that one molecule of dynein is sufficient to propel a microtubule, where A is the product of microtubule length (l) and two times the reach of the dynein molecule (w), as shown in (B, C) The experimental data obtained from the measurement using dynein-f. The inset shows the pivoting motion of a microtubule, which is presumably propelled by a single dynein-f molecule.

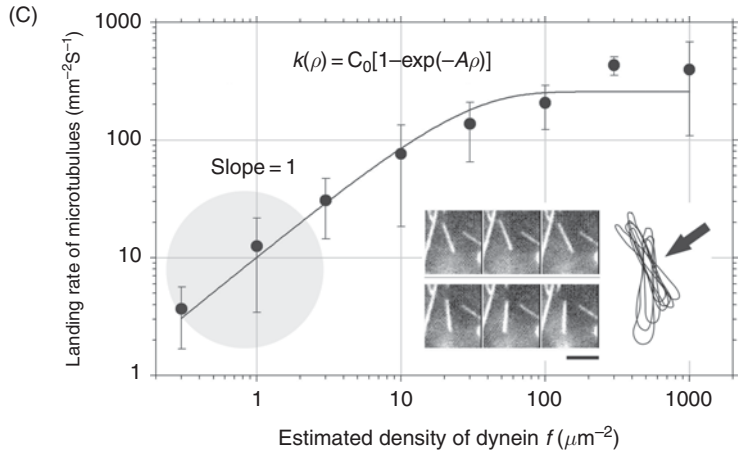

Fig. 2 (*Continued*)

single motors can move continuously along a microtubule per a diffusion encounter is called "processivity." Since motors with low processivity cannot maintain connection with protein filaments at the single-molecule level, we have to support the interactions between the motors and filaments with a double-beam optical trap system or fine glass needles.

On the other hand, in the bead assay, the number of motors absorbed onto the beads is titrated as needed to the single-molecule level. The relative frequency of binding depends on the number of motor molecules carried by the bead. Assuming that one active motor molecule attached to a bead with a geometry favorable for interaction suffices to bind the bead to a microtubule, the fraction of beads bound to microtubules should follow Poisson statistics. Measurements of force and movement are made using beads having less than 50% probability of binding and hence movement, so the Poisson probability that a bead carried two or more active motor molecules was less than 0.15. Assuming a random distribution of motor molecules over the bead surface and allowing a certain reach for the motor molecule's tether, the probability that two or more motor molecules were able to interact simultaneously with a microtubule is less than 0.01 (Block *et al*., 1990; Hirakawa *et al.*, 2000; Sakakibara *et al*., 1999). Under these conditions, only a single protein motor is expected to interact with the filament, yet continuous motion of the bead over a distance of 1 μm is observed for highly processive motors. In the case of motors with low processivity care should be taken to adjust the size of the bead and trap stiffness.

The motion of single motor molecules along filaments also can be observed more directly by using total internal reflection fluorescence microscopy (TIRFM) as described (Reck-Peterson *et al*., 2006; Toba *et al.*, 2006; Vale *et al*., 1996). The assay used in these experiments is an extension of the bead assay but instead of motor-coated beads, fluorescently labeled or fluorescently tagged motors are used (Fig. 1E and F).

2. *In Vitro* Motility Assay of Inner-Arm Dyneins

For inner-arm dyneins, the *in vitro* motility assay is carried out as described by Kagami and Kamiya (1992) or Sakakibara *et al*. (1999). A fractionated inner-arm dynein subspecies (200 μg/ml) is diluted to various concentrations in buffer solution containing 30 mM HEPES/KOH (pH 7.4), 5 mM $MgSO_4$, 1 mM DTT, 1 mM EGTA, and 0.5 mg/ml BSA. The flow cell is filled with 10 μl of the diluted dynein subspecies solution to coat the inner surface of the flow cell, incubated for 5 min, washed with buffer solution, and then 20 μl of buffer solution is infused into the flow cell, which contains 40 μg/ml microtubules, 0.5 mM ATP, 1 mM DTT (for fluorescence measurements, 100 μg/ml glucose oxidase, 20 μg/ml catalase, and 3–5 mg/ml glucose as an oxygen-depleting antifade mixture (Harada *et al*., 1990) are also added). The flow cell is then transferred to the stage of a microscope. Microtubule movement is observed and recorded with a dark-field optical microscope (BHF, Olympus Co., Tokyo, Japan), equipped with a 100× 1.3 NA oil-immersion objective with an iris (UPlanFL N, Olympus Co., Tokyo, Japan) and a high numerical aperture (NA) dark-field condenser (BH-DCW, Olympus Co., Tokyo, Japan) and a CCD camera. The light source we use is a high-voltage mercury lamp, USH-102D (Ushio Inc., Tokyo, Japan). UV (L420, Olympus Co., Tokyo, Japan), heat absorbing (B-76, Olympus Co., Tokyo, Japan), and interference filters (IF550, Olympus Co., Tokyo, Japan) are useful to avoid photochemical damage to the dyneins. When fluorescent microtubules (e.g., Cy3-labeled microtubules) are used, an epifluorescence microscope is applicable. Fluorophores are excited either by the spectrum line of a 100-W mercury arc lamp (HBO-100W/2, Osram GmbH, Munich, Germany) selected by an interference filter and a heat absorbing filter or a 1-mW 532-nm laser beam obtained by attenuation of the Nd-YAG laser output (μGreen Laser, model 4601-050-1000 (50 mW), Uniphase, San Jose, CA, USA). Imaging is carried out via a 560-nm dichroic reflector and a 580-nm interference filter with a 30-nm band width (560DRLP02 and 580DRF30, Omega Optical Inc., Brattelboro, VT, USA) using a Plan-Neofluar 100× 1.3 NA oil-immersion objective (Olympus Co., Tokyo, Japan) through a 2–4× magnifying lens onto a cooled CCD camera (e.g. ImagEM C9100-13, Hamamatsu Photonics Inc., Hamamatsu, Japan). The microscope stage and flow cell should be stabilized at the desired temperature (such as 25°C) for the assays.

Images of individual microtubules can be tracked using image analysis software. The speed and direction of microtubule sliding can then be determined. Under typical conditions, the slowest inner-arm dynein-f move microtubules at a velocity of around 1–2 μm/s while the fastest dynein-c move microtubules at 10 to 15 μm/s (see Supplementary movie 1), which is comparable to the maximum sliding velocity of the peripheral doublet microtubules within intact axonemes.

For evaluation of processivity of dyneins, the landing rate assay should be carried out (Fig. 2). In this assay, the rate at which microtubules come out of bulk solution, bind, and move over surfaces coated with dynein is measured. Landing rate plotted against dynein surface density (Fig. 2C) is examined by the theoretical relationship for a single dynein molecule being sufficient for attachment and motility of microtubules

(Hancock and Howard, 1998; Sakakibara *et al.*, 1999; Kotani *et al.*, 2007). The model in which a single molecule of dynein suffices to attach to and move a microtubule is expressed as follows:

$$k(\rho) = C_0[1 - \exp(-A \times \rho)], \quad (1)$$

where $k(\rho)$ is landing rate at the density of dynein (ρ) and A is the product of the microtubule length and the length in which single dynein fixed on the surface can interact with a microtubule (Fig. 2B). The fitting will provide the values of C_0 and A.

Another method of evaluating the processivity is to measure the fraction of microtubules that move further than their own length before their leaving the surface as a function of the dynein surface density. If the dynein is highly processive, microtubules observed at very low dynein surface densities will rotate erratically about a vertical axis through a fixed point on the surface, where a single dynein molecule is presumably located, while still progressing. In both assays, the surface density of dynein molecules can be calculated assuming that every dynein molecule infused into the flow cell evenly attached to the flow cell surface without losing its activity.

D. Optical Trap Nanometry

1. General

The optical trap is a popular and versatile technique for the manipulation of objects with micrometer dimensions. In this technique, refractive particles are captured by means of photon pressure from a laser beam focused to a diffraction-limited spot by a large NA objective lens (Fig. 3A). Although one might imagine that the optical trap would require a very complicated arrangement of optics, all that is, in fact, required is a high NA lens and a laser beam with a Gaussian intensity profile (Ashkin *et al.*, 1986) (Fig. 3B). For optical trap nanometry in cell biology, the textbook by Sheetz (1998) in this series may be consulted.

Because photons have a momentum, refraction changes the momentum of photons, generating a force that acts on the refracting particles. The momentum of a photon is nh/λ, where h is Planck's constant, n is the refractive index, and λ is the wavelength of the light in a vacuum. Light of a wavelength in the infrared region (1064 or 1047 nm) is most frequently used in optical traps for biological studies, because light of these wavelengths is sufficiently far from the absorption peaks of biological materials and is thus less harmful to them (Svoboda and Block, 1994). A particle in water ($n = 1.33$) reflecting one photon of wavelength 1064 nm (generated by a Nd-YAG laser) per second is subjected to an optical force of 1×10^{-15} pN. Although this is a very small force, the total force exerted by an optical trap becomes comparable to that generated by single-protein motor molecules when a laser beam of 0.1–1 W is focused to a diffraction-limited spot by using a large NA objective lens. For spherical objects, the restoring force increases linearly with displacement from the center of the trap, provided the particle does not move too far from the center of the trap, i.e., the optical

trap behaves like a Hookean spring (Fig. 3A and C). This linearity is important for measurement of force exerted on the trapped bead as described later.

Using an optical detector based on a quadrant photodiode (QPD) (e.g., S4349, Hamamatsu Photonics Inc., Hamamatsu, Japan), the position of the particle held in the optical trap can be measured with nanometer precision and millisecond temporal resolution. The optical trap can be used in combination with these precise position detectors as a force transducer to detect mechanical interactions between individual protein motor molecules. Using optical trap nanometry on various types of dynein, forces in the piconewton range and displacements in the nanometer range have been measured (Gennerich *et al*., 2007; Hirakawa *et al.*, 2000; Mallik and Gross, 2004; Mallik *et al.*, 2004; Sakakibara *et al.*, 1999; Shingyoji *et al.*, 1998; Toba *et al.*, 2006). For some protein motors, a combination of optical trap techniques and single-molecule fluorescence imaging techniques has provided a hint of the existence of a coupling between biochemical and mechanical events during ATPase cycles (Adachi *et al.*, 2007; Ishijima *et al.*, 1998; Nishizaka *et al*., 2004; Sakamoto *et al*., 2008). However, this technique has been applied to dyneins in only a few studies (Inoue and Shingyoji, 2007), because many of the fluorescent nucleotides suitable for single-molecule imaging [e.g., Cy3-EDA-ATP; (Oiwa *et al.*, 2000)] are poor substrates for axonemal dyneins.

2. Optical Layout

Those who are not familiar with laser optics and optical layout should seek advice from laser scientists or experts in laser optics. A microscope objective lens with high NA and a laser of a few hundred milliwatts power output is all that is required to capture and manipulate micrometer-sized glass or plastic beads suspended in water (Fig. 3B). Most optical traps are constructed around an inverted light microscope combined with a number of external optical components, required to align and direct an infrared laser beam (e.g., 4 W, Nd-YAG laser, CW, TEM_{00}, J201-BL-106C-JK1-W, *Spectra Physics*, model BL-106C, Mountain View, CA) toward the microscope objective lens. Normally, the system is built on a vibration isolation table. The quality of the laser beam should meet experimental requirements for trap stability and linearity. Measurement of nanometer displacement requires nanometer position stability of the trap in the specimen plane such that the beam pointing stability will be within a microradian for about half a minute. Thus, to achieve nanometer precision, one must avoid introducing any vibration into the trapping microscope.

The most common geometrical arrangement used to make dynein–microtubule mechanical measurements is the single bead arrangement (Figs. 1D and 3A). An optical trap requires filling the back aperture of a high NA objective with a parallel laser beam. Since change in the angle of incidence on the objective shifts the focal point of the beam laterally within the specimen plane, optical components are arranged in order to achieve this change. As illustrated in Fig. 3B, an expanded and collimated laser beam is introduced into an acousto-optic deflector (AOD) (e.g., LS110A-XY1.06XY, Isomet Corp., Springfield, VA, USA), which is placed at a point in the

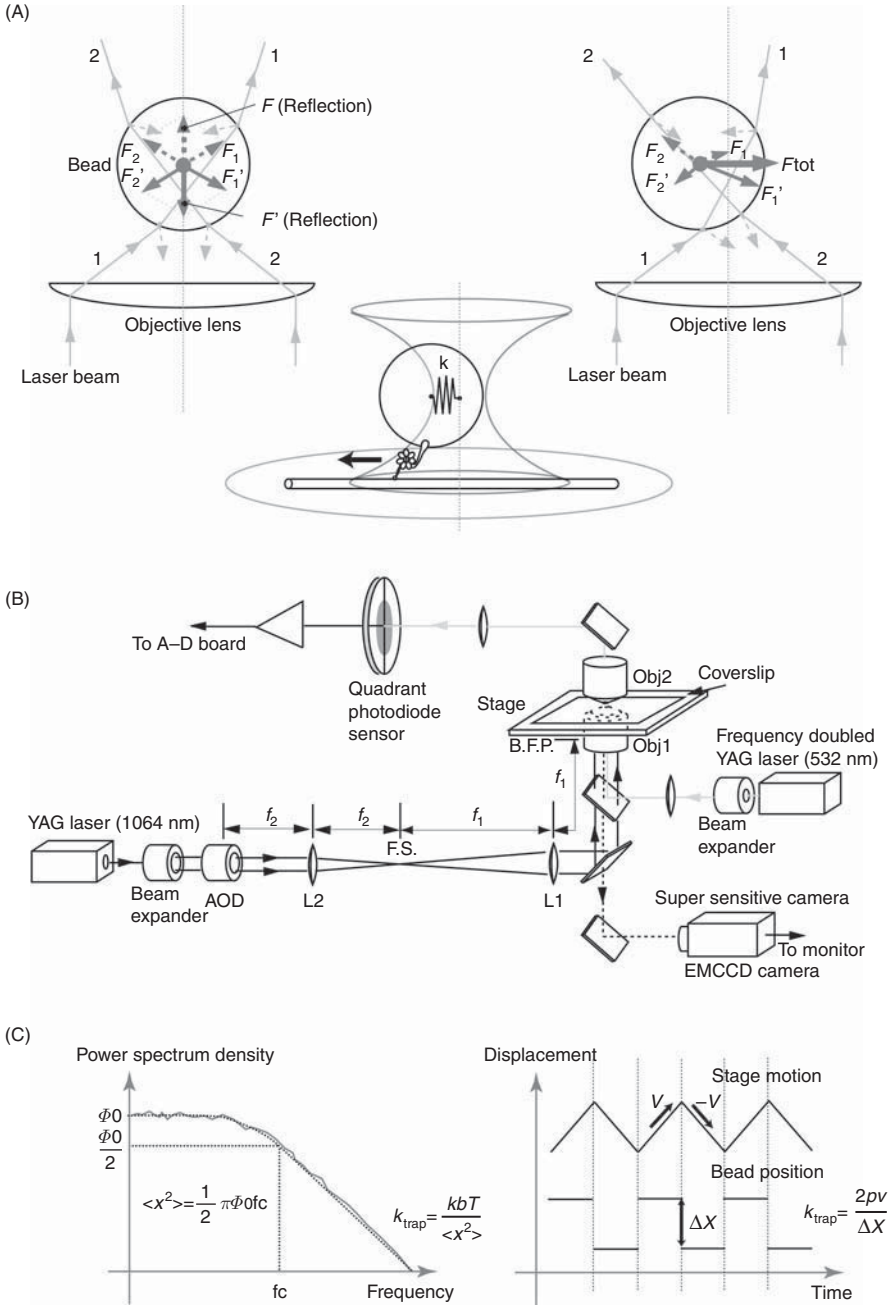

Fig. 3 (*Continued*)

rear focal plane of the lens L2. Lens L2 focuses the beam to Gaussian waist at the rear focal plane of L1. The beam then diverges from this plane and is collimated by lens L1. The angular deflection caused by AOD equals a lateral movement of the trap in the specimen plane, and then the trap can be moved within the *x–y* object plane of the microscope. An alternative steering option is to move the first lens (L2) of the telescope by a servo motor system, which costs less than AOD.

Double-beam arrangement can be created simply by splitting the input laser beam into two paths or by moving one beam much faster than the relaxation time of the trapped beads using the AOD, and each spot can be moved independently within the *x–y* object plane of the microscope.

In general, to prevent accidental exposure, introduction of an interlock shutter system into the optical path is recommended. An additional safety feature is to provide infrared blocking filters or attenuators in all parts of the visible light path.

In most apparatus, the bead position is measured using a QPD position sensor and either the scattered laser light emanating from the trapping laser or a focused image of the bead is projected onto the sensor. When the bead is imaged directly onto the sensor using bright- or dark-field microscopy, the signal reflects the absolute position of the bead. Under dark-field microscopy, the light intensity coming from the trapped bead is so low that a laser is recommended as a light source to increase the intensity of the scattered light for precise positioning of the bead (Nishiyama *et al.*, 2001). Typically, with sufficient intensity of the bead image, the sensor can determine the centroid of the bead position with a resolution of better than 0.5 nm.

3. Optical Trap Experiments Under Surface Assay Geometry

When using the surface assay geometry, a protein filament has to be captured by the optical trap through a bead or beads (Fig. 1C). For microtubules, tubulin antibodies, microtubule-associated proteins (MAPs, e.g., *tau*) are used as glues for microtubule-

Fig. 3 The setup for optical trap nanometry. (A) The micrometer-sized sphere is trapped slightly beneath the focal point where the optical forces applied on the sphere by the refraction and the reflection beams are balanced by each other (left). When the bead is located at an off-center position, the optical force acting toward the trap center is exerted on the sphere (right). Consequently, the trapped sphere acts like a sphere connected to a Hookean spring (center). (B) Schematic illustration of the optical system for optical trap nanometry. Optical trapping is performed by focusing the laser beam from the YAG laser ($\lambda = 1064$ nm) at the sample solution using an objective lens with a high numerical aperture (NA) (Obj1). The trap position is handled in two dimensions by controlling the light path using an acousto-optic deflector (AOD) placed at the front focus of the lens (L2). A frequency-doubled YAG laser ($\lambda = 532$ nm) is used as the light source for both nanometry and fluorescence microscopy. The fluorescence image is captured by a supersensitive camera. The image of the trapped sphere is focused onto the quadrant photodiode sensor (QPD) through another objective lens (Obj2). The position of the sphere is detected with nanometer accuracy by monitoring the differential output from the QPD. The trap stiffness is determined either by measuring the power of the thermal fluctuation $<x^2>$ shown by the trapped sphere and applying the energy equipartition theorem or by measuring the position change of the trapped sphere in response to the triangular motion of the sample stage and estimating the drag force, as shown in (C).

bead attachment. Protein-G-coated polystyrene carboxylated beads (300 nm in diameter) are incubated with 2 mg/ml of antitubulin–antibody (Sigma T9028) on ice in assay buffer (5 mM $MgSO_4$, 1 mM EGTA, 1 mM DTT, 150 mM HEPES/KOH, pH 7.4) for 3 h. The beads are then mixed with taxol-stabilized microtubules and incubated for 30 min. After introducing the bead–microtubule complexes into the flow cell, the resultant bead–microtubule complexes are then captured by the optical trap. The bead is brought to within 3 μm of the dynein-coated surface, allowing the free end of the microtubule to engage the dynein surface (Fig. 1C). As dynein pulls the microtubule, the bead is displaced in the optical trap. Displacement of the bead is measured using the QPD system with subnanometer-spatial and submillisecond-temporal resolution.

4. Determination of Stiffness of the Optical Trap

There are several ways to determine the trap stiffness. Here two methods are described.

1. Measure the motion of the bead in the trap and determine the 6-dB corner frequency of the power spectrum of the motion (Fig. 3C, the left panel). The corner frequency $f_{6\mathrm{dB}}$ is expressed as follows:

$$f_{6\mathrm{dB}} = \frac{k}{(12\pi^2\eta r)}, \tag{2}$$

   where η is the coefficient of viscosity, r is the radius of the bead, and k is the stiffness of the trap. This method requires a detector bandwidth that will cover almost all of the bead motion.
2. Apply solution flow to the trapped bead and measure the displacement of the bead from the center of the trap (Fig. 3C, the right panel). The force exerted on the bead (F) is calculated by using Stokes' law:

$$F = 6\pi\eta r V, \tag{3}$$

   where η is the coefficient of viscosity, r is the radius of the bead, and V is the flow speed. To obtain constant flow, the microscope stage is moved in a ramp-wave or triangular-wave manner at various velocities as shown in Fig. 3C. In consequence, the bead shows a square wave response corresponding to the viscous force. Measure the average displacement of the trapped bead.

E. Total Internal Reflection Fluorescence Microscopy

Progress in imaging devices makes the detection of a single fluorophore in aqueous environments feasible. The key technique for single fluorophore detection is to keep the intensity of background below the fluorescence of the target fluorophore. One solution to reduce the background fluorescence intensity is to minimize the sample volume in which fluorescence is detected. TIRFM provides a shallow excitation volume localized at the interface between the material with higher refractive index

and that with the lower refractive index, which is known as the evanescent field. The evanescent field generated at the interface penetrates into the material with lower refractive index for a few hundreds of nanometers (depending on the wavelength, refractory indices, and the incident angle) and will excite fluorophores that are at or near the interface. TIRFM was used in the first reported observation of single myosin molecules attached on a glass surface (Funatsu *et al*., 1995).

Two types of the total internal reflection fluorescence (TIRF) microscopy, the prism-type and the objective-type TIRF, have been reported. In this chapter, we focus on the objective-type TIRF. Figure 4 shows its optical arrangement. The key concept of this arrangement is that a laser beam is focused on the periphery of the back focal plane of the microscopic objective. The objective needs high NA > 1.4, which is produced by several manufacturers. For the excitation of fluorophores, a single-line laser with a few tens of milliwatts of power is recommended. For Cy3 fluorophore, frequency-doubled Nd-YAG laser with a 532-nm wavelength is suitable. The lens L1 is located one focal length away from the back focal plane of the objective. The output beam of the laser is attenuated and focused by the lens L1 at the back focal plane of the objective. The laser is then collimated again by the objective so that the rays of the laser beam are parallel to each other. If the beam passes through the center of the objective, it establishes epifluorescence excitation. When the mirror M1 is translated in the direction shown in Fig. 4, the laser beam moves laterally in the back focal plane of the objective. When the beam at the back focal plane reaches a critical radius, the incident angle to the glass–water interface is large enough to totally reflect at the interface and the evanescent field is established. The evanescent field penetrates approximately 80 nm (to $1/e^2$ intensity) beyond the glass–water interface into the solution above. Thus only fluorescent molecules very close to the surface are efficiently excited. However, fluorophores suspended in the medium but within the 100–200 nm extent of the evanescent field contribute to the background intensity. This poses an upper limit of approximately 50–100 nM on the concentration of fluorophore molecules.

Fluorescence is then collected by the objective lens (PlanApo 100×, NA 1.45 oil, Olympus Inc., Tokyo, Japan) and passed through a notch filter with center wavelength 532 nm (StopLine NF01-532U-25, Semrock Inc., Rochester, NY, USA) to cut excitation light of the frequency-doubled Nd-YAG laser and a band-pass filter with center wavelength 575 nm (HQ575/25, Chroma Technology. Corp., VT, USA) to select for Cy3 dye fluorescence. Detection is performed using commercially available camera sets, such as a cooled CCD (C4742-98, Hamamatsu photonics Inc., Hamamatsu, Japan), an image intensifier with a CCD camera in tandem (VS-1845, Video Scope International, Ltd. and CCD300T-RCX, Dage MTI, Michigan City, IN, USA), or an EMCCD camera (ImagEM C9100-13, Hamamatsu Photonics Inc., Hamamatsu, Japan). For the high-accuracy fluorophore localization methods described below, the EMCCD camera has dominated the experiments.

Objective-type TIRF illuminators are commercially available (e.g., IX2-RFAEVA-2, Olympus Inc., Tokyo, Japan), which use a movable fiber optic source instead of L1 and M1. Theoretical considerations of TIRF microscopy are available in Axelrod *et al.* (1984), Axelrod (2003), and Goldman (2008).

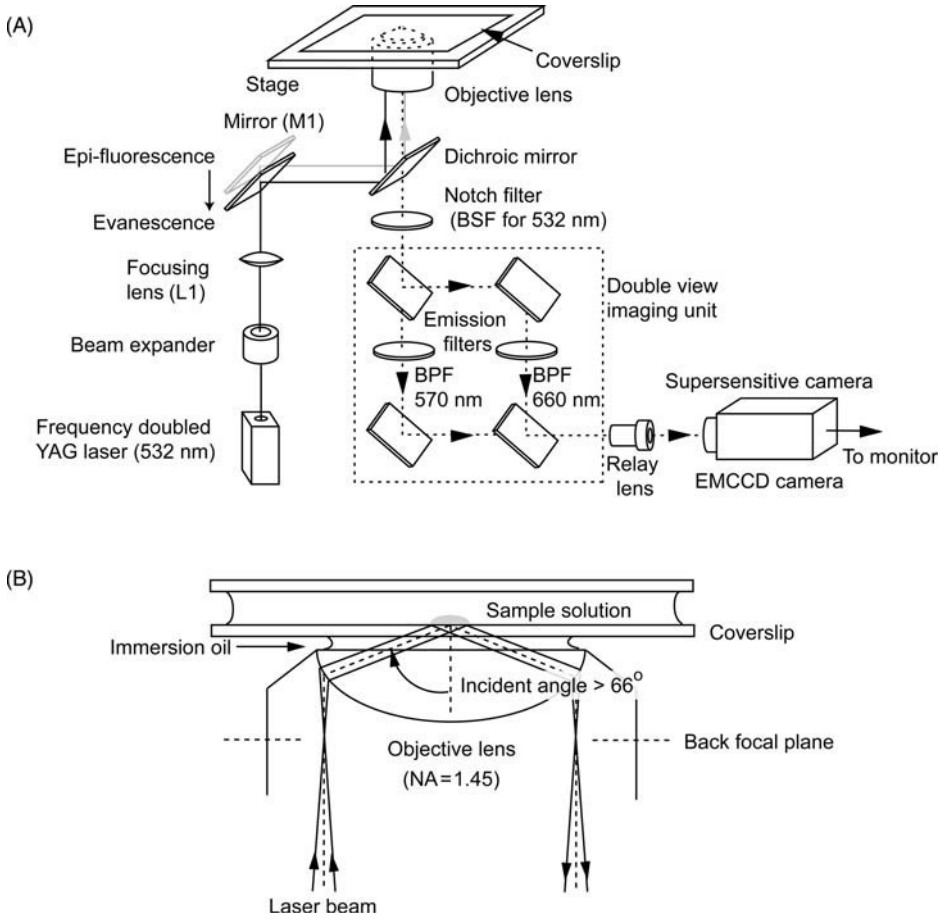

Fig. 4 The setup for TIRF microscopy. (A) Schematic illustration of the optical system for TIRF microscopy. The setup shown in this image is an objective-type TIRF system. The sample is illuminated by the frequency-doubled YAG laser ($\lambda = 532$ nm). The illumination mode is changed from epifluorescent illumination to evanescent illumination by changing the position of the mirror (M1). The fluorescence from the sample passes through a double-view unit in which the fluorescence from the Cy5-labeled microtubule and the Cy3- or Q-dot-labeled single molecule are separated and detected by a supersensitive camera. The illuminating laser beam entering the objective lens through the periphery of the back aperture is focused at the back focal plane and undergoes total reflection at the glass–solution boundary to generate an evanescent field localized on the coverslip at ~200 nm (B).

F. High-Accuracy Fluorophore Localization Methods

The image of a point source of light (wavelength = λ nm) that is produced by using the objective lens of a conventional microscope is a diffraction-limited spot with an Airy disk pattern (bright disk of light surrounded by alternating dark and bright

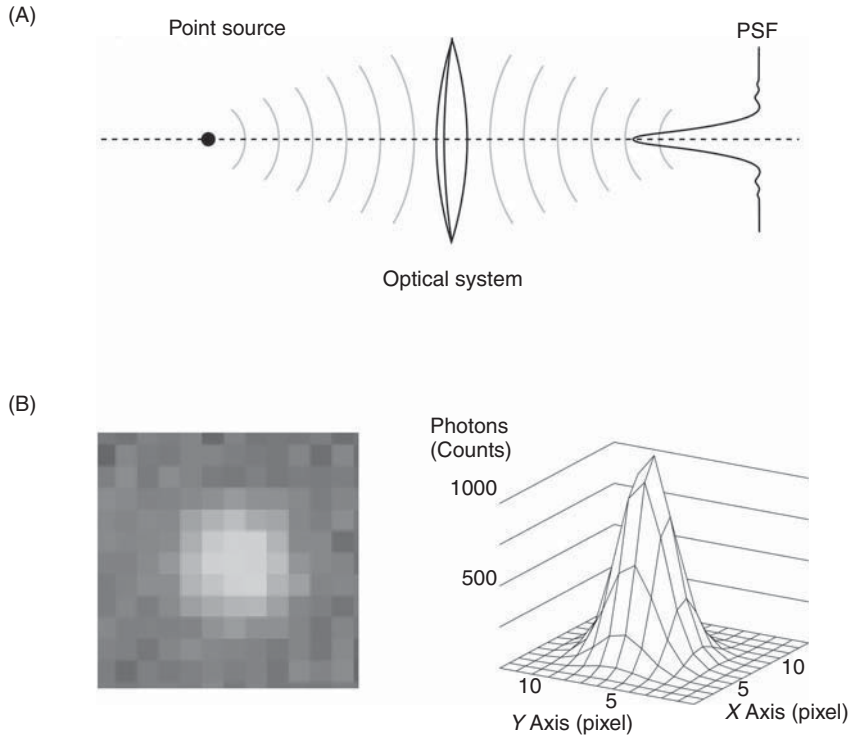

Fig. 5 High-accuracy fluorophore localization method, so-called FIONA (fluorescence imaging with one-nanometer accuracy) method. (A) A point light source forms a diffraction-limited image (point spread function, PSF) of width $\sim 0.5\,\lambda/\mathrm{NA}$ or $\sim 250\,\mathrm{nm}$ for visible light. The center of PSF corresponds to the position of the point light source. (B) To assign the center of PSF with nanometer accuracy, the image generated by a sufficient number of photons and captured by a high-sensitivity camera is fit to the two-dimensional Gaussian function. The number of photons at the peak position and the pixel size of the imaging detector are set to >1000 counts and $\sim 80\,\mathrm{nm}$, respectively, which represent the typical conditions for detection.

diffraction rings) (Fig. 5A). The spot approximates well to a two-dimensional Gaussian distribution (4) with a standard deviation σ given by $0.5\,\lambda/\mathrm{NA} \approx 250\,\mathrm{nm}$, where NA is the numerical aperture of the objective lens.

$$P(x,y) = \frac{1}{\sigma_x \sigma_y \sqrt{2\pi}} \exp\left[\frac{-(x-\Delta x)^2}{2\sigma_x^2}\right] \cdot \exp\left[\frac{-(y-\Delta y)^2}{2\sigma_y^2}\right]. \tag{4}$$

The size and shape of the image in three dimensions is known as the point spread function (PSF), which can be measured directly for any given imaging system. The error in determining the central position of a two-dimensional projection at the image plane is governed by system noise and photon-counting statistics. With proper adjustments of the experimental system, precision is limited simply by the photon count (n), where the

standard error of the mean (SEM) is equal to $\sigma\, n^{-0.5}$, where σ is the standard deviation of the spot image (Toprak and Selvin, 2007; Yildiz *et al.*, 2003, 2004). The mean position can be determined either by a center-of-mass calculation or by least squares fitting to a Gaussian distribution. For real systems where the signal-to-noise ratio is limited, the optimal determination of position is provided by the Gaussian fitting technique (Cheezum *et al.*, 2001). The two-dimensional Gaussian fit for the FIONA analysis is available in Mashanov and Molloy (2007), who extended FIONA into live cells. The computer software described in this chapter is available for academic use upon request. Visit http://www.nimr.mrc.ac.uk/gmimpro. Those who are not familiar with image data processing should seek advice from experts in image processing.

III. Results and Discussion

A. *In Vitro* Motility Assays

Since *in vitro* assays reduce the system to its simplest functional components much can be learned because of the ease with which the reaction conditions can be controlled. *In vitro* motility of dyneins, however, depends highly upon the surface conditions. We examined several types of surfaces; borosilicate glass, spin on glass (SOG) (Tokyo Ohka Kogyo Co. Ltd., Kawasaki, Japan), borosilicate glass cleaned with an anionic detergent, and the same glass cleaned with a plasma cleaner. We found that dynein-c and dynein-f retain their motile activity when bound to borosilicate glass that had been washed with 0.1 M HCl and 70% ethanol. On this glass surface, microtubules move smoothly over a distance of greater than 50 μm. However, even under these surface conditions, dynein-f displays only slow movement of microtubules (ca. 1.2 μm/s). For dynein-c, borosilicate glass cleaned with an anionic detergent also works well.

In vitro motility assays have not only paved the way to single-molecule studies on dynein but have given rise to several important findings about axonemal and cytoplasmic dyneins. A few of these are listed below:

1. Each of the heavy chains of axonemal dynein so far studied has motile activity (Kagami and Kamiya, 1992; Sakakibara and Nakayama, 1998).
2. The velocity of microtubule sliding varies with the type of dynein heavy chain (Kagami and Kamiya, 1992; Sakakibara and Nakayama, 1998).
3. Some inner-arm dyneins can rotate a microtubule about its long axis as it is moved on the dynein surface (Kagami and Kamiya, 1992; Kikushima and Kamiya, 2008; Vale and Toyoshima, 1988).
4. Some axonemal dyneins were found to require ADP for motility (Yagi, 2000).

B. Optical Trap Nanometry Studies on Dynein Motility

The mechanical properties of several types of dynein have been measured at nanometer and millisecond spatiotemporal resolution by means of the optical trap technique. However, the step sizes and modes of movement of these dyneins are still a

matter of controversy. For axonemal dyneins, the single-headed inner-arm dynein-c shows processive movement and has a step size of 8.2 nm (Sakakibara *et al.*, 1999). The maximal force generated by a dynein-c molecule was measured at 1.6 pN, which is smaller than the corresponding value for kinesin. The outer-arm dynein from *Tetrahymena* cilia, a 22S dynein that is a heterotrimer, also showed processive movement with an 8-nm step size at low concentrations of ATP ($<20\,\mu M$), whereas at higher concentrations ($\geq 20\,\mu M$), it does not move processively, but instead shows pulse-like force generation similar to that observed in skeletal muscle myosin II (Hirakawa *et al.*, 2000). Under high loads, both these dyneins often fail to step forward and slip backward (Hirakawa *et al.*, 2000; Sakakibara *et al.*, 1999).

In studies of cytoplasmic dyneins, their step sizes and modes of movement are also a matter of controversy. Mallik *et al.* (2004) reported that single cytoplasmic dynein molecules purified from bovine brain primarily took large steps (24–32 nm) at low loads, but the step size decreased from 32 to 8 nm with increasing load to its stall force. The stall force generated by the cytoplasmic dynein was reported to be $\sim$1 pN, which was smaller than that generated by kinesin. In addition, when multiple dynein molecules interact with a microtubule and contribute to movement, the dynein molecules move predominantly in 8-nm steps (Mallik *et al.*, 2004).

Toba *et al.* (2006) performed optical trap nanometric studies on cytoplasmic dynein purified from porcine brain. They observed processive movement of dynein with regular 8-nm steps, irrespective of the load, and they measured that the stall force generated by a single dynein molecule was 7–8 pN, a value that is comparable to that generated by a kinesin-1 molecule (Toba *et al.*, 2006). The large stall force of $\sim$7 pN also was measured in yeast cytoplasmic dynein (Gennerich *et al.*, 2007). These results contrast with the previous report on mammalian cytoplasmic dynein (Mallik *et al.*, 2004).

Gennerich *et al.* (2007) applied a force-feedback optical trap to native and artificially dimerized yeast cytoplasmic dynein and analyzed their stepping behavior as a function of load. Surprisingly, they found that dynein moves processively toward either the minus or plus ends of microtubules under an applied force in the absence of ATP hydrolysis. This force-induced, nucleotide-independent stepping shows the directional asymmetry: a small assisting force ($\sim$3 pN) causes dynein to step forward, while a much large force (7–10 pN) is required to induce backward stepping. In addition, by applying near-stall force to dynein in the presence of ATP, they observed nonadvancing forward–backward steps and then analyzed the dwell times between steps. The rate of nonadvancing backward stepping was increased by load but not affected by ATP, while the rate of nonadvancing forward stepping was unaffected by load and dependent on ATP.

C. High-Accuracy Fluorophore Localization Methods

In optical trap nanometry, a dynein molecule has to carry a relatively large bead (200 nm to 1 μm in diameter), so the measured position of the bead does not directly represent the position of the dynein molecule. Compliance between the bead and the dynein molecule attenuates displacement performed by the dynein molecules. Moreover, movement of the bead measured in an optical trap reflects movement of the center of

mass of the entire dynein molecule. To study the mechanism of processivity in more detail, the movement of individual heads should be monitored with high spatial and temporal resolutions. This can be achieved by the technique, high-accuracy positioning of fluorescent spot, FIONA (Toprak and Selvin, 2007; Yildiz *et al.*, 2003, 2004). This technique has been used for cytoplasmic dyneins, but not axonemal dyneins so far.

Toba *et al.* (2006) adopted this technique to analyze the movement of single cytoplasmic dynein molecules purified from porcine brain. To improve the temporal resolution and tolerance to photobleaching, they used quantum dots (Q-dots), which are stable and have an intense fluorescence. They achieved a temporal resolution of 2 ms and showed that the dynein undergoes stepwise movement with a regular 8-nm step size. A distribution of dwell times between successive steps was well fitted by a single exponential function, suggesting one transition rate is rate limiting for the stepwise movement. However, Toba *et al.* (2006) used a nonspecific cross-linker to label dynein molecules with Q-dots so the precise interpretation of their FIONA data was limited by not knowing the position of the fluorescent labels in the molecule.

Reck-Peterson *et al.* (2006), on the other hand, using a functional recombinant dimeric dynein from the budding yeast *S. cerevisiae*, labeled dynein in specific locations with fluorescent dyes or Q-dots and then tracked single molecules by FIONA. The trajectories of dynein movements showed a stepping behavior. When a dynein molecule was labeled at its tail domain, the step size measured was primarily 8 nm. In contrast, when the molecule was labeled at its head domain, the step size was 16 nm.

Based on findings from yeast cytoplasmic dynein, Reck-Peterson *et al.* (2006) proposed a molecular model (which they called the "alternating shuffling model") to explain how processive motion is achieved by cytoplasmic dynein. In the model, two dynein heads alternate taking 16-nm steps, while the centroid position of the molecule moves by 8 nm for each step. The large dimensions of the head ring do not allow the head to alternately "swing" forward at each step, but overlap part of the head ring during the stepping motion.

However, in dynein heteromers, as found in axonemal dyneins, the motor domains do not need to behave in an identical manner. Hence, processive movement of dynein could be described simply in terms of an inchworm model coupled with a diffusion search if we assume that two heads can separate by up to 32 nm when the dynein shows processive movements with 16-nm steps.

As described above, most biophysical measurements of dynein have been performed using cytoplasmic dyneins. For the understanding of axonemal dyneins, intensive biophysical measurements at the single-molecule level are required, although this is a real challenge.

IV. Summary

The aim of this chapter has been to introduce readers to some of the background on single-molecule studies of axonemal dyneins and specifically to illustrate this large body of work by discussing specific examples including work with

dynein-c and dynein-f. Single-molecule studies of dynein–microtubule interactions have been at the forefront in terms of technology development and in terms of applying new and emerging techniques to address specific questions of dyneins. We are obtaining an increasingly clear picture of how dynein works at the level of molecular rearrangements during the ATPase cycle but there is still much to learn.

Acknowledgments

We thank Dr. Yuji Shitaka for searching optimal conditions for *in vitro* motility assays. We also thank Ms. Yukako Sakai for technical support. This work was supported by the Grant-in-Aid for Scientific Research on the Priority Area "Regulation of Nano-systems in Cells" by the Ministry of Education, Science, and Culture of Japan.

References

Adachi, K., Oiwa, K., Nishizaka, T., Furuike, S., Noji, H., Itoh, H., Yoshida, M., and Kinosita, K. (2007). Coupling of rotation and catalysis in F_1-ATPase revealed by single-molecule imaging and manipulation. *Cell* **130**, 309–321.

Asai, D.J., and Lee, S.W. (1995). The structure and function of dynein heavy-chains. *Mol. Cells* **5**, 299–305.

Ashkin, A., Dziedzic, J.M., Bjorkholm, J.E., and Chu, S. (1986). Observation of a Single-beam gradient force optical trap for dielectric particles. *Optics Lett.* **11**, 288–290.

Avolio, J., Glazzard, A.N., Holwill, M.E., and Satir, P. (1986). Structures attached to doublet microtubules of cilia: Computer modeling of thin-section and negative-stain stereo images. *Proc. Natl. Acad. Sci. USA* **83**, 4804–4808.

Avolio, J., Lebduska, S., and Satir, P. (1984). Dynein arm substructure and the orientation of arm-microtubule attachments. *J. Mol. Biol.* **173**, 389–401.

Axelrod, D. (2003). Total internal reflection fluorescence microscopy in cell biology. *Methods Enzymol.* **361**, 1–33.

Axelrod, D., Burghardt, T.P., and Thompson, N.L. (1984). Total internal-reflection fluorescence. *Ann. Rev. Biophys. Bioeng.* **13**, 247–268.

Block, S.M., Goldstein, L.S., and Schnapp, B.J. (1990). Bead movement by single kinesin molecules studied with optical tweezers. *Nature* **348**, 348–352.

Burgess, S.A. (1995). Rigor and relaxed outer dynein arms in replicas of cryofixed motile flagella. *J. Mol. Biol.* **250**, 52–63.

Cheezum, M.K., Walker, W.F., and Guilford, W.H. (2001). Quantitative comparison of algorithms for tracking single fluorescent particles. *Biophys. J.* **81**, 2378–2388.

Funatsu, T., Harada, Y., Tokunaga, M., Saito, K., and Yanagida, T. (1995). Imaging of single fluorescent molecules and individual ATP turnovers by single myosin molecules in aqueous solution. *Nature* **374**, 555–559.

Gennerich, A., Carter, A.P., Reck-Peterson, S.L., and Vale, R.D. (2007). Force-induced bidirectional stepping of cytoplasmic dynein. *Cell* **131**, 952–965.

Goldman, Y.E. (2008). Imaging and molecular motors. *In* "Single Molecule Dynamics in Life Science" (T. Yanagida and Y. Ishii, eds.), pp. 41–76. Wiley-VCH GmbH., Berlin.

Goodenough, U.W., and Heuser, J.E. (1982). Substructure of the outer dynein arm. *J. Cell. Biol.* **95**, 798–815.

Goodenough, U., and Heuser, J.E. (1984). Structural comparison of purified dynein proteins with in situ dynein arms. *J. Mol. Biol.* **180**, 1083–1118.

Gorman, D.S., and Levine, R.P. (1965). Cytochrome f and plastocyanin: Their sequence in the photosynthetic electron transport chain of *Chlamydomonas reinhardi*. *Proc. Natl. Acad. Sci. USA* **54**, 1665–1669.

Hancock, W.O., and Howard, J. (1998). Processivity of the motor protein kinesin requires two heads. *J. Cell Biol.* **140**, 1395–1405.

Harada, Y., Sakurada, K., Aoki, T., Thomas, D.D., and Yanagida, T. (1990). Mechanochemical coupling in actomyosin energy transduction studied by *in vitro* movement assay. *J. Mol. Biol.* **216**, 49–68.

Hirakawa, E., Higuchi, H., and Toyoshima, Y.Y. (2000). Processive movement of single 22S dynein molecules occurs only at low ATP concentrations. *Proc. Natl. Acad. Sci. USA* **97**, 2533–2537.

Höök, P., Mikami, A., Shafer, B., Chait, B.T., Rosenfeld, S.S., and Vallee, R.B. (2005). Long range allosteric control of cytoplasmic dynein ATPase activity by the stalk and C-terminal domains. *J. Biol. Chem.* **280**, 33045–33054.

Hyman, A., Drechsel, D., Kellogg, D., Salser, S., Sawin, K., Steffen, P., Wordeman, L., and Mitchison, T. (1991). Preparation of modified tubulins. *Methods Enzymol.* **196**, 478–485.

Inoue, Y., and Shingyoji, C. (2007). The roles of noncatalytic ATP binding and ADP binding in the regulation of dynein motile activity in flagella. *Cell Motil. Cytoskelet.* **64**, 690–704.

Ishijima, A., Kojima, H., Funatsu, T., Tokunaga, M., Higuchi, H., Tanaka, H., and Yanagida, T. (1998). Simultaneous observation of individual ATPase and mechanical events by a single myosin molecule during interaction with actin. *Cell* **92**, 161–171.

Johnson, K.A., and Wall, J.S. (1983). Structure and molecular weight of the dynein ATPase. *J. Cell Biol.* **96**, 669–678.

Kagami, O., and Kamiya, R. (1992). Translocation and rotation of microtubules caused by multiple species of *Chlamydomonas* inner-arm dynein. *J. Cell Sci.* **103**, 653–664.

Kamiya, R. (2002). Functional diversity of axonemal dyneins as studied in Chlamydomonas mutants. *Inter. Rev. Cytol.* **219**, 115–155.

Kikushima, K., and Kamiya, R. (2008). Clockwise translocation of microtubules by flagellar inner-arm dyneins *in vitro*. *Biophys. J.* **94**, 4014–4019.

King, S.M. (1995). Large-scale isolation of Chlamydomonas flagella. *Methods Cell Biol.* **47**, 9–12.

Kotani, N., Sakakibara, H., Burgess, S.A., Kojima, H., and Oiwa, K. (2007). Mechanical properties of inner-arm dynein-F (dynein I1) studied with in vitro motility assays. *Biophys. J.* **93**, 886–894.

Mallik, R., Carter, B.C., Lex, S.A., King, S.J., and Gross, S.P. (2004). Cytoplasmic dynein functions as a gear in response to load. *Nature* **427**, 649–652.

Mallik, R., and Gross, S.P. (2004). Molecular motors: Strategies to get along. *Curr. Biol.* **14**, R971–R982.

Mashanov, G.I., and Molloy, J.E. (2007). Automatic detection of single fluorophores in live cells. *Biophys. J.* **92**, 2199–2211.

Nishiura, M., Kon, T., Shiroguchi, K., Ohkura, R., Shima, T., Toyoshima, Y.Y., and Sutoh, K. (2004). A single-headed recombinant fragment of *Dictyostelium* cytoplasmic dynein can drive the robust sliding of microtubules. *J. Biol. Chem.* **279**, 22799–22802.

Nishiyama, M., Muto, E., Inoue, Y., Yanagida, T., and Higuchi, H. (2001). Substeps within the 8-nm step of the ATPase cycle of single kinesin molecules. *Nat. Cell Biol.* **3**, 425–428.

Nishizaka, T., Oiwa, K., Noji, H., Kimura, S., Muneyuki, E., Yoshida, M., and Kinosita, K., Jr. (2004). Chemomechanical coupling in F_1-ATPase revealed by simultaneous observation of nucleotide kinetics and rotation. *Nat. Struct. Mol. Biol.* **11**, 142–148.

Oiwa, K., and Sakakibara, H. (2005). Recent progress in dynein structure and mechanism. *Curr. Opin. Cell Biol.* **17**, 98–103.

Oiwa, K., Eccleston, J.F., Anson, M., Kikumoto, M., Davis, C.T., Reid, G.P., Ferenczi, M.A., Corrie, J.E., Yamada, A., Nakayama, H., and Trentham, D.R. (2000). Comparative single-molecule and ensemble myosin enzymology: sulfoindocyanine ATP and ADP derivatives. *Biophys. J.* **78**, 3048–3071.

Reck-Peterson, S.L., and Vale, R.D. (2004). Molecular dissection of the roles of nucleotide binding and hydrolysis in dynein's AAA domains in Saccharomyces cerevisiae. *Proc. Natl. Acad. Sci. USA* **101**, 1491–1495.

Reck-Peterson, S.L., Yildiz, A., Carter, A.P., Gennerich, A., Zhang, N., and Vale, R.D. (2006). Single-molecule analysis of dynein processivity and stepping behavior. *Cell* **126**, 335–348.

Sakakibara, H., and Nakayama, H. (1998). Translocation of microtubules caused by the α, β and γ outer arm dynein subparticles of *Chlamydomonas*. *J. Cell Sci.* **111**, 1155–1164.

Sakakibara, H., Kojima, H., Sakai, Y., Katayama, E., and Oiwa, K. (1999). Inner-arm dynein c of *Chlamydomonas* flagella is a single-headed processive motor. *Nature* **400**, 586–590.

Sakamoto, T., Webb, M.R., Forgacs, E., White, H.D., and Sellers, J.R. (2008). Direct observation of the mechanochemical coupling in myosin Va during processive movement. *Nature* **455**, 128–132.

Sale, W.S., Goodenough, U.W., and Heuser, J.E. (1985). The substructure of isolated and in situ outer dynein arms of sea urchin sperm flagella. *J. Cell Biol.* **101**, 1400–1412.

Sheetz, M.P. (1998). "Methods in Cell Biology." Vol. 55. Academic Press, San Diego.

Shingyoji, C., Higuchi, H., Yoshimura, M., Katayama, E., and Yanagida, T. (1998). Dynein arms are oscillating force generators. *Nature* **393**, 711–714.

Svoboda, K., and Block, S.M. (1994). Biological applications of optical forces. *Annu Rev. Biophys. Biomol. Struct.* **23**, 247–285.

Toba, S., Watanabe, T.M., Yamaguchi-Okimoto, L., Toyoshima, Y.Y., and Higuchi, H. (2006). Overlapping hand-over-hand mechanism of single molecular motility of cytoplasmic dynein. *Proc. Natl. Acad. Sci. USA* **103**, 5741–5745.

Toprak, E., and Selvin, P.R. (2007). New fluorescent tools for watching nanometer-scale conformational changes of single molecules. *Annu. Rev. Biophys. Biomol. Struct.* **36**, 349–369.

Vale, R.D., and Toyoshima, Y.Y. (1988). Rotation and translocation of microtubules in vitro induced by dyneins from *Tetrahymena* cilia. *Cell* **52**, 459–469.

Vale, R.D., Funatsu, T., Pierce, D.W., Romberg, L., Harada, Y., and Yanagida, T. (1996). Direct observation of single kinesin molecules moving along microtubules. *Nature* **380**, 451–453.

Vallee, R.B. (1986). Reversible assembly purification of microtubules without assembly-promoting agents and further purification of tubulin, microtubule-associated proteins, and MAP fragments. *Methods Enzymol*. **134**, 89–104.

Witman, G.B. (1986). Isolation of Chlamydomonas flagella and flagellar axonemes. *Methods Enzymol.* **134**, 280–290.

Yagi, T. (2000). ADP-dependent microtubule translocation by flagellar inner-arm dyneins. *Cell Struct. Funct.* **25**, 263–267

Yagi, T., Minoura, I., Fujiwara, A., Saito, R., Yasunaga, T., Hirono, M., and Kamiya, R. (2005). An axonemal dynein particularly important for flagellar movement at high viscosity—Implications from a new Chlamydomonas mutant deficient in the dynein heavy chain gene DHC. *J. Biol. Chem.* **280**, 41412–41420.

Yildiz, A., Forkey, J.N., McKinney, S.A., Ha, T., Goldman, Y.E., and Selvin, P.R. (2003). Myosin V walks hand-over-hand: Single fluorophore imaging with 1.5-nm localization. *Science* **300**, 2061–2065.

Yildiz, A., Tomishige, M., Vale, R.D., and Selvin, P.R. (2004). Kinesin walks hand-over-hand. *Science* **303**, 676–678.

This page intentionally left blank

CHAPTER 7

Protein Electroporation into *Chlamydomonas* for Mutant Rescue

Masahito Hayashi *and* Ritsu Kamiya

Department of Biological Sciences, Graduate School of Science, University of Tokyo, 7-3-1 Hongo, Bunkyo-ku, Tokyo 113-0033, Japan

Abstract

Electroporation can be used to deliver proteins into *Chlamydomonas* cells. This technique is particularly useful to demonstrate rescue of paralyzed-flagella mutants with recombinant proteins that complement the mutations. The appearance of motile cells immediately provides assurance that the recombinant proteins have their native structures and are functional. It can be also used for the introduction of artificially modified proteins or other substances into live cells.

I. Introduction

Chlamydomonas, with its various excellent features, has been the most powerful model organism with which to study the assembly and function of cilia/flagella. However, it also has certain drawbacks when compared with other unicellular organism such as *Tetrahymena* and *Trypanosoma*. One such drawback is that it is not always easy to express large amounts of proteins from cloned cDNA.

METHODS IN CELL BIOLOGY, VOL. 92

978-0-12-374974-1
DOI: 10.1016/S0091-679X(08)92007-0

To circumvent this problem, we could introduce proteins directly into the cells by electroporation, instead of transforming them with the gene. Electroporation has been used to transform *Chlamydomonas* as a means of introducing cloned genes (Brown *et al*., 1991; Shimogawara *et al*., 1998). In other cells such as cultured cells and the cellular slime mold *Dictyostelium*, electroporation has been used for the introduction of a variety of substances in addition to DNA (Yumura *et al.,* 1995). Examples include myosin (Yumura and Uyeda, 1997), antibodies (Ushio-Fukai *et al*., 1999), mRNA (Teruel *et al*., 1999), GTP-γS (Haruta *et al*., 1998), and a calcium indicator (Yumura *et al*., 1996). In *Chlamydomonas*, we showed that muscle actin can be introduced by electroporation and the introduced actin can rescue the mutant *ida5* that lack several inner arm dyneins because of its loss of an actin gene (Hayashi *et al.,* 2001). Later, recombinant proteins of another inner arm dynein subunit (Hayashi *et al*., 2002), and a subunit of radial spokes (Yang *et al*., 2008), were also used to rescue mutants deficient in specific flagellar structures. Thus, protein electroporation is particularly useful when used in combination with mutants lacking the corresponding protein. When the mutant is nonmotile, we can easily detect the rescue by the emergence of motile cells after electroporation. Another merit is that electroporation allows us to introduce artificially modified proteins. For example, we can introduce proteins labeled with a fluorescent dye that is much brighter than green fluorescent protein. We have studied the turnover of inner arm dyneins by a fluorescence recovery after photobleaching method using rhodamine-labeled actin (Watanabe *et al*., 2004). The method described below is mostly based on our experience with the rescue of the nonmotile phenotype of *ida4oda6*, a double mutant of *ida4* (lacking several inner arm dyneins because of the absence of p28) and *oda6* (a slow-swimming mutant lacking outer arm dynein because of the absence of an outer arm subunit), by introduction of p28, the inner arm dynein subunit missing in this mutant (Hayashi *et al*., 2002).

II. Materials and Methods

A. Materials

1. Electroporation generator. Possibly most generators on the market can be used. We are using a BTX ECM600 (San Diego, CA).
2. Cuvette. BTX Model 620, or an equivalent, with a 2-mm gap.
3. Cells. Most *Chlamydomonas* strains can be used.
4. Solutions.

Autolysin solution: Gamete lysin for removing cell walls from vegetative cells. It can be obtained from mating gametes and stored frozen (Dutcher, 1995).

HMDKCaS: 30 mM HEPES, 5 mM $MgSO_4$, 1 mM DTT, 50 mM, potassium acetate, 1 mM calcium acetate, 60 mM sucrose, pH 7.4. The concentration of potassium acetate can be changed according to the solubility of the protein. In our study using actin, we used the following buffer to suppress actin polymerization: 0.2 mM ATP, 0.8 mM imidazole, 0.1 mM $CaCl_2$, 0.5 mM 2-mercaptoethanol,

pH 7.5. Presence of sucrose and $\geq$0.1 mM Ca^{2+} is important. In general, lower ionic strength results in lower optimal voltage.

TAPS: Tris-acetate-phosphate (TAP) culture medium (Harris, 2009), supplemented with 60 mM sucrose.

B. Methods

1. Cell wall is digested in an autolysin solution. The progress of digestion is checked under a phase contrast microscope. The digested cells are washed with HMDKCaS and suspended in the same solution (final concentration: 1×10^8 cells/ml).
2. The cell suspension and a protein solution made in HMDKCaS (0.2 mg/ml) are mixed at a 1:1 volume ratio. As a control, autolysin-treated cells are mixed with the HMDKCaS solution without protein and treated in the same manner as the experimental sample.
3. A 125-µl aliquot of the mixture is transferred to an electroporation cuvette and subjected to an electric pulse. Care should be taken to keep the temperature (15°C) and the time after cell washing (15 min) constant.
4. Electroporation is carried out at a variable voltage, with the resistance set to 24 Ω and the conductance to 600 µF. In our previous study with p28/*ida4oda6*, 1800 V/cm was optimal in the percentage of rescued cells; ~60% of total cells survived and about half of the survived cells recovered motility (Fig. 1). The overall time constant used in standard experiments is about 15 ms, although this is not a critical factor.
5. After pulse application, the cuvette is placed in a water bath at room temperature for 30 min and stirred every 5 min. The cells are then suspended in 300 µl of TAPS (Shimogawara *et al*., 1998), washed three times with the same solution, and incubated at room temperature.

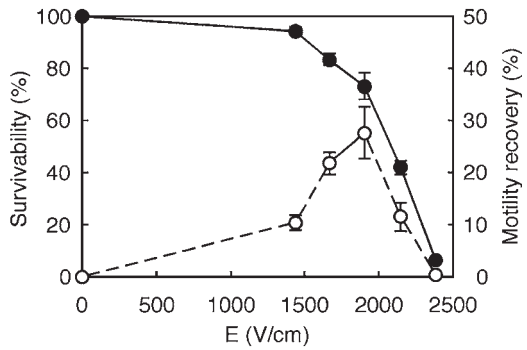

Fig. 1 Effect of voltage on the percentage of *ida*4*oda*6 that survived pulse application (survivability) (solid circles) and that recovered motility (motility recovery) (open circles). An electric pulse was applied in the presence of 10-µg/ml bacterially produced p28 at the indicated voltage. The number of cells was counted 4 h after pulse application. From Hayashi *et al*. (2002).

6. Cells are examined for motility recovery 1–2 h after electroporation. In the case of p28 and *ida4oda6*, motility recovery is complete in 2–3 h.

III. Discussion

Protein electroporation is a powerful method for determining whether a recombinant protein produced in bacteria or other cells has a native structure. We have thus far tested two subunits of inner arm dynein (actin, p28), three subunits of radial spokes (RSP4, RSP6, RSP9) (Kohno *et al*., in preparation), and two subunits of outer dynein arm-docking complex (ODA-DC) (DC1, DC2) (Ken-ichi Wakabayashi and Ritsu Kamiya, unpublished) in combination with mutants lacking these particular proteins. Also, a study with a radial spoke protein, HSP40, has been reported (Yang *et al*., 2008). In almost all cases, recombinant proteins were found to rescue the mutant phenotypes, indicating that they had native structures. In some cases, such as the experiment with ODA-DC (total molecular mass ~ 150 kD), we were unable to prepare a sufficiently high concentration of protein samples and only partial rescue appeared to take place; flagella displayed only twitching movements after electroporation. However, even such partial rescue is indicative of the native structure of the recombinant proteins.

In our experiments with p28, as many as 30% of the electroporated *ida4oda6* cells came to swim as fast as *oda6* cells and displayed clear phototaxis under optimal conditions (Fig. 1). An interesting future application is concentration of rescued cells using their phototaxis to obtain a pure population of cells that contain the recombinant protein. A second application is coelectroporation; we could carry out electroporation in the presence of a second protein (or other substance) in addition to the recombinant protein that can rescue the mutant phenotype. Since it is likely that rescued cells have incorporated the second protein also, we will be able to collect cells that are loaded with it.

References

Brown, L.E., Sprecher, S.L., and Keller, L.R. (1991). Introduction of exogenous DNA into *Chlamydomonas reinhardtii* by electroporation. *Mol. Cell Biol.* **11**, 2328–2332.

Dutcher, S.K. (1995). Purification of basal bodies and basal body complexes from *Chlamydomonas reinhardtii*. *Methods Cell Biol.* **47**, 323–334.

Harris, E.H. (2009). "The *Chlamydomonas* Sourcebook: Introduction to *Chlamydomonas* and Its Laboratory Use." 2nd edn., Vol. 1, pp. 444. Elsevier, Amsterdam.

Haruta, T., Morris, A.J., Vollenweider, P., Nelson, J.G., Rose, D.W., Mueckler, M., and Olefsky, J.M. (1998). Ligand-independent GLUT4 translocation induced by guanosine 5′-O-(3-thiotriphosphate) involves tyrosine phosphorylation. *Endocrinology* **139**, 358–364.

Hayashi, M., Hirono, M., and Kamiya, R. (2001). Recovery of flagellar dynein function in a *Chlamydomonas* actin/dynein-deficient mutant upon introduction of muscle actin by electroporation. *Cell Motil. Cytoskeleton* **49**, 146–153.

Hayashi, M., Yanagisawa, H., Hirono, M., and Kamiya, R. (2002). Rescue of a *Chlamydomonas* inner-arm-dynein-deficient mutant by electroporation-mediated delivery of recombinant p28 light chain. *Cell Motil. Cytoskeleton* **53**, 273–280.

Shimogawara, K., Fujiwara, S., Grossman, A., and Usuda, H. (1998). High efficiency transformation of *Chlamydomonas reinhardtii* by electroporation. *Genetics* **148**, 1821–1828.

Teruel, M.N., Blanpied, T.A., Shen, K., Augustine, G.J., and Meyer, T. (1999). A versatile microporation technique for the transfection of cultured CNS neurons. *J. Neurosci. Methods* **93**, 37–48.

Ushio-Fukai, M., Alexander, R.W., Akers, M., Lyons, P.R., Lassegue, B., and Griendling, K.K. (1999). Angiotensin II receptor coupling to phospholipase D is mediated by the bg subunits of heterotrimeric G proteins in vascular smooth muscle cells. *Mol. Pharmacol.* **55**, 142–149.

Watanabe, Y., Hayashi, M., Yagi, T., and Kamiya, R. (2004). Turnover of actin in *Chlamydomonas* flagella detected by fluorescence recovery after photobleaching (FRAP). *Cell Struct. Funct.* **29**, 67–72.

Yang, C., Owen, H.A., and Yang, P. (2008). Dimeric heat shock protein 40 binds radial spokes for generating coupled power strokes and recovery strokes of 9 + 2 flagella. *J. Cell Biol.* **180**, 403–415.

Yumura, S., Furuya, K., and Takeuchi, I. (1996). Intracellular free calcium responses during chemotaxis of *Dictyostelium* cells. *J. Cell Sci.* **109**, 2673–2678.

Yumura, S., Matsuzaki, R., and Kitanishi-Yumura, T. (1995). Introduction of macromolecules into living *Dictyostelium* cells by electroporation. *Cell Struct. Funct.* **20**, 185–190.

Yumura, S., and Uyeda, T.Q.P. (1997). Transport of myosin II to the equatorial region without its own motor activity in mitotic *Dictyostelium* cells. *Mol. Biol. Cell* **8**, 2089–2099.

This page intentionally left blank

CHAPTER 8

Analysis of the Role of Nucleotides in Axonemal Dynein Function

Chikako Shingyoji

Department of Biological Sciences, Graduate School of Science, University of Tokyo, Hongo, Tokyo 113-0033, Japan

Abstract

Axonemal dynein in flagella and cilia is a motor molecule that produces microtubule sliding, powered by the energy of ATP hydrolysis. Our goal is to understand how dynein motile activity is controlled to produce the characteristic oscillatory movement of flagella. ATP, the energy source for dynein, is also important as a regulator of dynein activity. Among the four nucleotide-binding sites of a dynein heavy chain, one is the primary ATP hydrolyzing site while the

METHODS IN CELL BIOLOGY, VOL. 92

978-0-12-374974-1
DOI: 10.1016/S0091-679X(08)92008-2

others are noncatalytic sites and thought to perform regulatory functions. Stable binding of both ATP and ADP to these regulatory sites is probably essential for the chemomechanical energy transduction in dynein. Although the ATP concentration in beating flagella is physiologically high and constant, at any moment in the oscillatory cycle some dynein molecules are active while others are not, and the motile activity of dynein oscillates temporally and spatially in the axoneme. It is likely that the basic mechanism underlying the highly dynamic control of dynein activity involves the ATP-dependent inhibition and ADP-dependent activation (or release of inhibition) of dynein. How the inhibition and activation can be induced in beating flagella is still unknown. It seems, however, that the mechanical force of bending is involved in the activation of dynein, probably through the control of noncatalytic nucleotide binding to dynein. This chapter provides an overview of several approaches, using sea urchin sperm flagella, to studying the roles of ATP and ADP in the regulation of dynein activity with or without the mechanical signal of bending.

I. Introduction

In sea urchin sperm flagella, the intracellular concentration of ATP is maintained at a high (mM) level by the activities of adenylate kinase and creatine kinase (Kinukawa *et al*., 2007). High ATP is not limited to sea urchin sperm; it is common in flagella and cilia. Flagellar oscillation depends primarily on the ATP concentration. However, dynein motile activity in flagella is not solely determined by ATP (Shingyoji *et al*., 1995) but is modulated by mechanical signals from bending (Gibbons *et al*., 1987; Hayashi and Shingyoji, 2008; Hayashibe *et al*., 1997; Morita and Shingyoji, 2004; Okuno and Hiramoto, 1976; Shingyoji *et al*., 1991, 1995) as well as by chemical signals such as protein phosphorylation/dephosphorylation, Ca^{2+}, and pH (Nakano *et al*., 2003; Porter and Sale, 2000; Smith and Yang, 2004; Yoshimura *et al*., 2007). Characteristic features of nucleotide conditions that influence dynein motile activity are also reported: in many cilia and flagella higher concentrations of ATP inhibit not only the oscillatory bending movement of demembranated flagella but also the sliding disintegration of protease-treated axonemes into individual doublets (Kinoshita *et al*., 1995; Omoto *et al*., 1996; Nakano *et al*., 2003; Yoshimura *et al*., 2007). These inhibitory effects of higher concentrations of ATP can be released by ADP (Kinoshita *et al*., 1995; Omoto *et al*., 1996; Yoshimura *et al*., 2007). The role of ADP in enhancing dynein motile activity has also been shown in microtubule gliding assay experiments using purified monomeric dynein (Furuta *et al*., 2009; Inoue and Shingyoji, 2007; Kikushima *et al*., 2004; Shiroguchi and Toyoshima, 2001; Yagi, 2000) and in mechanical bending experiments (Hayashi and Shingyoji, 2009; Ishikawa and Shingyoji, 2007). Furthermore, the binding of both ATP and ADP to dynein molecules appears to be essential for dynein motile activity (Inoue and Shingyoji, 2007). It seems likely that ATP and ADP are involved in the regulation of the

motile activity of dynein not only at the level of each molecule but also at the higher (cellular) level of the axoneme; the process probably occurs through stable ATP and ADP binding to the three noncatalytic nucleotide binding sites of the dynein heavy chain.

The purpose of this chapter is to provide a guide to analyzing the effects of ATP and ADP on dynein function in the axoneme. Understanding the dynamic control of dynein activity requires the analysis of dynein behavior within the axoneme as well as that of isolated dynein molecules. The basic mechanism of nucleotide-dependent regulation of dynein is similar in the cilia and flagella of various organisms such as *Chlamydomonas* flagella, *Tetrahymena* cilia, and sea urchin sperm flagella. The experiments described here have been carried out using sea urchin sperm because they have a long flagellum of about 50 μm and show almost planar beating; both are useful features for the study of mechanical aspects of flagellar movement.

Three approaches have been used. The first approach (A) is to examine the effects of ATP and ADP binding on dynein activity (Inoue and Shingyoji, 2007). Direct observation of ATP and ADP binding to dynein is achieved by using fluorescent ribose-modified ATP and ADP analogues (Bodipy® FL-ATP, TR-ATP, and TR-ADP) with a total internal reflection fluorescence (TIRF) microscope. The ATP analogues can be hydrolyzed by dynein at a level similar to that at which ATP is hydrolyzed but cannot induce sliding disintegration of protease-treated axonemes. This uncoupling between the ATPase activity and the motile activity of dynein gives us a clue to analyzing the mechanism of chemomechanical energy transduction, by searching for the nucleotide conditions necessary for dynein sliding activity.

The second approach (B) is the elastase-treatment assay, which is a novel microtubule sliding assay. In beating flagella we cannot directly observe the sliding activity of dynein, because beating requires some restriction of the free sliding between doublet microtubules in the axoneme. In this approach, the difficulty is overcome by using elastase (Brokaw, 1980) as protease to initiate the sliding disintegration of the axoneme (Nakano *et al*., 2003; Yoshimura and Shingyoji, 1999). Trypsin has been used more widely to digest axonemal substructures that restrict free sliding of doublets (Summers and Gibbons, 1971) but it causes considerable damages to the structure and function of dynein, resulting in the loss of the dynamic control of dynein activity in the axoneme (Imai and Shingyoji, 2003). The trypsin-treated axonemes do not show oscillatory bending movements in response to local, repetitive application of ATP, to which the elastase-treated axonemes respond with oscillatory bending movements, indicating that the latter retain certain regulatory mechanisms for producing local cyclical bending (Shingyoji and Takahashi, 1995). As the possible result of the regulation of dynein activity, the elastase-treated axonemes show in response to applied ATP characteristic sliding disintegration into paired bundles of doublet microtubules, indicating restricted activity of some dyneins (Fig. 1). Such restricted sliding occurs only at the physiologically high ATP concentration, while under lower

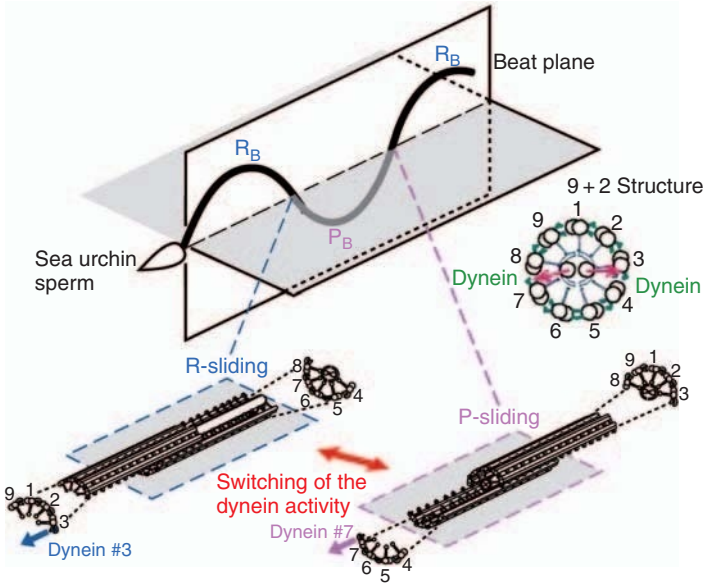

Fig. 1 Diagrams illustrating the flagellar beating of a sea urchin sperm and the regulation of dynein activity. Based on the "switching" model, the formation of P-bend (P_B) and R-bend (R_B) is due to P-sliding and R-sliding, respectively, induced by the dynein arms of the doublets 7 and 3 (or 4), respectively. Modified from Fig. 1 of Hayashi and Shingyoji (2008). (See Plate no. 3 in the Color Plate Section.)

ATP conditions all dyneins are capable of sliding [experiment B-1]. Interestingly, the restricted sliding can be released by ADP even at high ATP. The inhibition of sliding within each doublet bundle is probably caused by the dynein crossbridges that are formed only under the high ATP condition. This idea is supported by the observation of continuous beating in elastase-treated flagella [experiment B-2].

The third approach (C) is a dynein activation assay by mechanically imposed bending. This approach includes two experiments: (C-1) bending-induced switching of dynein activity in elastase-treated axonemes (Hayashi and Shingyoji, 2008, 2009) and (C-2) induction of beating in demembranated, motionless flagella at very low ATP concentrations (Ishikawa and Shingyoji, 2007). An essential process in the regulation of dynein in beating flagella is switching, that is, to alternate its activity between the two sides of the central pair (CP) microtubules (Fig. 1). When a bend is formed in the axoneme, dyneins on one side of the CP become active while those on the opposite side are less active, and the activity of dynein on opposite sides of the CP alternates during flagellar oscillation. By externally applied bending, the switching of dynein activity can be induced in the elastase-treated axonemes [experiment C-1]. Another example of dynein activation is induction of flagellar beating by imposed bending in immotile flagella at very low ATP [experiment C-2]. An involvement of ADP in the enhancement of the dynein activity is also shown in these two experiments.

II. Materials and Methods

A. Materials

Axonemes are prepared from the sea urchins, *Pseudocentrotus depressus, Clypeaster japonicus, Anthocidaris crassispina, Hemicentrotus pulcherrimus, Strongylocentrotus intermedius, Strongylocentrotus nudus, and Scaphechinus mirabilis*. As the beating plane is more stable in the sperm of *P. depressus* and *C. japonicus* due to their reduced ability to rotate in the beating plane compared to the other species (Takahashi *et al*., 1991), flagella of these two species show higher frequency of occurrence of sliding disintegration into paired bundles in elastase-treated axonemes (see Section IV). 21S dynein is isolated and purified from the axonemes of sea urchins according to the methods described in the references (Imai and Shingyoji, 2003; Inoue and Shingyoji, 2007). 21S dyneins of the sea urchins, *P. depressus, H. pulcherrimus, S. intermedius*, and *S. nudus*, respond to nucleotides similarly, but their interaction profiles with microtubules are different (Ueno *et al*., 2008).

B. Solutions and Chemicals

Ca^{2+}-free artificial seawater: 465 mM NaCl, 10 mM KCl, 25 mM $MgSO_4$, 25 mM $MgCl_2$, and 2 mM Tris-HCl, pH 8.0.

Demembranating solution: 0.04% (w/v) Triton X-100, 0.15 M potassium acetate, 2 mM $MgSO_4$, 2 mM glycoletherdiamine-*N, N, N′, N′*-tetraacetic acid (EGTA), 1 mM dithiothreitol (DTT), and 10 mM Tris-HCl, pH 8.0.

Ca^{2+}-free reactivating solution ($<10^{-9}$ M Ca^{2+}): 0.15 M potassium acetate, 2 mM $MgSO_4$, 2 mM EGTA, 1 mM DTT, 2% (w/v) polyethyleneglycol (MW 20,000), and 10 mM Tris-HCl (or 20 mM HEPES), pH 8.0, with 0.02–1.0 mM ATP.

10^{-4} M Ca^{2+} reactivating solution: reactivating solution containing 1 mM ATP with 2.2 mM Ca^{2+} provides 10^{-4} M Ca^{2+}.

Elastase treatment: elastase solution [5 μg/ml elastase (Sigma, type III) and 5 μg/ml trypsin inhibitor (Sigma, type I-S) in the reactivating solution (HEPES) without ATP]; ovoinhibitor solution [50 μg/ml ovoinhibitor from chicken egg white (Sigma, type IV-O) in the reactivating solution (HEPES) without ATP]; casein solution [~1 mg/ml casein in the reactivating solution (HEPES) without ATP].

Assay buffer for fluorescence microscopy: an oxygen reduction system [1% (v/v) β-mercaptoethanol, 20 mM glucose, 36 μg/ml catalase, 220 μg/ml glucose oxidase] in reactivating solution (HEPES) at pH 7.8.

Caged ATP and caged ADP: 0.5 and 1 mM caged ATP (p^3-[1-(2-nitrophenyl) ethyl] ATP, Dojindo 349-05501) in reactivating solution with hexokinase (Toyobo, HXK-301; 40 units/ml under low Ca^{2+} condition and 30 units/ml under high Ca^{2+} condition) or apyrase (Sigma, A6535; 40 units/ml or 15 units/ml). 0.02–0.4 mM caged ADP (Invitrogen A-7056).

Fluorescent analogues: Bodipy® TR-ATP (A22352), Bodipy® TR-ADP (A22359), and Bodipy® FL-ATP (A12410) from Invitrogen.

C. Observation and Micromanipulation

Observation of flagellar beating: An inverted microscope equipped with a dark-field condenser (Nikon TMD) or phase contrast optics (Zeiss Axiovert 35) and with a ×40 objective lens. A CCD camera (Watec Neptune 100, Watec Co., Japan) with an image intensifier (DII-2050, Nakanishi Image Lab Inc., Tokyo, Japan).

Observation of sliding disintegration: A dark-field microscope with a halogen lamp (Nikon TMD) or an inverted fluorescent microscope equipped with a caged system (Olympus, IX-70 with IX-RFA/CAGED) with a ×100 objective lens (Olympus UPlanApo, NA = 1.35). Mercury arc lamps for illumination and UV flashes to photorelease ATP (or ADP) from caged ATP (or caged ADP) built into the fluorescent microscope (Fig. 2A).

TIRF microscopy: Details of an objective-type TIRF microscope are shown in the reference (Inoue and Shingyoji, 2007). For observation of the fluorescence of Bodipy® TR and Bodipy® FL-ATP, a laser beam of 532 nm (from a diode-pumped Nd:YVO_4 laser, 100 mW, GCL-100-S, CrystaLaser, USA) with a band-pass filter 620DF50 (transmission wavelength = 595–645 nm, Omega) and that of 488 nm (Ion Laser Technology, USA) with filters (a dichroic mirror, BA515, Olympus; a low-pass filter of transmission wavelength <570 nm) are used, respectively.

Micromanipulation: A glass microneedle made of a glass rod of 1 mm diameter using a micropipette puller (Narishige, Model PP-830) is attached to a hydraulic micromanipulator (Narishige, MW-3 or WR-88) mounted on the body of the inverted microscope (Fig. 2B).

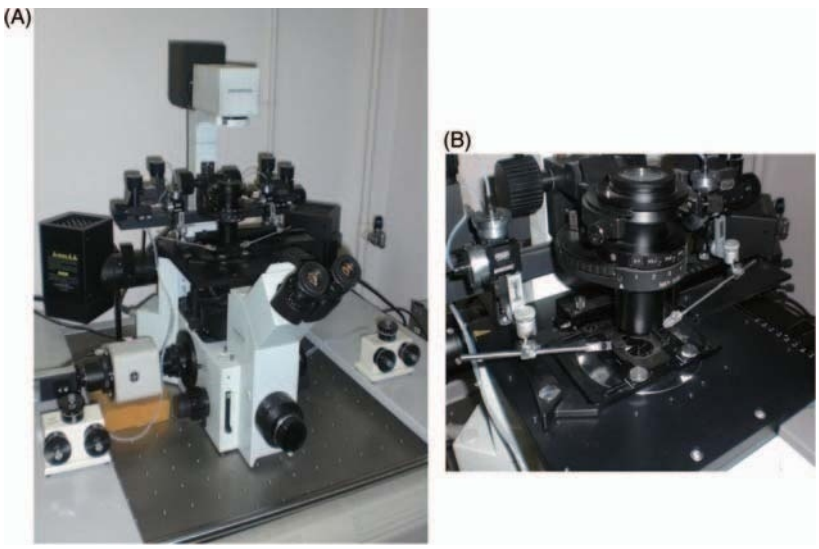

Fig. 2 The inverted fluorescent microscope on an air-suspension laboratory bench (A) equipped with two sets of hydraulic micromanipulators, to which glass microneedles are attached (B).

III. Methods

A. Binding Assay of Fluorescent ATP and ADP Analogues

[Experiment A-1]: A perfusion chamber of ~15μl, constructed with cover slips, is coated with BSA. The chamber is perfused first with the reactivating solution without ATP (buffer) and then with 0.1 mg/ml 21S dynein in buffer and kept still for 5 min. Removal of the unbound 21S dynein, by perfusing buffer again, is followed by perfusion of 0.1–5 nM nucleotide analogues in the assay buffer with an oxygen reduction system. Imaging of Bodipy® TR-ATP (TR-ATP), Bodipy® TR-ADP (TR-ADP), and Bodipy® FL-ATP (FL-ATP) is carried out by an objective-type TIRF microscope at room temperature (24–26°C). To analyze the stable binding of the nucleotide analogues for longer than the fluorescence lifetime, the dynein-coated glass surface should be surveyed in one area and then a neighboring region (Fig. 3A).

[Experiment A-2]: For observation of stable binding of ADP to dynein in the axoneme, demembranated flagella are placed in a 2-μl chamber and the reactivating solution containing 0.02 mM ATP and 30 nM TR-ADP at pH 7.0 is used (Fig. 3A).

B. Sliding Disintegration of Elastase-Treated Axonemes

To obtain demembranated flagella (axonemes), spermatozoa suspended in 7–20 volumes of Ca^{2+}-free artificial seawater are treated with 7.5 volumes of demembranating solution for 60 s at 20–23°C (*Pseudocentrotus, Hemicentrotus*) or 24–26°C (other species) (Fig. 3B). The demembranation is stopped by adding 10 volumes of Ca^{2+}-free reactivating solution without ATP. [For observation under a fluorescent microscope the demembranated sperm are labeled with 9.4 μM tetramethylrhodamine (Invitrogen, C-1171)]. Demembranated flagella are reactivated in Ca^{2+}-free reactivating solutions containing 1 and 0.02 mM ATP [experiment B-2] or 1.5–3 μM ATP [experiment C-2]. In the experiment B-2, 5 μg/ml elastase with trypsin inhibitor is added to the reactivating solution.

In some of the sliding experiments [experiments B-1 and C-1], the demembranated sperm are homogenized and sperm heads are removed to obtain axonemal fragments. To observe sliding disintegration, a suspension of the axonemes is introduced into a 10 ~ 15 μl (for ATP in the experiment B-1) or a 5 μl (for caged ATP in the experiment C-1) perfusion chamber. In the perfusion chamber the axonemes are treated with the elastase solution for 1.5 min; the treatment is stopped with ovoinhibitor, which is followed by perfusion with the casein solution and the assay buffer containing ATP or caged ATP (with or without caged ADP). ATP (or ADP) is released from caged ATP (or caged ADP) by 60-ms UV illumination through a 360 ± 5 nm band-pass filter and an electronic shutter to induce sliding movements.

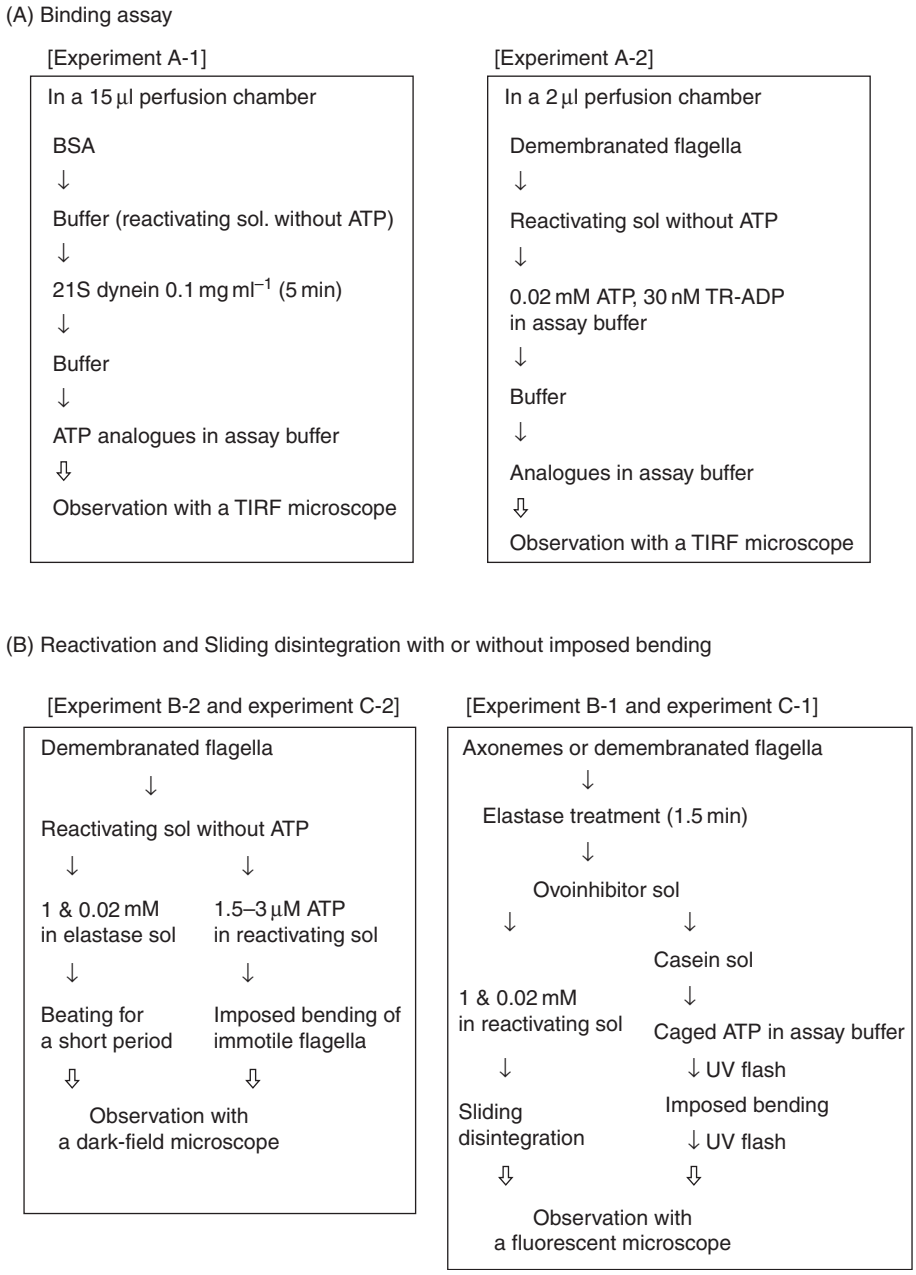

Fig. 3 Flow summaries of the methods.

C. Micromanipulation for Imposed Bending

In the experiment C-1, axonemes attached to the bottom surface of the perfusion chamber are bent with a glass microneedle. For inserting a glass microneedle into the assay buffer in the chamber, an open surface is needed over the axonemes (Fig. 4). When the elastase-treated axonemes labeled with rhodamine are bent, the phase contrast image of the microneedle and the fluorescent image of the axonemes can be observed simultaneously with the halogen lamp and the excitation light.

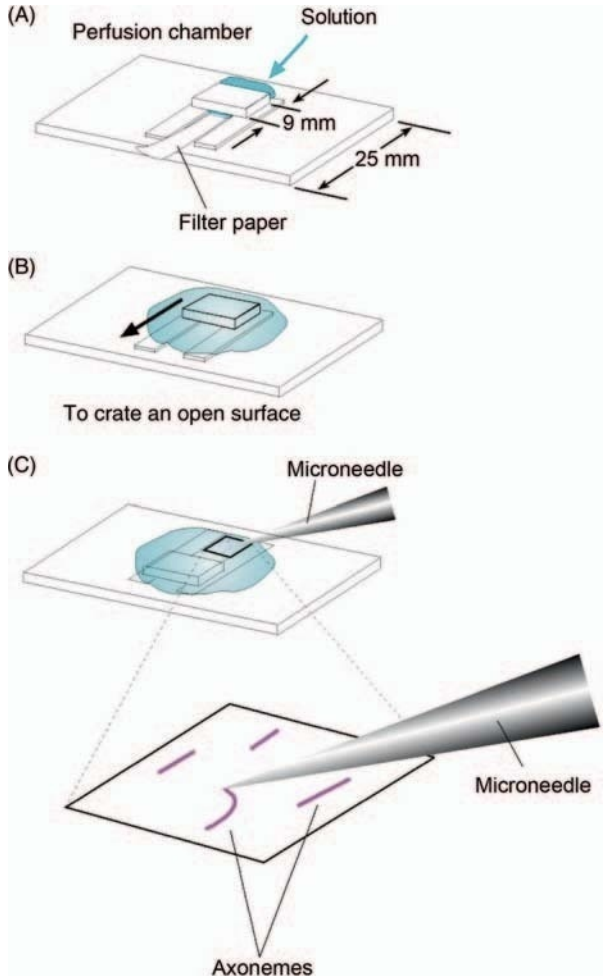

Fig. 4 Schematic diagram showing the chamber used for perfusion of experimental solutions (A) and the method for bringing the microneedle into contact with the axonemes (B and C). Modified from Fig. S1 of Morita and Shingyoji (2004). (See Plate no. 4 in the Color Plate Section.)

In the experiment C-2, demembranated sperm reactivated at low (1.5–3 μM) ATP concentrations, which are close to the threshold ATP concentration for spontaneous beating, are used. A motionless sperm is caught with two glass microneedles coated with 0.1% poly-L-lysine (Sigma, P-126) by attaching one needle to the head and the other one to the distal end of the axoneme. To bend the flagellar axoneme, the microneedle attached to the distal end is moved with respect to the head.

IV. Results and Discussion

A. Effects of Stable ATP and ADP Binding on Dynein Motile Activity

When 0.1–5 nM fluorescent ATP analogues, such as FL-ATP and TR-ATP, are applied onto a dynein-coated glass surface, binding of their molecules to 21S dynein can be observed by TIRF microscopy as fluorescent spots (Fig. 5A) [experiment A-1] (Inoue and Shingyoji, 2007). The fluorescent intensity of each spot shows quantized changes, consisting of transient spike-like changes and more prolonged changes: the transient changes probably reflect hydrolysis in dynein, while the prolonged changes reflect stable binding of analogues to dynein. FL-ATP is hydrolyzed by 21S dynein at the rate of 10.6 ± 1.4/s at 1 mM, which is close to the rate of ATP hydrolysis (13.6 ± 2.8/s). Microtubules (4 mg/ml) increase the rate of hydrolysis of ATP at 1 mM by 1.9-fold. Similar activation by microtubules is observed in FL-ATP (1.4-fold) at 1 mM. The stable binding of the nucleotide analogues are characterized by estimating the dissociation rates (Fig. 5B). They are well fitted to single exponential curves with dissociation rates of 0.0055–0.0082/s, which are 87- to 1300-fold slower than the rate of hydrolysis.

The ATP analogues can be hydrolyzed by dynein at rates similar to that at which ATP is hydrolyzed but cannot induce sliding disintegration of the elastase-treated axonemes (Fig. 5C left). This uncoupling between the ATPase activity and the motile activity of dynein in the presence of FL-ATP seems to be caused by the stable binding of FL-ATP to noncatalytic sites of dynein heavy chains (Fig. 5D left). FL-ATP stably bound to dynein probably behaves differently from ATP and inhibits the force generation of dynein for microtubule sliding. However, after being pretreated for 1–10 min with 1 mM AMPPNP, a nonhydrolyzable ATP analogue, FL-ATP causes microtubule sliding in the elastase-treated axonemes (Fig. 5C right). As the sliding disintegration continues for a few minutes (<3.5 min) after removal of AMPPNP, AMPPNP is probably bound to dynein stably and behaves similarly to ATP (Fig. 5D right). Several reports show that ADP is involved in the activation of dynein motility (Inoue and Shingyoji, 2007; Kikushima *et al*., 2004; Yagi, 2000), indicating that the stable binding of both ATP and ADP to dynein regulatory sites is essential for dynein motile activity (Fig. 5D right).

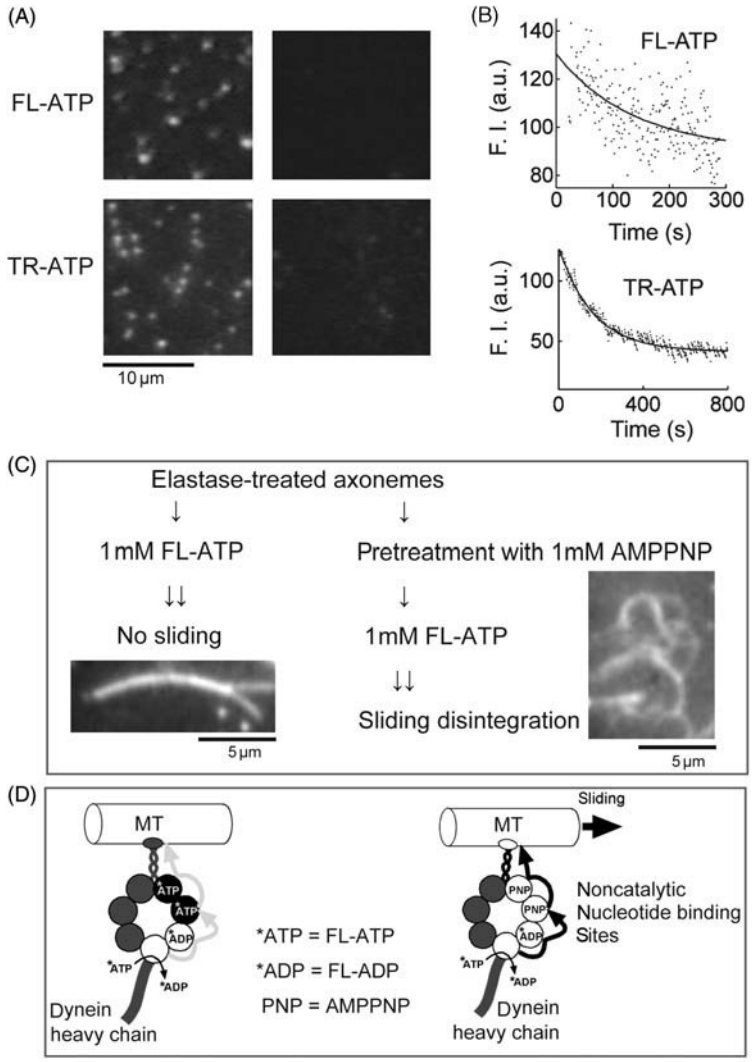

Fig. 5 Effects of ATP and ADP binding on dynein activity [experiment A-1]. (A) Video images showing fluorescent spots, observed for 1 nM FL-ATP and TR-ATP on 21S dynein-coated glass surfaces (left). No fluorescent spots were observed on the glass surface without dynein in the presence of 1 nM ATP analogues (right). (B) Dissociation profiles of the fluorescent nucleotide analogues, expressed as changes of fluorescent intensity (arbitrary units) of FL-ATP and TR-ATP stably bound to dynein on the glass surface. After incubation of dynein with 5 nM nucleotide analogues for 4–5 min in the perfusion chamber, unbound nucleotide analogues were removed by perfusion with buffer without nucleotides. (C) Responses of elastase-treated axonemes to 1 mM FL-ATP after preincubation with (right) or without (left) ATP analogues. Only when the elastase-treated axonemes were pretreated with 1 mM AMPPNP, did application of FL-ATP induce disintegration of the axonemes into individual bundles. (D) A model for dynein–nucleotide interactions explaining the results of experiment A-1. A loss of sliding ability in dynein molecules in the presence of FL-ATP (left), which is probably caused by stable binding of FL-ATP to noncatalytic binding sites of dynein, can be rescued by stable binding of AMPPNP instead of FL-ATP (right). Modified from the figures in Inoue and Shingyoji (2007).

Direct observation of ADP binding to dynein, relevant to dynein motility, can be made by using TR-ADP in axonemes either untreated or treated with protein phosphatase 1 (PP1) [experiment A-2] (Fig. 6 in Yoshimura *et al*., 2007). A time-dependent increase of TR-ADP binding is observed in the untreated flagella at pH 7.0 and 0.02 mM ATP, but not in the PP1-treated axonemes.

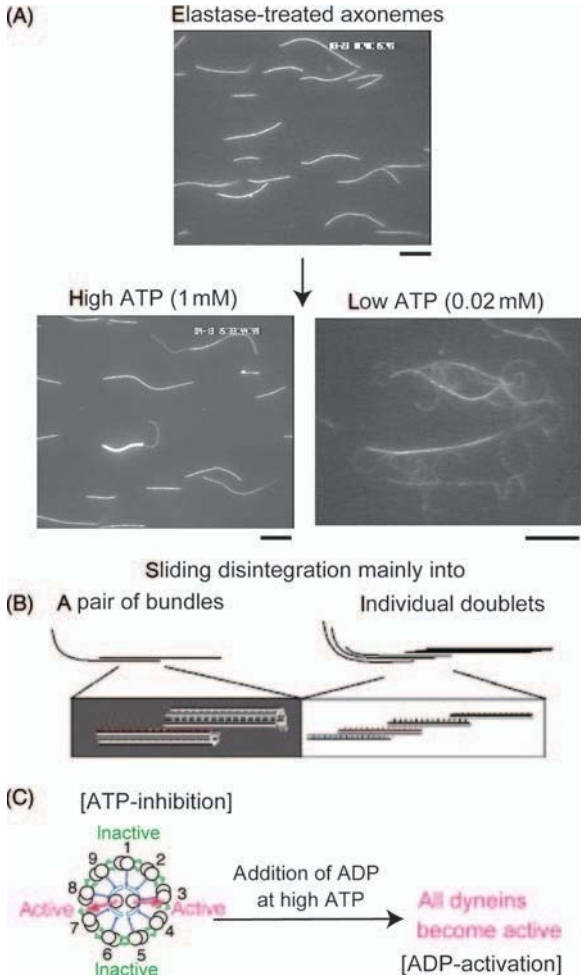

Fig. 6 The elastase-treatment assay [experiment B-1]. Video images (A) and their diagrammatic illustrations (B) showing the characteristic microtubule sliding of elastase-treated axonemes mainly into paired bundles and individual doublets under high- and low-ATP conditions, respectively. Dynein arms on both sides of the CP are active but those in other positions are inactive at high ATP; this regulation of dynein activity causes splitting of the axoneme into a pair of bundles (C left and Fig. 1). By addition of ADP, the inhibition of some dynein activity at high ATP (ATP inhibition) can be released, resulting in the sliding of elastase-treated axonemes into individual doublets (C). Nakano *et al*., 2003; Yoshimura *et al*., 2007.

Under this low pH and ATP condition the flagella can be reactivated to beat, while the PP1-treated axonemes do not beat. This experiment indicates the relationship between ADP binding to dynein and the dynein motility underlying flagellar beating.

B. ATP Inhibition and ADP Activation in the Regulation of Dynein in Beating Flagella

Elastase-treated axonemes of sea urchin sperm flagella, which retain the ability for local oscillatory bending (Shingyoji and Takahashi, 1995), show characteristic microtubule sliding into a pair of doublet bundles at high ATP, while they disintegrate into individual doublets at low ATP (Fig. 6A and B) (Nakano *et al*., 2003; Yoshimura and Shingyoji, 1999). The boundary ATP concentration between the two types of sliding is around 0.1 mM. The limited microtubule sliding into paired bundles indicates that the activity of dyneins in the axoneme is regulated so that only those on specific doublets become active. This regulation can be observed as characteristic splitting patterns in the ultrastructural analysis of the split bundles (Nakano *et al*., 2003). Basically, the dyneins on the two sides of the CP are active, while other dyneins are less active or inactive. A role for ADP can be observed as a change in the sliding types. An addition of ADP released the limited sliding at high ATP (Fig. 6C) (Yoshimura *et al*., 2007). The results indicate that ADP as well as ATP is involved in the regulation of dynein activity.

In elastase-treated axonemes, substructures such as the nexin links that are thought to restrict the sliding apart of doublets are either absent or weak enough for the bundles to undergo sliding disintegration into individual doublets in the presence of a low concentration of ATP (Fig. 6A right) (Shingyoji and Takahashi, 1995). The sliding into paired bundles at high ATP (Fig. 6A left) suggests that, in addition to the nexin links, dynein crossbridges may play an important role as linkers between doublets during flagellar motility at high ATP. This idea can be tested by experiment B-2 (Fig. 7A and B) (Yoshimura *et al*., 2007). The duration of flagellar beating, or the time to the onset of sliding disintegration, at 1 and 0.02 mM ATP in the presence of 5 μg/ml elastase (Fig. 7A) shows a Gaussian distribution (Fig. 7B). For sliding disintegration, elastase treatment for about 1–1.5 min is necessary. The time to the onset of sliding disintegration at 1 mM ATP is twice as long as that at 0.02 mM ATP. These results indicate that the physiological concentration of ATP plays, in addition to its role as the source of chemical energy, a role as an inhibitory factor that prevents dynein arms from causing microtubule sliding probably by maintaining crossbridges between certain dynein arms and microtubules (Fig. 7C).

C. Dynein Activation by Mechanical Force from Bending

Dynein arms on both sides of the CP are those that are assigned by the CP to produce the microtubule sliding necessary for bend formation (Figs. 1 and 7C). Since the dynein molecule is a minus-end-directed motor protein (Sale and Satir, 1977; Vale and Toyoshima, 1988), for cyclical bending in alternate directions the activity of

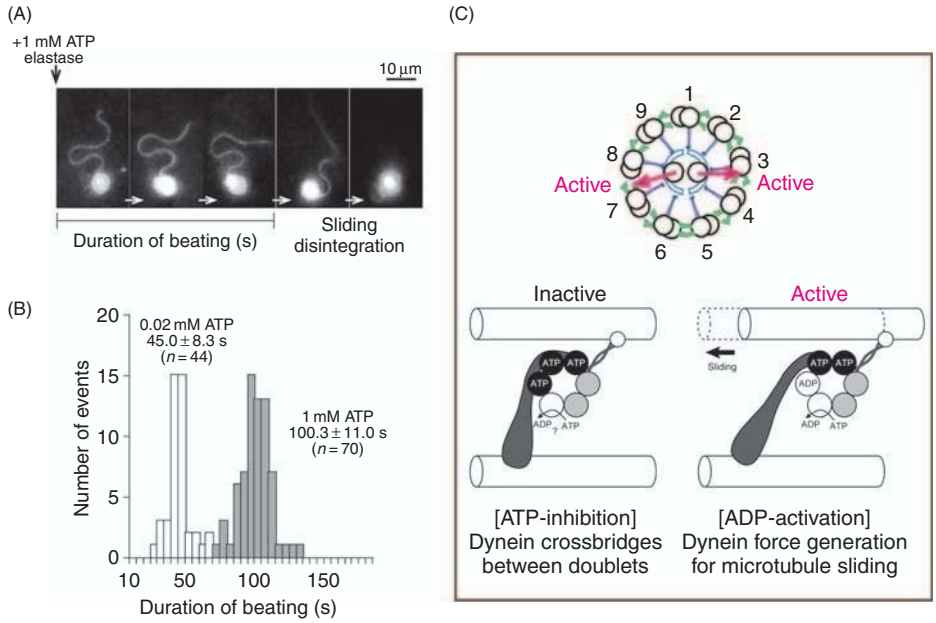

Fig. 7 Dynein crossbridges between doublets at high ATP [experiment B-2]. (A) Sequential video images of a flagellum that beat for a while after an application of 1 mM ATP with elastase before it disintegrated. (B) The duration of beating was significantly shorter at 0.02 mM ATP than at 1 mM ATP. Modified from Fig. 8 of Yoshimura *et al*. (2007). (C) A model for dynein–nucleotide interactions explaining the two states of dynein: the ATP-inhibition state, in which dynein forms a crossbridge between doublets (left) and the ADP-activation state, in which dynein generates force for microtubule sliding (right). Based on the reports by Inoue and Shingyoji (2007), Yoshimura *et al*. (2007), and Ueno *et al*. (2008).

dynein arms on the two sides of the CP should alternate (or switch) cyclically. Experiments C-1 and C-2 show that the mechanical force of bending plays an important role for switching dynein activity in the axoneme, not only at high ATP but also at low ATP.

C-1. Bending-induced switching of dynein activity in elastase-treated axonemes: In elastase-treated axonemal fragments, high ATP (1 mM) at high Ca^{2+} (10^{-4} M) induces sliding disintegration that splits the axoneme into two doublet bundles of unequal thickness, due mainly to the activity of dynein arms on doublet #7 (Hayashi and Shingyoji, 2008; Nakano *et al*., 2003). This is depicted in Fig. 8C as forward sliding, in which the thinner bundle moves leftward. Successive applications of ATP, released from caged ATP by repetitive UV flashes, induce further sliding of the thinner bundle in the same, forward, direction. However, bending the region of overlap between the two bundles by more than 90° can induce in some fragments a reversal of the direction of sliding between the bundles (Fig. 8C, backward sliding) (Morita and Shingyoji, 2004). The reversal is probably induced by the switching of dynein activity from

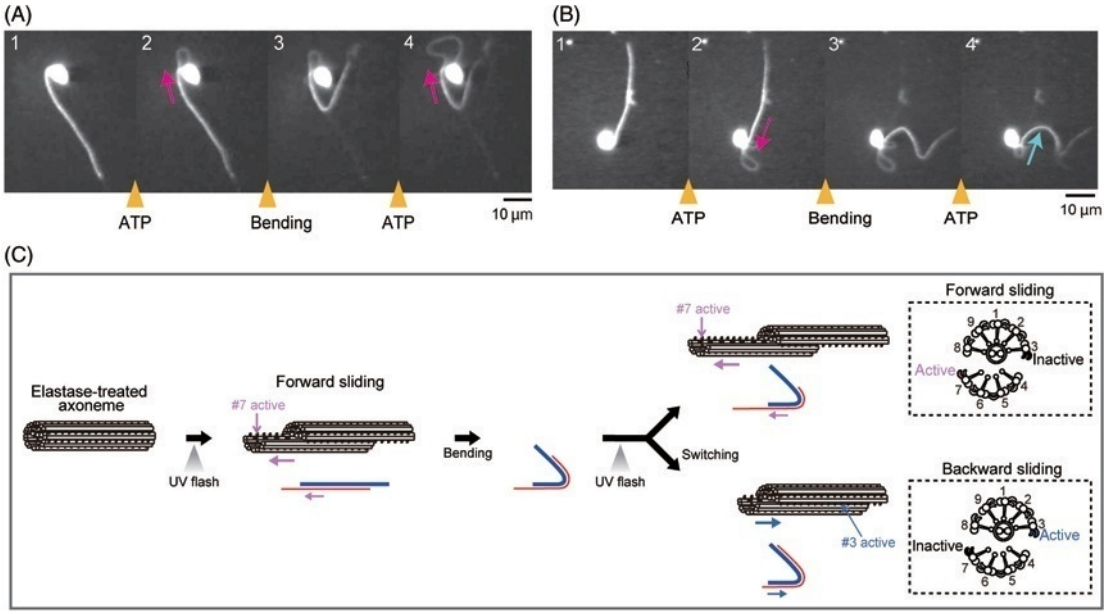

Fig. 8 Bending-induced reversal of microtubule sliding [experiment C-1]. (A) and (B) Video images showing forward (red arrows in A and B-2) and backward sliding (blue arrow in B-4) before and after imposed bending (bending). Sliding was induced by UV flashes in the elastase-treated quiescent flagella that had a P-bend at the base. Bending was applied in the same direction to the P-bend (A) and in the opposite direction (B). (C) Diagram showing interpretation of the experiment. Modified from Fig. 3 in Hayashi and Shingyoji (2008, 2009). (See Plate no. 5 in the Color Plate Section.)

doublet #7 to doublet #3 (or #4). The rate of reversal (about 48%) in the axonemal fragments is not high, meaning that bending itself is not the sole dynein-regulating factor related to the switching mechanism. In contrast, when the bending direction is controlled by using elastase-treated Ca^{2+}-induced quiescent flagella as shown in Fig. 8A and B, reversal of the sliding direction is induced at a high rate (71%) depending on the direction of imposed bending (Hayashi and Shingyoji, 2008). Furthermore, in elastase-treated axonemal fragments the rate of bending-induced reversal is increased by the presence of ADP (Hayashi and Shingyoji, 2009).

It is tempting to speculate that bending-induced activation of dynein arms on doublet #3 occurs upon ADP binding to dynein, although ADP binding to the regulatory sites of dyneins on doublet #3 has not been demonstrated when their activity is switched on by bending. It seems likely that stable ADP binding to dynein is necessary for the bending-induced activation of dynein in the ATP-inhibited state, but the regulation of the activity of dynein that is already active may not involve association and dissociation of ADP with dynein during beating. In other words, once ADP binds to dynein, the dynein can probably

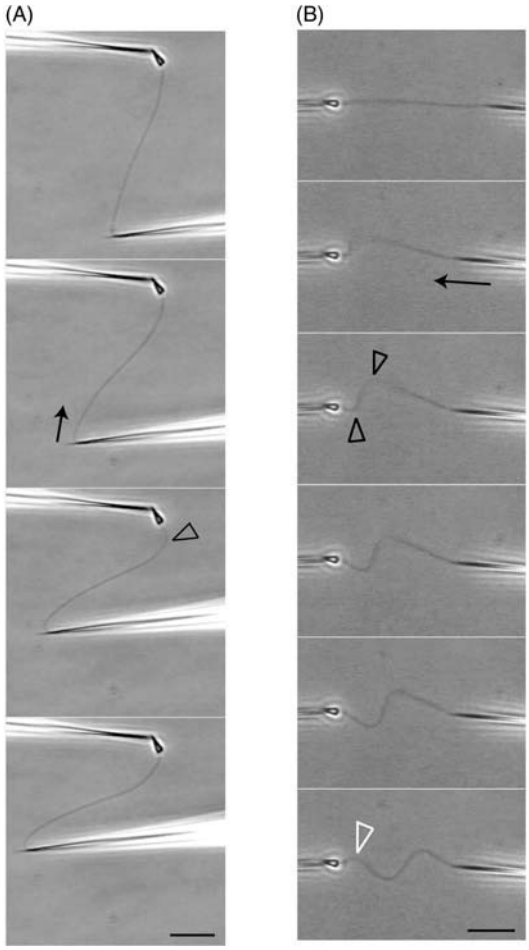

Fig. 9 Bending-induced oscillation in immotile flagella at 2.0 μM ATP [experiment C-2]. Sequential video images showing imposed bending with two microneedles, one (left microneedle) attached to the head and the other (right microneedle) to the end of the flagellum. Bending of the flagellum by moving the right microneedle toward the head (arrows) induced a bend near the head (A) and a pair of bends (B) (black arrowheads). Bending-induced single bend (A) did not induce a new flagellar response, while paired bends (B) induced a new bend (white arrowhead) in the proximal region of the flagellum that was followed by oscillation. The oscillation continued under the mechanical constraint.

respond more sensitively to mechanical signals than before ADP binding (Hayashi and Shingyoji, 2009).

C-2. Induction of beating in demembranated, motionless flagella at very low ATP concentrations: The microtubule sliding in elastase-treated axonemes, restricted to specific interdoublet sites beside the CP, is associated with the regulation of dynein motile activity at high ATP. Thus, the CP plays a key role in the regulation of dynein

activity at high ATP. At low ATP, however, the situation seems different: demembranated axonemes of *Chlamydomonas* flagellar mutans lacking the CP are capable of Ca^{2+} concentration-dependent beating at low ATP, indicating that the CP is probably not an essential determinant regulating dynein activity (Wakabayashi *et al*., 1997). Although no experimental procedures are available to directly identify the factors important for dynein regulation at low ATP, experiment C-2 provides a clue: the results lead to the conclusion that even at low ATP, the mechanical force of bending is important for the enhancement and switching of dynein activity in the axoneme.

Demembranated flagella that are immotile at low ATP (2.0–3.0 μM), which is around the threshold concentration for beating, become motile and oscillate when they are distorted with two microneedles, one attached to the head and the other to the distal end of the flagellum. Simple bending, however, of the axoneme so as to increase the angle of a single bend does not induce oscillation (Fig. 9A). A key step for oscillation by imposed bending is to form a pair of bends (Fig. 9B) (Ishikawa and Shingyoji, 2007). This effective bending may be related to the direction-dependent factor important for the bending-induced reversal described earlier in experiment C-1 (Hayashi and Shingyoji, 2008). The bending-induced oscillation in experiment C-2 continues under the mechanical constraint, but is terminated by the removal of the constraint by detaching the microneedle from the distal end of the flagellum. In the presence of low ADP (2.0–2.5 μM) in addition to ATP (2.0–2.5 μM), however, the removal of the microneedle does not terminate the oscillation (Ishikawa and Shingyoji, 2007). This indicates that the presence of ADP is necessary for the switching of dynein activity for oscillatory bending.

V. Outlook

The sliding disintegration assay using elastase-treated axonemes is useful for studying the regulation of dynein activity in flagella. Most importantly, it enables us to analyze the dynein motile activity that is likely to occur in beating flagella. Because the rotation of the CP microtubules reported for some flagella makes the analysis of active dynein in disintegrated axonemes more complex, this method is more suitable for sea urchin sperm flagella, whose beating plane is nearly stable during beating. However, the work of Smith's group on *Chlamydomonas* flagella (Wargo and Smith, 2003) demonstrated that a similar method is useful for flagella with a rotating CP. When combined with ultrastructural studies, the sliding assay method becomes an even stronger tool for understanding dynein regulation in beating flagella.

Mechanical signals are an important factor to be considered in studying the role of nucleotides in the regulation of dynein activity in flagella. How the mechanical force controls the motile activity of dynein at the molecular level and how it regulates the binding of ATP and ADP to dynein are interesting questions. To answer them, development of new methods adequate to assay both nucleotide binding and motile activity in dynein molecules under the control of mechanical force is awaited.

Acknowledgments

I thank Prof. Keiichi Takahashi for valuable discussion and the members of my group, past and present, who have collaborated with me on dynein and sea urchin sperm flagella (M. Yoshimura, T. Kobayashi, H. Imai, I. Nakano, Y. Inoue, Y. Morita, R. Ishikawa, A. Yoshimura, S. Hayashi, and Y. Watanabe).

References

Brokaw, C.J. (1980). Elastase digestion of demembranated sperm flagella. *Science* **207**, 1365–1367.

Furuta, A., Yagi, T., Yanagisawa, H.A., Higuchi, H., and Kamiya, R. (2009). Systematic comparison of in vitro motile properties between Chlamydomonas wild-type and mutant outer arm dyneins each lacking one of the three heavy chains. *J. Biol. Chem.* **284**, 5927–5935.

Gibbons, I.R., Shingyoji, C., Murakami, A., and Takahashi, K. (1987). Spontaneous recovery after experimental manipulation of the plane of beat in sperm flagella. *Nature* **325**, 351–352.

Hayashi, S., and Shingyoji, C. (2008). Mechanism of flagellar oscillation – bending-induced switching of dynein activity in elastase-treated axonemes of sea urchin sperm. *J. Cell Sci.* **121**, 2833–2843.

Hayashi, S., and Shingyoji, C. (2009). Bending-induced switching of dynein activity in elastase-treated axonemes of sea urchin sperm – Roles of Ca^{2+} and ADP. *Cell Motil. Cytoskeleton.* **66**, 292–301.

Hayashibe, K., Shingyoji, C., and Kamiya, R. (1997). Induction of temporary beating in paralyzed flagella of *Chlamydomonas* mutants by application of external force. *Cell Motil. Cytoskeleton* **37**, 232–239.

Imai, H., and Shingyoji, C. (2003). Effects of trypsin-digested outer-arm dynein fragments on the velocity of microtubule sliding in elastase-digested flagellar axonemes. *Cell Struct. Funct.* **28**, 71–86.

Inoue, Y., and Shingyoji, C. (2007). The roles of noncatalytic ATP binding and ADP binding in the regulation of dynein motile activity in flagella. *Cell Motil. Cytoskeleton* **64**, 690–704.

Ishikawa, R., and Shingyoji, C. (2007). Induction of beating by imposed bending or mechanical pulse in demembranated, motionless sea urchin sperm flagella at very low ATP concentrations. *Cell Struct. Funct.* **32**, 17–27.

Kikushima, K., Yagi, T., and Kamiya, R. (2004). Slow ADP-dependent acceleration of microtubule translocation produced by an axonemal dynein. *FEBS Lett.* **563**, 119–122.

Kinoshita, S., Miki-Noumura, T., and Omoto, C.K. (1995). Regulatory role of nucleotides in axonemal function. *Cell Motil. Cytoskeleton* **32**, 46–54.

Kinukawa, M., Nomura, M., and Vacquier, V.D. (2007). A sea urchin sperm flagellar adenylate kinase with triplicated catalytic domains. *J. Biol. Chem.* **282**, 2947–2955.

Morita, Y., and Shingyoji, C. (2004). Effects of imposed bending on microtubule sliding in sperm flagella. *Curr. Biol.* **14**, 2113–2118.

Nakano, I., Kobayashi, T., Yoshimura, M., and Shingyoji, C. (2003). Central-pair-linked regulation of microtubule sliding by calcium in flagellar axonemes. *J. Cell Sci.* **116**, 1627–1636.

Okuno, M., and Hiramoto, Y. (1976). Mechanical stimulation of starfish sperm flagella. *J. Exp. Biol.* **65**, 401–413.

Omoto, C.K., Yagi, T., Kurimoto, E., and Kamiya, R. (1996). Ability of paralyzed flagella mutants of *Chlamydomonas* to move. *Cell Motil. Cytoskeleton* **33**, 88–94.

Porter, M.E., and Sale, W.S. (2000). The 9 + 2 axoneme anchors multiple inner arm dyneins and a network of kinases and phosphatases that control motility. *J. Cell Biol.* **151**, F37–42.

Sale, W.S., and Satir, P. (1977). Direction of active sliding of microtubules in *Tetrahymena* cilia. *Proc. Natl. Acad. Sci. USA* **74**, 2045–2049.

Shingyoji, C., Gibbons, I.R., Murakami, A., and Takahashi, K. (1991). Effect of imposed head vibration on the stability and waveform of flagellar beating in sea urchin spermatozoa. *J. Exp. Biol*. **156**, 63–80.

Shingyoji, C., and Takahashi, K. (1995). Cyclical bending movements induced locally by successive iontophoretic application of ATP to an elastase-treated flagellar axoneme. *J. Cell Sci.* **108**, 1359–1369.

Shingyoji, C., Yoshimura, K., Eshel, D., Takahashi, K., and Gibbons, I.R. (1995). Effect of beat frequency on the velocity of microtubule sliding in reactivated sea urchin sperm flagella under imposed head vibration. *J. Exp. Biol.* **198**, 645–653.

Shiroguchi, K., and Toyoshima, Y.Y. (2001). Regulation of monomeric dynein activity by ATP and ADP concentrations. *Cell Motil. Cytoskeleton* **49**, 189–199.

Smith, E.F., and Yang, P. (2004). The radial spokes and central apparatus: Mechano-chemical transducers that regulate flagellar motility. *Cell Motil. Cytoskeleton.* **57**, 8–17.

Summers, K.E., and Gibbons, I.R. (1971). Adenosine triphosphate-induced sliding of tubules in trypsin-treated flagella of sea-urchin sperm. *Proc. Natl. Acad. Sci. USA* **68**, 3092–3096.

Takahashi, K., Shingyoji, C., Katada, J., Eshel, D., and Gibbons, I.R. (1991). Polarity in spontaneous unwinding after prior rotation of the flagellar beat plane in sea-urchin spermatozoa. *J. Cell Sci.* **98**, 183–189.

Ueno, H., Yasunaga, T., Shingyoji, C., and Hirose, K. (2008). Dynein pulls microtubules without rotating its stalk. *Proc. Natl. Acad. Sci. USA* **105**, 19702–19707.

Vale, R.D., and Toyoshima, Y.Y. (1988). Rotation and translocation of microtubules in vitro induced by dyneins from *Tetrahymena* cilia. *Cell* **52**, 459–469.

Wakabayashi, K., Yagi, T., and Kamiya, R. (1997). Ca^{2+}-dependent waveform conversion in the flagellar axoneme of *Chlamydomonas* mutants lacking the central-pair/radial spoke system. *Cell Motil. Cytoskeleton* **38**, 22–28.

Wargo, M.J., and Smith, E.F. (2003).Asymmetry of the central apparatus defines the location of active microtubule sliding in *Chlamydomonas* flagella. *Proc. Natl. Acad. Sci., USA* **100**, 137–142.

Yagi, T. (2000). ADP-dependent microtubule translocation by flagellar inner-arm dyneins. *Cell Struct. Funct.* **25**, 263–267.

Yoshimura, A., Nakano, I., and Shingyoji, C. (2007). Inhibition by ATP and activation by ADP in the regulation of flagellar movement in sea urchin sperm. *Cell Motil. Cytoskeleton* **64**, 777–793.

Yoshimura, M., and Shingyoji, C. (1999). Effects of the central pair apparatus on microtubule sliding velocity in sea urchin sperm flagella. *Cell Struct. Funct.* **24**, 43–54.

This page intentionally left blank

CHAPTER 9

The Regulation of Dynein-Driven Microtubule Sliding in *Chlamydomonas* Flagella by Axonemal Kinases and Phosphatases

Candice A. Elam, Winfield S. Sale, *and* Maureen Wirschell

Department of Cell Biology, Emory University School of Medicine, 465 Whitehead Biomedical Research Building, 615 Michael Street, Atlanta, Georgia 30322

Abstract

The purpose of this chapter is to review the methodology and advances that have revealed conserved signaling proteins that are localized in the 9 + 2 ciliary axoneme for regulating motility. Diverse experimental systems have revealed that ciliary and

METHODS IN CELL BIOLOGY, VOL. 92

978-0-12-374974-1
DOI: 10.1016/S0091-679X(08)92009-4

eukaryotic flagellar motility is regulated by second messengers including calcium, pH, and cyclic nucleotides. In addition, recent advances in *in vitro* functional studies, taking advantage of isolated axonemes, pharmacological approaches, and biochemical analysis of axonemes have demonstrated that otherwise ubiquitous, conserved protein kinases and phosphatases are transported to and anchored in the axoneme. Here, we focus on the functional/pharmacological, genetic, and biochemical approaches in the model genetic system *Chlamydomonas* that have revealed highly conserved kinases, anchoring proteins (e.g., A-kinase anchoring proteins), and phosphatases that are physically located in the axoneme where they play a direct role in control of motility.

I. Introduction

Experimental data have revealed that eukaryotic ciliary/flagellar motility is regulated by second messengers such as calcium or cyclic nucleotides that, in many or most cases, interact directly with the axoneme for control of dynein-driven motility. These conclusions are based in part on *in vitro* biochemical, functional, and pharmacological analysis with isolated axonemes. Informative experimental systems include both invertebrate and vertebrate sperm (Burton and McKnight, 2007; Inaba, 2007; Lindemann *et al*., 1991), mammalian cilia (Salathe, 2007), and model genetic organisms including *Paramecium* (Bonini *et al*., 1991), *Tetrahymena* (Hennessey *et al*., 2002; Pennock, 2000), Trypanosomes (Hill, 2003; Kohl and Bastin, 2005; Ralston and Hill, 2008), and *Chlamydomonas* (Porter and Sale, 2000; Smith and Yang, 2004; Wirschell *et al*., 2007).

Approaches for studying the regulation of ciliary motility have included pharmacological analysis of motility in live cells and tissues and analysis of ATP-reactivated motility in axonemes including altered motility introduced by changes in calcium, cyclic nucleotides, or pharmacological reagents in the reactivation buffers (Lindemann and Schmitz, 2001). For example, *in vitro* ATP-induced reactivation studies of sperm tail axonemes have shown that increased calcium results in increased axonemal curvature (Brokaw, 1979). Similarly, changes in calcium or cyclic nucleotides in reactivation buffers can alter beat frequency in mammalian ciliary axonemes (Salathe, 2007) and alter motility in ciliary axonemes from *Paramecium, Tetrahymena*, and *Chlamydomonas* (Bonini and Nelson, 1988; Christensen *et al*., 2001; Hasegawa *et al*., 1987; Kamiya and Witman, 1984). Together, these approaches have revealed that changes in calcium or cyclic nucleotides can alter motility through interactions of second messengers directly with proteins in the axoneme. Consistent with this conclusion, biochemical/proteomic analyses of isolated ciliary axonemes have revealed conserved kinases and phosphatases, as well as calcium-binding proteins that are localized in the axoneme. The challenge is to identify the axonemal signaling proteins (calcium-binding proteins, kinases, and phosphatases) and the signal transduction pathway that leads to altered dynein motor activity and changes in ciliary bending.

In this chapter, we focus on the model experimental system, *Chlamydomonas*, and describe a network of conserved axonemal structures, including the central pair (CP)

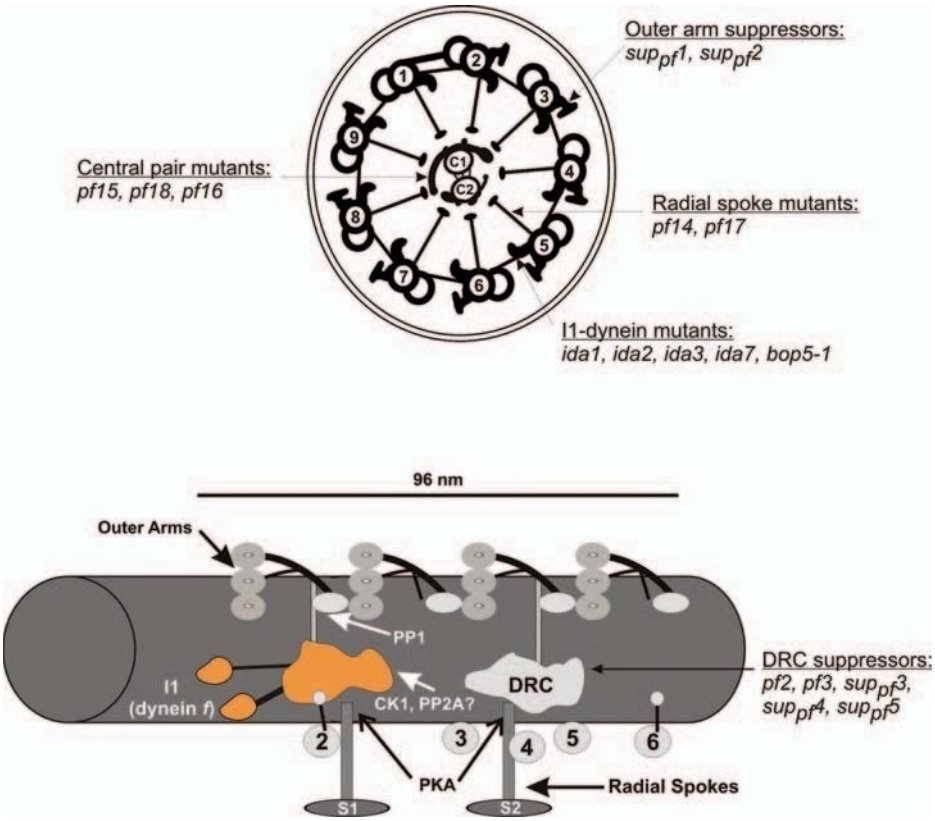

Fig. 1 Structural components of the axoneme. The *Chlamydomonas* axoneme is depicted in cross section (top) and longitudinal section (bottom). Axonemal structures include the inner (I1 dynein and 2–6) and outer dynein arms, the radial spokes (RS) (S1 and S2), the central pair (CP) apparatus, and the dynein regulatory complex (DRC). Key mutations that affect the assembly of the CP/RS structures are indicated. Also shown are the suppressor mutations of the DRC and dynein arms that restore motility to the paralyzed CP/RS flagella. The predicted locations of critical signaling kinases and phosphatases (CK1, PKA, PP1, and PP2A) are shown (white arrows). (See Plate no. 6 in the Color Plate Section.)

apparatus and the radial spokes (RSs), which impinge upon equally conserved axonemal kinases and phosphatases for control of dynein activity and axonemal bending (Fig. 1). We emphasize the methodology and results of *in vitro* analysis of microtubule sliding in isolated axonemes from *Chlamydomonas* (Okagaki and Kamiya, 1986; Summers and Gibbons, 1971). The microtubule sliding assay in axonemes has proven to be extremely reliable and informative, revealing features of dynein activity fundamental to our understanding of axonemal bend oscillation and features of a "switching" model for alternating forward and reverse bending (Aoyama and Kamiya, 2005; Brokaw, 2009; Hayashi and Shingyoji, 2008; Sale and Satir, 1977; Satir and Matsuoka, 1989; Smith and Yang, 2004). In addition, analysis of microtubule sliding in

Chlamydomonas axonemes from wild-type and flagellar mutants has revealed a distinctive functional capability of each dynein subform (Brokaw, 2009; Kamiya, 2002) and has also revealed an axonemal phosphorylation-based regulatory mechanism that controls dynein activity, the focus of this chapter.

Here, we review the methodology of axoneme purification (Fig. 2A), the microtubule sliding disintegration assay, and the use of informative structural mutants (e.g., lacking the CP, RSs, or subsets of dynein arms; Figs. 1 and 2B) in *Chlamydomonas* that have revealed the protein kinase, CK1, and the phosphatases, PP1 and

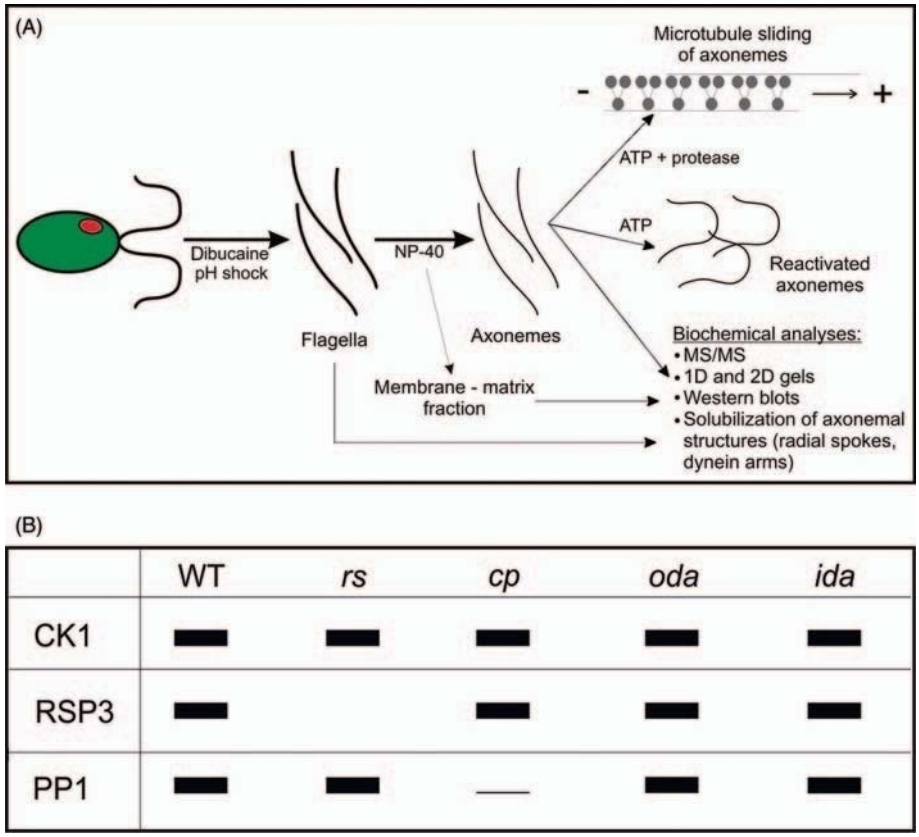

Fig. 2 Assays used for identifying the role and localization of kinases and phosphatases in the *Chlamydomonas* axoneme. (A) *Chlamydomonas* flagella and axonemes, readily isolated by well-defined methods (dibucaine/pH shock), can be used for a variety of functional, pharmacological, and biochemical methods including reactivation of axonemal motility, dynein-driven microtubule sliding assays, and several biochemical techniques. (B) Isolated axonemes from wild type and a series of mutants that are missing specific axonemal structures, such as the radial spokes (*rs*), central pair apparatus (*cp*), outer dynein arms (*oda*), and inner dynein arms (*ida*) can be screened by western blot, or blot overlay, to determine the localization of a protein of interest (diagram represents a cartoon of a western blot). (See Plate no. 7 in the Color Plate Section.)

PP2A, are localized and anchored in the axoneme in position to control dynein phosphorylation (Porter and Sale, 2000; Smith and Yang, 2004; Wirschell *et al*., 2007). This chapter is complemented by other chapters in this volume focused on the dynein motors (S. King), radial spokes (P. Yang), the central pair apparatus (D. Mitchell), the dynein regulatory complex (DRC; M. E. Porter), and calcium-binding proteins (E. F. Smith) for the regulation of motility. Together, these chapters will provide the reader with the methodology and our current understanding of how ciliary/flagellar motility is regulated.

II. The *Chlamydomonas* Experimental System: Axoneme Isolation and the Flagellar Mutants

We focus on experimental studies that have taken advantage of axonemes isolated from wild-type and mutant *Chlamydomonas reinhardtii.* This unicellular, biflagellate is a powerful model system for the study of ciliary/flagellar motility revealing extraordinary conservation in axonemal structure, the functional role of each dynein subform, and the signaling proteins and enzymes that control flagellar motility. Additionally, *Chlamydomonas* has revealed the mechanisms by which cilia and flagella are assembled and function, mechanisms that are also very highly conserved in ciliated organisms.

A. Method—Axoneme Isolation

One important feature of *Chlamydomonas* is that the flagella are easily isolated and large amounts of purified flagella can be used for a wide range of biochemical, structural, and functional assays, making *Chlamydomonas* one of the best model systems for studies of the cilia/flagella and the axoneme (Fig. 2A).

As illustrated in Fig. 2A, flagella can be actively excised by treating the cells with the drug dibucaine or by pH shock. The details of flagellar isolation have been reviewed before (Witman, 1986; Witman *et al*., 1972). The cell bodies can then be separated from flagella by differential centrifugation, resulting in highly purified flagella. Purified flagella can then be suspended in a buffer containing a nonionic detergent, such as Triton X-100 or Nonidet-P40, and axonemal and membrane–matrix fractions separated and recovered by centrifugation. Any of the fractions (flagella, membrane–matrix, or axonemes) can then be analyzed by biochemical approaches including 1D and 2D gel electrophoresis, immunoblots, blot overlays, and tandem mass spectrometry (MS/MS) analysis to name a few (Fig. 2A). Specific axonemal structures can also be biochemically solubilized from the isolated axonemes. For example, the dynein arm structures and RSs can be solubilized by extraction of axonemes with high salt or chaotropic buffers and subsequently purified (Gibbons and Rowe, 1965; King and Kamiya, 2009; Yang *et al*., 2001). Moreover, the dyneins and spoke structures can be reconstituted back to their original positions in the

axoneme *in vitro* (Gibbons, 1981; Gibbons and Gibbons, 1976; Smith and Sale, 1992b; Yamamoto *et al*., 2006; Yang *et al*., 2001).

Importantly, isolated axonemes can be reactivated in ATP-containing reactivation buffers to form oscillatory bends and move in a manner that mimics the movement of flagella in live cells (Gibbons and Gibbons, 1972). This result alone indicated that the machinery—motors and regulatory mechanisms—required for motility were physically localized to the axoneme. Additionally, dynein-driven microtubule sliding can be measured by treating the isolated axonemes with proteases and ATP for assessment of microtubule sliding by video microscopy (see Section III). This assay can be performed with axonemes from wild-type or paralyzed flagellar (*pf*) mutant cells lacking specific axonemal structures, facilitating the identification of structures important for regulating flagellar motility.

B. The Flagellar Structural Mutants

Chlamydomonas is an ideal model genetic system because the flagella are not required for viability, therefore mutations that affect flagellar assembly and function can be readily isolated and characterized. Additionally, isolated axonemes from *Chlamydomonas* structural mutants (e.g., axonemes from mutants lacking the entire RS structures, the entire CP apparatus, or the dynein arms) can be used for indirect localization of proteins or enzymes. For example, immunoblots can be used to determine if a protein, such as the phosphatase PP1 or the kinase CK1, is localized to the RSs, the CP, or the outer doublet microtubules (Fig. 2B). In this example, since PP1 is largely missing in axonemes from a CP mutant, it is likely enriched in the CP apparatus (Yang *et al*., 2000). Similarly, the A-kinase anchoring protein (AKAP) RSP3 is missing from axonemes lacking the RSs and thus is presumed to be a spoke protein (Gaillard *et al*., 2001). In the final example, the kinase, CK1, is present in wild-type amounts in axonemes lacking the RSs, the CP structures, and the inner and outer dynein arms. Thus, CK1 is presumed to be localized to the outer doublet microtubules (Gokhale *et al*., 2009; Yang and Sale, 2000). The use of structural mutants has revealed the location of key signaling components, such as AKAPs, CK1, PP1, and PP2A in the axoneme (detailed in Section IV). Thus, experimental data obtained from these mutants have provided us with a model for targeting of proteins in specific positions within the axoneme for direct interaction with their substrates.

III. *In Vitro* Microtubule Sliding Assays: The Method and Discovery of Kinases and Phosphatases that Regulate Dynein

A. History

The measurement of microtubule sliding in isolated axonemes is used as a means of measuring the mechanochemical properties of dyneins in cilia and flagella. The first demonstration of dynein-driven sliding of outer doublet microtubules was reported by

Summers and Gibbons using sea urchin axonemes (Summers and Gibbons, 1971). This pioneering achievement was the first direct visualization of dynein-driven microtubule sliding and featured the use of dark-field light microscopy to view microtubules. Since then, the microtubule sliding assay in axonemes has been adapted for ciliary and flagellar axonemes from a wide variety of cells (Bannai *et al*., 2000; Kamimura and Takahashi, 1981; Lindemann and Gibbons, 1975; Mogami and Takahashi, 1983; Okagaki and Kamiya, 1986; Sale and Satir, 1977; Summers, 1974; Tamm and Tamm, 1984; Witman *et al*., 1978). In particular, Witman *et al*. (1978) took advantage of *Chlamydomonas* axonemes isolated from paralyzed flagellar mutants and demonstrated that the dynein arms in mutants lacking the CP or RSs are capable of generating interdoublet shearing forces. This was a critical observation indicating that the CP and RS structures are essential for conversion of interdoublet sliding into axonemal bending.

Using isolated flagella from wild-type and mutant *Chlamydomonas* cells, Okagaki and Kamiya (1986) refined the microtubule sliding assay in a number of ways, including measurement of the sliding velocity and analysis of the microtubule sliding pattern in axonemes from wild-type and mutant cells. Additional advances included fragmenting the flagella by sonication to produce axoneme pieces that were free of the basal/proximal axonemal portion—which underwent sliding events more frequently than intact axonemes. They further improved the method by testing microtubule sliding using various proteases and determined that nagarse, a protease with broad specificity, gave excellent results regarding efficiency and velocity of sliding. Current methods often utilize the protease, subtilisin A Type VIII, to induce microtubule sliding events with similar results. With the improved method and given sets of conditions, Okagaki and Kamiya were able to obtain highly reproducible results and determined the sliding velocities for mutants lacking specific dynein arms or other axonemal components.

Notably, microtubule sliding velocities obtained using this method were significantly lower than the velocity calculated from the waveform of beating axonemes. To further improve the method, Kurimoto and Kamiya (1991) changed the buffer to one used routinely for reactivating demembranated *Chlamydomonas* cell models that included potassium acetate in place of potassium chloride. In other studies, potassium acetate has been shown to improve motility in reactivated sperm models (Gibbons *et al*., 1985). Based on a variety of data, Gibbons *et al*. (1985) determined that reduced sliding velocities appeared to be a consequence of Cl^- inhibition of dynein activity. Thus, the key element in the buffer conditions is the omission of chloride containing salts (NaCl/KCl) and replacement with the organic anion acetate.

B. The Method

The *in vitro* microtubule sliding, or sliding disintegration, assay provides an extremely reliable means to directly observe and measure active microtubule sliding in isolated axonemes. The method, described below, is routinely used to measure sliding disintegration in *Chlamydomonas* axonemes for an indirect assessment of axonemal

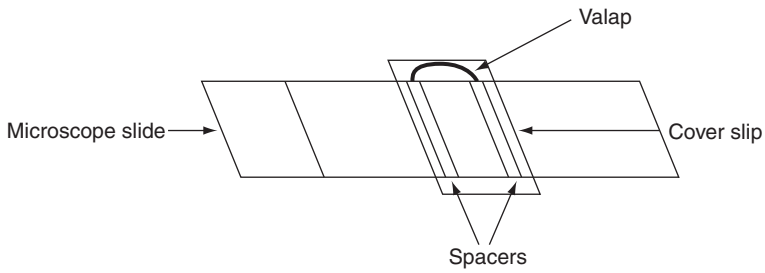

Fig. 3 Schematic of the perfusion chambers used in the microtubule sliding disintegration assay. A simple perfusion chamber can be made using a microscope slide and cover slip. A 22 × 40 mm cover slip is affixed to the microscope slide using two thin strips of double stick tape as spacers, leaving the ends of the cover slip protruding from each side of the slide. A thin coating of valap (1:1:1 mixture of Vaseline, lanolin and paraffin wax) is placed on one side of the cover slip to make a well for loading buffers into the perfusion chamber. The other side is left open to be accessible to capillary filtration with filter paper.

dynein function. It is based on the method of Okagaki and Kamiya (1986) with the modifications in buffer conditions described earlier (Habermacher and Sale, 1996, 1997; Howard *et al*., 1994).

For these experiments, simple perfusion chambers can be made using standard microscope slides, cover slips, double stick tape, and a sealant such as valap (a 1:1:1 mixture of Vaseline, lanolin, and paraffin) (Fig. 3). Briefly, two narrow strips of double stick tape are affixed to a microscope slide, serving as spacers for a cover slip which is laid on top of the tape. One side of the cover slip is coated with a U-shaped line of valap, forming a reservoir that is used to load the perfusion chamber. Perfusion through the chamber is facilitated by adsorption from the opposite end of the chamber using strips of filter paper.

Flagella are isolated from either vegetative or gametic cells by the dibucaine method described by Witman (1986). Isolated flagella can be stored on ice in a buffer containing 10 mM HEPES, pH 7.4, 5 mM $MgSO_4$, 1 mM DTT, 0.5 mM EDTA, 5% polyethylene glycol 8000, and 25 mM potassium acetate. Flagella are demembranated in buffer containing 0.5% Nonidet-P40 and added to a perfusion chamber (Fig. 3). We typically do not sonicate the flagella, as we have found no difference in sliding velocities between sonicated and unsonicated flagella. If sonication is desired, a Kontes cell disrupter set at a power of 6 for 30 s typically yields transversely fractured flagella about one-third the original length. Flagellar segments are then demembranated using the method described above and added to a perfusion chamber. Nonsticking axonemes are washed away in buffer without detergent. Microtubule sliding is initiated by addition of buffer containing 1 mM ATP and 3 μg/ml subtilisin A Type VIII protease. Sliding disintegration of axonemes will occur over the next ~60 s. All sliding events are recorded and several sliding events can often be observed from a single slide or field of view. However, as previously reported (Kurimoto and Kamiya, 1991; Sale *et al*., 1993), prolonged illumination of axonemes tends to inhibit ATP-induced sliding

events in the region of illumination. Thus, it is imperative to work quickly and it may be necessary to move to a new field of view after initiation of sliding.

Microtubule sliding disintegration is observed using dark-field microscopy. The key features of dark-field illumination include an intense light source, a dark-field oil immersion condenser with high numerical aperture, a high-quality 40× objective, and a sensitive recording system. For these experiments, we typically use an inverted Zeiss Axiovert 35 microscope body equipped with a 100-W mercury lamp, heat and interference filters, and a Zeiss ultra dark-field oil immersion condenser. For most experiments, we use a 40 × Zeiss Plan Neofluar oil immersion lens and the images are captured with a silicon-intensified target camera that is mounted on a trinocular head through a 10–20 × zoom eyepiece. This optical configuration allows for high-resolution detection of purified axonemes and doublet microtubules required for the sliding assay. Our current recording system converts video images to a digital format using Labview 7.1 software (National Instruments, Austin, TX). (Note, compared to the video recording we describe, sensitive digital cameras are now available that offer many advantages for recording and analysis. The minimum frame rate necessary for a suitable digital camera should be equivalent to the rates used for video recording while maintaining the sensitivity required for dark-field visualization of microtubules.) Microtubule sliding velocities are calculated by manually measuring microtubule displacement on tracings calibrated with a micrometer versus time. In 1 mM Mg ATP, microtubules slide at about 17–18 μm/s in axonemes from wild-type cells and about 8–9 μm/s in axonemes from paralyzed flagellar mutants lacking the RSs or RS heads (e.g., *pf17*). Note, that we have observed that sliding velocities may vary depending on the concentration and type of protease used (Okagaki and Kamiya, 1986; Kikushima, 2009). Thus, for every experiment, we measure microtubule sliding in wild-type and RS mutant axonemes (e.g., *pf17*) as controls.

C. Discovery of Regulation of Microtubule Sliding by Axonemal Kinases and Phosphatases

The microtubule sliding assay has been fundamental in revealing the role of the RSs and the CP apparatus in regulation of microtubule sliding (Howard *et al*., 1994; Smith and Sale, 1992a; Witman *et al*., 1978). This mechanism involves protein kinases and phosphatases located in the axoneme for the control of dynein phosphorylation (Porter and Sale, 2000; Wirschell *et al*., 2007). This conclusion is founded in part by combining a pharmacological approach with microtubule sliding assays using isolated axonemes from specific paralyzed *Chlamydomonas* flagellar mutants which manifest reduced microtubule sliding velocities. For example, treatment of RS or CP mutant axonemes, with inhibitors of cAMP-dependent protein kinases, PKA, or inhibitors of CK1, increased microtubule sliding velocities to wild-type levels (Habermacher and Sale, 1996; Howard *et al*., 1994; Yang *et al*., 2000) demonstrating that the axoneme contains these kinases and that they control dynein activity.

Subsequent studies, using double mutants lacking the RSs and selected subsets of dynein arms, identified I1 dynein as a critical target for regulation of microtubule sliding (Habermacher and Sale, 1997; King and Dutcher, 1997; Yang and Sale, 2000).

Furthermore, in these studies, phosphorylation of the I1-dynein intermediate chain, IC138, was correlated with inhibition of I1-dynein activity, and dephosphorylation of IC138 was correlated with rescue of microtubule sliding (see later; reviewed in Porter and Sale, 2000; Wirschell *et al*., 2007). As a consequence of defects in the CP/RS pathway which regulates I1 dynein, IC138 becomes uniformly phosphorylated throughout the axoneme (hyperphosphorylated) and I1 dynein is inhibited throughout the axoneme, resulting in reduced microtubule sliding velocities (Hendrickson *et al*., 2004). Rescue of dynein activity also depended on the action of tightly bound axonemal phosphatases, PP1 and PP2A, as selective phosphatase inhibitors could block rescue of dynein-driven sliding by the kinase inhibitors (Habermacher and Sale, 1996; Yang *et al*., 2000). Thus, pharmacological analyses of microtubule sliding in isolated axonemes provided the initial evidence that conserved kinases and phosphatases are located in the axoneme.

IV. Biochemical Analysis of Kinases and Phosphatases Localized to the *Chlamydomonas* Axoneme

Biochemical and molecular studies have revealed that protein kinases and phosphatases are localized to specific structures within the axoneme. These studies have taken advantage of the library of axonemal structural mutants in *Chlamydomonas* described earlier (Fig. 2B), revealing the presence and location of conserved kinases, kinase anchoring proteins, and phosphatases in the axoneme. Additionally, genomic and proteomic studies have independently revealed that the axoneme contains a surprisingly wide range of conserved signaling proteins including those we focus upon in this chapter (Pazour *et al*., 2005).

Part of the foundation for these biochemical studies are the functional and pharmacological studies, cited in the previous section, that indicate dynein-driven microtubule sliding in isolated axonemes is regulated by kinases, including PKA and CK1, and phosphatases, including PP1 and PP2A. An important feature of the phosphorylation-based regulatory mechanism is the discovery that the kinases, phosphatases (CK1, PP2A, PP1), and the kinase-anchoring proteins (AKAPs and other predicted anchoring proteins, Fig. 4) that regulate dynein motor function are inherently built into the axonemal structure. Given this permanent incorporation into the axoneme, we postulate that these kinases and phosphatases are physically anchored in the axoneme near the phosphoprotein substrates such as IC138 in the I1-dynein motor to regulate motility (Fig. 4).

A. The Axonemal Kinases

1. PKA and Axonemal AKAPs

Given the pharmacological data that indicated a role for PKA in regulation of dynein-driven microtubule sliding, it was proposed that PKA must be localized to axonemal structures involved in the CP/RS phosphorylation regulatory pathway. To

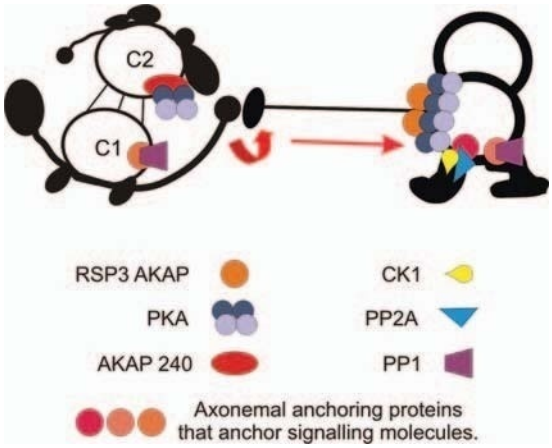

Fig. 4 Model for anchoring signaling proteins in the axoneme. The axonemal AKAPs, RSP3, and AKAP240 are thought to be responsible for localizing PKA to specific structures within the axoneme (the central pair and base of the radial spokes). A similar mechanism may exist for localizing other regulatory proteins, for example, there may be specific anchoring proteins responsible for localizing CK1 and the regulatory phosphatases, PP1 and PP2A, near their substrates in the axoneme. (See Plate no. 8 in the Color Plate Section.)

date, PKA subunits and genes have not been characterized in *Chlamydomonas*. However, conserved AKAPs have been identified and localized in the axoneme. Gaillard *et al*. (2001) took advantage of a well-characterized method for identifying AKAPs, using a blot overlay and the regulatory subunit of PKA (RII) as a probe, to assess whether candidate AKAPs are located in the axoneme. A panel of axonemes from *Chlamydomonas* flagellar structural mutants was used for analysis. These studies identified two prominent candidate axonemal AKAPs; one located in the CP apparatus associated with the C2 microtubule (AKAP240) and the other located in the RS, the well-studied protein RS protein 3 (RSP3).

To further test the hypothesis that RSP3 is an AKAP and responsible for regulation of flagellar motility, a mutation in the PKA-binding domain was made in the RSP3 gene. A null mutant of RSP3 (*pf14*) was transformed with the mutant gene and the motility of the transformants was analyzed (Gaillard *et al*., 2006). The results indicated that disruption of the PKA-binding domain results in failure in motility and that localization of PKA is critical for control of flagellar motility. RSP3 is a highly conserved protein of all motile cilia (Wirschell *et al*., 2008), thus predictably the RSP3 AKAP plays a conserved regulatory role in all cilia and flagella. Further tests of these ideas now require the identification and characterization of PKA in *Chlamydomonas* flagella and analysis of RSP3 in cilia from other organisms. These and additional findings led to the hypothesis that other kinases and phosphatases must also be targeted to the axoneme to specific locations mediated by a series of specific anchoring proteins (Fig. 4).

2. Casein Kinase 1

Although inhibitors to PKA can rescue microtubule sliding in paralyzed flagellar mutants, further examination revealed that PKA may not be the only axonemal kinase that can control microtubule sliding and regulate IC138 phosphorylation (Yang and Sale, 2000). In order to identify the additional axonemal kinases, in gel kinase assays were used to screen isolated axonemes and fractionated axonemal salt extracts (Yang and Sale, 2000). An axonemal casein kinase 1 (CK1) was identified and shown to be an abundant protein in isolated axonemes. The use of *Chlamydomonas* structural mutants demonstrated that CK1 is located on the outer doublet microtubules (Fig. 2B; Yang and Sale, 2000). In support of this data, several CK1 peptides were identified in the *Chlamydomonas* proteome and indicated that CK1 is an axonemal protein (Pazour *et al*., 2005). The relatively specific CK1 inhibitor, CK1-7, was shown to directly block IC138 phosphorylation and rescue microtubule sliding inhibition in RS and CP mutants (Smith, 2002b; Yang *et al*., 2000). These data support the hypothesis that CK1 is anchored on the axoneme in proximity to I1 dynein. Furthermore, *in vitro* analysis reveals IC138 may be a substrate for CK1 (Gokhale *et al*., 2009; Yang and Sale, 2000). Future studies for CK1 include direct localization of the kinase within the axoneme and identification of potential targeting proteins for positioning along the axoneme.

B. The Axonemal Phosphatases

The first evidence for identification of axonemal phosphatases was observed in microtubule sliding assays using the phosphatase inhibitors, okadaic acid and microcystin-LR, and potent inhibitors of both PP1 and PP2A. Treatment of RS mutant axonemes with the phosphatase inhibitors blocked PKI-induced activation and rescue of wild-type microtubule sliding velocity (Habermacher and Sale, 1996). Based on these functional studies, direct biochemical analysis, using the phosphatase inhibitor microcystin-LR, which binds to the catalytic (C-) subunits of both PP1 and PP2A, was used to precipitate the PP1 and PP2A C-subunits and the A-subunit of PP2A from salt-extracted axonemes, thus providing direct evidence for the presence of these two phosphatases in the axoneme (Yang *et al*., 2000).

Using an array of structural mutants missing specific axonemal structures, PP1 was localized primarily to the CP apparatus with a minor amount distributed on the outer doublets (Fig. 2B; Yang *et al*., 2000). Using the same approach (illustrated in Fig. 2B), PP2A was localized to the outer doublet microtubules. As a result, these data suggested that PP2A is localized near I1 dynein, while PP1 most likely plays a role further upstream in the regulatory pathway. Since PP2A is a heterotrimer of A-, C-, and B-subunits, we predict that there will also be a specific B-subunit that localizes to the axoneme. Future directions regarding the phosphatases include direct localization within the axoneme, determining how the phosphatases are targeted to specific sites along the axoneme, and the direct substrates for these phosphatases.

C. The Flagellar Proteome and Axonemal Signaling Proteins

Thanks to the completed sequence of the *Chlamydomonas* genome and the large-scale proteomic analysis used to create the *Chlamydomonas* flagellar proteome (Merchant *et al*., 2007; Pazour *et al*., 2005), we have been able to identify gene models for a large number of potential axonemal kinases and phosphatases (http://genome.jgi-psf.org/Chlre4/Chlre4. home.html; http://labs.umassmed.edu/chlamyfp/protector_login.php). Of the estimated ~600 flagellar proteins, at least 21 are protein kinases and 11 are protein phosphatases (Pazour *et al*., 2005). This number is not surprising given the predicted number of phosphorylated flagellar proteins located in the axoneme alone (Boesger *et al*., 2009; Piperno *et al*., 1981; Piperno and Luck, 1976; Segal and Luck, 1985) and the fact that phosphorylation plays a role in many important flagellar functions including motility (Porter and Sale, 2000; Wirschell *et al*., 2007), signaling (Pan and Snell, 2000), and assembly (Rosenbaum and Witman, 2002). Estimates regarding the number and function of ciliary kinases and phosphatases are in agreement with another ciliary proteome containing data from various ciliated organisms (http://v3.ciliaproteome. org/cgi-bin/index.php).

V. Discussion of the Regulatory Model and Concluding Remarks

Based on the functional analysis, genetics and biochemical/proteomic dissection described above, we have developed a working model for regulation of axonemal microtubule sliding by phosphorylation (Fig. 5; Porter and Sale, 2000; Smith and Yang, 2004; Wirschell *et al*., 2007). As indicated earlier, functional/pharmacological analyses using an *in vitro* assay of dynein activity, along with informative paralyzed

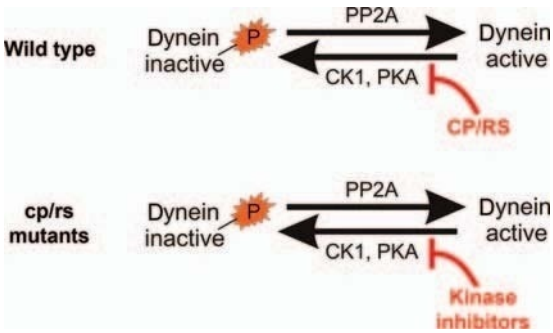

Fig. 5 Model for regulation of I1 dynein by axonemal kinases and phosphatases. Several lines of evidence indicate that I1-dynein activity is regulated by axonemal kinases and phosphatases. When IC138 is hyperphosphorylated, I1 dynein is inactive; when dephosphorylated, I1 dynein is active. In wild-type axonemes, the central pair and radial spokes (CP/RS) function to regulate the kinases that phosphorylate IC138. When the regulatory pathway is disrupted, such as in CP/RS mutants, the kinases are unregulated and IC138 becomes uniformly phosphorylated throughout the axoneme resulting in a global inhibition of dynein throughout the axoneme. This inhibition can be relieved *in vitro* by the use of kinase inhibitors which restore microtubule sliding velocities of RS or CP mutant axonemes to wild-type levels.

flagellar mutant cells from *Chlamydomonas*, have revealed that microtubule sliding can be regulated by phosphorylation and that the key kinases and phosphatases are physically anchored and localized in the axoneme.

The regulatory machinery includes the CP apparatus, RSs, I1 dynein and the signaling proteins CK1 and PP2A. Although not yet demonstrated directly, it is likely the CP/RS phosphoregulatory mechanism responds to changes in second messengers including cyclic nucleotides and calcium (Chapter 10 by Smith, this volume; Hayashi and Shingyoji, 2009; Smith, 2002a,b; Smith and Yang, 2004). The CP/RS phosphoregulatory mechanism does not appear to be required for initiation of bending and bend oscillation, features that may be inherent to the dynein motors and to mechanical feedback control mechanisms that are not well understood (Brokaw, 2008). Rather, this CP/RS phosphoregulatory mechanism appears to be required for controlling the form of forward and reverse bends important for normal movement and behavior. We do not yet know whether this same CP/RS phosphoregulatory mechanism operates in motile cilia from other organisms. However, we do know that each structure and component is highly conserved, for example, certain components of the CP such as hydin (Lechtreck *et al*., 2008; Lechtreck and Witman, 2007; Pazour *et al*., 2005) and I1-dynein subunits (Hendrickson *et al*., 2004; Wirschell *et al*., 2009; Ikeda *et al.,* 2009; Bower *et al.*, 2009). Moreover, mutations in I1-dynein components in *Tetrahymena* result in failure of normal ciliary bending and motile behavior (Angus *et al*., 2001; Hennessey *et al*., 2002; Liu *et al*., 2005) and as emphasized above, the RSP3 AKAP is highly conserved in all organisms with motile cilia (Wirschell *et al*., 2008).

A major challenge is to understand how signals from the CP apparatus are conveyed to the outer doublet microtubules for control of dynein activity (Chapters 11 and 12 by Yang and Mitchell, this volume; Smith and Yang, 2004). The mechanism appears to involve structural interactions of the RS head with the CP projections and induction of physical strain in the spoke shaft as outer doublet microtubules slide relative to the CP, or as the CP twists or rotates relative to the outer doublets. Consistent with this idea, electron microscopy has demonstrated tilting of spokes in bent regions of axonemes (Mitchell and Nakatsugawa, 2004; Warner and Satir, 1974). Predictably, since the CP is highly asymmetric in structure (Mitchell, 2003a,b; Mitchell and Sale, 1999), each projection of the CP apparatus interacts with the spoke head from each doublet microtubule in a different manner. Thus, different signals will be relayed to each outer doublet microtubule on each side of the axis of the axoneme, influencing the pattern of microtubule sliding across the axis and controlling the size and shape of the bend (see Chapter 12 by Mitchell and Smith, this volume).

Another major challenge is to determine how altered spoke structure or tilting can alter dynein activity. One idea is that CP/RS interactions result in a local drag on sliding, thus changing the pattern of sliding and the form of the bend (Warner and Satir, 1974; Yang *et al*., 2004). A change in the spoke structure or a strain at the base of the spoke could lead to changes in activity of kinases or phosphatases located at the base of the spokes and near the site of attachment of the inner dynein arms, including near the position of the phosphoregulatory protein IC138 and the postulated positions of CK1 and PP2A. The idea that strain can alter control of dynein phosphorylation requires

more direct, detailed understanding of the positions of the catalytic subunits of the axonemal kinases and phosphatases relative to the base of the spoke and base of I1 dynein, as well as a detailed understanding of I1 dynein, spoke composition (Yang *et al*., 2001, 2005), and associated complexes such as the calmodulin–RS complex (CRC), thought to mediate signals from the spoke to I1 dynein (Dymek and Smith, 2007). This resolution of structure may be possible given that recent advances in cryo-electron tomography are revealing the position of single proteins in the 96-nm axonemal repeat (Heuser *et al*., 2008). With these new data, optical approaches including FRET could be designed to test whether changes in spoke structure or strain could alter kinase activity in the outer doublet microtubule.

In summary, analyses of isolated axonemes from *Chlamydomonas* by functional, pharmacological, and direct biochemical methods have revealed a number of highly conserved, otherwise ubiquitous, protein kinases and phosphatases that are located in the axoneme. The general mechanism for controlling dynein activity and regulating microtubule sliding is through phosphorylation of dynein subunits (e.g., IC138 of I1 dynein), using a network of structures (CP/RS) and enzymes (CK1, PP2A). Additional important questions include: How and where are these kinases and phosphatases targeted and anchored in the axoneme? The RSP3 AKAP provides an important model (Gaillard *et al*., 2001, 2006) for the targeting of axonemal signaling proteins within the axoneme (Fig. 4). How are signals transmitted from the CP to the RS heads, and then from the RSs to the kinases and phosphatases on the outer doublets? How does phosphorylation of dynein subunits alter dynein motor activity? A better understanding of the phosphoregulatory mechanism will require the identification of proteins responsible for the transport and anchoring of the kinases/phosphatases to the axoneme, high-resolution structural imaging of wild-type and mutant axonemes, biophysical analyses of dyneins with altered subunit composition, and the identification and mutation of the target phosphoresidues in the key regulatory proteins.

References

Angus, S.P., Edelmann, R.E., and Pennock, D.G. (2001). Targeted gene knockout of inner arm 1 in Tetrahymena thermophila. *Eur. J. Cell Biol.* **80**, 486–497.

Aoyama, S., and Kamiya, R. (2005). Cyclical interactions between two outer doublet microtubules in split flagellar axonemes. *Biophys. J.* **89**, 3261–3268.

Bannai, H., Yoshimura, M., Takahashi, K., and Shingyoji, C. (2000). Calcium regulation of microtubule sliding in reactivated sea urchin sperm flagella. *J. Cell Sci.* **113**(Pt. 5), 831–839.

Boesger, J., Wagner, V., Weisheit, W., and Mittag, M. (2009). Analysis of flagellar phosphoproteins from Chlamydomonas reinhardtii. *Eukaryot. Cell*. **8**, 922–932.

Bonini, N.M., Evans, T.C., Miglietta, L.A., and Nelson, D.L. (1991). The regulation of ciliary motility in Paramecium by Ca^{2+} and cyclic nucleotides. *Adv. Second Messenger Phosphoprotein Res.* **23**, 227–272.

Bonini, N.M., and Nelson, D.L. (1988). Differential regulation of Paramecium ciliary motility by cAMP and cGMP. *J. Cell Biol*. **106**, 1615–1623.

Bower, R., Vanderwaal, K., O'Toole, E., Fox, L., Perrone, C., Mueller, J., Wirschell, M., Kamiya, R., Sale, W. S., and Porter, M.E., (2009). IC138 Defines a Sub-Domain at the Base of the I1 Dynein That Regulates Microtubule Sliding and Flagellar Motility. *Mol Biol Cell.* **20**, 3055–3063.

Brokaw, C.J. (1979). Calcium-induced asymmetrical beating of triton-demembranated sea urchin sperm flagella. *J. Cell Biol.* **82**, 401–411.

Brokaw, C.J. (2009). Thinking about flagellar oscillation. *Cell Motil. Cytoskeleton* **66**, 425–436.

Burton, K.A., and McKnight, G.S. (2007). PKA, germ cells, and fertility. *Physiology* (*Bethesda*) **22**, 40–46.

Christensen, S.T., Guerra, C., Wada, Y., Valentin, T., Angeletti, R.H., Satir, P., and Hamasaki, T. (2001). A regulatory light chain of ciliary outer arm dynein in Tetrahymena thermophila. *J. Biol. Chem.* **276**, 20048–20054.

Dymek, E.E., and Smith, E.F. (2007). A conserved CaM- and radial spoke associated complex mediates regulation of flagellar dynein activity. *J. Cell Biol.* **179**, 515–526.

Gaillard, A.R., Diener, D.R., Rosenbaum, J.L., and Sale, W.S. (2001). Flagellar radial spoke protein 3 is an A-kinase anchoring protein (AKAP). *J. Cell Biol.* **153**, 443–448.

Gaillard, A.R., Fox, L.A., Rhea, J.M., Craige, B., and Sale, W.S. (2006). Disruption of the A-kinase anchoring domain in flagellar radial spoke protein 3 results in unregulated axonemal cAMP-dependent protein kinase activity and abnormal flagellar motility. *Mol. Biol. Cell* **17**, 2626–2635.

Gibbons, B.H., and Gibbons, I.R. (1972). Flagellar movement and adenosine triphosphatase activity in sea urchin sperm extracted with triton X-100. *J. Cell Biol.* **54**, 75–97.

Gibbons, B.H., and Gibbons, I.R. (1976). Functional recombination of dynein 1 with demembranated sea urchin sperm partially extracted with KC1. *Biochem. Biophys. Res. Commun.* **73**, 1–6.

Gibbons, B.H., Tang, W.J., and Gibbons, I.R. (1985). Organic anions stabilize the reactivated motility of sperm flagella and the latency of dynein 1 ATPase activity. *J. Cell Biol.* **101**, 1281–1287.

Gibbons, I.R. (1981). Cilia and flagella of eukaryotes. *J. Cell Biol.* **91**, 107–124s.

Gibbons, I.R., and Rowe, A.J. (1965). Dynein: A protein with adenosine triphosphatase activity from cilia. *Science* **149**, 424–426.

Gokhale, A.,Wirschell, M., and Sale, W.S. (2009). Regulation of dynein-driven microtubule sliding by the axonemal protein kinase CK1 in *Chlamydomonas* flagella. *J. Cell Biol.* Sep 14. [Epub ahead of print]. Habermacher, G., and Sale, W.S. (1996). Regulation of flagellar dynein by an axonemal type-1 phosphatase in *Chlamydomonas*. *J. Cell Sci.* **109**(Pt. 7), 1899–1907.

Habermacher, G., and Sale, W.S. (1997). Regulation of flagellar dynein by phosphorylation of a 138-kD inner arm dynein intermediate chain. *J. Cell Biol.* **136**, 167–176.

Hasegawa, E., Hayashi, H., Asakura, S., and Kamiya, R. (1987). Stimulation of in vitro motility of Chlamydomonas axonemes by inhibition of cAMP-dependent phosphorylation. *Cell Motil. Cytoskeleton* **8**, 302–311.

Hayashi, S., and Shingyoji, C. (2008). Mechanism of flagellar oscillation-bending-induced switching of dynein activity in elastase-treated axonemes of sea urchin sperm. *J. Cell Sci.* **121**, 2833–2843.

Hayashi, S., and Shingyoji, C. (2009). Bending-induced switching of dynein activity in elastase-treated axonemes of sea urchin sperm – roles of Ca2+ and ADP. *Cell Motil. Cytoskeleton* **66**, 292–301.

Hendrickson, T.W., Perrone, C.A., Griffin, P., Wuichet, K., Mueller, J., Yang, P., Porter, M.E., and Sale, W.S. (2004). IC138 is a WD-repeat dynein intermediate chain required for light chain assembly and regulation of flagellar bending. *Mol. Biol. Cell* **12**, 5431–5442.

Hennessey, T.M., Kim, D.Y., Oberski, D.J., Hard, R., Rankin, S.A., and Pennock, D.G. (2002). Inner arm dynein 1 is essential for Ca++-dependent ciliary reversals in Tetrahymena thermophila. *Cell Motil. Cytoskeleton* **53**, 281–288.

Heuser, T., Raytchev, M., Krell, J., Porter, M.E., and Nicastro, D. (2008). Cryo-electron tomography reveals new structures in the flagellar axoneme. *In* "American Society for Cell Biology" *Vol. Mol. Biol. Cell* **19** (Suppl.), (CD-ROM) #16, San Francisco.

Hill, K.L. (2003). Biology and mechanism of trypanosome cell motility. *Eukaryot. Cell* **2**, 200–208.

Howard, D.R., Habermacher, G., Glass, D.B., Smith, E.F., and Sale, W.S. (1994). Regulation of *Chlamydomonas* flagellar dynein by an axonemal protein kinase. *J. Cell Biol.* **127**, 1683–1692.

Ikeda, K., Yamamoto, R., Wirschell, M., Yagi, T. Bower, R. Porter, M.E., Sale, W.S., and Kamiya, R. (2009). A novel ankyrin-repeat protein interacts with the regulatory proteins of inner arm dynein f (I1) of *Chlamydomonas reinhardtii. Cell Motil Cytoskeleton.* **66**, 448–456.

Inaba, K. (2007). Molecular basis of sperm flagellar axonemes: Structural and evolutionary aspects. *Ann. N. Y. Acad. Sci.* **1101**, 506–526.

Kamimura, S., and Takahashi, K. (1981). Direct measurement of the force of microtubule sliding in flagella. *Nature* **293**, 566–568.

Kamiya, R. (2002). Functional diversity of axonemal dyneins as studied in *Chlamydomonas* mutants. *Int. Rev. Cytol.* **219**, 115–155.

Kamiya, R., and Witman, G.B. (1984). Submicromolar levels of calcium control the balance of beating between the two flagella in demembranated models of *Chlamydomonas. J. Cell Biol.* **98**, 97–107.

King, S.J., and Dutcher, S.K. (1997). Phosphoregulation of an inner dynein arm complex in Chlamydomonas reinhardtii is altered in phototactic mutant strains. *J. Cell Biol.* **136**, 177–191.

King, S.M., and Kamiya, R. (2009). Axonemal dyneins: Assembly, structure, and force generation. In "The *Chlamydomonas* Sourcebook: Cell Motility and Behavior" (G. B. Witman, ed.), Vol. 3, pp. 131–208. Academic Press, Oxford.

Kikushima, K. (2009). Central pair apparatus enhances outer-arm dynein activities through regulation of inner-arm dyneins. *Cell Motil Cytoskeleton.* **66**, 272–280.

Kohl, L., and Bastin, P. (2005). The flagellum of trypanosomes. *Int. Rev. Cytol.* **244**, 227–285.

Kurimoto, E., and Kamiya, R. (1991). Microtubule sliding in flagellar axonemes of Chlamydomonas mutants missing inner- or outer-arm dynein: Velocity measurements on new types of mutants by an improved method. *Cell Motil. Cytoskeleton* **19**, 275–281.

Lechtreck, K.F., Delmotte, P., Robinson, M.L., Sanderson, M.J., and Witman, G.B. (2008). Mutations in Hydin impair ciliary motility in mice. *J. Cell Biol.* **180**, 633–643.

Lechtreck, K.F., and Witman, G.B. (2007). Chlamydomonas reinhardtii hydin is a central pair protein required for flagellar motility. *J. Cell Biol.* **176**, 473–482.

Lindemann, C.B., Gardner, T.K., Westbrook, E., and Kanous, K.S. (1991). The calcium-induced curvature reversal of rat sperm is potentiated by cAMP and inhibited by anti-calmodulin. *Cell Motil. Cytoskeleton* **20**, 316–324.

Lindemann, C.B., and Gibbons, I.R. (1975). Adenosine triphosphate-induced motility and sliding of filaments in mammalian sperm extracted with Triton X-100. *J. Cell Biol.* **65**, 147–162.

Lindemann, C.B., and Schmitz, K.A. (2001). Detergent-extracted models for the study of cilia or flagella. *Methods Mol. Biol.* **161**, 241–252.

Liu, S., Hennessey, T., Rankin, S., and Pennock, D.G. (2005). Mutations in genes encoding inner arm dynein heavy chains in Tetrahymena thermophila lead to axonemal hypersensitivity to Ca2+. *Cell Motil. Cytoskeleton* **62**, 133–140.

Merchant, S.S., Prochnik, S.E., Vallon, O., Harris, E.H., Karpowicz, S.J., Witman, G.B., Terry, A., Salamov, A., Fritz-Laylin, L.K., Marechal-Drouard, L., Marechal-Marshall, W.F. *et al*. (2007). The Chlamydomonas genome reveals the evolution of key animal and plant functions. *Science* **318**, 245–250.

Mitchell, D.R. (2003a). Orientation of the central pair complex during flagellar bend formation in Chlamydomonas. *Cell Motil. Cytoskeleton* **56**, 120–129.

Mitchell, D.R. (2003b). Reconstruction of the projection periodicity and surface architecture of the flagellar central pair complex. *Cell Motil. Cytoskeleton* **55**, 188–199.

Mitchell, D.R., and Nakatsugawa, M. (2004). Bend propagation drives central pair rotation in Chlamydomonas reinhardtii flagella. *J. Cell Biol.* **166**, 709–715.

Mitchell, D.R., and Sale, W.S. (1999). Characterization of a *Chlamydomonas* insertional mutant that disrupts flagellar central pair microtubule-associated structures. *J. Cell Biol.* **144**, 293–304.

Mogami, Y., and Takahashi, K. (1983). Calcium and microtubule sliding in ciliary axonemes isolated from Paramecium caudatum. *J. Cell Sci* **61**, 107–121.

Okagaki, T., and Kamiya, R. (1986). Microtubule sliding in mutant *Chlamydomonas* axonemes devoid of outer or inner dynein arms. *J. Cell Biol.* **103**, 1895–902.

Pan, J., and Snell, W.J. (2000). Signal transduction during fertilization in the unicellular green alga, Chlamydomonas. *Curr. Opin. Microbiol.* **3**, 596–602.

Pazour, G.J., Agrin, N., Leszyk, J., and Witman, G.B. (2005). Proteomic analysis of a eukaryotic cilium. *J. Cell Biol.* **170**, 103–113.

Pennock, D.G. (2000). Selection of motility mutants. *Methods Cell. Biol.* **62**, 281–290.
Piperno, G., Huang, B., Ramanis, Z., and Luck, D.J. (1981). Radial spokes of *Chlamydomonas* flagella: Polypeptide composition and phosphorylation of stalk components. *J. Cell Biol.* **88**, 73–79.
Piperno, G., and Luck, D.J. (1976). Phosphorylation of axonemal proteins in *Chlamydomonas reinhardtii*. *J. Biol. Chem.* **251**, 2161–2167.
Porter, M.E., and Sale, W.S. (2000). The 9 + 2 axoneme anchors multiple inner arm dyneins and a network of kinases and phosphatases that control motility. *J. Cell Biol.* **151**, F37–42.
Ralston, K.S., and Hill, K.L. (2008). The flagellum of Trypanosoma brucei: New tricks from an old dog. *Int. J. Parasitol.* **38**, 869–884.
Rosenbaum, J.L., and Witman, G.B. (2002). Intraflagellar transport. *Nat. Rev. Mol. Cell Biol.* **3**, 813–825.
Salathe, M. (2007). Regulation of mammalian ciliary beating. *Annu. Rev. Physiol.* **69**, 401–422.
Sale, W.S., Fox, L.A., and Smith, E.F. (1993). Assays of axonemal dynein-driven motility. *Methods Cell Biol.* **39**, 89–104.
Sale, W.S., and Satir, P. (1977). Direction of active sliding of microtubules in Tetrahymena cilia. *Proc. Natl. Acad. Sci. USA* **74**, 2045–2049.
Satir, P., and Matsuoka, T. (1989). Splitting the ciliary axoneme: Implications for a "switch-point" model of dynein arm activity in ciliary motion. *Cell Motil. Cytoskeleton* **14**, 345–358.
Segal, R.A., and Luck, D.J. (1985). Phosphorylation in isolated Chlamydomonas axonemes: A phosphoprotein may mediate the Ca2+-dependent photophobic response. *J. Cell Biol.* **101**, 1702–1712.
Smith, E.F. (2002a). Regulation of flagellar dynein by calcium and a role for an axonemal calmodulin and calmodulin-dependent kinase. *Mol. Biol. Cell* **13**, 3303–3313.
Smith, E.F. (2002b). Regulation of flagellar dynein by the axonemal central apparatus. *Cell Motil. Cytoskeleton* **52**, 33–42.
Smith, E.F., and Sale, W.S. (1992a). Regulation of dynein-driven microtubule sliding by the radial spokes in flagella. *Science* **257**, 1557–1559.
Smith, E.F., and Sale, W.S. (1992b). Structural and functional reconstitution of inner dynein arms in *Chlamydomonas* flagellar axonemes. *J. Cell Biol.* **117**, 573–581.
Smith, E.F., and Yang, P. (2004). The radial spokes and central apparatus: Mechano-chemical transducers that regulate flagellar motility. *Cell Motil. Cytoskeleton* **57**, 8–17.
Summers, K. (1974). ATP-induced sliding of microtubules in bull sperm flagella. *J. Cell Biol.* **60**, 321–324.
Summers, K.E., and Gibbons, I.R. (1971). Adenosine triphosphate-induced sliding of tubules in trypsin-treated flagella of sea-urchin sperm. *Proc. Natl. Acad. Sci. USA* **68**, 3092–3096.
Tamm, S.L., and Tamm, S. (1984). Alternate patterns of doublet microtubule sliding in ATP-disintegrated macrocilia of the ctenophore Beroe. *J. Cell. Biol.* **99**, 1364–1371.
Warner, F.D., and Satir, P. (1974). The structural basis of ciliary bend formation. Radial spoke positional changes accompanying microtubule sliding. *J. Cell Biol.* **63**, 35–63.
Wirschell, M., Hendrickson, T., and Sale, W.S. (2007). Keeping an eye on I1: I1 dynein as a model for flagellar dynein assembly and regulation. *Cell Motil. Cytoskeleton* **64**, 569–579.
Wirschell, M., Yang, C., Yang, P., Fox, L., Yanagisawa, H.A., Kamiya, R., Witman, G.B., Porter, M.E., and Sale, W.S. (2009). IC97 is a novel intermediate chain of I1 dynein that interacts with tubulin and regulates interdoublet sliding. *Mol. Biol. Cell*. **20**, 3044–3054.
Wirschell, M., Zhao, F., Yang, C., Yang, P., Diener, D., Gaillard, A., Rosenbaum, J.L., and Sale, W.S. (2008). Building a radial spoke: Flagellar radial spoke protein 3 (RSP3) is a dimer. *Cell Motil. Cytoskeleton* **65**, 238–248.
Witman, G.B. (1986). Isolation of *Chlamydomonas* flagella and flagellar axonemes. *Methods Enzymol.* **134**, 280–290.
Witman, G.B., Carlson, K., Berliner, J., and Rosenbaum, J.L. (1972). *Chlamydomonas* flagella. I. Isolation and electrophoretic analysis of microtubules, matrix, membranes, and mastigonemes. *J. Cell Biol.* **54**, 507–539.
Witman, G.B., Plummer, J., and Sander, G. (1978). Chlamydomonas flagellar mutants lacking radial spokes and central tubules. Structure, composition, and function of specific axonemal components. *J. Cell Biol.* **76**, 729–747.

Yamamoto, R., Yagi, T., and Kamiya, R. (2006). Functional binding of inner-arm dyneins with demembranated flagella of Chlamydomonas mutants. *Cell Motil. Cytoskeleton* **63**, 258–265.

Yang, C., Compton, M.M., and Yang, P. (2005). Dimeric novel HSP40 is incorporated into the radial spoke complex during the assembly process in flagella. *Mol. Biol. Cell* **16**, 637–648.

Yang, P., Diener, D.R., Rosenbaum, J.L., and Sale, W.S. (2001). Localization of calmodulin and dynein light chain LC8 in flagellar radial spokes. *J. Cell Biol.* **153**, 1315–1326.

Yang, P., Fox, L., Colbran, R.J., and Sale, W.S. (2000). Protein phosphatases PP1 and PP2A are located in distinct positions in the *Chlamydomonas* flagellar axoneme. *J. Cell Sci.* **113**(Pt. 1), 91–102.

Yang, P., and Sale, W.S. (2000). Casein kinase I is anchored on axonemal doublet microtubules and regulates flagellar dynein phosphorylation and activity. *J. Biol. Chem.* **275**, 18905–18912.

Yang, P., Yang, C., and Sale, W.S. (2004). Flagellar radial spoke protein 2 is a calmodulin binding protein required for motility in Chlamydomonas reinhardtii. *Eukaryot. Cell* **3**, 72–81.

This page intentionally left blank

CHAPTER 10

Analysis of Redox-Sensitive Dynein Components

Ken-ichi Wakabayashi
Department of Biological Sciences, Graduate School of Science, The University of Tokyo, Tokyo, Japan

Abstract

Redox-based regulation plays important roles in many cellular activities. Thioredoxins, one of the best characterized class of proteins involved in cellular redox regulation, are conserved components of eukaryotic ciliary/flagellar axonemal dyneins. Studies with *Chlamydomonas* showed that, under varying redox conditions, dynein-associated thioredoxins interact with different proteins through disulfide bonds and, as a consequence, flagella change their manner of beating. This chapter provides an overview of techniques for estimating and modulating the redox state of axonemal proteins, as well as for searching for redox-regulated proteins in the axoneme.

METHODS IN CELL BIOLOGY, VOL. 92

978-0-12-374974-1
DOI: 10.1016/S0091-679X(08)92010-0

I. Introduction

Intracellular redox (*red*uction–*ox*idation) poise is kept reduced mainly by the glutathione and thioredoxin systems. However, it can become more oxidized due to the generation of reactive oxygen species (ROS) in response to stress or intrinsic cellular activity. Such alterations in the cellular redox poise are important in the regulation of many kinds of cellular functions, such as transcription factor activation, defense against oxidative stress, apoptosis [for review see Oktyabrsky and Smirnova (2007)]. Previously, *Chlamydomonas* outer arm dynein ATPase and flagellar beating were both shown to be modulated by redox poise (Harrison *et al*., 2002; Wakabayashi and King, 2006), which changes in response to alterations in ambient light conditions *in vivo* (Forti *et al*., 2003).

Chlamydomonas outer arm dynein contains at least three subunits that have redox-sensitive vicinal dithiol(s): LC3, LC5, and DC3. LC3 is a 17-kDa polypeptide which binds the N-terminal stem of the β and γ heavy chains (Sakakibara *et al*., 1993; Sakato *et al*., 2007) and has one complete redox-active thioredoxin motif ($_{36}$W*C*GP*C*K$_{41}$) and a second potentially redox-sensitive vicinal dithiol ($_{65}$V*C*AEK*C*N$_{71}$) (Harrison *et al*., 2002; Patel-King *et al*., 1996; Sakato *et al*., 2007). LC5 is a 14-kDa protein which has one complete thioredoxin motif ($_{33}$W*C*GP*C*K$_{38}$) and binds the stem of the α heavy chain (Harrison *et al*., 2002). DC3 is a 21 kDa protein that is the smallest subunit of the outer dynein arm-docking complex (ODA-DC); this structure mediates the binding of outer arm dyneins to specific sites on the doublet microtubules (Casey *et al*., 2003b; Takada and Kamiya, 1994). DC3 has a vicinal dithiol ($_{65}$D*C*DG*C*I$_{70}$) within an EF hand and binds Ca^{2+} only when it is reduced (Casey *et al*., 2003a). These three redox-sensitive proteins associate with other proteins in a redox-sensitive manner, and these redox targets can change in response to alterations in ambient light conditions or following treatment with H_2O_2 (Wakabayashi and King, 2006). These data strongly suggest that a redox regulatory pathway functions in the *Chlamydomonas* flagellum and that redox-sensitive dynein subunits participate in this pathway.

The presence of thioredoxins in dynein is not specific to *Chlamydomonas*, as similar modules have been found in the intermediate chain 1 (IC1) protein of sperm flagellar outer arm dynein from the sea urchin *Anthocidaris crassispina* (Ogawa *et al*., 1996) and the ascidian *Ciona intestinalis* (Padma *et al*., 2001). In addition, two proteins related to *Chlamydomonas* LC5 and *Ciona* IC1, TXNDC3 and TXNDC6, are expressed in human ciliated organisms (Padma *et al*., 2001; Pazour *et al*., 2006; Sadek *et al*., 2003, 2001). Thus, the presence of thioredoxins in axonemal dyneins has been evolutionarily conserved. DC3 is a member of a subfamily of EF-hand proteins termed *c*almodulin, *t*roponin C (CTER and the *e*ssential and *r*egulatory light chains of myosin). DC3 has a homologue in *Plasmodium*, and these proteins represent a distinct subfamily within the CTER grouping (Casey *et al*., 2003b).

Here I describe (1) how to modulate the redox state of flagellar proteins including three redox-sensitive dynein subunits *in vitro* (including motility assessment of demembranated cell models after modulation of the redox state), (2) how to assess the *in vivo* redox state of those proteins, and (3) how to screen for proteins which interact with these dynein components in a redox-sensitive manner. These techniques

can be adapted to proteins other than dynein subunits that contain cysteine residues, to determine whether those proteins are redox sensitive, and/or whether they interact with other polypeptides *via* intermolecular disulfide bonds.

II. Materials and Reagents

A. Materials

1. *Chlamydomonas* flagellar axonemes (for preparation, see Chapter 3 by King, this volume)
2. *Chlamydomonas* demembranated cell models (for preparation, see Chapter 12 by Kamiya, volume 91)

B. Reagents

1. 4-Acetamido-4-maleimidylstilbene-2,2-disulfonic acid (AMS)
2. Iodoacetamide (IAA)
3. 100% (w/v) trichloroacetic acid (TCA)
4. 1 M acetic acid
5. 5,5′-Dithiobis (2-nitrobenzoic acid) (DTNB)
6. Dithiothreitol (DTT)
7. Reduced L-glutathione (GSH)
8. Oxidized L-glutathione (GSSG)
9. HMEK buffer (30 mM HEPES, pH 7.4, 5 mM $MgSO_4$, 1 mM EGTA, 50 mM potassium acetate)
10. HMEKP [HMEK + 1% polyethylene glycol (M_r 20,000)] containing 70 units/ml creatine kinase and 5 mM phosphocreatine as an ATP-regenerating system.
11. 2× Nonreducing SDS sample buffer (0.1 M Tris-HCl, pH 6.8, 4% SDS, 20% glycerol, 0.01% bromophenol blue)

III. Methods

A. *In vitro* Modulation of Axonemal Redox State

Redox buffers are prepared with reduced and oxidized L-glutathione (GSH and GSSG, respectively) in HMEK buffer. Examples of the GSH/GSSG ratio and the final concentrations are shown in Table I. Fully oxidized or reduced control buffers are prepared with 10 mM DTNB or 10 mM DTT in HMEK buffer, respectively. Purified axonemes are resuspended at a concentration of ~6 μg/μl in these buffers, incubated at room temperature for 30 min, and then fixed with TCA (final 5% v/v) to freeze the redox state of the axonemal proteins. Fixed axonemes are harvested by centrifugation at 18,000 × *g* for 10 min and washed three times with acetone to remove the TCA. After drying by vacuum centrifugation, samples are alkylated with 20 mM AMS in 0.1 M Tris-HCl, pH 7.4, 1%

Table I
Redox Buffers for Modulation of the Redox state of Axonemes

GSH (mM)	2.5	2.5	2.5	2.5	2.5	2.5	5	5	25	25
GSSG (mM)	250	200	150	100	75	50	50	25	25	5
[GSH]:[GSSG]	1:100	1:80	1:60	1:40	1:30	1:20	1:10	1:5	1.1	5.1
Common reagents	30 mM HEPES (pH 7.4), 5 mM $MgSO_4$, 1 mM EGTA, 50 mM Potassium acetate									

SDS, and incubated for 30 min at room temperature; if it is difficult to dissolve the pellets, use an ultrasonic bath. AMS adds 490 Da per modified thiol (Fig. 1A) to the mass of a protein. All samples are mixed with an equal volume of 2× nonreducing SDS sample buffer and incubated for 30 min at 37°C prior to electrophoresis. Following electrophoresis, gels are blotted to nitrocellulose (NC) or polyvinylidene difluoride (PVDF) membranes and probed with specific antibodies. Figure 1B shows the redox states of LC3, LC5, and DC3 in the redox buffers; proteins were detected using specific antibodies.

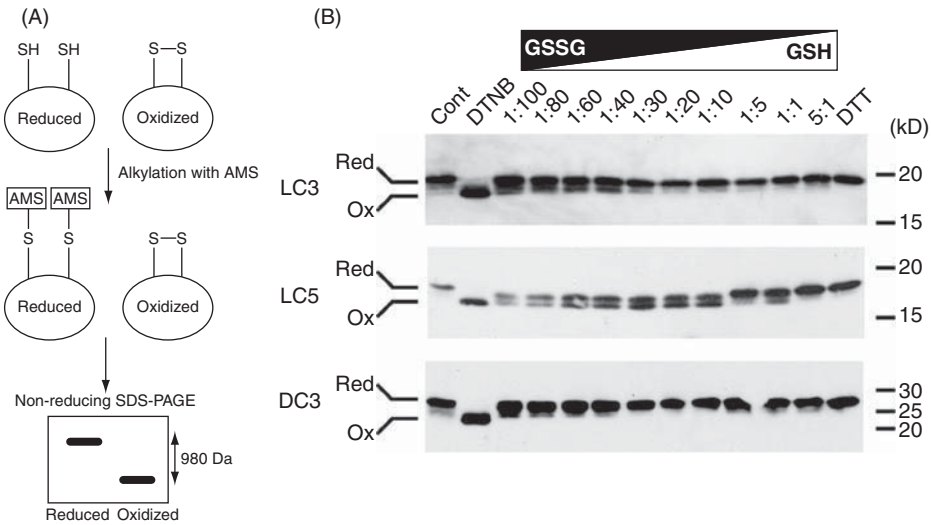

Fig. 1 (A) Scheme detailing the 4-acetamido-4-maleimidylstilbene-2,2-disulfonic acid (AMS) method to distinguish oxidized and reduced dithiols. The maleimide group of AMS reacts only with reduced thiols and, thus a protein with a reduced vicinal dithiol will incorporate two AMS moieties (980 Da). In contrast, oxidized dithiols are protected from modification. Consequently, reduced proteins may be readily separated from the oxidized forms by nonreducing SDS-PAGE. (B) Axonemes were incubated with redox buffers containing different GSH/GSSG ratios; alkylated with AMS; electrophoresed in the absence of reducing agents; and probed with antiLC3, -LC5, and -DC3 antibodies. Axonemes alkylated after incubation with 10 mM DTNB or DTT were used as fully oxidized and reduced controls, respectively. The lane marked "Cont" was only treated with HMEK buffer before AMS modification. The redox state of the three dynein/ODA-DC proteins is altered depending on the GSH/GSSG ratio. The location of the M_r markers ($\times 10^3$) is at right. Modified from Wakabayashi and King (2006).

B. Reactivation of Demembranated Cell Models in Redox Buffers

Cell models are resuspended in a series of redox buffers in HMEKP buffer. Examples of redox buffers are shown in Table II. (For this physiological experiment, buffers were designed to mimic the intracellular glutathione concentration (~10 mM) (Oktyabrsky and Smirnova, 2007), and the total amounts of GSH and GSSG are reduced from those shown in Table I.) Incubate on ice for 1 h and then add ATP to a final concentration of 1 mM to reactivate the cell models. When mixing the solutions, avoid vigorous pipetting or axonemes become detached from the cell models and beat frequency analysis is difficult. Mixing by light tapping is recommended. The method for analysis of axonemal beat frequency is described in Chapter 12 by Kamiya, volume 91. Figure 2 shows the beat frequency of reactivated cell model axonemes from a wild-type strain and a mutant lacking outer arm dynein [*oda1* (Kamiya, 1988)] after treatment with the series of redox buffers.

C. Estimation of the *In Vivo* Redox State of Dynein Subunits

A 50 ml culture of *Chlamydomonas* (~3×10^6 cells/ml) is deflagellated by addition of acetic acid (final concentration of 25 mM) and immediately treated with TCA (final concentration of 5%, v/v) to freeze the *in vivo* redox state of the flagellar proteins; to avoid changing the *in vivo* redox state, acetic acid and TCA are added in rapid succession to a stirred culture. Note that the color of the culture will turn from green to brown after addition of TCA. Following elimination of cell bodies by differential centrifugation, flagella are harvested by centrifugation at 18,000 × *g* for 10 min and washed with acetone three times to remove TCA. After drying by vacuum centrifugation, samples are then alkylated with 20 mM AMS in 0.1 M Tris-HCl, pH 7.4, 1% SDS, and incubated for 30 min at room temperature. Fully oxidized and reduced standards were obtained as described in Section III.A. All samples are mixed with an equal volume of 2× nonreducing SDS sample buffer and incubated for 30 min at 37°C prior to electrophoresis. The *in vivo* redox state of these proteins can be estimated by comparison with the western blot patterns obtained from samples in Section A. This methodology has been adapted from that described by (Kobayashi *et al.*, 1997). Figure 3 shows the *in vivo* redox state of LC3, LC5, and DC3 from cells grown under different light conditions. All the proteins are almost always reduced, but in the dark, the amount of oxidized proteins is slightly increased.

Table II
Redox Buffers for Reactivation of Cell Models

GSH (mM)	10	5	3	1	0.3	0.06	0
GSSG (mM)	0	1	3	5	6	6	10
[GSH]:[GSSG]	–	5:1	1:1	1:5	1:20	1:100	–
Common reagents	In addition to HMEK (Table I), 1% polyethylene glycol (M_r 20,000), 70 units/ml creatine kinase, 5 mM phosphocreatine						

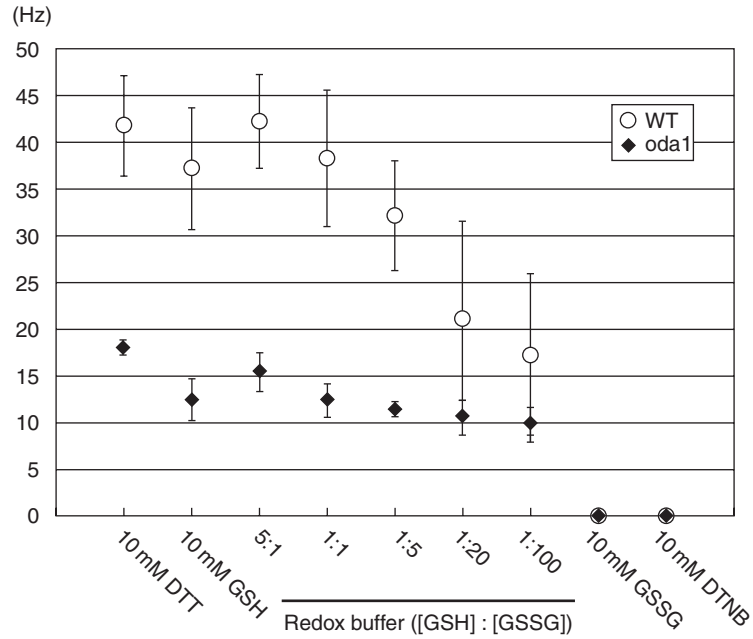

Fig. 2 Axonemal beat frequency of cell models prepared from wild-type cells and a mutant lacking the entire outer arm dynein (*oda1*). Models were reactivated by addition of ATP and an ATP-regenerating system under fully reducing (10 mM DTT and GSH) and oxidizing (10 mM DTNB and GSSG) conditions and in the presence of various redox buffers. Flagellar beat frequency was determined by FFT analysis (see Chapter 12 by Kamiya, volume 91), and the data plotted as the mean ± SEM for three independent experiments. Note that in the presence of 10 mM DTNB or GSSG, all cell models lost their flagella and were therefore immotile; visual inspection determined that these detached axonemal structures did not reactivate in the presence of ATP. The axonemal beat frequency of wild-type cell models decreased by ~60% when the [GSH]:[GSSG] ratio was changed from 5:1 to 1:100, while that of *oda1* cell models decreases by ~30%, suggesting that outer arm dyneins are more sensitive to alterations in redox poise than are inner arm dyneins. Modified from Wakabayashi and King (2006).

D. Redox 2D PAGE of Flagellar Proteins

Nonreducing–reducing 2D polyacrylamide gel electrophoresis (or redox 2D PAGE) is a method to (1) comprehensively screen for redox-sensitive proteins from organisms of interest and (2) screen for protein(s) which interact with known redox-sensitive proteins in a redox-dependent manner. Spots below the diagonal represent potential redox-sensitive proteins, and spots on the same vertical axis, that is, parallel to the direction of the second dimension electrophoresis, represent potential binding partners that interact *via* disulfides (Fig. 4A).

Chlamydomonas flagella isolated from 200-ml cultures (~4×10^6 cells/ml) are fixed with TCA and washed with acetone as described in Section C. Dried flagella samples are then treated with an alkylation solution (0.1 M Tris-HCl, pH 7.4, 1% SDS, 0.1 M IAA) for 30 min at room temperature to prevent free sulfhydryl groups from forming

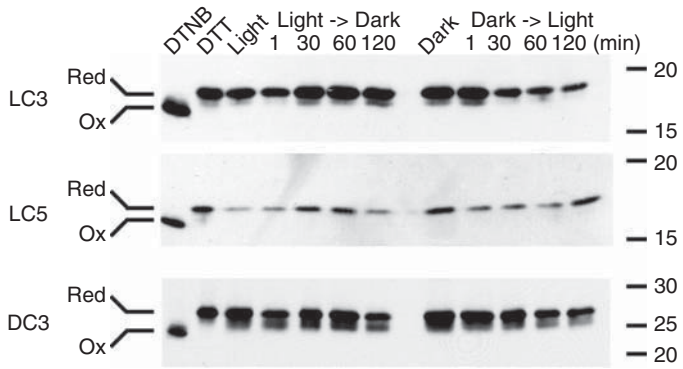

Fig. 3 The *in vivo* redox state of LC3, LC5, and DC3 in cells grown under different light conditions. A *C. reinhardtii* preculture was grown under a 15/9 h light/dark cycle for 2–3 days. This culture was then inoculated into several bottles and grown for 1–2 days more (total 3–4 days). On the day before the experiment, half of the bottles were kept under the regular illumination regime, and the other half were wrapped with aluminum foil and kept completely in the dark. Experiments were initiated 6 h after the beginning of the light phase. We prepared samples for each treatment group, and then switched the light conditions; that is, light-adapted cells were placed in total darkness and vice versa. Samples were taken 1, 30, 60, and 120 min after the light switch. Flagella were fixed with TCA immediately after deflagellation and treated with 4-acetamido-4-maleimidylstilbene-2,2-disulfonic acid. Samples were separated in a 15% acrylamide gel without reducing reagents; transferred to nitrocellulose membranes; and probed with antiLC3, -LC5, and -DC3 antibodies. Although LC5 is essentially always reduced, small amounts of LC3 (~10%) and DC3 (~30%) are present in the oxidized form. The fully oxidized and reduced markers are at left. Modified from Wakabayashi and King (2006).

nonspecific intermolecular disulfide bonds. Samples are mixed with 2× nonreducing SDS sample buffer and incubated at 37°C for 30 min.

Initially, samples are electrophoresed in a 5–15% gradient polyacrylamide gel. The gel lanes are excised, soaked in 1× SDS sample buffer containing 0.1 M DTT for 30 min, and subsequently in 1× SDS sample buffer containing 0.1 M DTT and 0.1 M IAA for 30 min. After a brief wash with 1× SDS sample buffer without DTT and IAA for 30 min to reduce streaking artifacts, gel strips are placed onto the second dimension gel (another 5–15% polyacrylamide gradient) and sealed with 1% agarose in 50 mM Tris-HCl, pH 6.8; to easily place the gel strips, make the second gel thicker than that used for the first dimension. Following electrophoresis, gels are either stained with SYPRO Ruby (Molecular Probes, Eugene, OR) or silver (for protein identification *via* mass spectrometry, do not use procedures that include glutaraldehyde), or blotted to NC or PVDF membranes and probed with specific antibodies. For detection of LC3, LC5, and DC3, use affinity-purified antiLC3 (R4930), -LC5 (R4929) antibodies (Patel-King *et al*., 1996), and antiDC3 antiserum (Casey *et al*., 2003b). Antibodies against proteins which do not contain any cysteine residues are useful as a negative control, such as R7178 against LC7a, an outer arm light chain (Bowman *et al*., 1999). Figure 4B shows a redox-2D SDS-PAGE gel of *Chlamydomonas* wild-type flagella isolated from cells grown in the light.

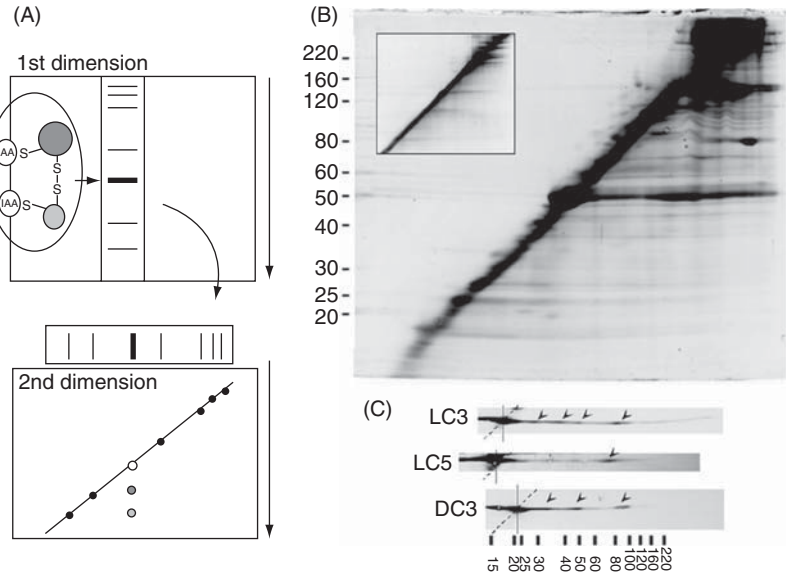

Fig. 4 (A) Schematic of the redox 2D gel method. Samples were initially alkylated with IAA in the absence of reducing reagents and electrophoresed in the first dimension (intermolecular disulfides are stable under these conditions). The gel lane was excised, reduced, and alkylated and then electrophoresed again. Any proteins initially crosslinked by intermolecular disulfide bonds focus below the diagonal. (B) Redox 2D gel analysis of *C. reinhardtii* flagella from light-adapted cells and stained with SYPRO Ruby; multiple spots are observed below the diagonal. The inset shows a similar 2D gel that used reducing reagents in both dimensions; note that no spots were detected below the diagonal. The location of the M_r markers are indicated at the left ($\times 10^3$). (C) Immunoblots of redox-2D gels probed with antibodies against LC3, LC5, and DC3. Flagellar samples were obtained from cells adapted to the light. In each immunoblot, off-diagonal spots which derive from binding other proteins are indicated with arrowheads. Solid lines are references for M_r and dotted lines mark the diagonal on which most proteins align. The location of M_r markers is indicated at the bottom ($\times 10^3$). Modified from Wakabayashi and King (2006).

Acknowledgments

The author thanks Drs. Stephen M. King (University of Connecticut Health Center) and Gregory J. Pazour (University of Massachusetts Medical School) for critically reading this manuscript. This work was supported by a Grant-in-Aid for Young Scientists (Start-up) and from the Japan Society for Promotion of Sciences and a grant from the Asahi Glass Foundation.

References

Bowman, A.B., Patel-King, R.S., Benashski, S.E., McCaffery, J.M., Goldstein, L.S., and King, S.M. (1999). Drosophila roadblock and Chlamydomonas LC7: A conserved family of dynein-associated proteins involved in axonal transport, flagellar motility, and mitosis. *J. Cell Biol.* **146**, 165–180.

Casey, D., Yagi, T., Kamiya, R., and Witman, G. (2003a). DC3, the smallest subunit of the Chlamydomonas flagellar outer dynein arm-docking complex, is a redox-sensitive calcium-binding protein. *J. Biol. Chem.* **278**, 42652–42659.

Casey, D.M., Inaba, K., Pazour, G.J., Takada, S., Wakabayashi, K., Wilkerson, C.G., Kamiya, R., and Witman, G.B. (2003b). DC3, the 21-kDa subunit of the outer dynein arm-docking complex (ODA-DC), is a novel EF-hand protein important for assembly of both the outer arm and the ODA-DC. *Mol. Biol. Cell* **14**, 3650–3663.

Forti, G., Furia, A., Bombelli, P., and Finazzi, G. (2003). In vivo changes of the oxidation-reduction state of NADP and of the ATP/ADP cellular ratio linked to the photosynthetic activity in Chlamydomonas reinhardtii. *Plant Physiol.* **132**, 1464–1474.

Harrison, A., Sakato, M., Tedford, H.W., Benashski, S.E., Patel-King, R.S., and King, S.M. (2002). Redox-based control of the gamma heavy chain ATPase from Chlamydomonas outer arm dynein. *Cell Motil. Cytoskeleton* **52**, 131–143.

Kamiya, R. (1988). Mutations at twelve independent loci result in absence of outer dynein arms in Chlamydomonas reinhardtii. *J. Cell Biol.* **107**, 2253–2258.

Kobayashi, T., Kishigami, S., Sone, M., Inokuchi, H., Mogi, T., and Ito, K. (1997). Respiratory chain is required to maintain oxidized states of the DsbA-DsbB disulfide bond formation system in aerobically growing Escherichia coli cells. *Proc. Natl. Acad. Sci. USA* **94**, 11857–11862.

Ogawa, K., Takai, H., Ogiwara, A., Yokota, E., Shimizu, T., Inaba, K., and Mohri, H. (1996). Is outer arm dynein intermediate chain 1 multifunctional? *Mol. Biol. Cell* **7**, 1895–1907.

Oktyabrsky, O.N., and Smirnova, G.V. (2007). Redox regulation of cellular functions. *Biochemistry* (*Mosc*) **72**, 132–145.

Padma, P., Hozumi, A., Ogawa, K., and Inaba, K. (2001). Molecular cloning and characterization of a thioredoxin/nucleoside diphosphate kinase related dynein intermediate chain from the ascidian, Ciona intestinalis. *Gene* **275**, 177–183.

Patel-King, R.S., Benashki, S.E., Harrison, A., and King, S.M. (1996). Two functional thioredoxins containing redox-sensitive vicinal dithiols from the Chlamydomonas outer dynein arm. *J. Biol. Chem.* **271**, 6283–6291.

Pazour, G.J., Agrin, N., Walker, B.L., and Witman, G.B. (2006). Identification of predicted human outer dynein arm genes: Candidates for primary ciliary dyskinesia genes. *J. Med. Genet.* **43**, 62–73.

Sadek, C., Jimenez, A., Damdimopoulos, A., Kieselbach, T., Nord, M., Gustafsson, J.-A., Spyrou, G., Davis, E., Oko, R., van der Hoorn, F., and Miranda-Vizuete, A. (2003). Characterization of human thioredoxin-like 2. A novel microtubule-binding thioredoxin expressed predominantly in the cilia of lung airway epithelia and spermatid manchette and axoneme. *J. Biol. Chem.* **278**, 13133–13142.

Sadek, C.M., Damdimopoulos, A.E., Pelto-Huikko, M., Gustafsson, J.A., Spyrou, G., and Miranda-Vizuete, A. (2001). Sptrx-2, a fusion protein composed of one thioredoxin and three tandemly repeated NDP-kinase domains is expressed in human testis germ cells. *Genes Cells* **6**, 1077–1090.

Sakakibara, H., Takada, S., King, S.M., Witman, G.B., and Kamiya, R. (1993). A Chlamydomonas outer arm dynein mutant with a truncated beta heavy chain. *J. Cell Biol.* **122**, 653–661.

Sakato, M., Sakakibara, H., and King, S.M. (2007). Chlamydomonas outer arm dynein alters conformation in response to Ca2+. *Mol. Biol. Cell* **18**, 3620–3634.

Takada, S., and Kamiya, R. (1994). Functional reconstitution of Chlamydomonas outer dynein arms from alpha- beta and gamma subunits: Requirement of a third factor. *J. Cell Biol.* **126**, 737–745.

Wakabayashi, K., and King, S.M. (2006). Modulation of Chlamydomonas reinhardtii flagellar motility by redox poise. *J. Cell Biol.* **173**, 743–754.

This page intentionally left blank

CHAPTER 11

Calcium Regulation of Ciliary Motility: Analysis of Axonemal Calcium-Binding Proteins

Christen DiPetrillo *and* Elizabeth Smith
Department of Biological Sciences, Dartmouth College, Hanover, New Hampshire

Abstract

Substantial data have contributed to a model in which the axonemal microtubules act as a scaffold for the assembly of molecules that form a signal transduction pathway that ultimately regulates dynein. We have also known for some time that for virtually all motile cilia and flagella, the second messenger, calcium, impacts upon these signaling pathways to modulate beating in response to extracellular cues. Yet we are only beginning to identify the axonemal proteins that bind this second messenger and determine their role in regulating dynein-driven microtubule sliding to alter the size and shape of ciliary bends. Here, we review our current understanding of calcium

METHODS IN CELL BIOLOGY, VOL. 92

978-0-12-374974-1
DOI: 10.1016/S0091-679X(08)92011-2

regulation of motility, emphasizing recent advances in the detection and characterization of calcium-binding proteins anchored to the axoneme.

I. Introduction

While the motility of virtually all cilia and flagella is modulated in response to changes in intraflagellar calcium, the response varies greatly between cell types. For example, for the biflagellate green alga *Chlamydomonas reinhardtii*, small increases in calcium (pCa9–pCa7; pCa refers to the negative log of the calcium concentration) induce a shift in flagellar dominance, differentially activating one or the other flagellum and causing the cell to turn toward light (Kamiya and Witman, 1984). A larger increase in calcium (pCa5–pCa4) causes a momentary cessation of motility followed by a complete switch from an asymmetric to a symmetric waveform (Bessen *et al*., 1980). Cilia and flagella in other organisms respond to increases in calcium by changing from a symmetric waveform to an asymmetric waveform (Brokaw, 1979; Brokaw *et al*., 1974), reversing the direction of the effective stroke (Izumi and Miki-Noumura, 1985; Naitoh and Kaneko, 1972), or increasing beat frequency (Verdugo, 1980).

Despite the diversity of responses to changes in calcium concentration, modulation of motility necessarily requires the following general sequence of events. First, the signal triggers an increase in intracellular, and more specifically intraflagellar/intraciliary, calcium. Second, the intraflagellar calcium associates with calcium sensors anchored to precise structures within the axoneme. And finally, binding of calcium to these axonemal proteins ultimately modulates dynein-driven microtubule sliding to produce changes in ciliary and flagellar motility. Significant advances have been made in understanding each of these events for a variety of ciliated/flagellated cell types. In this chapter, we briefly highlight the major advances in each of these areas; however, we focus our discussion on the detection and characterization of axonemal calcium-binding proteins in the model organism *C. reinhardtii.*

II. How Does Calcium Enter Motile Cilia?

While it is possible that calcium entry into motile cilia and flagella occurs through the release of calcium from internal stores (for review of calcium sources in ciliates see Plattner and Klauke, 2001), the most obvious answer to this question is through calcium channels localized to the ciliary or flagellar membrane. Several studies in a variety of organisms have provided evidence for the existence of calcium channels localized to cilia/flagella (see, for example, Adoutte *et al*., 1981; Andrivon, 1988; Beck and Uhl, 1994; Darszon *et al*., 2007; Kung and Eckert, 1972; Kung and Naito, 1973; Navarro *et al*., 2008). More recently, four calcium channels (referred to as CatSper1-4) have been discovered in mammals that are uniquely localized to the sperm flagellar membrane and that are absolutely required for hyperactivation and fertility (Carlson *et al*., 2003, 2005; Qi *et al*., 2007; Ren *et al*., 2001; Xia *et al*., 2007; Xia and Ren,

2009). In addition, a voltage-dependent calcium channel, CAV2, has been discovered in *Chlamydomonas* which is required for flagellar waveform conversion (Fujiu *et al*., 2009). Interestingly, Fuijiu *et al*. report that this channel is primarily localized to the distal part of the flagellum (for further discussion of the significance of this localization see also Quarmby, 2009). It is important to note that the calcium channels so far described for motile cilia and flagella are distinct from the calcium channels associated with immotile, primary cilia [such as polycystin-2 (Chen *et al*., 1999)].

Visualizing and quantifying calcium influx into cilia and flagella, other than by electrophysiological methods, has been challenging. This difficulty has been due in large part to the small volume of this organelle, as well as the fact that they are beating. To accomplish this technical feat would require highly sensitive calcium sensors and high-speed methods for image capture. Tamm and Teraski had early success visualizing calcium in the ctenophore comb plate (Tamm and Terasaki, 1994). More recently, Wood *et al*. have succeeded at quantifying intraflagellar calcium fluxes for reactivated sea urchin sperm (Wood *et al*., 2005), and Shiba *et al*. have recently had success with ascidian sperm (Shiba *et al*., 2008). To date, visualization of calcium flux in beating *Chlamydomonas* flagella using fluorescent calcium indicators has not been possible. It would be fascinating to observe calcium fluxes in the two flagella as cells differentially modulate one flagellum or another to turn toward light.

III. What Ciliary Proteins Serve as Calcium Sensors?

Early work using *in vitro* reactivation assays of demembranated *Chlamydomonas* flagella provided solid evidence that key calcium sensors are anchored to the axoneme (Bessen *et al*., 1980; Gibbons and Gibbons, 1980). These studies illustrate the power of a model organism in which motility can be exquisitely controlled and quantified *in vitro* and consequently for generating testable hypotheses. Based on their *in vitro* functional studies of isolated *Chlamydomonas* flagella, Omoto and Brokaw (1985) observed differential effects of increasing calcium on waveform and beat frequency. They concluded from these studies that regulation in response to calcium is a multicomponent process. Based on these observations combined with additional data from *Chlamydomonas* mutants, Omoto and Brokaw hypothesized that the component of the calcium signaling pathway that regulates beat frequency includes calcium sensors closely associated with the dynein arms, and that the component of the calcium signaling pathway that regulates waveform includes a calcium sensor associated with structures required for modulating waveform, such as the radial spokes and central apparatus. The challenge is to identify the calcium sensors, determine their precise localization relative to specific structures in the axoneme, and establish their unique contributions to changes in motility. In this section we describe the known axonemal calcium-binding proteins and include recent advances in identifying proteins that interact with the ubiquitous calcium sensor, calmodulin.

A. Identifying Calcium Sensors by Molecular and Biochemical Methods

The acquisition of genomic and proteomic information for ciliated cells (Gherman *et al*., 2006; Inglis *et al*., 2006; Li *et al*., 2004; Ostrowski *et al*., 2002; Pazour, 2004; Pazour *et al*., 2005) has allowed for the identification of putative calcium-binding proteins in cilia and flagella. One common feature of most, but not all, calcium-binding proteins is the presence of a structural motif known as an EF-hand, a helix–loop–helix motif that coordinates the binding of calcium ions. Based on analysis of the *Chlamydomonas* flagellar proteome, the axoneme is estimated to be comprised of over 650 different polypeptides, 27 of which have EF-hand motifs (Pazour *et al*., 2005). Of these 27 proteins, four are confirmed calcium-binding proteins, including calmodulin, centrin, ODA-DC3, and LC4 (Fig. 1) (Casey *et al*., 2003a; Gitelman and Witman, 1980; Huang *et al*., 1988; King and Patel-King, 1995; Piperno *et al*., 1992; Salisbury *et al*., 1984; Yang *et al*., 2001).

Both calmodulin and centrin (also named caltractin) were identified as calcium-binding proteins by their shift in electrophoretic mobility in the presence of calcium ions as well as their calcium-dependent binding to phenyl sepharose (Gitelman and

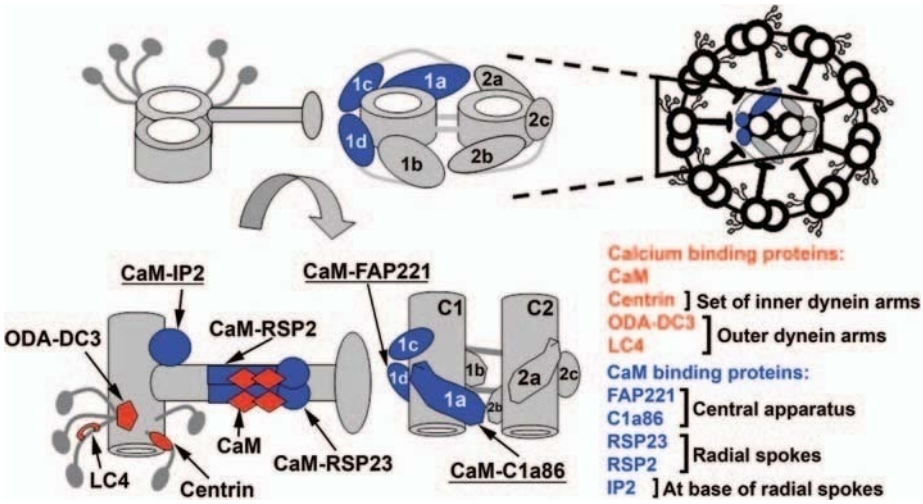

Fig. 1 Transverse section of cilium/flagellum (top right). The central apparatus and a single doublet with associated structures are enlarged and then rotated. Known calcium-binding proteins, including calmodulin (CaM)-associated proteins, are labeled. The underlined proteins (C1a86, IP2, and FAP221) are components of multipolypeptide complexes we recently identified in calmodulin immunoprecipitation experiments (Dymek and Smith, 2007; Wargo *et al*., 2005) and unpublished data by DiPetrillo and Smith). Confirmed calcium-binding proteins are shown in orange and include calmodulin, centrin, ODA-DC3, and LC4 (Casey *et al*., 2003a; Gitelman and Witman, 1980; Huang *et al*., 1988; King and Patel-King, 1995; Piperno *et al*., 1992; Salisbury *et al*., 1984; Yang *et al*., 2001). Confirmed calmodulin-binding proteins are shown in blue and include RSP23 (Patel-King *et al*., 2004), RSP2 (Yang *et al*., 2004), C1a86 (Wargo *et al*., 2005), IP2 (Dymek and Smith, 2007), and FAP221 (unpublished data by DiPetrillo and Smith). (See Plate no. 9 in the Color Plate Section.)

Witman, 1980; Huang *et al*., 1988; Salisbury *et al*., 1984). Initial studies in *Chlamydomonas* revealed that calmodulin was associated with both the flagellar membrane and the axoneme; however, a more precise axonemal localization could not be determined based on simple western blot analysis of flagella isolated from mutants lacking specific structures. Additional biochemical studies have now demonstrated that calmodulin is associated with both the radial spokes and central apparatus (Dymek and Smith, 2007; Wargo *et al*., 2005; Yang *et al*., 2001, 2004). Centrin was originally described as being associated with the basal bodies and contractile striated fibers present in the cytoplasm (Huang *et al*., 1988; Salisbury*et al*., 1984). However, centrin was later identified as a component of a subset of inner dynein arms (Piperno *et al*., 1992). Based on FPLC fractionation of extracted dynein arms, centrin is associated with three different inner arm heavy chains, Dhc5, Dhc8, and Dhc7, which are thought to represent single-headed dynein arms (Yanagisawa and Kamiya, 2001).

The two outer arm-associated proteins, ODA-DC3 and LC4, were confirmed to bind calcium using the radioisotope 45-Ca^{2+} (Casey *et al*., 2003b; King and Patel-King, 1995). The advantage of this assay is that quantitative information about the affinity of the protein for calcium is obtained. For example, King and Patel-King determined that the binding affinity of LC4 is approximately 3×10^{-5} M. As noted above, this affinity would be in the concentration range for triggering changes in waveform and reverse swimming in *Chlamydomonas*. Interestingly, Casey *et al.* using a similar assay discovered that the affinity of ODA-DC3 for calcium is within this same range, approximately 1×10^{-5} M Casey *et al*., 2003b. LC4 is an outer dynein arm associated light chain. Based on their analyses of dynein arm structure in the presence and absence of calcium, Sakato *et al.* have demonstrated that when LC4 binds calcium, the light chain undergoes a conformational change that affects the stem domain of the γ heavy chain (Sakato *et al*., 2007). They propose that this change in interaction may alter mechanochemical interactions between the motor domains of the outer dynein arm and the microtubules (Sakato *et al*., 2007). ODA-DC3 is an outer dynein arm-docking complex protein (Casey *et al*., 2003a). The functional significance of calcium binding to this protein remains unknown (see Casey *et al*., 2003b).

For all four of these confirmed calcium-binding proteins, antibodies have been generated which have proven invaluable in additional biochemical and functional studies (Casey *et al*., 2003a; Huang *et al*., 1988; King and Patel-King, 1995; Sakato *et al*., 2007; Salisbury *et al*., 1988; Wargo *et al*., 2005). Anti-calmodulin antibodies are available from a variety of companies and centrin antibodies are available from Santa Cruz Biotechnology, Inc (Santa Cruz, CA). Yang *et al.* used an anti-Dictyostelium calmodulin antibody that cross-reacts with *Chlamydomonas* calmodulin (Yang *et al*., 2001). However, Wargo *et al*. developed a *Chlamydomonas*-specific antibody generated against a synthetic peptide (Wargo *et al*., 2005). This *Chlamydomonas*-specific calmodulin antibody, unlike most commercially available calmodulin antibodies, recognizes calmodulin by both immunoblot and in immunoprecipitation assays (Dymek *et al*., 2002; Wargo *et al*., 2005). The ability of this antibody to immunoprecipitate calmodulin has allowed the identification of many calmodulin interactors (see Section III.B).

For the additional 23 putative calcium-binding proteins identified in the *Chlamydomonas* flagellar proteome, confirming their calcium-binding properties and determining their function awaits further study. For the four proteins described above, an important advance in understanding their role in motility includes identification of their axonemal-binding partners. As noted, centrin, LC4, and ODA-DC3 are associated with dynein arms. A review of dynein biochemistry can be found in Chapters 3 and 4. Here, we focus our discussion on the identification of calmodulin interacting proteins in the axoneme.

B. Identifying Calmodulin-Binding Proteins

Calmodulin is the most conserved and most studied of all calcium-binding proteins. As a component of cilia and flagella, calmodulin has been actively studied in *Chlamydomonas, Paramecium, Tetrahymena, Elliptio*, and sperm cells from mammals and echinoderms (reviewed in Otter, 1989; Plattner and Klauke, 2001). For flagella isolated from all of these organisms, a pool of calmodulin appears to be associated with the ciliary/flagellar membrane and is solubilized by the addition of detergent; a second pool remains tightly associated with the axoneme. In *Chlamydomonas*, the axonemal pool is divided into at least three different subfractions; axonemal calmodulin is associated with the radial spoke stalk (Patel-King *et al*., 2002, 2004; Yang *et al*., 2001), with a complex localized to the base of the spoke (Dymek and Smith, 2007) and with the C1 tubule of the central apparatus (Wargo *et al*., 2005).

Proteins which interact with calmodulin fall into four general classes: those that bind calmodulin in high calcium, those that bind in low calcium; and for each of these, those that are activated by binding and those that are inactivated by binding (reviewed in Chin and Means, 2000). Although the flagellar axoneme is typically thought of as a nearly crystalline array of highly organized protein structures, when considering calmodulin-binding proteins one must consider the possibility that calmodulin may interact with a different subset of proteins in high- versus low-calcium conditions. Below we describe several methods for identifying calmodulin-interacting proteins. However, it is important to keep in mind the calcium concentration of the buffer for each of these methods.

1. Affinity Purification Using Calmodulin-Coupled Sepharose

One method that has been successfully used to confirm and characterize calmodulin interactions is a calmodulin-binding assay using calmodulin-coupled sepharose beads. This technique was used by Yang *et al*. for the affinity purification of recombinant RSP2 and to demonstrate that calmodulin preferentially binds RSP2 in high calcium (Yang *et al*., 2004). Patel-King *et al*. used a similar method to characterize the calmodulin-binding properties of recombinant RSP23 (p61) (Patel-King *et al*., 2004). RSP23 contains three putative calmodulin-binding domains or IQ motifs. In their experiments using truncated expressed RSP23, Patel-King *et al*. were able to demonstrate that the IQ1 domain exhibits calcium-insensitive calmodulin binding whereas IQ2 and IQ3 exhibit calcium-sensitive calmodulin binding.

2. Calmodulin Gel Overlay Assay

a. Rationale. A second approach to identify calmodulin interactors is a gel overlay assay, or far-western. For this assay, proteins of interest are prepared as for a standard western blot. However, the blot is incubated with calmodulin and then processed for calmodulin detection. One benefit to this approach is that calmodulin interactions can be identified in both high- and low-calcium buffers and in either complex mixtures (such as isolated axonemes) or isolated expressed proteins. In organisms such as *Chlamydomonas* where flagellar mutants are available which lack specific structures, one can also obtain information about the localization of the interacting proteins. One disadvantage of this approach, however, is that proteins denatured for SDS-PAGE may fail to interact with calmodulin. In addition, this approach does not provide information about the identity of the interacting protein, only its approximate molecular weight. It should be noted that gel overlay assays have been used with success to identify specific interactions between axonemal proteins other than calmodulin (Dymek and Smith, 2007; Gaillard *et al*., 2001; Wargo *et al*., 2005).

Regardless of the interaction being tested, one needs a source of purified protein for the overlay. Although purified calmodulin can be purchased commercially, it is more economical to express and purify the protein in the laboratory, given the large amounts required for overlay. For calmodulin gel overlays, our lab cloned the cDNA of *Chlamydomonas* calmodulin into the pET expression vector and expressed the 6xHis-tagged construct in BL21(DE3) pLys *E. coli* cells (Novagen, Madison, WI). The 6xHis-CaM was purified using either Ni-NTA resin (Novagen, Madison, WI) or phenyl sepharose (GE Healthcare, Piscataway, NJ). In our hands the phenyl sepharose column provides a yield of higher purity and concentration.

There are several methods for detecting the overlaid calmodulin. Our lab used a *Chlamydomonas*-specific synthetic peptide to generate polyclonal anti-calmodulin antibodies in rabbits (Wargo *et al*., 2005). However, there are numerous commercially available anti-calmodulin antibodies. It is also possible to express calmodulin with a specific tag that can be detected [such as an S-tag fusion protein (Novagen, Inc)] or to biotinylate-purified calmodulin for detection using streptavidin-HRP (GE Healthcare, Piscataway, NJ). Our lab has used the EZ-Link Sulfo-NHS-LC-Biotinylation Kit (Pierce Biotech., Rockford, IL) according to the manufacturer's instructions for this purpose. For simplicity, the methods below only describe calmodulin detection using antibodies generated against calmodulin.

b. Materials.

- SDS-PAGE gel, running buffer, transfer buffer, and nitrocellulose membrane.
- Block buffer: 5% nonfat dry milk in TBS-T(150 mM NaCl, 20 mM Tris-HCl, pH 7.6, 0.1% Tween-20)
- Wash buffer: TBS-T
- Purified nondenatured calmodulin protein diluted to 10 μg/ml in TBS-T with 1% BSA and either 0.1 mM $CaCl_2$ or 5 mM EGTA
- Anti-calmodulin antibody diluted in TBS-T

- HRP-conjugated secondary antibody diluted in TBS-T (anti-rabbit IgG, GE Healthcare, Piscataway, NJ)
- ECL-Plus kit (GE Healthcare, Piscataway, NJ)

c. Methods.

1. Use the SDS-PAGE conditions appropriate to resolve the proteins of interest on acrylamide gels and transfer the proteins onto nitrocellulose membrane.
   Note: If comparing high- and low-calcium conditions for calmodulin binding, duplicate blots should be prepared. Nitrocellulose is the preferred membrane for this assay (not PVDF). However, nitrocellulose is more fragile than nylon membranes and is not as readily stripped for reprobing.
2. Block with 5% nonfat dry milk in TBS-T overnight at 4°C. All other incubations are performed at room temperature.
3. Briefly wash the membrane twice with TBS-T.
4. Incubate membrane with calmodulin at a concentration of 10 μg/ml in TBS-T and 1% BSA with either 0.1 mM $CaCl_2$ (high calcium condition) or 5 mM EGTA (low calcium) for 2 h at room temperature.
5. Wash with TBS-T three times for 5 min each.
6. Block the membrane again with 5% milk in TBS-T for 1 h.
7. Briefly wash membrane twice with TBS-T.
8. Incubate the membrane with an anti-calmodulin antibody diluted in TBS-T for 1 h.
   Note: Alternatively, use a tag-specific antibody or streptavidin-HRP if the calmodulin protein is tagged or biotinylated.
10. Wash the membrane three times for 5 min each with TBS-T.
11. Incubate the membrane with secondary antibody diluted in TBS-T for 30 min. In our lab we use anti-rabbit-HRP (GE Healthcare, Piscataway, NJ) diluted 1:30,000.
12. Wash the membrane four times for 5 min each with TBS-T.
13. Visualize the overlaid protein. In our lab the ECL Plus Western Blotting kit is used for detection (GE Healthcare, Piscataway, NJ) according to the manufacturer's directions.

Figure 2 shows a representative example of a calmodulin overlay assay. To demonstrate calcium-dependent calmodulin binding, we have loaded equal amounts of bacterially expressed proteins which were known to bind calmodulin. CaM-IP2 (also known as

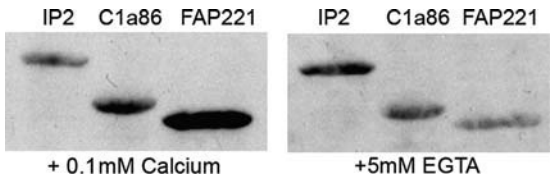

Fig. 2 Calmodulin gel overlay assay. IP2, C1a86, and FAP221 recombinant protein fragments were purified and subjected to calmodulin gel overlay analysis in the presence of either 0.1 mM calcium or 5 mM EGTA. FAP221 preferentially binds to calmodulin in the presence of calcium, while IP2 associates with calmodulin more in the presence of EGTA.

FAP91 and localized to the base of the spokes) exhibits a higher affinity for calmodulin in low calcium conditions compared to high calcium (Dymek and Smith, 2007). FAP221, however, exhibits a very high affinity for calmodulin in high calcium conditions; this protein is tentatively localized to the C1d projection of the C1 central tubule (unpublished results by DiPetrillo and Smith). C1a-86 which is localized to the C1a projection (Wargo *et al*., 2005) has a higher affinity for calmodulin in high calcium buffer, but not as dramatic as FAP221.

3. Calmodulin Immunoprecipitation

a. Rationale. Calmodulin immunoprecipitation has been an invaluable technique for identifying calmodulin-binding proteins, as well as additional members of calmodulin-containing complexes. For example, calmodulin-containing complexes localized to the base of the radial spoke (Dymek and Smith, 2007) and the C1a projection of the central pair of microtubules (Wargo *et al*., 2005) were identified by this approach. The success of this technique is entirely dependent on the quality of the precipitating antibody. As noted above, we generated a *Chlamydomonas*-specific anti-calmodulin antibody against a synthetic peptide (RMMTSGATDDKDKKGHK) (Wargo *et al*., 2005). Peptide synthesis, peptide conjugation to KLH, and polyclonal antibody production in rabbits were performed at Spring Valley Laboratories (Woodbine, MD). The resulting antibody was affinity purified using synthetic peptide conjugated to a Sulfolink column according to the manufacturer's instructions (Pierce Biotech., Rockford, IL). For our antibody, affinity purification is not necessary for western blots, but is absolutely essential for obtaining clean results in immunoprecipitation experiments.

For starting material, cilia or flagella are severed from the cell bodies, demembranated, and extracted using high-salt buffers (for isolating flagella from *Chlamydomonas*, see Witman, 1986). The choice of salt, the concentration of salt, and the time of extraction is determined empirically depending on the source of the flagella and the substructures of interest. (For isolating dyneins, central apparatus proteins, or radial spokes, see the Chapters 3, 12, 11 by King, Mitchell and Yang. respectively, this volume.) In our lab we have used either 0.6 M NaCl or 0.5 M KI to extract proteins from *Chlamydomonas* axonemal microtubules. It is important to note that the use of high concentrations of salt may disrupt interactions between complex members. Therefore, we routinely dialyze extracts into low-salt buffer (30 mM NaCl) to allow for the reconstitution of protein interactions. By manipulating the salt concentration of the extract so that only a subset of interactions reform, we have had some success in determining specific interactions between proteins in larger calmodulin-associated complexes (Wargo *et al*., 2005). It is also possible to partially purify suspected interactors by FPLC or sucrose density gradient centrifugation prior to immunoprecipitation. This step may be important if nonspecific binding is problematic.

One of the biggest advantages to using immunoprecipitation to identify calmodulin interactors is that the members of an entire complex can be identified. We have had terrific success performing mass spectrometry for the precipitated proteins and determining their identity (Dymek and Smith, 2007; Wargo *et al*., 2005). Furthermore, precipitation can be repeated using extracts from mutants missing specific structures to

determine the putative localization of the complex. A second advantage is that in addition to identifying calmodulin interactors, it is possible to use immunoprecipitation to determine if these interactions are calcium sensitive. For example, the precipitation can be performed in high- or low-calcium conditions. In the case of high-calcium conditions, the flagella and extracts should be prepared and maintained in high-calcium buffer (pCa3 or 4) during precipitation. It is possible to determine calcium sensitivity by washing the protein A beads with a different calcium concentration than was present during precipitation. For example, Dymek and Smith performed calmodulin immunoprecipitation in low-calcium buffer to isolate a specific calmodulin-containing complex localized to the base of the radial spokes (Dymek and Smith, 2007). The protein A beads were then washed in high-calcium buffer (see Fig. 3). The complex was released from calmodulin in high calcium; however, the calmodulin remained associated with beads. These results demonstrated that the interaction with calmodulin was calcium sensitive.

b. Materials.

- Axonemal extract at a known concentration prepared as described above
- Affinity purified anti-calmodulin antibody
- Protein-A beads (Invitrogen, Carlsbad, CA)

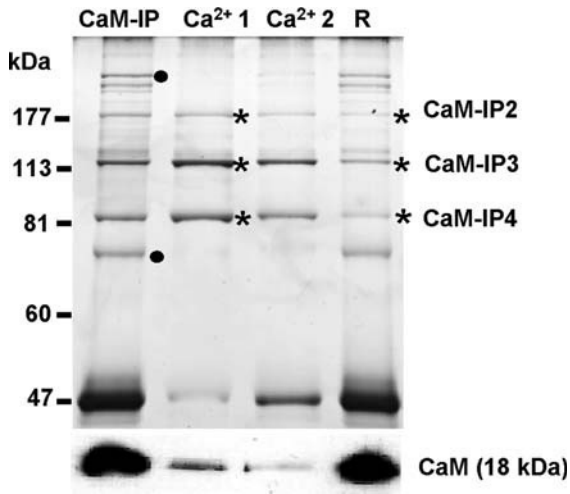

Fig. 3 Silver-stained gel of calmodulin immunoprecipitation from radial spokeless axonemal extracts (*pf14*) followed by treatment with $CaCl_2$ (upper panel). Following precipitation (CaM-IP), the protein A beads were washed twice with 2 mM $CaCl_2$ ($Ca^{2+}1$ and $Ca^{2+}2$) and the resulting extract loaded onto the gel. Proteins remaining (lane R) associated with the beads following the $CaCl_2$ wash were eluted with sample buffer. CaM-IP2, -IP3, and -IP4 (asterisks) are extracted from the beads. In contrast, two additional proteins (dots) are not extracted with $CaCl_2$. Western blots using anti-CaM antibodies (lower panel) reveal that $CaCl_2$ extracts very little CaM from the beads. These results indicate that binding of CaM-IP2, -IP3, and -IP4 to CaM is calcium sensitive. (This figure is Fig. 4A from Dymek and Smith (2007) and reproduced with permission from the *Journal of Cell Biology*, Rockefeller Press.)

- Low-calcium TBS-T (150 mM NaCl, 50 mM Tris-HCl, pH 7.5, 0.5 mM EDTA, 0.1% Tween-20)
- High-calcium TBS-T (150 mM NaCl, 50 mM Tris-HCl, pH 7.5, 1 mM $CaCl_2$, 0.1% Tween-20)

c. Methods.

1. In a 1.5 ml tube, add enough slurry to equal 50 µl of protein-A beads. Wash beads with an equal volume of TBS-T with appropriate calcium concentration. Aspirate off liquid, leaving 50 µl of protein-A beads settled at the bottom of the tube.
2. Add 250–350 µg axonemal extract, 50–70 µg affinity purified anti-calmodulin antibody, and 200 µl TBS-T with the appropriate calcium composition to the tube containing the washed protein-A beads. Note that for many immunoprecipitation protocols, the antibody is conjugated to the protein-A beads. This ensures that the antibody is not eluted with the precipitated proteins. However, we have had much greater success by not conjugating our antibody to the beads.
3. Mix for 2 h at 4°C.
4. Wash samples four times with 1 ml of TBS-T with the appropriate calcium composition for 5 min each.
5. If the samples are to be directly analyzed by SDS-PAGE, we resuspend the sample in 60 µl TBS-T and 30 µl 5X SDS sample buffer to elute the proteins from the beads.

d. Discussion. We have presented several methods for the identification of calcium-binding proteins in the axoneme; and using calmodulin as an example, we have described several methods for determining protein interactors for calcium-binding proteins. Based on the specific advantages and disadvantages of each method, the best approach is to use them in combination. In addition, by taking advantage of available flagellar mutants in the model organism *Chlamydomonas*, these proteins can be partially localized to specific structures in the axoneme. As noted above, there are some 23 additional axonemal proteins that have EF-hand domains and may, therefore, be calcium-binding proteins. To generate a complete map of the calcium signaling pathways, researchers must continue to characterize these proteins by confirming their calcium-binding properties, identifying their interactors, and localizing them within the axoneme.

IV. How Does a Change in Calcium Concentration Modulate Motility?

Once calcium enters the cilium or flagellum and binds to the calcium sensors, observed changes in motility must result from modulation of dynein-driven microtubule sliding. The question is, what is the molecular mechanism by which the calcium sensors alter microtubule sliding to produce the observed changes in waveform and beat frequency? Advances toward answering this question include the use of several *in vitro* motility assays. In this section we briefly review the recent contributions

several of these assays have made on our understanding of calcium regulation of motility, and again we focus our discussion on the model organism *C. reinhardtii*.

The most critical feature for any of the assays we discuss is the amount of free calcium in the buffers. The actual concentration of free calcium ions in a solution may be significantly lower than its total concentration, depending on the ratio of ions to ligands (Goldstein, 1979). Typically, the correct amounts of calcium ($CaCl_2$) and calcium chelators must be combined in order to maintain the desired free calcium concentration. Wakabayashi *et al*. used the methods of Goldstein to calculate the free calcium concentration in buffers used for *Chlamydomonas* reactivation studies (Wakabayashi *et al*., 1997). Knowing the exact free calcium concentrations in these studies was crucial because they were studying the effects of varying calcium concentrations on flagellar waveform. In this case, the amount of $CaCl_2$ compared to EGTA and EDTA was used to determine the concentration of free calcium. See Table I in Wakabayashi *et al*. for the composition of pCa4–pCa8 reactivation buffers (Wakabayashi *et al*., 1997).

A. Inducing and Imaging Phototaxis and Photoshock in *Chlamydomonas*

Chlamydomonas is a photosynthetic organism and must optimize its orientation to light. In order to positively phototax, *Chlamydomonas* preferentially increases beat frequency in one flagellum, causing the cell to turn toward the light (reviewed in Witman, 1993). Photoshock occurs when *Chlamydomonas* is confronted with an intense light source and results in the cell momentarily pausing then swimming in reverse by switching from an asymmetric to a symmetric waveform. Both of these processes are the result of changes in intraflagellar calcium. Small increases in calcium (pCa9–pCa7) induce a shift in flagellar dominance, differentially activating one or the other flagellum and causing the cell to turn toward light (Kamiya and Witman, 1984). A larger increase in calcium (pCa5–pCa4) causes a momentary cessation of motility followed by a complete switch from an asymmetric to a symmetric waveform (Bessen *et al*., 1980).

Both phototaxis and photoshock can be induced and analyzed by video microscopy *in vitro*. The methods for conducting these experiments have been previously described (Horst and Witman, 1993; Moss *et al*., 1995). These assays have also been used to analyze the ability of mutant cells to respond to changes in light (Hirschberg and Stavis, 1977; Horst and Witman, 1993; Matsuda *et al*., 1998; Okita *et al*., 2005; Pazour *et al*., 1995; Ruffer and Nultsch, 1997). In the future, for those calcium-binding proteins in which mutants do not exist, one can imagine knockdown of expression for specific axonemal calcium-binding proteins by RNA interference (see Chapter 5 by Cerutti, volume 93) and testing whether the cells retain the phototaxis or photoshock responses. This experiment would provide evidence for the participation of specific proteins in these calcium-based behaviors.

B. Reactivation Studies Using Cell Models or Isolated Axonemes

To study the direct effect of varying calcium concentrations on parameters, such as beat frequency or waveform, reactivation studies can be performed on permeabilized

cell models or isolated axonemes. In either case, the axoneme is reactivated to beat in the appropriate buffer containing ATP and analyzed by video microscopy. The advantage of this technique is that the concentration of calcium bathing the axoneme is exquisitely controlled. In addition, it can be used for any cell type as long as sufficient quantities of isolated axonemes can be obtained and visualized by video microscopy. Excellent examples of and methods used for applying this technique to wild-type and mutant *Chlamydomonas* cells have been previously described (Brokaw and Kamiya, 1987; Brokaw and Luck, 1985; Brokaw *et al*., 1982; Horst and Witman, 1995; Kamiya and Witman, 1984; Wakabayashi *et al*., 1997) and are also presented in the Chapter 6 by Kamiya, this volume. Analysis of flagellar beat in *Chlamydomonas* is presented in the Chapter 11 by Foster, volume 91. Use of these techniques for isolated sperm flagella have also been previously described, particularly with respect to calcium modulation of motility (Brokaw, 1979, 1987, 1991; Brokaw *et al*., 1974; Brokaw and Nagayama, 1985). The biggest advance in imaging beating cilia and flagella is the development of high-speed digital cameras which can capture images at a sufficiently high frame rate (>500 fps) to provide meaningful digital information (see Yang *et al*., 2008, for example).

C. Microtubule Sliding Assays

The *in vitro* microtubule sliding assay is similar to reactivation of isolated axonemes, with the vital difference being that axonemes are also exposed to a specific protease that cleaves the protein linkages between neighboring microtubules. As a result, when the dynein arms are activated with ATP, the microtubules slide past one another. By recording the sliding events by video microscopy, dynein activity can be quantified as a function of sliding velocity. Importantly, this technique can be used to analyze dynein activity in mutants with paralyzed flagella.

The microtubule sliding assay was first described by Summers and Gibbons to visualize microtubules sliding past one another in trypsin-treated sea urchin sperm axonemes (Summers and Gibbons, 1971). These studies provided the basis for the hypothesis that propagated bending is the result of ATP-induced sliding forces on neighboring microtubules. Forces generated by the dynein arms are resisted in the intact axonemal structure, which results in localized sliding and ultimately flagellar bending. Trypsin-treated sea urchin sperm axonemes were later used to investigate calcium regulation of dynein activity as well as to explore the role of the radial spoke and central apparatus system for regulating microtubule sliding (Bannai *et al*., 2000; Brokaw, 1979, 1987, 1991; Brokaw and Nagayama, 1985; Hayashi and Shingyoji, 2009; Nakano *et al*., 2003; Sale, 1986; Yoshimura and Shingyoji, 1999).

Our lab and others have used this assay for understanding calcium regulation of microtubule sliding in *Chlamydomonas*. We used this technique in key experiments showing that calcium-regulated motility involves modulation of dynein-driven microtubule sliding, that calmodulin mediates this calcium signal, and that the central apparatus and radial spokes are important components of the calcium signaling pathway (Smith, 2002). Wakabayashi *et al*. have also used this technique to understand the

role of the central apparatus and radial spokes in calcium-dependent waveform conversion (Wakabayashi *et al*., 1997). In combination with mutants and electron microscopic analysis of slid axonemes, we determined that calcium affects the patterns of microtubule sliding (Wargo *et al*., 2004). More recently we have used the sliding assay in combination with the antibodies we generated against components of a calmodulin-associated complex to asses the contribution of this complex to dynein-driven microtubule sliding (Dymek and Smith, 2007). As evidenced, the microtubule sliding assay is extremely robust and can provide very direct evidence for the involvement of particular axonemal components in regulating dynein-driven microtubule sliding. For additional information and details of methods, see also the Chapters 6, 7, 8 by Kamiya, Shingyoji, and Sale, this volume.

V. Summary

Significant advances have been made in identifying calcium channels in the ciliary/flagellar membrane as well as in imaging free calcium concentration within this specialized organelle. The identification of the calcium sensors as well as their binding partners has greatly benefited from the availability of genomic and proteomic information. As Omoto and Brokaw predicted nearly 25 years ago from key observation of flagella reactivated to beat *in vitro*, a subset of the sensors is associated with the dynein arms and additional sensors are localized to the radial spokes and central apparatus, structures known to modulate waveform. Despite these advances we are still only beginning to understand how calcium modulates ciliary and flagellar motility. In addition, multiple studies have indicated that the calcium signaling pathway most likely impacts upon the network of kinases and phosphatases associated with the axoneme (for example, Ignotz and Suarez, 2005; Marquez *et al*., 2007; Salathe, 2007; Salathe and Bookman, 1999; Salathe *et al*., 1993; Segal and Luck, 1985; Smith, 2002; Suarez, 2008; see also Chapter 8 by Sale, this volume) Through continued identification of the calcium sensors and their interactors, combined with biochemical, structural, and functional experimental approaches, the data we obtain will ultimately reveal how this complex signaling network is modulated by calcium.

References

Adoutte, A., Ling, K.Y., Forte, M., Ramanathan, R., Nelson, D., and Kung, C. (1981). Ionic channels of Paramecium: From genetics and electrophysiology to biochemistry. *J. Physiol. (Paris)* **77**, 1145–1159.

Andrivon, C. (1988). Membrane control of ciliary movement in ciliates. *Biol. Cell* **63**, 133–142.

Bannai, H., Yoshimura, M., Takahashi, K., and Shingyoji, C. (2000). Calcium regulation of microtubule sliding in reactivated sea urchin sperm flagella. *J. Cell Sci.* **113**(Pt. 5), 831–839.

Beck, C., and Uhl, R. (1994). On the localization of voltage-sensitive calcium channels in the flagella of Chlamydomonas reinhardtii. *J. Cell Biol.* **125**, 1119–1125.

Bessen, M., Fay, R.B., and Witman, G.B. (1980). Calcium control of waveform in isolated flagellar axonemes of Chlamydomonas. *J. Cell Biol.* **86**, 446–455.

Brokaw, C.J. (1979). Calcium-induced asymmetrical beating of triton-demembranated sea urchin sperm flagella. *J. Cell Biol.* **82**, 401–411.

Brokaw, C.J. (1987). Regulation of sperm flagellar motility by calcium and cAMP-dependent phosphorylation. *J. Cell Biochem.* **35**, 175–184.

Brokaw, C.J. (1991). Calcium sensors in sea urchin sperm flagella. *Cell Motil. Cytoskeleton* **18**, 123–130.

Brokaw, C.J., Josslin, R., and Bobrow, L. (1974). Calcium ion regulation of flagellar beat symmetry in reactivated sea urchin spermatozoa. *Biochem. Biophys. Res. Commun.* **58**, 795–800.

Brokaw, C.J., and Kamiya, R. (1987). Bending patterns of Chlamydomonas flagella: IV. Mutants with defects in inner and outer dynein arms indicate differences in dynein arm function. *Cell Motil. Cytoskeleton* **8**, 68–75.

Brokaw, C.J., and Luck, D.J. (1985). Bending patterns of chlamydomonas flagella: III. A radial spoke head deficient mutant and a central pair deficient mutant. *Cell Motil.* **5**, 195–208.

Brokaw, C.J., Luck, D.J., and Huang, B. (1982). Analysis of the movement of Chlamydomonas flagella: The function of the radial-spoke system is revealed by comparison of wild-type and mutant flagella. *J. Cell Biol.* **92**, 722–732.

Brokaw, C.J., and Nagayama, S.M. (1985). Modulation of the asymmetry of sea urchin sperm flagellar bending by calmodulin. *J. Cell Biol.* **100**, 1875–1883.

Carlson, A.E., Quill, T.A., Westenbroek, R.E., Schuh, S.M., Hille, B., and Babcock, D.F. (2005). Identical phenotypes of CatSper1 and CatSper2 null sperm. *J. Biol. Chem.* **280**, 32238–32244.

Carlson, A.E., Westenbroek, R.E., Quill, T., Ren, D., Clapham, D.E., Hille, B., Garbers, D.L., and Babcock, D.F. (2003). CatSper1 required for evoked Ca2+ entry and control of flagellar function in sperm. *Proc. Natl. Acad. Sci. USA* **100**, 14864–14868.

Casey, D.M., Inaba, K., Pazour, G.J., Takada, S., Wakabayashi, K., Wilkerson, C.G., Kamiya, R., and Witman, G.B. (2003a). DC3, the 21-kDa subunit of the outer dynein arm-docking complex (ODA-DC), is a novel EF-hand protein important for assembly of both the outer arm and the ODA-DC. *Mol. Biol. Cell* **14**, 3650–3663.

Casey, D.M., Yagi, T., Kamiya, R., and Witman, G.B. (2003b). DC3, the smallest subunit of the Chlamydomonas flagellar outer dynein arm-docking complex, is a redox-sensitive calcium-binding protein. *J. Biol. Chem* **278**, 42652–42659.

Chen, X.Z., Vassilev, P.M., Basora, N., Peng, J.B., Nomura, H., Segal, Y., Brown, E.M., Reeders, S.T., Hediger, M.A., and Zhou, J. (1999). Polycystin-L is a calcium-regulated cation channel permeable to calcium ions. *Nature* **401**, 383–386.

Chin, D., and Means, A.R. (2000). Calmodulin: A prototypical calcium sensor. *Trends Cell Biol.* **10**, 322–328.

Darszon, A., Trevino, C.L., Wood, C., Galindo, B., Rodriguez-Miranda, E., Acevedo, J.J., Hernandez-Gonzalez, E.O., Beltran, C., Martinez-Lopez, P., and Nishigaki, T. (2007). Ion channels in sperm motility and capacitation. *Soc. Reprod. Fertil. Suppl.* **65**, 229–244.

Dymek, E., Wargo, M., and Smith, E.F. (2002). Characterization of calmodulin and calmodulin binding proteins associated with the flagellar central apparatus. *Mol. Biol. Cell* **13**, 328a.

Dymek, E.E., and Smith, E.F. (2007). A conserved calmodulin and radial spoke associated complex mediates regulation of flagellar dynein activity. *J. Cell Biol.* **179**, 515–526.

Fujiu, K., Nakayama, Y., Yanagisawa, A., Sokabe, M., and Yoshimura, K. (2009). Chlamydomonas CAV2 encodes a voltage-dependent calcium channel required for the flagellar waveform conversion. *Curr. Biol.* **19**, 133–139.

Gaillard, A.R., Diener, D.R., Rosenbaum, J.L., and Sale, W.S. (2001). Flagellar radial spoke protein 3 is an A-kinase anchoring protein (AKAP). *J. Cell Biol.* **153**, 443–448.

Gherman, A., Davis, E.E., and Katsanis, N. (2006). The ciliary proteome database: An integrated community resource for the genetic and functional dissection of cilia. *Nat. Genet.* **38**, 961–962.

Gibbons, B.H., and Gibbons, I.R. (1980). Calcium-induced quiescence in reactivated sea urchin sperm. *J. Cell Biol.* **84**, 13–27.

Gitelman, S.E., and Witman, G.B. (1980). Purification of calmodulin from Chlamydomonas: Calmodulin occurs in cell bodies and flagella. *J. Cell Biol.* **87**, 764–770.

Goldstein, D.A. (1979). Calculation of the concentrations of free cations and cation-ligand complexes in solutions containing multiple divalent cations and ligands. *Biophys. J.* **26**, 235–242.

Hayashi, S., and Shingyoji, C. (2009). Bending-induced switching of dynein activity in elastase-treated axonemes of sea urchin sperm–roles of Ca2+ and ADP. *Cell Motil. Cytoskeleton* **66**, 292–301.

Hirschberg, R., and Stavis, R. (1977). Phototaxis mutants of Chlamydomonas reinhardtii. *J. Bacteriol.* **129**, 803–808.

Horst, C.J., and Witman, G.B. (1993). ptx1, a nonphototactic mutant of Chlamydomonas, lacks control of flagellar dominance. *J. Cell Biol.* **120**, 733–741.

Horst, C.J., and Witman, G.B. (1995). Reactivation of Chlamydomonas cell models. *Methods Cell. Biol.* **47**, 207–210.

Huang, B., Watterson, D.M., Lee, V.D., and Schibler, M.J. (1988). Purification and characterization of a basal body-associated Ca2+-binding protein. *J. Cell Biol.* **107**, 121–131.

Ignotz, G.G., and Suarez, S.S. (2005). Calcium/calmodulin and calmodulin kinase II stimulate hyperactivation in demembranated bovine sperm. *Biol. Reprod.* **73**, 519–526.

Inglis, P.N., Boroevich, K.A., and Leroux, M.R. (2006). Piecing together a ciliome. *Trends Genet.* **22**, 491–500.

Izumi, A., and Miki-Noumura, T. (1985). Tetrahymena cell model exhibiting Ca-dependant behavior. *Cell Motil.* **5**, 323–331.

Kamiya, R., and Witman, G.B. (1984). Submicromolar levels of calcium control the balance of beating between the two flagella in demembranated models of Chlamydomonas. *J. Cell Biol.* **98**, 97–107.

King, S.M., and Patel-King, R.S. (1995). Identification of a Ca(2+)-binding light chain within Chlamydomonas outer arm dynein. *J. Cell Sci.* **108**(Pt. 12), 3757–3764.

Kung, C., and Eckert, R. (1972). Genetic modification of electric properties in an excitable membrane (paramecium-calcium conductance-electrophysiological measurements-membrane mutant). *Proc. Natl. Acad. Sci. USA* **69**, 93–97.

Kung, C., and Naito, Y. (1973). Calcium-induced ciliary reversal in the extracted models of "Pawn", a behavioral mutant of Paramecium. *Science* **179**, 195–196.

Li, J.B., Gerdes, J.M., Haycraft, C.J., Fan, Y., Teslovich, T.M., May-Simera, H., Li, H., Blacque, O.E., Li, L., Leitch, C.C., Lewis, R.A., Green, J.S. et al. (2004). Comparative genomics identifies a flagellar and basal body proteome that includes the BBS5 human disease gene. *Cell* **117**, 541–552.

Marquez, B., Ignotz, G., and Suarez, S.S. (2007). Contributions of extracellular and intracellular Ca2+ to regulation of sperm motility: Release of intracellular stores can hyperactivate CatSper1 and CatSper2 null sperm. *Dev. Biol.* **303**, 214–221.

Matsuda, A., Yoshimura, K., Sineshchekov, O.A., Hirono, M., and Kamiya, R. (1998). Isolation and characterization of novel Chlamydomonas mutants that display phototaxis but not photophobic response. *Cell Motil. Cytoskeleton* **41**, 353–362.

Moss, A.G., Pazour, G.J., and Witman, G.B. (1995). Assay of Chlamydomonas phototaxis. *Methods Cell Biol.* 47, 281–287.

Naitoh, Y., and Kaneko, H. (1972). Reactivated triton extracted models of Paramecium: Modification of ciliary movement by calcium ions. *Science* **176**, 523–524.

Nakano, I., Kobayashi, T., Yoshimura, M., and Shingyoji, C. (2003). Central-pair-linked regulation of microtubule sliding by calcium in flagellar axonemes. *J. Cell Sci.* **116**, 1627–1636.

Navarro, B., Kirichok, Y., Chung, J.J., and Clapham, D.E. (2008). Ion channels that control fertility in mammalian spermatozoa. *Int. J. Dev. Biol.* **52**, 607–613.

Okita, N., Isogai, N., Hirono, M., Kamiya, R., and Yoshimura, K. (2005). Phototactic activity in Chlamydomonas 'non-phototactic' mutants deficient in Ca2+-dependent control of flagellar dominance or in inner-arm dynein. *J. Cell Sci.* **118**, 529–537.

Omoto, C.K., and Brokaw, C.J. (1985). Bending patterns of Chlamydomonas flagella: II. Calcium effects on reactivated Chlamydomonas flagella. *Cell Motil.* **5**, 53–60.

Ostrowski, L.E., Blackburn, K., Radde, K.M., Moyer, M.B., Schlatzer, D.M., Moseley, A., and Boucher, R.C. (2002). A proteomic analysis of human cilia: Identification of novel components. *Mol. Cell Proteomics* **1**, 451–465.

Otter, T. (1989). Calmodulin and the control of flagellar movement. *In* "Cell Movement." Vol. 1, pp. 281–298. Alan R. Liss, New York.

Patel-King, R.S., Benashski, S.E., and King, S.M. (2002). A Bipartite Ca2+-regulated Nucleoside-diphosphate Kinase System within the Chlamydomonas Flagellum. THE REGULATORY SUBUNIT p72. *J. Biol. Chem.* **277**, 34271–34279.

Patel-King, R.S., Gorbatyuk, O., Takebe, S., and King, S.M. (2004). Flagellar radial spokes contain a Ca2+-stimulated nucleoside diphosphate kinase. *Mol. Biol. Cell* **15**, 3891–3902.

Pazour, G.J. (2004). Comparative genomics: Prediction of the ciliary and basal body proteome. *Curr. Biol.* **14**, R575–R577.

Pazour, G.J., Agrin, N., Leszyk, J., and Witman, G.B. (2005). Proteomic analysis of a eukaryotic cilium. *J. Cell Biol.* **170**, 103–113.

Pazour, G.J., Sineshchekov, O.A., and Witman, G.B. (1995). Mutational analysis of the phototransduction pathway of Chlamydomonas reinhardtii. *J. Cell Biol.* **131**, 427–440.

Piperno, G., Mead, K., and Shestak, W. (1992). The inner dynein arms I2 interact with a "dynein regulatory complex" in Chlamydomonas flagella. *J. Cell Biol.* **118**, 1455–1463.

Plattner, H., and Klauke, N. (2001). Calcium in ciliated protozoa: Sources, regulation, and calcium-regulated cell functions. *Int. Rev. Cytol.* **201**, 115–208.

Qi, H., Moran, M.M., Navarro, B., Chong, J.A., Krapivinsky, G., Krapivinsky, L., Kirichok, Y., Ramsey, I.S., Quill, T.A., and Clapham, D.E. (2007). All four CatSper ion channel proteins are required for male fertility and sperm cell hyperactivated motility. *Proc. Natl. Acad. Sci. USA* **104**, 1219–1223.

Quarmby, L. (2009). Ciliary ion channels: Location, location, location. *Curr. Biol.* **19**, R158–R160.

Ren, D., Navarro, B., Perez, G., Jackson, A.C., Hsu, S., Shi, Q., Tilly, J.L., and Clapham, D.E. (2001). A sperm ion channel required for sperm motility and male fertility. *Nature* **413**, 603–609.

Ruffer, U., and Nultsch, W. (1997). Flagellar photoresponses of ptx1, a nonphototactic mutant of Chlamydomonas. *Cell Motil. Cytoskeleton* **37**, 111–119.

Sakato, M., Sakakibara, H., and King, S.M. (2007). Chlamydomonas outer arm dynein alters conformation in response to Ca2+. *Mol. Biol. Cell* **18**, 3620–3634.

Salathe, M. (2007). Regulation of mammalian ciliary beating. *Annu. Rev. Physiol.* **69**, 401–422.

Salathe, M., and Bookman, R.J. (1999). Mode of Ca2+ action on ciliary beat frequency in single ovine airway epithelial cells. *J. Physiol.* **520**(Pt. 3), 851–865.

Salathe, M., Pratt, M.M., and Wanner, A. (1993). Protein kinase C-dependent phosphorylation of a ciliary membrane protein and inhibition of ciliary beating. *J. Cell Sci.* **106**(Pt. 4), 1211–1220.

Sale, W.S. (1986). The axonemal axis and Ca2+-induced asymmetry of active microtubule sliding in sea urchin sperm tails. *J. Cell Biol.* **102**, 2042–2052.

Salisbury, J.L., Baron, A., Surek, B., and Melkonian, M. (1984). Striated flagellar roots: Isolation and partial characterization of a calcium-modulated contractile organelle. *J. Cell Biol.* **99**, 962–970.

Salisbury, J.L., Baron, A.T., and Sanders, M.A. (1988). The centrin-based cytoskeleton of Chlamydomonas reinhardtii: Distribution in interphase and mitotic cells. *J. Cell Biol.* **107**, 635–641.

Segal, R.A., and Luck, D.J. (1985). Phosphorylation in isolated Chlamydomonas axonemes: A phosphoprotein may mediate the Ca2+-dependent photophobic response. *J. Cell Biol.* **101**, 1702–1712.

Shiba, K., Baba, S.A., Inoue, T., and Yoshida, M. (2008). Ca2+ bursts occur around a local minimal concentration of attractant and trigger sperm chemotactic response. *Proc. Natl. Acad. Sci. USA* **105**, 19312–19317.

Smith, E.F. (2002). Regulation of flagellar dynein by calcium and a role for an axonemal calmodulin and calmodulin-dependent kinase. *Mol. Biol. Cell* **13**, 3303–3313.

Suarez, S.S. (2008). Control of hyperactivation in sperm. *Hum. Reprod. Update* **14**, 647–657.

Summers, K.E., and Gibbons, I.R. (1971). Adenosine triphosphate-induced sliding of tubules in trypsin-treated flagella of sea-urchin sperm. *Proc. Natl. Acad. Sci. USA* **68**, 3092–3096.

Tamm, S.L., and Terasaki, M. (1994). Visualization of calcium transients controlling orientation of ciliary beat. *J. Cell Biol.* **125**, 1127–1135.

Verdugo, P. (1980). Ca2+-dependent hormonal stimulation of ciliary activity. *Nature* **283**, 764–765.

Wakabayashi, K., Yagi, T., and Kamiya, R. (1997). Ca2+-dependent waveform conversion in the flagellar axoneme of Chlamydomonas mutants lacking the central-pair/radial spoke system. *Cell Motil. Cytoskeleton* **38**, 22–28.

Wargo, M.J., Dymek, E.E., and Smith, E.F. (2005). Calmodulin and PF6 are components of a complex that localizes to the C1 microtubule of the flagellar central apparatus. *J. Cell Sci.* **118**, 4655–4665.

Wargo, M.J., McPeek, M.A., and Smith, E.F. (2004). Analysis of microtubule sliding patterns in Chlamydomonas flagellar axonemes reveals dynein activity on specific doublet microtubules. *J. Cell Sci.* **117**, 2533–2544.

Witman, G.B. (1986). Isolation of Chlamydomonas flagella and flagellar axonemes. *Methods Enzymol.* **134**, 280–290.

Witman, G.B. (1993). Chlamydomonas phototaxis. *Trends Cell Biol.* **3**, 403–408.

Wood, C.D., Nishigaki, T., Furuta, T., Baba, S.A., and Darszon, A. (2005). Real-time analysis of the role of Ca(2+) in flagellar movement and motility in single sea urchin sperm. *J. Cell Biol.* **169**, 725–731.

Xia, J., Reigada, D., Mitchell, C.H., and Ren, D. (2007). CATSPER channel-mediated Ca2+ entry into mouse sperm triggers a tail-to-head propagation. *Biol. Reprod.* **77**, 551–559.

Xia, J., and Ren, D. (2009). Egg coat proteins activate calcium entry into mouse sperm via CATSPER channels. *Biol. Reprod.* **80**, 1092–1098.

Yanagisawa, H.A., and Kamiya, R. (2001). Association between actin and light chains in Chlamydomonas flagellar inner-arm dyneins. *Biochem. Biophys. Res. Commun.* **288**, 443–437.

Yang, C., Owen, H.A., and Yang, P. (2008). Dimeric heat shock protein 40 binds radial spokes for generating coupled power strokes and recovery strokes of 9 + 2 flagella. *J. Cell Biol.* **180**, 403–415.

Yang, P., Diener, D.R., Rosenbaum, J.L., and Sale, W.S. (2001). Localization of calmodulin and dynein light chain LC8 in flagellar radial spokes. *J. Cell Biol.* **153**, 1315–1326.

Yang, P., Yang, C., and Sale, W.S. (2004). Flagellar radial spoke protein 2 is a calmodulin binding protein required for motility in Chlamydomonas reinhardtii. *Eukaryot. Cell* **3**, 72–81.

Yoshimura, M., and Shingyoji, C. (1999). Effects of the central pair apparatus on microtubule sliding velocity in sea urchin sperm flagella. *Cell Struct. Funct.* **24**, 43–54.

CHAPTER 12

Isolation and Analysis of Radial Spoke Proteins

Pooja Kelekar, Mei Wei, *and* Pinfen Yang
Department of Biological Sciences, Marquette University, Milwaukee, Wisconsin

Abstract

The 9 + 2 axoneme that mediates the highly controlled oscillatory beating of cilia and flagella is an elaborate supramolecular complex. Proteomics and genomics have revealed more than 400 distinct polypeptides that presumably are built into axonemal subcomplexes for specific tasks. However, only a handful of proteins can be assigned to the most prominent structural modules visible by electron microscopy. Much less is known about the function and mechanism of individual molecules and complexes. Isolation of intact complexes will hasten discoveries and open the door to a wide range of analyses as showcased by axonemal dynein motors. However, many axonemal components, such as the radial spoke complex, either are not extracted by conditions that solubilize axonemal dynein or at best are only partially released. This chapter

METHODS IN CELL BIOLOGY, VOL. 92

978-0-12-374974-1
DOI: 10.1016/S0091-679X(08)92012-4

discusses strategies and methods to circumvent this problem in order to characterize radial spokes. With appropriate modifications, the lessons learned from the radial spoke complex may be applicable to other axonemal complexes.

I. Introduction

The radial spoke (RS), which is central for the control of axonemal dyneins, is located at a key position in the $9+2$ axoneme. Its thin stalk is anchored to the outer doublet microtubules near the dynein motors and dynein regulatory complex (DRC), while its bulbous head projects toward the mobile central pair apparatus (CP). During oscillatory beating, the spokehead transiently engages the CP. It is postulated that through transient engagements during oscillatory beating, the RS transduces a mechanical feedback of unknown nature between the CP and the motors on the outer doublets (Smith and Yang, 2004). This feedback is thought to coordinate the dynein motors around the circumference and along the length of the axoneme. Consequently, defects in the spokehead and thus the RS/CP contact cause paralysis or aberrant motility. In addition, the RS is critical for motility changes regulated by second messengers and phosphoenzymes. The challenge is to substantiate this model by defining the molecular mechanisms involved.

In general, many methods developed for axonemal dyneins are applicable to the RS. However, unlike dynein arms, but similar to the DRC, MBO (*m*ove *b*ackward *o*nly) complex and part of the CP, the RS cannot be effectively extracted by 0.6 M NaCl. To isolate the RS, a buffer of higher ionic strength or a different extraction strategy is necessary. Furthermore, unlike the heavy chains that constitute a major portion of the dynein motors and exhibit an enzymatic activity (ATPase) that is indicative of the functional mechanism, none of the 19 subunits in the RS is singularly prominent or revealing of function. Thus, there is no clear indication of the molecular mechanism underpinning the mechanical and chemical transduction that occurs between the RS and CP.

The biochemical constraints are partially mitigated by motility mutants defective in the RS complex and the unusual isoelectric points (pI) of most radial spoke proteins (RSPs). Compared to wild-type (WT) axonemes, 17 polypeptides are absent in the two-dimensional (2D) map of *pf*14 axonemes that lack the RS. Hence these proteins are termed RSP1-17 (Huang *et al.*, 1981; Piperno *et al.*, 1981). Unlike the majority of the $>$400 proteins that comprise the axoneme, the pIs of 12 RSPs are similar to or lower than those of tubulins and can be unequivocally identified in 2D gels. Among these, five are absent in *pf*1 and *pf*17 axonemes in which the spokehead appears less conspicuous (Piperno *et al*., 1977; Huang *et al.*, 1981). Furthermore, these five proteins also dissociate from the rest of the RS after prolonged dialysis against low-salt buffer. Therefore, these five proteins are denoted as constituents of the head domain. Taking advantage of the behavior of RSPs in 2D gels, several acidic RSPs have been purified and used to raise specific antibodies (Williams *et al*., 1986, 1989). These antibodies proved to be powerful tools for addressing several critical questions in flagellar biology. These findings and reagents paved the way to devise additional procedures as discussed below.

II. Isolation of Intact RS Complexes

A. Background

The original indication that RSs could be extracted by salt came from studies of dynein motors. To identify the subunits of the 20S dynein motors, double mutant *pf*28*pf*30 cells that lack 20S motors were compared to wild-type cells. Even though the dyneins were not present in *pf*28*pf*30 cells, a pattern of faint bands routinely emerged in silver-stained gels of the 20S fractions. These bands shared similar molecular masses with the large RSPs and were found to be a small fraction of RSPs released from axonemes by 0.6 M NaCl. Test extractions with other salts showed that the RSPs became largely soluble following 0.6 M KI extraction and could be partially released by 0.6 M NaBr (Yang *et al*., 2001). The differential effectiveness of these three salts in extracting the RS corresponds to their position in the Hofmeister series and suggests that salt disrupts the ionic interactions within the axoneme and that use of various salts is likely to provide a powerful approach to the disintegration of the axoneme into discrete subcomplexes.

In fact, it was originally demonstrated that KI and other chaotropic compounds are very effective at disassembling the outer doublets of sea urchin axonemes into subunits and a particularly stable filament located between the A and B outer doublets (Linck, 1976). Fortuitously, despite the drastic extraction conditions, the *Chlamydomonas* RS remains intact in 0.6 M KI buffer. Following dialysis to reduce the salt concentration, the RS migrates as a 20S particle during velocity sedimentation through a 5–20% sucrose gradient. The sedimentation of the RS as a large particle is advantageous for purification as the majority of solubilized axonemal components are much smaller. NaBr treatment achieves similar results; although the extraction is somewhat less effective, use of NaBr results in less precipitation following dialysis.

Silver-stained protein gels show that despite preextraction with 0.6 M NaCl, a significant amount of the 20S dyneins remain in the NaBr extract of *pf*14 axonemes (Fig. 1, right panel). Therefore, if the 20S dynein motors interfere with analysis, the extract should be prepared from double mutant *pf*28*pf*30 cells lacking both outer arm and inner arm I1/f dynein species (Fig. 1, left panel). The proteins in the 20S fractions of *pf*28*pf*30 are RSPs, as evidenced by the fact that they are largely absent in *pf*14. This approach illustrates the power of sequential extraction in combination with the use of mutant axonemes to produce relatively pure RSs.

The isolated intact complex has been used for electron microscopy, reconstitution (Yang *et al*., 2001), production of antibodies against the entire complex (Yang *et al*., 2005), and enzymatic assays (Patel-King *et al*., 2004; Yang *et al*., 2004). This procedure also led to the discovery of a RS-associated complex (Dymek and Smith, 2007).

As revealed by negative-stain electron microscopy, RS particles in the 20S fraction appear polymorphic, ranging from monomers to oligomers in which the spokeheads face the periphery. The larger aggregates may explain why the RS complex sediments at 20S even though the molecular mass of the RS complex is significantly smaller than 20S multiheaded dynein arms.

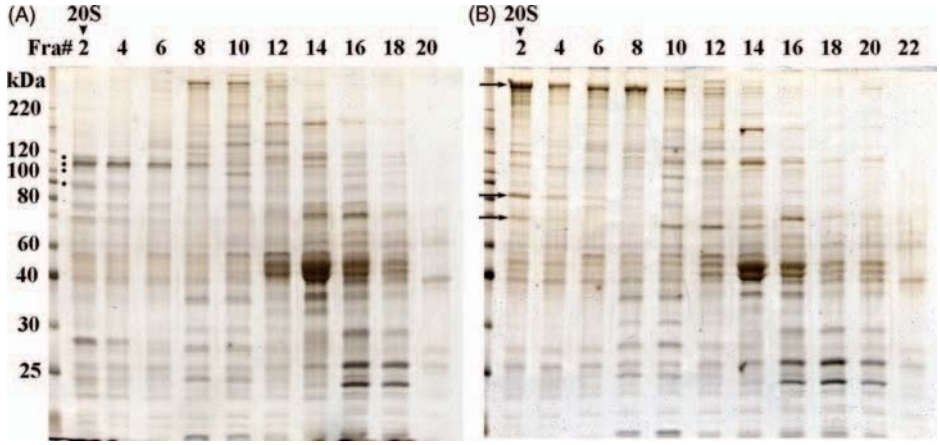

Fig. 1 Sucrose gradient profiles of axonemal extracts from *pf*28*pf*30, a mutant that lacks the 20S outer dynein arm and inner dynein arm I1/f (A), and from *pf*14 that lacks radial spokes (B). The axonemes were first extracted with 0.6 M NaCl and then with 0.6 M NaBr. The NaBr extract, after dialysis against buffer A, was sedimented through a 5–20% sucrose gradient. The fractions were separated in 9% acrylamide gels and proteins revealed by ammoniacal silver staining. The protein bands corresponding to RSP1, RSP2, RSP23, and RSP3 (dots) in the 20S fractions were only present in (A). In contrast, residual dynein subunits, such as heavy chains, IC1(IC78), and IC2(IC69) (arrows) were present in (B) but absent in (A). (See Plate no. 10 in the Color Plate Section.)

B. Materials and Methods

Axonemes (prepared as described in Chapter 3 by King, this volume)
Buffer A—10 mM HEPES, 5 mM $MgSO_4$, 1 mM dithiothreitol, 0.5 mM EDTA, 30 mM NaCl, 0.1 mM PMSF, 0.5 TIU/ml aprotinin, pH 7.4
Extraction buffer—0.6 M KI or NaBr in Buffer A
5 and 25% Sucrose in Buffer A

1. Pellet axonemes at 12,000 × g centrifugation for 10 min.
2. Resuspend the pellet in extraction buffer at a protein concentration of 5–10 mg/ml and incubate for 20–30 min at room temperature. This step can be carried out on ice but the extraction appears to be slightly less efficient.
3. Centrifuge the mixture as in step 1, or if the volume is appropriate, 13,000 × g for 5 min in a microfuge. The RS will be in the supernatant while the pellet will be significantly smaller than before and appear more translucent.
4. Dialyze the supernatant against 200 ml buffer A for 30 min on ice. Prolonged dialysis is unnecessary.
5. During dialysis, prepare 11-ml 5–25% continuous sucrose gradients in 12-ml ultracentrifuge tubes on ice with a gradient maker.
6. Centrifuge the extract as in step 3.
7. Carefully layer up to 0.7 ml supernatant on top of each sucrose gradient.

8. Centrifuge balanced pairs of tubes containing the gradients at 222,000 × g in an ultracentrifuge at 4°C overnight for 12–16 h (see later). This corresponds to 36,000 rpm using a Beckman SW41 Ti rotor.
9. Fractionate each gradient into ~20 fractions with a peristaltic pump.

C. Variations and Tips

Methods for the isolation of axonemal complexes can be modified significantly to yield optimal results. The main parameters that are typically altered are the centrifugation conditions and the use of alternative salts and different salt concentrations.

1. Centrifugation Conditions

Numerous variations of sucrose gradients have been developed for specific applications. The most common parameters that are altered to maximize the desired separation range are the concentrations of sucrose and the duration of sedimentation (e.g., Mitchell and Sale, 1999). It is important to point out that during velocity sedimentation through a sucrose gradient the sedimentation does not reach equilibrium. The concentration of the gradient, the duration of centrifugation, and the size and shape of the particles will influence where the particles sediment. Large particles can exit the gradient and pellet at the bottom of the tube if the sample is centrifuged long enough. As shown in Figs. 1 and 2A, after 16-h centrifugation,

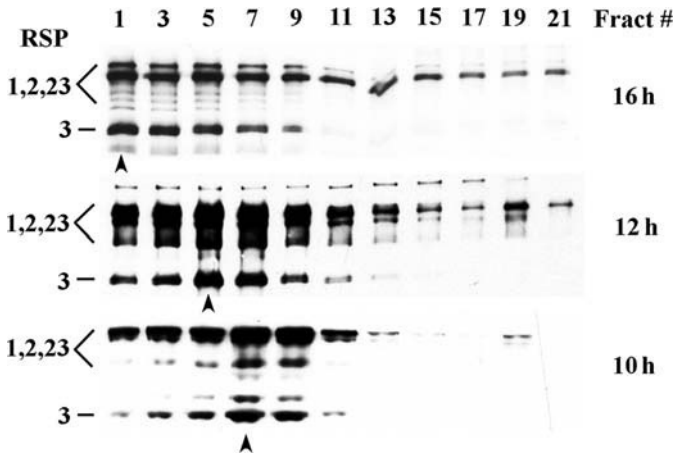

Fig. 2 The duration of centrifugation significantly influences the sedimentation profile of the RS particles. Western blots of sucrose gradient fractions of KI extracts from wild-type (cc124) axonemes following centrifugation for 16 h (A), 12 h (B), or 10 h (C) were probed with the antibody raised against the isolated RS complex. The RS peak (arrowhead) sedimented deeper into the gradient after longer centrifugation. Note that this polyclonal antibody recognized multiple large RSPs including RSP1, RSP2, and RSP23 that migrated at similar positions in SDS-PAGE. RSP23, a phosphoprotein, in particular, was resolved into multiple bands, some of which overlap with RSP1 and RSP2 bands (see western blots of 2D electrophoresis in Fig. 4B). The band patterns often varied, likely due to differences in phosphorylation levels.

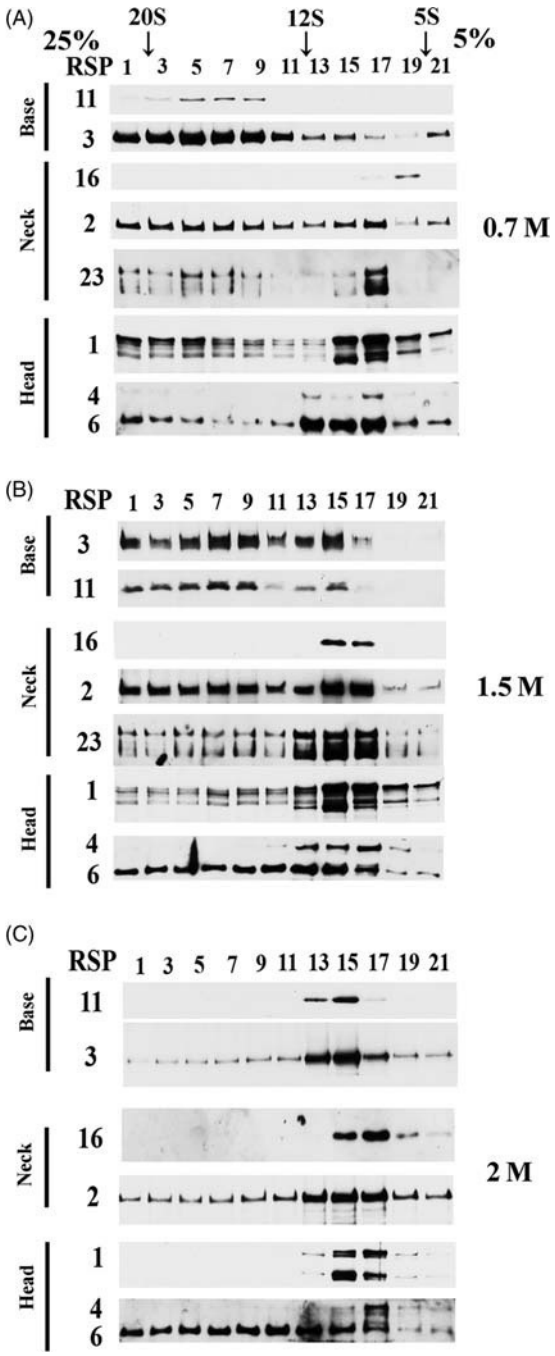

Fig. 3 (*Continued*)

the peak of RS has passed the bottom of the gradient and a major portion has sedimented into the pellet. If a discrete peak is desired, centrifugation duration should be reduced. Following 12- or 10-h centrifugation, the RS peak occurs in fractions #5 and #7, respectively (Fig. 2B and C). The downside of the shorter centrifugation period is less separation between the desired particles and contaminants of similar S value.

2. Relative Concentrations of Proteins and Salt

The optimal protein and salt concentrations for axonemal extractions have been empirically determined. Most extraction procedures are performed at 5–10 mg/ml protein with 0.5–0.6 M salt. Under these conditions, dynein and RS complexes remain intact. Variations in these two parameters can result in unanticipated, but potentially advantageous, outcomes. For example, at low protein concentrations the RS complex partially dissociates in buffers containing a high concentration of KI (Fig. 3). As the protein concentration is reduced and the KI concentration increased, the particles become more dissociated. This progressive dissociation can be exploited to characterize various RS subcomplexes.

If the RSPs are extracted from axonemes with a buffer containing $\geq$0.7 M KI and at a protein concentration of 2.5 mg/ml, the RSPs no longer cosediment as 20S particles following 16 h centrifugation. Following fractionation of a 0.7 M KI extract (Fig. 3A), the spokehead proteins (e.g., RSP1) and associated neck proteins (RSP2, RSP16, and RSP23) largely sediment near the top of the gradient, while RSP3 and RSP11 sediment at ~15 S. Furthermore, RSP16, an HSP40-related protein, that joins the spoke precursor complex in flagella (Yang *et al*., 2005), completely dissociates while RSP2 and RSP23 still cosediment. Note that under these conditions, RSP1, which normally migrates as a single band, becomes a doublet of equal prominence, suggesting degradation related to denaturation and iodine treatment. Interestingly, under these conditions, the closely related spokehead proteins, RSP4 and RSP6, cosediment with each other, but not with RSP1; this suggests that these two proteins interact directly.

Following extraction with 1.5 M KI (Fig. 3B), a subset of the ~15 S particles containing RSP3 and RSP11 further dissociate and these two proteins cosediment in a smaller particle. In contrast, RSP6 is distributed throughout the gradient, suggesting that it becomes denatured under these conditions. In 2 M KI extracts (Fig. 3C), all RSPs tested sediment near the top of the gradient, indicating a drastic dissociation of the entire RS complex. However, even under these conditions, RSP3

Fig. 3 The concentration of KI determines the dissociation level of the RS complex. Western blots of sucrose gradient fractions of wild-type axonemal extracts. The axonemes were extracted at 2 mg/ml with buffer containing 0.7 M (A), 1.5 M (B), and 2 M (C) KI. Under these conditions, RSPs no longer sedimented as a single peak, indicative of the dissociation of the complex, contrary to the intact RS particles extracted at 5–10 mg/ml with 0.5–0.6 M KI buffer as shown in Fig. 2. The dissociation extents correlate with the salt concentrations. The blots were probed with antibodies that recognize specific RSPs as indicated.

and RSP11 still cosediment. This result provides *in situ* evidence for the direct interaction of RSP3 and RSP11, a prediction founded on the complementary interaction motifs present in these two molecules (Yang *et al*., 2006). Together, these results indicate that salt concentrations beyond the typical 0.5–0.6 M range can further disrupt inter as well as intramolecular interactions. This high-salt-mediated dissociation can provide additional information to reveal molecular interactions among axonemal components.

III. Two-Dimensional Gel Electrophoresis of the RS Complexes

Two-dimensional (2D) electrophoresis offers an alternative separation method to standard one-dimensional (1D) SDS-PAGE. There are a few variations, mostly differing in the separation principles for the first dimension of electrophoresis. The most commonly used method is isoelectric focusing, which fractionates polypeptides based on their different pI. Commercially available software and tools, developed for the current explosion of proteomic studies, have made this approach much more powerful and easier for many applications.

However, in our hands, these new tools do not work as well for fractionating axonemes and RSPs as the methods first developed 30 years ago by Piperno and Luck (see Piperno, 1995). The first-dimension separation of this method is nonequilibrium pH gradient electrophoresis (NEPHGE). This method is more suitable for polypeptides of extreme pIs than is isoelectric focusing. During NEPHGE, molecules are not focused to their respective isoelectric points but theoretically migrate at different rates based on their charge. Under NEPHGE, nearly all axonemal proteins are clearly resolved. The acidic RSPs are particularly well separated from the other axonemal proteins. In contrast, commercially available gel strips produce extensive horizontal and vertical streaks, which are indicative of incomplete dissociation or precipitation. Without modification, the capacities and sample buffers designed for commercial apparatuses are not suitable for axonemes consisting of highly stable molecular complexes and a large quantity of tubulin. Therefore, the procedures presented here are largely based on Piperno's method with minor modifications to include new reagents and a commercially available gel apparatus (Bio-Rad Protean II).

The original method of Piperno utilized customized slab gels for both the first- and the second-dimension gels. We prefer tube gels for the first dimension of electrophoresis as these eliminate the need to cut the first-dimension slab gel into thin strips; however, they pose different challenges. Due to the small diameter, the resistance is high and the current is low, particularly near the end of focusing when molecules approach their isoelectric points. To overcome this problem, run at least four tube gels at a time; it is not necessary for all to contain protein samples. In addition, if the power supply is equipped with a no-load detection system, it should be turned off before starting the electrophoresis.

Gel recovery can be challenging. Prior to casting, the tubes need to be thoroughly cleaned by soaking in Chromerge for at least 24 h and extensively rinsed, otherwise it will be difficult to extrude the gel after electrophoresis. On the other hand, the action of Chromerge can cause the gels to prematurely slip out of the tubes during electrophoresis. This problem can be prevented by covering the bottom end of the tube with wet dialysis membrane secured by a rubber band. Note that Chromerge is a 50% aqueous solution of chromium trioxide and is highly corrosive. Extreme caution should be taken to avoid skin/eye contact and inhalation.

After focusing, the tube gel or gel strip is equilibrated in loading buffer and laid on the top of a slab gel for the second dimension of electrophoresis. If only a particular part of the separation is needed, the region of interest can be excised and run on a mini-gel to save time. For instance, since all RSPs migrate in the acidic region of the first-dimension gel, this section can be fractionated on a 1.5-mm thick mini-gel (Bio-Rad, Mini-Protean 3 system). The following procedures are suitable for samples of axonemes or sucrose gradient fractions.

A. Materials and Methods

Ampholine (pH 3.5–9.5 premixed, GE HealthCare)

Acrylamide stock: 28.38% acrylamide and 1.62% bisacrylamide (filtered, kept at 4°C, less than 1 month old)

First-dimension sample buffer: 9.5 M ultrapure urea, 0.8% ampholine, 8% Nonidet-P40, 5% β-mercaptoethanol. (Dissolve 14.27 g ultrapure urea in 9 ml H_2O at 60°C. Add 2 g Nonidet-P40 and 1.25 ml β-mercaptoethanol. Before the solution cools down to room temperature, add 0.2 ml ampholine. Bring the final volume to 25 ml with H_2O. Save the mixture in 1-ml aliquots at –20°C.)

Overlay buffer: 1 M urea, 1% ampholine (store in 2-ml aliquots at −20°C)

Anode (upper chamber, positive) running buffer: 0.01 M H_3PO_4 (577 µl of an ~86% solution/500 ml H_2O)

Cathode (lower chamber, negative) running buffer: 0.02 M NaOH (2.08 g/2.6 l)

5X second-dimension sample buffer stock: 10% SDS, 50% glycerol, 0.3 M Tris (pH 6.8), and 0.005% bromophenol blue. Before usage, add to the stock β-mercaptoethanol a final concentration of 5% and dilute the concentrated complete sample buffer to 2X with water.

1. Sample preparation—Each gel of 1.5-mm diameter can fractionate a sample of less than 100 µg protein in less than 50 µl. Buffer A with or without sucrose is compatible with the first-dimension electrophoresis. Add SDS and β-mercaptoethanol to freshly prepared samples to final concentrations of 2 and 1%, respectively. After boiling for 3 min, the mixture can be divided into 15-µl aliquots. Immediately prior to electrophoresis, each aliquot is mixed with 5 µl 10% Nonidet-P40 and 30 µl first-dimension sample buffer. Discard any precipitate after centrifugation. Additional aliquots could be stored at –80°C although degradation and aggregation may occur.

Table I
Composition of the First-Dimension Tube Gel

Acrylamide stock	0.5 ml
10% Nonidet-P40	0.75 ml
Ampholine, pH 3.5–9.5	0.24 ml
H_2O	0.8 ml
Ultrapure urea	2.06 g
12.5% ammonium persulfate	5 µl
TEMED	3 µl

2. Cast the tube gel—Set up multiple devices made from a 3-ml syringe and a clean tube connected with a short piece of tightly fitted Tygon tubing. Seal the junction with a fragment of Parafilm. The first five ingredients in Table I are added sequentially followed by 30-min degassing and then addition of ammonium persulfate (APS) and TEMED. After thorough mixing, add 0.5-ml of the mixture to a 10-ml clean culture tube secured in a tube rack. Place the syringe/tube device into the acrylamide mixture to withdraw the fluid into the tube with the syringe up to the 14-cm mark. Leave the setup in a rack for at least 2 h until polymerization is complete. If the seal is defective, the fluid will leak out of the tube.
3. Remove the syringe and the residual fluid from the gel tube. Set up the first-dimension electrophoresis apparatus as instructed by the manufacturers. Use a sample-loading syringe to load the sample supernatant on top of the gel and then add the overlay buffer up to the top of the tube. Bubbles should be avoided to prevent interference with the flow of current.
4. Fill the upper and lower chambers with the respective running buffer. Importantly, as the acidic buffer is in the upper chamber, the customary direction for electrophoresis should be reversed by connecting the electrodes in opposite orientation.
5. Electrophoresis is powered by a suitable power supply at 200 V for 2 h, 500 V for 2 h, and 800 V for 14–16 h.
6. To eject the gel, each tube, after rinsing with water, is reconnected to the Tygon tubing/syringe device with the plunger in a withdrawn position. The junction is resealed with Parafilm. Gently push the plunger to eject part of the gel into 2X regular SDS-PAGE sample buffer in a clean container. A long trough made from a folded piece of Parafilm is useful to maintain the orientation of the extruded gel. Apply more force if necessary to release the rest of the gel.
7. After 30 min incubation to allow denaturation in sample buffer, the tube gel, with the aid of a metal spatula if necessary, can be inserted into a long well of a regular SDS-PAGE gel. The dimensions of this gel should be comparable with the length and width of the tube gel and preferably with a reference well for protein markers. Figure 4 shows the fractionation of the acidic half of a tube gel in 1.5-mm thick mini-gels. Percentages of acrylamide can be varied to achieve optimal separation of proteins of interest. The spots are revealed by silver staining (Fig. 4A, C, and D) or

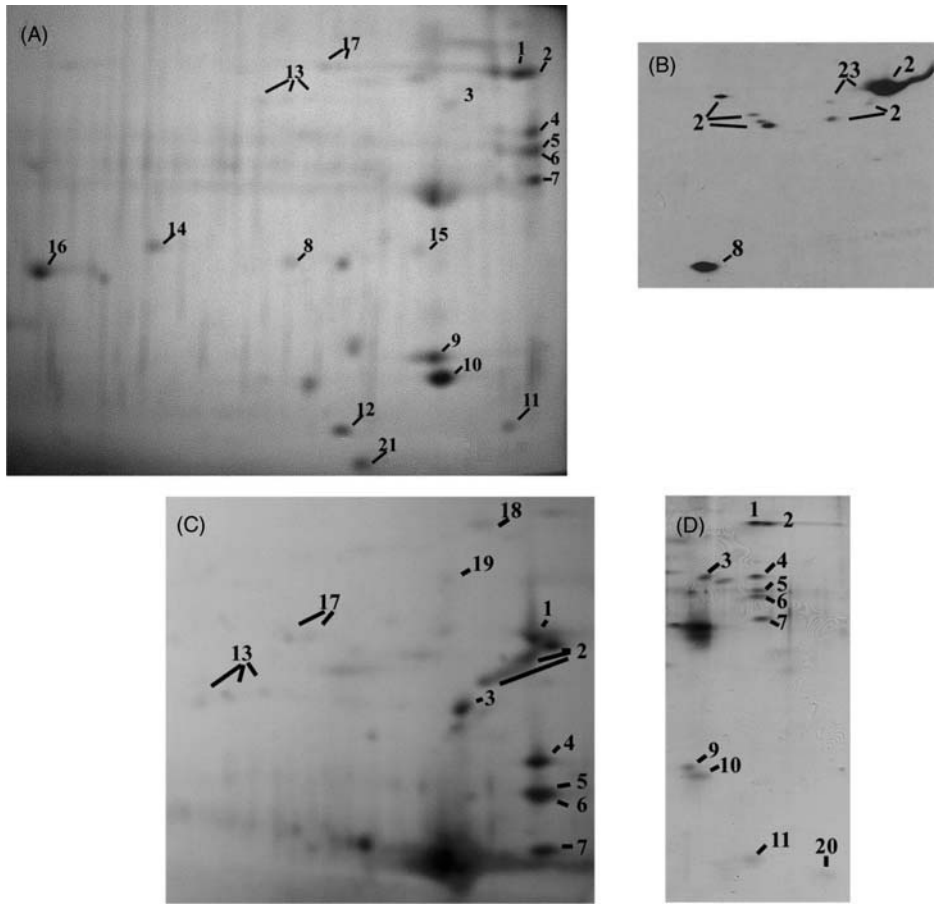

Fig. 4 Two-dimensional gel electrophoresis of RSPs from the 20S fractions of a *pf*28*pf*30 axonemal KI extract. The first dimension was separated by nonequilibrium pH gradient electrophoresis (NEPHGE). Only the acidic end of the first-dimension tube gels was further fractionated in mini SDS-PAGE gels. Different percentages of acrylamide were used to separate RSP5 and RSP6 as they migrate close to each other. Protein spots were revealed by silver staining (A, C, and D). Note that the relative intensities of the RSPs varied significantly in the different stained gels. Calmodulin, the most acidic RSP (D), was often not detected as it focuses on the very acidic end of the first-dimension tube gel which tears easily during gel extrusion. Furthermore, this protein is only very weakly stained by various silver staining methods. Similarly, the RSP23 spot was not detected during the initial identification of RSPs as it is hard to observe in the 2D gels. Its presence can be readily revealed by western blotting (B). To relate these RSP23 spots to other RSPs, the membrane was subsequently probed for RSP8 and RSP2. Notably, both RSP2 and RSP23, two phosphoproteins, were resolved as multiple spots including some which overlap (see Fig. 2A).

with Coomassie blue (Williams *et al*., 1986, 1989). RSP23, which migrates adjacent to RSP2, is not readily detectable by this method but can be revealed by western blotting (Fig. 4B).

IV. Blue Native PAGE for Characterizing Subparticles in RS Complexes

A. Background

Both 1D and 2D SDS-PAGE are broadly used for assessing flagellar samples. The advantage of SDS-PAGE is that both inter- and intramolecular interactions are completely disrupted by heating in the presence of SDS. Furthermore, individual proteins are evenly coated by charged detergent, which causes them to fractionate primarily by size. While this is a powerful technique, the relationship between proteins in complexes is lost. Investigation of extracted axonemal complexes has relied heavily on velocity sedimentation in sucrose gradients to define the composition of complexes. Native gel electrophoresis also separates particles without denaturing the proteins or disrupting the complexes and is an alternative to sucrose gradient centrifugation. Native gel electrophoresis provides an additional means of investigating axonemal complexes and may yield higher resolution separations than velocity sedimentation. Since native gel procedures are widely available, this section will only discuss a modified version termed blue native gel electrophoresis.

In native gels that do not contain SDS, the migration of proteins or protein complexes largely relies on the intrinsic charge of proteins, which is determined by the amino acid composition of the protein and the pH of the buffer. Thus, the migration in native gels is slower and the position of protein particles in the gel is not a good indicator of the molecular mass. Neutral particles do not migrate well and potentially may precipitate. These problems can be partially ameliorated by inclusion of the anionic Coomassie blue dye in both the sample and running buffers. The dye binds to proteins via hydrophobic interactions while its charge promotes migration. Thus blue native gel electrophoresis (BN-PAGE) reflects particle size better than native gel electrophoresis without dye. This method has been widely used in the study of membranous complexes extracted from mitochondria (Wittig *et al*., 2006).

Modification of the original method is needed for axonemal complexes. The major issue is compatibility between the buffer needed for extraction and for electrophoresis of native gels. Contrary to SDS-PAGE, native gels are sensitive to the salt concentration. Thus, the sample needs to be soluble in a buffer containing less than 50 mM NaCl and with minimal divalent cations.

The following method was developed to fractionate partial RS complexes extracted from a RS mutant and is modified from the original procedure (Schagger and von Jagow, 1991). Additional variations were recently published (Wittig *et al*., 2006) and could be incorporated into this protocol.

B. Materials and Methods

Acrylamide stock (49.5% T, 3% C): 48% acrylamide, 1.5% bisacrylamide

Clear cathode buffer—50 mM Tricine, 15 mM Bis-Tris, pH 7.0. Inclusion of 0.002% Coomassie dye is optional but will reveal prominent proteins during electrophoresis.

Blue cathode buffer—Cathode buffer and 0.02% Coomassie blue G-250
Anode buffer—50 mM Bis-Tris, pH 7.0
Gel buffer, 3X—1.5 M aminocaproic acid in 150 mM Bis-Tris, pH 7.0
Sample buffer, 10X—5% Coomassie blue G-250 in 500 mM aminocaproic acid (6-aminohexanoic acid), pH 7.

1. Prepare samples by adding 50% glycerol and 10X sample buffer to the dialyzed axonemal extract (~5 mg ml^{-1}) or gradient fractions at a 1:10 ratio (v/v).
2. Cast gels of appropriate concentrations as shown in Table II. A 5–10% gradient gel was used for separating polymorphic RS complexes from RSP2 mutant *pf*24.
3. Set up a mini-gel apparatus with blue cathode buffer and anode buffer. Run the gel at 150 V until the blue dye enters ~one-third of the gel. Replace the blue buffer with clear cathode buffer. Continue the electrophoresis until the dye runs off. It takes about 2–4 h. The standard protein markers for gel filtration chromatography can be used for BN-PAGE. If the apparatus heats up excessively, the electrophoresis should be conducted at 4°C.
4. The gel can be stained for proteins using standard procedures or processed for 2D SDS-PAGE and/or western blotting. To improve the blotting efficiency, the gel should first be immersed in the transfer buffer for 30 min.

The resolution power of BN-PAGE for axonemal complexes is demonstrated by the separation of polymorphic RS particles from RSP2 mutant *pf*24 (Fig. 5, modified after Yang *et al*., 2005). *pf*24 axonemes still contain a small amount of RSP2 that is involved in, but not essential for, linking the spokehead to the stalk. Consequently, all *pf*24 RS particles contain the stalk base while some lack components near the spokehead (e.g., RSP1, RSP2, and RSP23). RSs were first extracted from *pf*24 axonemes and fractionated through a 10–25% sucrose gradient. As shown by SDS-PAGE and western blots probed with antispoke complex antibody (Fig. 5A, upper panel) and antiRSP11 (lower panel), *pf*24 spoke particles appear to sediment as two overlapping peaks (arrowheads), while RSP1, RSP2, and RSP23 sediment slightly deeper into the gradient (Fig. 5A). Yet in BN gels (Fig. 5B), spoke particles represented

Table II
Composition of the BN-PAGE

Stock	Separating gel				Stacking gel
	5%	7%	10%	13%	
Acrylamide (ml)	0.78	1.1	1.54	1.76	0.6
3X Gel Buffer (ml)	2.19	3.06	1.73	2.25	2.5
Glycerol (g)	–	–	1.038	1.35	–
H_2O (ml)	4.87	3.68	2.23	1.3	4.33
10% APS (μl)	33.8	33.8	22.5	22.5	60
TEMED (μl)	3.4	3.4	2.3	2.3	6

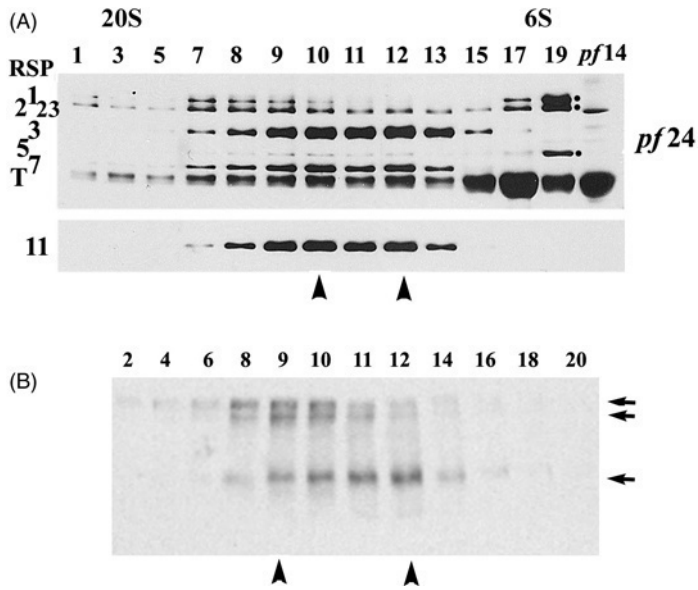

Fig. 5 Blue native PAGE resolved defective polymorphic RS particles in sucrose gradient fractions. The RSP2 mutant *pf*24 is partially deficient in the components around the spokehead, including RSP1, RSP2, and RSP23. The defective RS particles extracted by KI buffer sediment as two major overlapping peaks in fractions #10 and #12 in a 10–25% sucrose gradient (A) as shown by western blots of stalk proteins, RSP3, RSP7, and RSP11, revealed by the antispoke complex antibody (top panel) and antiRSP11 (bottom panel). However, in a 5–10% BN gel followed by western blotting for RSP3 (B), the spoke particles migrate as three bands that peak in different fractions (arrow). From Yang *et al*. (2005). Reproduced from *Mol. Biol. Cell* **16**, 637–648 by copyright permission of the *American Society for Cell Biology.*

by spoke docking protein RSP3 migrate as three discrete bands/complexes. Two slow-migrating complexes were found predominately in fractions near the bottom of the sucrose gradient while a faster-migrating complex was found in fractions from the top of the sucrose gradient (Fig. 5B). Thus, while SDS-PAGE reveals the overall content in each fraction, BN-PAGE further resolves the content into discrete particles. Although the experiment shown here documented the separation of sucrose gradient fractions, BN-PAGE likely can separate dialyzed axonemal extracts directly.

BN-PAGE can be used for other analyses that require native conformation. For example, to determine the molecules in each particle, the desired bands from a Coomassie blue-stained gel could be excised for mass spectrometry. Alternatively, blots of native gels could be probed for candidate proteins. In the case of *pf*24 RS particles, RSPs around the spokehead likely will be absent in the smaller particles while the common components, such as RSP3, will be present in all particles. Some antibodies cannot recognize antigens in complexes due to steric hindrance or conformational differences of epitopes. This problem can be overcome by processing a strip of BN gel for second-dimension SDS-PAGE prior to western blotting in a manner

similar to that described above for isoelectric focusing gels (Yang and Yang, 2006). The proteins in one particle will dissociate in the sample buffer and migrate as spots in the same line at the predicted sizes. Thus BN-PAGE, like chemical crosslinking and sucrose gradient fractionation, can be used for establishing the molecular relationship in a native complex. In addition, as shown by mitochondrial ATPases, BN-PAGE preserves the activities of certain enzymatic complexes.

V. Summary

The extraordinary stability of axonemes is essential for function but poses a great challenge for the elucidation of individual functional units. Nevertheless, it is worthwhile to note that this highly stable structure is assembled from precursors delivered to the tip and that the structure disassembles during resorption. Therefore, many complexes must be able to remain soluble outside of the context of the microtubule cytoskeleton. Until the control of the assembly and disassembly of the axonemal framework is elucidated, dissection of individual complexes has to rely on chemical, enzymatic, and physical means to break axonemes into pieces. Traditionally, NaCl extraction, velocity sedimentation, and chemical crosslinking have been the main approaches. Yet many variations, new reagents, conditions, and approaches remain to be explored. The described procedures developed for the RS could serve as a launching pad for exploration of the numerous unknown complexes in flagella and axonemes.

References

Dymek, E.E., and Smith, E.F. (2007). A conserved CaM- and radial spoke associated complex mediates regulation of flagellar dynein activity. *J. Cell Biol*. **179**, 515–526.

Huang, B., Piperno, G., Ramanis, Z., and Luck, D.J. (1981). Radial spokes of Chlamydomonas flagella: Genetic analysis of assembly and function. *J. Cell Biol*. **88**, 80–88.

Linck, R.W. (1976). Flagellar doublet microtubules: Fractionation of minor components and alpha-tubulin from specific regions of the A-tubule. *J. Cell Sci.* **20**, 405–439.

Mitchell, D.R., and Sale, W.S. (1999). Characterization of a Chlamydomonas insertional mutant that disrupts flagellar central pair microtubule-associated structures. *J. Cell Biol*. **144**, 293–304.

Patel-King, R.S., Gorbatyuk, O., Takebe, S., and King, S.M. (2004). Flagellar radial spokes contain a Ca2+-stimulated nucleoside diphosphate kinase. *Mol. Biol. Cell* **15**, 3891–3902.

Piperno, G. (1995). Two-dimensional separation of axonemal proteins. *Methods Cell Biol*. **47**, 107–112.

Piperno, G., Huang, B., and Luck, D.J. (1977). Two-dimensional analysis of flagellar proteins from wild-type and paralyzed mutants of *Chlamydomonas reinhardtii*. *Proc. Natl. Acad. Sci*. USA **74**, 1600–1604.

Piperno, G., Huang, B., Ramanis, Z., and Luck, D.J. (1981). Radial spokes of Chlamydomonas flagella: Polypeptide composition and phosphorylation of stalk components. *J. Cell Biol.* 88, 73–79.

Schagger, H., and von Jagow, G. (1991). Blue native electrophoresis for isolation of membrane protein complexes in enzymatically active form. *Anal. Biochem*. **199**, 223–231.

Smith, E.F., and Yang, P. (2004). The radial spokes and central apparatus: Mechano-chemical transducers that regulate flagellar motility. *Cell Motil. Cytoskeleton* **57**, 8–17.

Williams, B.D., Mitchell, D.R., and Rosenbaum, J.L. (1986). Molecular cloning and expression of flagellar radial spoke and dynein genes of Chlamydomonas. *J. Cell Biol*. **103**, 1–11.

Williams, B.D., Velleca, M.A., Curry, A.M., and Rosenbaum, J.L. (1989). Molecular cloning and sequence analysis of the Chlamydomonas gene coding for radial spoke protein 3: Flagellar mutation pf-14 is an ochre allele. *J. Cell Biol*. **109**, 235–245.

Wittig, I., Braun, H.P., and Schagger, H. (2006). Blue native PAGE. *Nat. Protoc*. **1**, 418–428.

Yang, C., Compton, M.M., and Yang, P. (2005). Dimeric novel HSP40 is incorporated into the radial spoke complex during the assembly process in flagella. *Mol. Biol. Cell* **16**, 637–648.

Yang, C., and Yang, P. (2006). The flagellar motility of Chlamydomonas pf25 mutant lacking an AKAP-binding protein is overtly sensitive to medium conditions. *Mol. Biol. Cell* **17**, 227–238.

Yang, P., Diener, D.R., Rosenbaum, J.L., and Sale, W.S. (2001). Localization of calmodulin and dynein light chain LC8 in flagellar radial spokes. *J. Cell Biol*. **153**, 1315–1326.

Yang, P., Diener, D.R., Yang, C., Kohno, T., Pazour, G.J., Dienes, J.M., Agrin, N.S., King, S.M., Sale, W.S., Kamiya, R., Rosenbaum, J.L., and Witman, G.B. (2006). Radial spoke proteins of Chlamydomonas flagella. *J. Cell Sci*. **119**, 1165–1174.

Yang, P., Yang, C., and Sale, W.S. (2004). Flagellar radial spoke protein 2 is a calmodulin binding protein required for motility in Chlamydomonas reinhardtii. *Eukaryot. Cell* **3**, 72–81.

CHAPTER 13

Analysis of the Central Pair Microtubule Complex in *Chlamydomonas reinhardtii*

David R. Mitchell *and* Brandon Smith
Department of Cell and Developmental Biology, SUNY Upstate Medical University, Syracuse, New York

Abstract

The central pair microtubule complex in *Chlamydomonas* flagella has been well characterized as a regulator of flagellar dynein activity, but many aspects of this regulation depend on specific interactions between the asymmetric central pair structure and radial spokes, which appear symmetrically arranged along all nine outer doublet microtubules. Relationships between central pair–radial spoke interactions and dynein regulation have been difficult to

METHODS IN CELL BIOLOGY, VOL. 92

978-0-12-374974-1
DOI: 10.1016/S0091-679X(08)92013-6

understand because the *Chlamydomonas* central pair is twisted *in vivo* and rotates during bend propagation. Here we describe genetic and biochemical methods of dissecting the *Chlamydomonas* central pair and electron microscopic methods useful to determine structure–function relationships in this complex.

I. Introduction

The central pair complex is a nearly universal feature of motile cilia and flagella and plays an essential role as an asymmetric regulatory complex for axonemal dyneins. Mutations that disrupt assembly of the central pair generally result in a nearly complete inhibition of organelle motility, as seen in humans (Stannard *et al*., 2004), mice (Zhang *et al*., 2006), algae (Warr *et al*., 1966), and trypanosomes (Branche *et al*., 2006). Most of the genetic, structural, and biochemical work on the central pair has taken advantage of one model organism, *Chlamydomonas reinhardtii*. A summary of major structural elements in the *Chlamydomonas* central pair, as determined from thin section electron microscopy, is shown in Fig. 1. Two 13-protofilament microtubules are joined by short linkers. The microtubule designated C1 has two longer projections (1a and 1b) that represent structures with 16 nm periodicity and shorter projections (1c and 1d) that include material with a 32 nm periodicity. In contrast, the C2 microtubule has only a single long projection (2b) and two shorter projections (2a and 2c), and all C2-associated structures appear to have 16 nm periodicities. Two basic approaches used for analysis of central pair structure–function relationships are the correlation of structural defects with functional abnormalities, and the correlation of central pair orientation with presumed

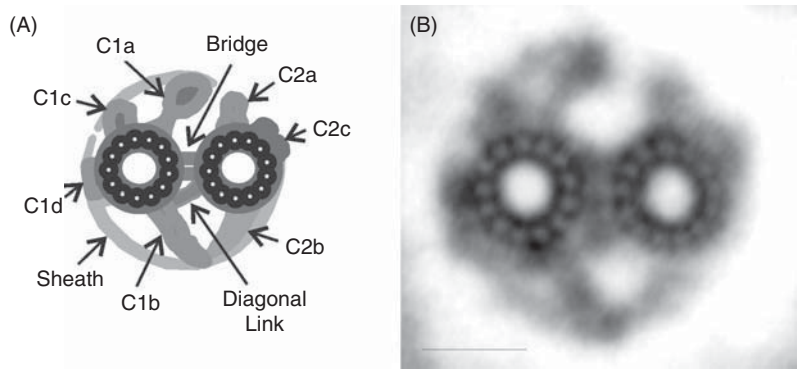

Fig. 1 Summary of central pair structure as seen in cross-sectional image averages. (A) Diagram labeling densities in the averaged image. (B) Image average from thin sections of *pf14* axonemes, which lack radial spokes but retain wild-type central pair structure. Bar = 20 nm. Modified from Mitchell and Sale (1999) by permission of The Rockefeller University Press.

patterns of dynein activity. While neither approach has provided complete answers to some of the nagging questions of axonemal dynein regulation, these methods may prove useful for further analysis of the enigmatic mechanism of motility regulation by the central pair complex.

II. Basic Methods for Central Pair Structure Analysis by Thin Section Electron Microscopy

The procedures for preparing samples for thin section electron microscopy do not differ from those commonly used and previously described in this series (Hoops, 1995; O'Toole *et al*., 1995). Because flagellar structures are much more difficult to visualize *in situ* than in isolated, demembranated axonemes, all high-resolution analyses start with axonemes. Only details pertinent to work on the central pair are emphasized here.

For routine thin section electron microscopy, a 1l culture grown to ~5×10^6 cells/ml provides sufficient material, and volumes listed in the remainder of this procedure are suitable for processing flagella from this number of cells. For biochemical fractionation prior to microscopy, especially if several fractions are to be processed to make samples from a single experiment or if separate samples are to be saved for gel analysis, initial starting culture volumes should be increased. Cell density may be increased by using a growth medium supplemented with sodium acetate, but some mutant strains tend to assemble shorter flagella in richer media, and thus growth in larger volumes of a minimal medium such as M I (Sager and Granick, 1953) may be advantageous.

A. Solutions

- Wash buffer (HMDEK): 30 mM HEPES, 5 mM $MgSO_4$, 1 mM DTT, 0.5 mM EGTA, 25 mM potassium acetate, pH 7.4 (prepare as a 10X stock of HMEK and 1 M stock of DTT; dilute stocks on the day of use and add protease inhibitors such as 1 mM PMSF)
- Demembranation buffer: HMDEK + 0.4% NP-40
- Primary fixative: 1% glutaraldehyde, 1% tannic acid in HMDEK.
- Secondary fixative: 1% osmium tetroxide in HMDEK

B. Procedures

1. We deflagellate *Chlamydomonas* cells by treatment with dibucaine and purify flagella by differential centrifugation, following published procedures (Witman, 1986).
2. Flagella are resuspended in 1 ml HMDEK and then mixed with an equal volume of HMDEK containing 0.4% NP-40. After trituration with a 1 ml pipettor (avoid

foaming), pellet the axonemes and wash by resuspending in 1 ml HMDEK without detergent.

Note: Care must be taken to choose the correct source of NP-40, as recent changes in detergent properties can result in incomplete removal of membrane (Wirschell *et al*., 2004). If larger starting amounts of flagella are processed, either the volume or the detergent concentration should be increased proportionately. NP-40 concentrations as high as 1% do not appear to adversely affect central pair structure, but caution is advised based on the detergent sensitivity of some axonemal proteins, including dynein regulator Lis1 (Pedersen *et al*., 2007) and a dynein-associated adenylate kinase (Wirschell *et al*., 2004). Variations in the salt concentration and choice of anion may affect stability of central pair structures, especially in some mutants as noted below.

3. Pellet axonemes under moderately high force (15,000 × g) in a round-bottomed tube, remove buffer, and overlay the pellet with 1 ml primary fix. Incubate on ice for 1 h. After the first 15 min, the pellet may be gently lifted from the surface of the centrifuge tube with a sharpened applicator stick to permit better penetration of solutions.

   Note: Tannic acid is not a standardized material. Concentrations may need to be adjusted to provide the desired level of contrast enhancement. Care must also be taken that the tannic acid does not change the pH of your fixation solutions. We prepare a 10% stock of tannic acid, adjust the pH to near neutral with NaOH (too high and the tannic acid will precipitate), and freeze in aliquots.
4. Remove primary fixative, wash pellet with two changes of buffer, postfix in osmium for 1 h on ice, wash as before, and proceed through normal dehydration in graded ethanol. Transfer pellet in 100% ethanol to a small dish and cut into several segments prior to infiltration with embedding resin. After infiltration, segments of the pellet may be aligned parallel or perpendicular to the end of an embedding mold so that thin sections favor longitudinal or cross-sectional views when cut from the end of the block.
5. Thin sections are stained with uranyl acetate and lead citrate by standard EM methods, and images are collected at an initial magnification of 40–50k.

As central pair structures have 16 and 32 nm periodicities, routine thin sections of 60–80 nm thickness include more than one copy of each projection and perfect alignment is essential to obtain a high-quality image. Image averages generated from as few as 15–20 good cross-sectional images can markedly improve resolution of material that is uniformly present and can be used to generate difference images that highlight structures altered by specific mutations (Mitchell and Sale, 1999). Ultrathin (20–30 nm) sections can be useful when analyzing longitudinal images, to avoid superposition of structures. In addition, mutations that disrupt the assembly of radial spokes, such as *pf14*, are particularly useful for distinguishing central pair projections from radial spoke heads in longitudinal views. Because of the difficulty of finding multiple sections that present identical longitudinal views (180° rotational variation as well as section depth variation must be taken into account), image averages have not been used on longitudinal thin sections. Advances in cryo-electron tomography

(Hoenger and Nicastro, 2007) are likely to provide superior images of the central pair in the near future, but are unlikely to supplant thin section studies for the initial characterization of new mutants or of new biochemical treatments for dissecting central pair structure.

III. Genetic Dissection of the Central Pair

Chlamydomonas has been used extensively to genetically dissect flagellar motility and assembly. This haploid, single-celled alga swims in liquid environments by beating its two nearly identical flagella, but also occurs in nature as a soil microorganism and does not require flagellar motility for its survival. Mutations that disrupt flagellar motility or that even block flagellar assembly completely are nonlethal. Many such mutations have been characterized at the level of genetics, motility, ultrastructure, and sequence identity, and some of the first motility defective strains studied (paralyzed flagella or *pf* mutants) were later found to have defects in assembly of the central pair (Randall *et al*., 1964). Further analysis shows that a simple phenotypic difference can be used to separate mutations that disrupt the entire central pair structure from those with more subtle structural defects: central pairless mutants have full-length paralyzed flagella that remain nearly straight, except for occasional twitches or slow bends (http://www.elsevierdirect.com/companions/9780123749734, Supplemental movie 1). In contrast, mutations that produce only partial central pair disruption generally retain more motility (http://www.elsevierdirect.com/companions/9780123749734, Supplemental movie 2), whereas mutations that disrupt another flagellar regulatory complex, the radial spoke, produce paralyzed flagella with curved shapes (http://www.elsevierdirect.com/companions/9780123749734, Supplemental movie 3). Most mutations in dynein subunits produce flagella that continue to beat and support swimming at a reduced velocity (Kamiya, 2002). Methods are summarized for using central pair mutants and knockdown approaches to assign proteins to specific central pair structures. A list of characterized mutations and knockdown strains affecting the *Chlamydomonas* central pair is given in Table I.

A. Mutations That Disrupt Assembly of Both Central Pair Microtubules

Mutations at four loci disrupt assembly or stability of both central pair microtubules. In cross sections of *in situ* flagella, the central pair region usually appears as a dense core of amorphous material, which often appears to retain periodicity when observed in longitudinal images. Upon isolation of flagella and demembranation to form axonemes, these mutants usually appear to completely lack a central pair structure ($9 + 0$ axonemes) (Witman *et al*., 1978). Antibodies to newly characterized flagellar proteins are frequently used to probe western blots that compare wild-type axonemes to axonemes from one of these mutant strains, where absence of the antigen in mutant

Table I
Mutations and Knockdowns Affecting Central Pair Structure

Mutant locus	Structural defect in flagella	Structural defect in axonemes	Gene product	Mammalian homolog	References[a]
pf6	9 + 2, 1a missing	9 + 2, projection 1a missing	PF6 AAK38270	MmSPAG17 AAV66533	Dutcher *et al*. (1984); Rupp *et al*. (2001)
pf15	9 + dense core	9 + 0	Katanin p80		Starling and Randall (1971); Witman *et al*. (1978); Adams *et al*. (1981); Dymek *et al*. (2004a)
pf16	9 + 2	9 + 1, C1 microtubule missing	PF16 AAC49169	MmSPAG6 AAV66534	Dutcher *et al*. (1984); Smith and Lefebvre (1996)
pf18	9 + dense core	9 + 0	?	?	Starling and Randall (1971); Adams *et al*. (1981)
pf19	9 + dense core	9 + 0	?	?	Starling and Randall (1971); Witman *et al*. (1978); Adams *et al*. (1981)
pf20	9 + 2, 9 + 1, 9 + 0	9 + 0	PF20 AAB41727	MmSPAG16L NP_083436	Starling and Randall (1971); Adams *et al*. (1981); Smith and Lefebvre (1997)
cpc1	Projection 1b missing	Projection 1b missing	CPC1 AAT40992	RnKPL2 AAD56310	Mitchell and Sale (1999); Zhang and Mitchell (2004)
H2	?	Projection 2b reduced	?	?	Smith and Lefebvre (1996)
Klp1-KD	?	Projection 2a and 2b (partial)	KLP1 EDP06592	MmKIF9 CAB46016	Bernstein *et al*. (1994); Yokoyama *et al*. (2004)
Hydin-KD	?	Projections 2a and 2b (partial)	EDP09735	MmHydin AAH80316	Lechtreck and Witman (2007)

[a] References are for *Chlamydomonas* knockdown or mutant characterization.

axonemes defines the antigen as a central pair protein. Two of the loci that generate this phenotype in *Chlamydomonas, pf18* and *pf19*, have not been characterized at the molecular level. A third, *pf15*, encodes a subunit related to p80 (noncatalytic) subunits of the microtubule severing protein Katanin (Dymek *et al*., 2004b). The *PF15* gene product has not been localized to flagella, and thus may function during an assembly process rather than as a structural component of the central pair. Because the mode of action that leads to lack of central pair assembly in *pf15* is not understood, some caution should be used in assigning a protein as part of the central pair structure based on its absence from mutant flagella. The fourth locus, *pf20*, encodes a WD repeat protein that has been localized to the region that joins the C1 and C2 microtubules (Smith and Lefebvre, 1997). These four mutations have been used nearly interchangeably as signatures defining central pair proteins.

B. Mutations That Destabilize Single Central Pair Microtubules

One mutation, *pf16*, destabilizes a single microtubule of the central pair complex, C1, and results in nearly complete flagellar paralysis. PF16 is an armadillo repeat protein that has been localized to the C1 microtubule (Smith and Lefebvre, 1996). Based on interactions between the mammalian homologs of PF16 and PF20, the PF16 protein may localize to the interface between C1 and C2 microtubules. Central pair structure remains essentially intact in *pf16* flagella *in situ*, but shows a variable loss of C1 in isolated axonemes, from a partial opening of the C1 microtubule and loss of C1a to a complete loss of C1 and all associated structures. Variability in the extent of C1 loss can be controlled by varying the monovalent salt and its concentration in axoneme isolation buffers. When flagella are isolated and demembranated in buffers containing 30–50 mM NaCl, the C1 microtubule is highly labile (Dutcher *et al*., 1984; Mitchell and Sale, 1999; Smith and Lefebvre, 1996). When isolation buffers contain 25 mM K acetate in place of NaCl, less than 10% of *pf16* axonemes are completely missing C1 and many have an apparently intact central pair complex (Mitchell and Sale, 1999).

We have recently isolated a *Chlamydomonas* mutant (provisionally designated *unc1*) with flagella that twitch but fail to form coordinated bending waves. This mutation has been mapped to a previously uncharacterized locus on LG V (B. Smith and D. Mitchell, unpublished observations). EM thin sections of *unc1* axonemes show selectively destabilized C2 microtubules (Fig. 2), similar to the variability in C1 structure of *pf16* axonemes. In the future, this mutation should be useful for identifying C2-associated proteins and should complement identification of C2 proteins by biochemical fractionation.

C. Mutations and Knockdowns That Disrupt Central Pair Microtubule-Associated Complexes

The *pf6* mutation blocks assembly of projection 1a and results in flagella that twitch and beat, but too slowly and intermittently to support progressive cell movement. The 240-kDa *PF6* gene product (Rupp *et al*., 2001) functions as a molecular scaffold for a calmodulin-associated complex (Wargo *et al*., 2005), and may function in calcium regulation of

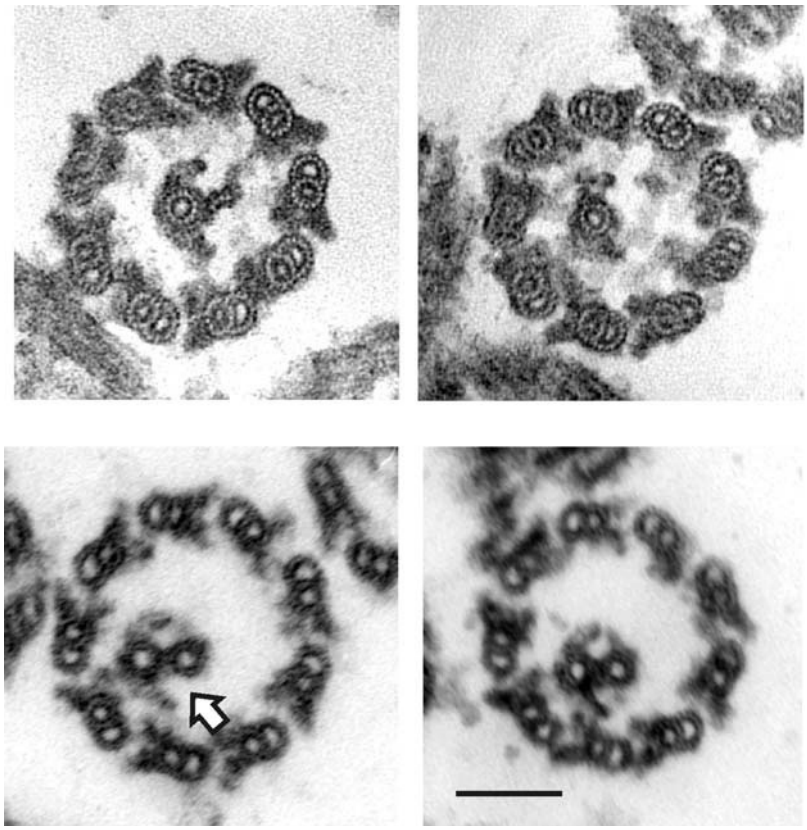

Fig. 2 Defects in C2-associated structures seen in axonemes of *Chlamydomonas* mutants. (Upper row) Axonemes from *unc1* show instability of the C2 microtubule. (Lower row) Axonemes from an H2*pf14* strain frequently lack the 2b projection (arrow). Bar = 100 nm.

flagellar motility. Although it is tempting to think that some protein in this complex engages radial spoke heads directly, no such specific interaction has yet been identified.

Proteins in C1-associated complex 1b were identified through analysis of the *cpc1* mutation. The 265 kDa CPC1 protein contains signature domain elements of an adenylate kinase, but these blocks of sequence similarity are separated by sequences much larger than the loops found between domains in typical adenylate kinases, and we have no evidence that CPC1 is a functional adenylate kinase (Zhang and Mitchell, 2004). CPC1 copurifies in a complex containing an even larger protein that has one domain with weak similarity to adenylate kinases and five domains with weak similarity to guanylate kinases. Other proteins in this complex include an armadillo repeat protein, the chaperone HSP70, and the glycolytic enzyme enolase (Mitchell *et al*., 2005).

Although no well-characterized mutants block assembly of specific C2-associated structures, the H2 strain carries a mutation that partially disrupts structures associated

with the C2 microtubule (Smith and Lefebvre, 1996), and some *Chlamydomonas* proteins identified as central pair components have been disrupted by RNAi approaches and result in C2 defects. These include a kinesin-like protein of the KIF9 family, KLP1 (Yokoyama *et al*., 2004), and the hydrocephalus-associated protein Hydin (Lechtreck and Witman, 2007), which both alter the appearance or stability of the 2b projection and a portion of the 2a projection. We have further characterized the H2 strain, mapped the mutation, and find that the motility phenotype of the mutation in H2 is similar to that of other strains with disruptions of C2-associated structures, including *unc1* and strains with reductions in expression of KLP1 or Hydin (B. Smith and D. Mitchell, unpublished observations). At the ultrastructural level, H2 axonemes show frequent loss of projection 2b (Fig. 2). Although this defect is similar to the defect observed upon knockdown of Hydin, the mutation in H2 does not map to the Hydin locus. Further characterization of this mutation should provide additional useful material for dissecting the contribution of C2 structures to central pair motility regulation and biochemistry.

IV. Biochemical Dissection of the Central Pair

Differential extraction of portions of the central pair with increasingly chaotropic salt solutions provides useful fractionation of central pair proteins for biochemical analyses and also generates structural intermediates that can be used for localizing proteins within parts of the central pair. As noted by the Luck lab (Dutcher *et al*., 1984), treatment of axonemes with 0.5–0.6 M NaCl solubilizes the C2 microtubule and its associated proteins with moderate efficiency. Because dyneins and some additional outer doublet-associated proteins are also extracted at this salt concentration, this method should be considered enrichment, at best. However, the appearance of C1 and associated projections appears essentially unaltered by these conditions (Fig. 3), and thus proteins that appear to be central pair components based on analysis of mutants and that are extracted by 0.6 M NaCl are likely to be C2 associated, whereas proteins that remain pelletable are likely to be C1 associated (see Fig. 4).

The alternative method of determining whether a protein is part of the C1 or C2 complex is to compare the protein composition of axonemes from wild-type and central pairless (e.g., *pf18*) axonemes, with those of *pf16*. However, the incomplete extraction of C1 sometimes seen in preparations of *pf16* axonemes can result in substantial residual amounts of some C1-associated proteins. A further problem arises for complexes such as projection 1b, which retain connections to both C1 and C2. Blot analysis of the CPC1 protein, which functions as a scaffold for the 1b projection, shows only a small reduction in abundance of *pf16* axonemes (Zhang and Mitchell, 2004), and electron microscopy confirms that 1b projections can remain associated with the C2 microtubule when the C1 microtubule is absent (Mitchell and Sale, 1999). Most of the CPC1 protein is retained on C1 following extraction of C2 with 0.5 M NaCl (Fig. 4).

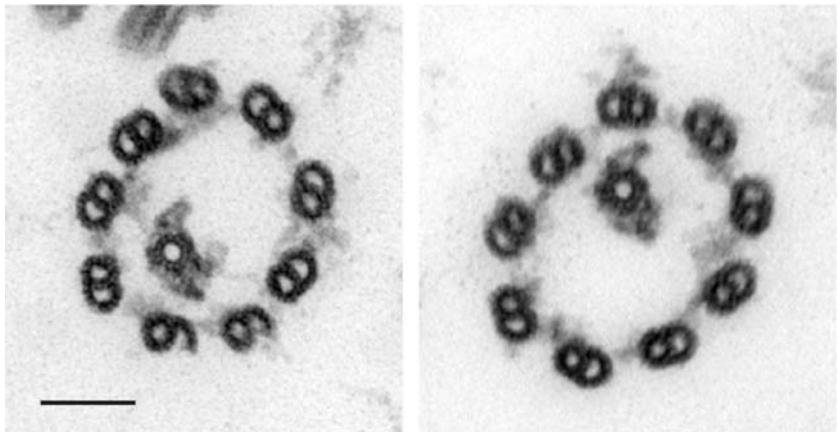

Fig. 3 Cross sections through *pf14* axonemes extracted with 0.6 M NaCl showing the projections that remain associated with C1 following extraction. Bar = 100 nm.

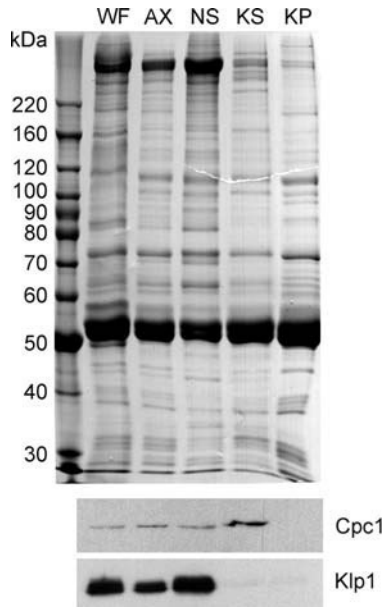

Fig. 4 Stained gel and immunoblots of axonemes fractionated by salt extraction. WF, whole flagella; AX, axonemes following NP-40 treatment; NS, fraction solubilized by 0.6 M NaCl; KS, fraction solubilized by 0.2 M KI; KP, insoluble material following KI extraction. Upper panel, gel stained with Coomassie blue. Lower panels, blots probed for C1-associated CPC1 (265 kDa) and C2-associated KLP1 (85 kDa).

To generate a soluble fraction containing C1 proteins, axonemes can be first extracted with 0.6 M NaCl to remove dyneins and C2 proteins and the pellet then extracted with 0.2 M or greater concentrations of KI (Mitchell and Sale, 1999). Since

doublet-associated radial spokes are extracted by 0.5 M KI but not by 0.2 M KI (Yang *et al*., 2006), we routinely use 0.2 M KI to create fractions enriched in C1-associated proteins, such as CPC1. At least some of the proteins made soluble in this way retain interactions with other central pair proteins in higher order complexes. Separation of a 0.2 M KI extract by sucrose gradient sedimentation was used to show that CPC1 cosediments with four additional proteins. Blots of *cpc1* mutant axonemes show that some of these additional proteins are entirely dependent on CPC1 for their assembly onto axonemes. Others, such as HSP70 and enolase, still appear at reduced levels in *cpc1* axonemes but are completely dependent on the central pair for axonemal association, suggesting that they form contacts with additional central pair components (Mitchell *et al*., 2005).

A. Materials

- HMDEK with 0.6 M NaCl (prepare fresh on day of use from a 10X stock of HMEK and 1 M stock of NaCl)
- HMDEK with 0.2 M KI (prepare fresh on day of use from a 10X stock of HMEK and 1 M stocks of DTT and KI).

B. Methods

1. Axonemes are resuspended in HMDEK + 0.6 M NaCl and left on ice for 20 min, then pelleted at 4°C in a microfuge for 10 min. The supernatant contains C2 proteins, some of which remain in complexes.
2. Resuspend the extracted axonemes in HMDEK + 0.2 M KI, leave on ice for 20 min, pellet in microfuge for 20 min. Supernatant contains C1 proteins. If the starting material is unextracted axonemes, all central pair proteins can be solubilized in a single step.

V. Methods to Study Central Pair Structural Conformation

A. Thin Section TEM of the Central Pair *In Situ*

As a regulatory complex, the central pair is thought to modify dynein activity patterns through interactions between the central pair and doublet-associated radial spokes. Evidence for the importance of such interactions comes from analysis of doublet sliding activity in disrupted axonemes, which shows that doublets associated with an intact central pair have a different intrinsic dynein activity profile from doublets that lack central pair association. Similar conclusions have been reached from studies of metazoan axonemes, such as those from sea urchin spermatozoa (Yoshimura and Shingyoji, 1999), and protistan axonemes, such as those from *Chlamydomonas* (Smith, 2002). However, studies of these systems reveal a surprising difference in the overall mechanics of central pair–radial spoke interactions. Metazoan cilia and flagella have a central pair complex that maintains a fixed orientation along

the entire axoneme, with C1 facing doublet 8 and C2 facing doublet 3 (Gibbons, 1961; Linck *et al*., 1981). In some cases, strong interactions between spoke heads from these doublets and the surface of each central pair microtubule can be seen in highly disrupted axonemes, where doublets 3 and 8 remain attached to the central pair (Tamm and Tamm, 1984). In contrast, the central pair easily separates from outer doublets in disrupted axonemes from such protists as *Chlamydomonas* and *Paramecium*, and central pair orientation appears random in cross sections of these protistan axonemes. This variable orientation has been seen in all organisms tested from at least two branches of eukaryotic phylogeny, the Chromalveolates (ciliates and their kin) and the Viridaplantae (which includes *Chlamydomonas*). We used thin section microscopy of rapidly fixed cells to find the relationship between central pair orientation and bend formation in *Chlamydomonas* (Mitchell, 2003). Here we describe methods essential for such analysis.

Key to observations of *in vivo* central pair orientation is a method to rapidly preserve normal flagellar bends. Because *Chlamydomonas* flagella beat at 60 Hz, the preservation must be fast indeed. The most rapid methods of preservation currently available for EM specimens involve rapid freezing followed by freeze substitution chemical fixation or by direct observation of the cryopreserved specimen. Neither of these methods can be applied to intact, swimming *Chlamydomonas* cells. Cryopreservation by plunging an EM grid into an ultracool liquid cannot be used, because the cells require a layer of liquid thicker than the diameter of the cell (~5 μm) in order to swim with a normal waveform. Such thick layers of liquid are difficult to freeze rapidly enough to prevent ice crystal formation and are too thick for direct observation of unstained specimens. Cryopreservation of *Chlamydomonas* cells by high-pressure freezing has only been successful with thick slurries of cells surrounded by little remaining extracellular fluid, which prevents analysis of swimming cells. Therefore, more traditional chemical fixation of the most rapid form is necessary. Previous work with ciliates and ciliated epithelia has relied on osmium as a primary fixative to preserve the waveform of metachronally beating cilia. We find superior fixation of swimming waveforms in *Chlamydomonas* when the initial fixative is glutaraldehyde at a relatively high concentration. However, for reasons not presently understood, the preparation must be diluted to 1% glutaraldehyde after the first 4 min of fixation or else waveforms that were visible immediately after addition of glutaraldehyde begin to relax (straighten).

A second necessary parameter for observation of central pair orientation in fixed preparations of whole *Chlamydomonas* cells is to obtain thin sections that pass along the plane of a flagellar bend. Although bends are nearly planar in *Chlamydomonas*, each cell has only two flagella and it is thus difficult to find a random thin section with the correct orientation to reveal the central pair over an extended length of the flagellum. To improve the frequency of success, cells are allowed to settle onto the surface of a glass slide or cover slip during the initial period of fixation. Most cells settle with their flagella approximately parallel to the glass surface. After fixation and dehydration, these cells are flat embedded in epoxy resin, the glass is removed, and the specimen is remounted to allow sections to be cut parallel to the flat surface.

1. Materials

- Cells resuspended at ~5 × 10E6/ml in growth medium
- 50 mM cacodylate buffer, pH 7.5
- 6% glutaraldehyde in 50 mM cacodylate, pH 7.5
- 1% low-melt agarose in 50 mM cacodylate, pH 7.5
- 1% OsO_4 in 50 mM cacodylate, pH 7.5

2. Methods

1. To 1 ml of swimming cells in a 15 ml conical tube add 1 ml of 6% buffered glutaraldehyde for a final glutaraldehyde concentration of 3%.
2. After 3–4 min, add 4 ml of 50 mM cacodylate to reduce the glutaraldehyde concentration to 1%. Transfer samples onto glass slides and continue fixation for 1 h at room temperature in a humid chamber, allowing cells to settle onto the glass surface.
3. Gently remove glutaraldehyde solution and replace with 1% low-melt agarose in 50 mM cacodylate buffer.
4. Rinse by immersing slide in cacodylate buffer, postfix in 1% osmium tetroxide, dehydrate through graded acetone.
5. Infiltrate in epon/araldite resin (50% overnight, 100% for 4 h), then replace with a thin layer of fresh embedding resin and transfer to 60° curing oven.
6. Immerse slide in liquid nitrogen to aid removal of cured resin from slide. Cut the resin into small squares and remount on dummy blocks for sectioning.

Chlamydomonas, like many other flagellated protists, can adhere to surfaces using their flagella and move along the surface through a poorly understood flagellar gliding mechanism. During gliding, flagellar beating is suppressed. We have used such quiescent cells to examine central pair orientation in nonbeating flagella. In this case, live cells are permitted to attach to a glass surface and begin gliding prior to the application of glutaraldehyde. Specimens are flat embedded and remounted, and longitudinal views of flagella are seen in the first few sections cut from the flat surface (Mitchell and Nakatsugawa, 2004). By using fixation and embedding methods more suited to the preservation of antibody recognition, Rosenbaum and colleagues have adapted this method for immunogold EM localization of intraflagellar transport proteins (Pedersen *et al*., 2006).

B. EM and Light Microscopy of Extruded Central Pair Complexes

One essential element for generating the twisted shape of the central pair in *Chlamydomonas* flagella *in vivo* is likely to be the overall helical shape of the central pair complex itself when separated from outer doublets. Such helical curvature can be seen either by splaying axonemes so that the distal ends of all nine doublets separate from each other as well as from the central pair (Johnson,

1995) or by extruding the central pair complex from an otherwise intact axoneme, as described here.

Several methods have been explored to disrupt axonemes, with the intent of making a pure population of central pair complexes, but with little success. Squid sperm central pair microtubules were isolated following treatment of axonemes with 0.5 M NaCl (Linck *et al*., 1981) and *Tetrahymena* central pair may also be released by treatment of axonemes with 0.2 M NaCl (D. Mitchell, unpublished observation), but the effects of such treatment on the protein composition of the central pair have not been determined. Sonication of *Tetrahymena* or *Chlamydomonas* axonemes results in axonemal breakage into short fragments, rather than splaying of doublet microtubules and does not release the central pair. Treatment of axonemes with a protease in the presence of ATP will result in doublet sliding, and in some cases sliding proceeds to the point where all nine doublets slide apart and the central pair is released. More commonly, however, sliding occurs between bundles of doublet microtubules, and the central pair remains associated with one bundle, as was used advantageously by Smith and colleagues to monitor central pair orientation relative to doublet sliding pattern (Wargo and Smith, 2003). We also considered it advantageous to obtain central pair complexes that had not been purposely exposed to proteolysis. To date our most successful extrusions of the *Chlamydomonas* central pair have been seen after prolonged exposure to a standard reactivation protocol. Flagella isolated from dibucaine-treated cells are demembranated with a nonionic detergent, such as NP-40, and resuspended in a reactivation buffer containing 1 mM ATP. Such preparations contain a built-in ATP-regenerating system in the form of substantial adenylate kinase activity, thus ATP is not depleted until most of the nucleotide has been converted to AMP. Neither higher nor lower concentrations of ATP were as effective as 1 mM. We leave a tube of reactivating axonemes at room temperature and check samples periodically by darkfield light microscopy. A typical preparation of axonemes will continue to beat for 8–10 min under these conditions, and during the last 1–2 min an increasing number of central pair complexes begin to extrude from the distal tip of many axonemes. When all movement stops, the sample is chilled and any additional manipulations are carried out in the cold.

Simple dilution of a preparation of post-reactivated axonemes can be used to observe the helical shape of the extruded central pair complexes by darkfield light microscopy and negative stain electron microscopy (Fig. 5). Such preparations can also be fixed for immunofluorescent microscopy, to distinguish central pair versus outer doublet localization of axonemal antigens (Lechtreck and Witman, 2007).

Although this method does produce some central pair complexes free of other axonemal components, many more central pair complexes are only partially extruded with their proximal ends remaining inserted in the axoneme. In addition, as with any such disruption methods, some axoneme fragments are produced which unfortunately have similar sedimentation properties to the released central pair complexes. Thus while it is possible to enrich for the central pair after extrusion we have not developed a method of purifying these central pair

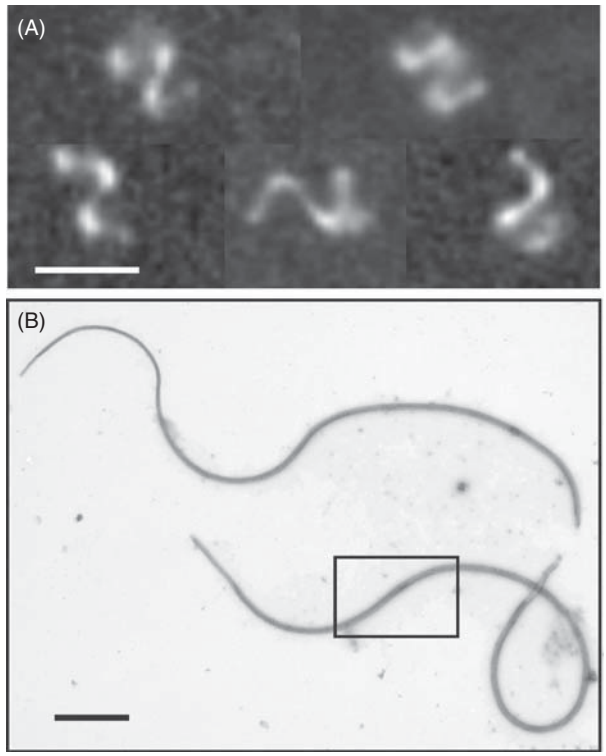

Fig. 5 Extruded central pair complexes imaged by darkfield light microscopy (A) and negative stain electron microscopy (B). Bar = 5 μm in (A), 1 μm in (B). Reproduced from Mitchell and Nakatsugawa (2004), by permission of The Rockefeller University Press.

complexes in large quantities. Finally, it should be noted that once released, the *Chlamydomonas* central pair is surprisingly brittle, fragmenting easily into short arcs upon pelleting and resuspension.

VI. Summary

The *Chlamydomonas* central pair complex provides a unique model for studying the mechanical and biochemical pathways by which radial spoke–central pair interactions regulate axonemal dynein activity patterns. Using biochemical and genetic dissection of central pair structure, combined with electron microscopic observations of the relationship between central pair orientation and microtubule sliding patterns, it should be possible to clarify the role of specific interactions between spoke heads and central pair projections in regulating dynein activity.

References

Adams, G.M.W., Huang, B., Piperno, G., and Luck, D.J.L. (1981). Central-pair microtubular complex of *Chlamydomonas* flagella: Polypeptide composition as revealed by analysis of mutants. *J. Cell Biol*. **91**, 69–76.

Bernstein, M., Beech, P.L., Katz, S.G., and Rosenbaum, J.L. (1994). A new kinesin-like protein (Klp1) localized to a single microtubule of the *Chlamydomonas* flagellum. *J. Cell Biol*. **125**, 1313–1326.

Branche, C., Kohl, L., Toutirais, G., Buisson, J., Cosson, J., and Bastin, P. (2006). Conserved and specific functions of axoneme components in trypanosome motility. *J. Cell Sci*. **119**, 3443–3455.

Dutcher, S.K., Huang, B., and Luck, D.J.L. (1984). Genetic dissection of the central pair microtubules of the flagella of *Chlamydomonas reinhardtii*. *J. Cell Biol*. **98**, 229–236.

Dymek, E.E., Lefebvre, P.A., and Smith, E.F. (2004a). PF15p is the *Chlamydomonas* homologue of the Katanin p80 subunit and is required for assembly of flagellar central microtubules. *Eukaryot. Cell* **3**, 870–879.

Dymek, E.E., Lefebvre, P.A., and Smith, E.F. (2004b). PF15p is the *Chlamydomonas* homologue of the Katanin p80 subunit and is required for assembly of flagellar central microtubules. *Eukaryot. Cell* **3**, 870–879.

Gibbons, I.R. (1961). The relationship between the fine structure and direction of beat in gill cilia of a lamellibranch mollusc. *J. Biophys. Biochem. Cytol*. **11**, 179–205.

Hoenger, A., and Nicastro, D. (2007). Electron microscopy of microtubule-based cytoskeletal machinery. *Methods Cell Biol*. **79**, 437–462.

Hoops, H.J. (1995). Preparation of cilia and flagella for thin-section transmission electron microscope analysis. *Methods Cell Biol*. **47**, 193–197.

Johnson, K.A. (1995). Immunoelectron microscopy. *Methods Cell Biol*. **47**, 153–162.

Kamiya, R. (2002). Functional diversity of axonemal dyneins as studied in *Chlamydomonas* mutants. *Int. Rev. Cytol*. **219**, 115–155.

Lechtreck, K.F., and Witman, G.B. (2007). *Chlamydomonas* reinhardtii hydin is a central pair protein required for flagellar motility. *J. Cell Biol*. **176**, 473–482.

Linck, R.W., Olson, G.E., and Langevin, G.L. (1981). Arrangement of tubulin subunits and microtubule-associated proteins in the central pair microtubule apparatus of squid (*Loligo pealei)* sperm flagella. *J. Cell Biol*. **89**, 309–322.

Mitchell, B.F., Pedersen, L.B., Feely, M., Rosenbaum, J.L., and Mitchell, D.R. (2005). ATP production in *Chlamydomonas reinhardtii* flagella by glycolytic enzymes. *Mol. Biol. Cell* **16**, 4509–4518.

Mitchell, D.R. (2003). Orientation of the central pair complex during flagellar bend formation in *Chlamydomonas*. *Cell Motil. Cytoskeleton* **56**, 120–129.

Mitchell, D.R., and Nakatsugawa, M. (2004). Bend propagation drives central pair rotation in Chlamydomonas reinhardtii flagella. *J. Cell Biol*. **166**, 709–715.

Mitchell, D.R., and Sale, W.S. (1999). Characterization of a *Chlamydomonas* insertional mutant that disrupts flagellar central pair microtubule-associated structures. *J. Cell Biol*. **144**, 293–304.

O'Toole, E., Mastronarde, D., McIntosh, J.R., and Porter, M.E. (1995). Computer-assisted analysis of flagellar structure. *Methods Cell Biol*. **47**, 183–191.

Pedersen, L.B., Geimer, S., and Rosenbaum, J.L. (2006). Dissecting the molecular mechanisms of intraflagellar transport in *Chlamydomonas. Curr. Biol*. **16**, 450–459.

Pedersen, L.B., Rompolas, P., Christensen, S.T., Rosenbaum, J.L., and King, S.M. (2007). The lissencephaly protein Lis1 is present in motile mammalian cilia and requires outer arm dynein for targeting to Chlamydomonas flagella. *J. Cell Sci*. **120**, 858–867.

Randall, J., Warr, J.R., Hopkins, J.M., and McVittie, A. (1964). A single-gene mutation of *Chlamydomonas reinhardtii* affecting motility: A genetic and electron microscope study. *Nature* **203**, 912–914.

Rupp, G., O'Toole, E., and Porter, M.E. (2001). The *Chlamydomonas PF6* locus encodes a large alanine/proline-rich polypeptide that is required for assembly of a central pair projection and regulates flagellar motility. *Mol. Biol. Cell* **12**, 739–751.

Sager, R., and Granick, S. (1953). Nutritional studies with *Chlamydomonas reinhardtii*. *Ann. NY Acad. Sci*. **466**, 18–30.

Smith, E.F. (2002). Regulation of flagellar dynein by the axonemal central apparatus. *Cell Motil. Cytoskeleton* **52**, 33–42.

Smith, E.F., and Lefebvre, P.A. (1996). *PF16* encodes a protein with armadillo repeats and localizes to a single microtubule of the central apparatus in *Chlamydomonas flagella*. *J. Cell Biol*. **132**, 359–370.

Smith, E.F., and Lefebvre, P.A. (1997). *PF20* gene product contains WD repeats and localizes to the intermicrotubule bridges in *Chlamydomonas* flagella. *Mol. Biol. Cell* **8**, 455–467.

Stannard, W., Rutman, A., Wallis, C., and O'Callaghan, C. (2004). Central microtubular agenesis causing primary ciliary dyskinesia. *Am. J. Respir. Crit. Care Med*. **169**, 634–637.

Starling, D., and Randall, J. (1971). The flagella of temporary dikaryons of *Chlamydomonas reinhardtii*. *Genet. Res. Camb*. **18**, 107–113.

Tamm, S.L., and Tamm, S. (1984). Alternate patterns of doublet microtubule sliding in ATP-disintegrated macrocilia of the Ctenophore *Beroe*. *J. Cell Biol*. **99**, 1364–1371.

Wargo, M.J., Dymek, E.E., and Smith, E.F. (2005). Calmodulin and PF6 are components of a complex that localizes to the C1 microtubule of the flagellar central apparatus. *J. Cell Sci*. **118**, 4655–4665.

Wargo, M.J., and Smith, E.F. (2003). Asymmetry of the central apparatus defines the location of active microtubule sliding in *Chlamydomonas flagella*. *Proc. Natl. Acad. Sci. USA* **100**, 137–142.

Warr, J.R., McVittie, A., Randall, J., and Hopkins, J.M. (1966). Genetic control of flagellar structure in Chlamydomonas reinhardii. *Genet. Res. Camb*. **7**, 335–351.

Wirschell, M., Pazour, G., Yoda, A., Hirono, M., Kamiya, R., and Witman, G.B. (2004). Oda5p, a novel axonemal protein required for assembly of the outer dynein arm and an associated adenylate kinase. *Mol. Biol. Cell* **15**, 2729–2741.

Witman, G.B. (1986). Isolation of *Chlamydomonas* flagella and flagellar axonemes. *Methods Enzymol*. **134**, 280–290.

Witman, G.B., Plummer, J., and Sander, G. (1978). *Chlamydomonas* flagellar mutants lacking radial spokes and central tubules. *J. Cell Biol*. **76**, 729–747.

Yang, P., Diener, D.R., Yang, C., Kohno, T., Pazour, G.J., Dienes, J.M., Agrin, N.S., King, S.M., Sale, W.S., Kamiya, R., Rosenbaum, J.L., and Witman, G.B. (2006). Radial spoke proteins of *Chlamydomonas* flagella. *J. Cell Sci*. **119**, 1165–1174.

Yokoyama, R., O'Toole, E., Ghosh, S., and Mitchell, D.R. (2004). Regulation of flagellar dynein by a central pair kinesin. *Proc. Natl. Acad. Sci. USA* **101**, 17398–17403.

Yoshimura, M., and Shingyoji, C. (1999). Effects of the central pair apparatus on microtubule sliding velocity in sea urchin sperm flagella. *Cell Struct. Funct*. **24**, 43–54.

Zhang, H., and Mitchell, D.R. (2004). Cpc1, a Chlamydomonas central pair protein with an adenylate kinase domain. *J. Cell Sci*. **117**, 4179–4188.

Zhang, Z., Kostetskii, I., Tang, W., Haig-Ladewig, L., Sapiro, R., Wei, Z., Patel, A.M., Bennett, J., Gerton, G.L., Moss, S.B., Radice, G.L., and Strauss, J.F., III (2006). Deficiency of SPAG16L causes male infertility associated with impaired sperm motility. *Biol. Reprod*. **74**, 751–759.

This page intentionally left blank

INDEX

C

N

O

P

Q

R

S

T

U

This page intentionally left blank

VOLUMES IN SERIES

Founding Series Editor
DAVID M. PRESCOTT

Volume 1 (1964)
Methods in Cell Physiology
Edited by David M. Prescott

Volume 2 (1966)
Methods in Cell Physiology
Edited by David M. Prescott

Volume 3 (1968)
Methods in Cell Physiology
Edited by David M. Prescott

Volume 4 (1970)
Methods in Cell Physiology
Edited by David M. Prescott

Volume 5 (1972)
Methods in Cell Physiology
Edited by David M. Prescott

Volume 6 (1973)
Methods in Cell Physiology
Edited by David M. Prescott

Volume 7 (1973)
Methods in Cell Biology
Edited by David M. Prescott

Volume 8 (1974)
Methods in Cell Biology
Edited by David M. Prescott

Volume 9 (1975)
Methods in Cell Biology
Edited by David M. Prescott

Volume 10 (1975)
Methods in Cell Biology
Edited by David M. Prescott

Volume 11 (1975)
Yeast Cells
Edited by David M. Prescott

Volume 12 (1975)
Yeast Cells
Edited by David M. Prescott

Volume 13 (1976)
Methods in Cell Biology
Edited by David M. Prescott

Volume 14 (1976)
Methods in Cell Biology
Edited by David M. Prescott

Volume 15 (1977)
Methods in Cell Biology
Edited by David M. Prescott

Volume 16 (1977)
Chromatin and Chromosomal Protein Research I
Edited by Gary Stein, Janet Stein, and Lewis J. Kleinsmith

Volume 17 (1978)
Chromatin and Chromosomal Protein Research II
Edited by Gary Stein, Janet Stein, and Lewis J. Kleinsmith

Volume 18 (1978)
Chromatin and Chromosomal Protein Research III
Edited by Gary Stein, Janet Stein, and Lewis J. Kleinsmith

Volume 19 (1978)
Chromatin and Chromosomal Protein Research IV
Edited by Gary Stein, Janet Stein, and Lewis J. Kleinsmith

Volume 20 (1978)
Methods in Cell Biology
Edited by David M. Prescott

Advisory Board Chairman
KEITH R. PORTER

Volume 21A (1980)
Normal Human Tissue and Cell Culture, Part A: Respiratory, Cardiovascular, and Integumentary Systems
Edited by Curtis C. Harris, Benjamin F. Trump, and Gary D. Stoner

Volume 21B (1980)
Normal Human Tissue and Cell Culture, Part B: Endocrine, Urogenital, and Gastrointestinal Systems
Edited by Curtis C. Harris, Benjamin F. Trump, and Gray D. Stoner

Volume 22 (1981)
Three-Dimensional Ultrastructure in Biology
Edited by James N. Turner

Volume 23 (1981)
Basic Mechanisms of Cellular Secretion
Edited by Arthur R. Hand and Constance Oliver

Volume 24 (1982)
The Cytoskeleton, Part A: Cytoskeletal Proteins, Isolation and Characterization
Edited by Leslie Wilson

Volume 25 (1982)
The Cytoskeleton, Part B: Biological Systems and *In Vitro* Models
Edited by Leslie Wilson

Volume 26 (1982)
Prenatal Diagnosis: Cell Biological Approaches
Edited by Samuel A. Latt and Gretchen J. Darlington

Series Editor
LESLIE WILSON

Volume 27 (1986)
Echinoderm Gametes and Embryos
Edited by Thomas E. Schroeder

Volume 28 (1987)
***Dictyostelium discoideum:* Molecular Approaches to Cell Biology**
Edited by James A. Spudich

Volume 29 (1989)
Fluorescence Microscopy of Living Cells in Culture, Part A: Fluorescent Analogs, Labeling Cells, and Basic Microscopy
Edited by Yu-Li Wang and D. Lansing Taylor

Volume 30 (1989)
Fluorescence Microscopy of Living Cells in Culture, Part B: Quantitative Fluorescence Microscopy—Imaging and Spectroscopy
Edited by D. Lansing Taylor and Yu-Li Wang

Volume 31 (1989)
Vesicular Transport, Part A
Edited by Alan M. Tartakoff

Volume 32 (1989)
Vesicular Transport, Part B
Edited by Alan M. Tartakoff

Volume 33 (1990)
Flow Cytometry
Edited by Zbigniew Darzynkiewicz and Harry A. Crissman

Volume 34 (1991)
Vectorial Transport of Proteins into and across Membranes
Edited by Alan M. Tartakoff

Selected from Volumes 31, 32, and 34 (1991)
Laboratory Methods for Vesicular and Vectorial Transport
Edited by Alan M. Tartakoff

Volume 35 (1991)
Functional Organization of the Nucleus: A Laboratory Guide
Edited by Barbara A. Hamkalo and Sarah C. R. Elgin

Volume 36 (1991)
***Xenopus laevis:* Practical Uses in Cell and Molecular Biology**
Edited by Brian K. Kay and H. Benjamin Peng

Series Editors
LESLIE WILSON AND PAUL MATSUDAIRA

Volume 37 (1993)
Antibodies in Cell Biology
Edited by David J. Asai

Volume 38 (1993)
Cell Biological Applications of Confocal Microscopy
Edited by Brian Matsumoto

Volume 39 (1993)
Motility Assays for Motor Proteins
Edited by Jonathan M. Scholey

Volume 40 (1994)
A Practical Guide to the Study of Calcium in Living Cells
Edited by Richard Nuccitelli

Volume 41 (1994)
Flow Cytometry, Second Edition, Part A
Edited by Zbigniew Darzynkiewicz, J. Paul Robinson, and Harry A. Crissman

Volume 42 (1994)
Flow Cytometry, Second Edition, Part B
Edited by Zbigniew Darzynkiewicz, J. Paul Robinson, and Harry A. Crissman

Volume 43 (1994)
Protein Expression in Animal Cells
Edited by Michael G. Roth

Volume 44 (1994)
***Drosophila melanogaster:* Practical Uses in Cell and Molecular Biology**
Edited by Lawrence S. B. Goldstein and Eric A. Fyrberg

Volume 45 (1994)
Microbes as Tools for Cell Biology
Edited by David G. Russell

Volume 46 (1995)
Cell Death
Edited by Lawrence M. Schwartz and Barbara A. Osborne

Volume 47 (1995)
Cilia and Flagella
Edited by William Dentler and George Witman

Volume 48 (1995)
***Caenorhabditis elegans:* Modern Biological Analysis of an Organism**
Edited by Henry F. Epstein and Diane C. Shakes

Volume 49 (1995)
Methods in Plant Cell Biology, Part A
Edited by David W. Galbraith, Hans J. Bohnert, and Don P. Bourque

Volume 50 (1995)
Methods in Plant Cell Biology, Part B
Edited by David W. Galbraith, Don P. Bourque, and Hans J. Bohnert

Volume 51 (1996)
Methods in Avian Embryology
Edited by Marianne Bronner-Fraser

Volume 52 (1997)
Methods in Muscle Biology
Edited by Charles P. Emerson, Jr. and H. Lee Sweeney

Volume 53 (1997)
Nuclear Structure and Function
Edited by Miguel Berrios

Volume 54 (1997)
Cumulative Index

Volume 55 (1997)
Laser Tweezers in Cell Biology
Edited by Michael P. Sheetz

Volume 56 (1998)
Video Microscopy
Edited by Greenfield Sluder and David E. Wolf

Volume 57 (1998)
Animal Cell Culture Methods
Edited by Jennie P. Mather and David Barnes

Volume 58 (1998)
Green Fluorescent Protein
Edited by Kevin F. Sullivan and Steve A. Kay

Volume 59 (1998)
The Zebrafish: Biology
Edited by H. William Detrich III, Monte Westerfield, and Leonard I. Zon

Volume 60 (1998)
The Zebrafish: Genetics and Genomics
Edited by H. William Detrich III, Monte Westerfield, and Leonard I. Zon

Volume 61 (1998)
Mitosis and Meiosis
Edited by Conly L. Rieder

Volume 62 (1999)
Tetrahymena thermophila
Edited by David J. Asai and James D. Forney

Volume 63 (2000)
Cytometry, Third Edition, Part A
Edited by Zbigniew Darzynkiewicz, J. Paul Robinson, and Harry Crissman

Volume 64 (2000)
Cytometry, Third Edition, Part B
Edited by Zbigniew Darzynkiewicz, J. Paul Robinson, and Harry Crissman

Volume 65 (2001)
Mitochondria
Edited by Liza A. Pon and Eric A. Schon

Volume 66 (2001)
Apoptosis
Edited by Lawrence M. Schwartz and Jonathan D. Ashwell

Volume 67 (2001)
Centrosomes and Spindle Pole Bodies
Edited by Robert E. Palazzo and Trisha N. Davis

Volume 68 (2002)
Atomic Force Microscopy in Cell Biology
Edited by Bhanu P. Jena and J. K. Heinrich Ho¨rber

Volume 69 (2002)
Methods in Cell-Matrix Adhesion
Edited by Josephine C. Adams

Volume 70 (2002)
Cell Biological Applications of Confocal Microscopy
Edited by Brian Matsumoto

Volume 71 (2003)
Neurons: Methods and Applications for Cell Biologist
Edited by Peter J. Hollenbeck and James R. Bamburg

Volume 72 (2003)
Digital Microscopy: A Second Edition of Video Microscopy
Edited by Greenfield Sluder and David E. Wolf

Volume 73 (2003)
Cumulative Index

Volume 74 (2004)
Development of Sea Urchins, Ascidians, and Other Invertebrate Deuterostomes: Experimental Approaches
Edited by Charles A. Ettensohn, Gary M. Wessel, and Gregory A. Wray

Volume 75 (2004)
Cytometry, 4th Edition: New Developments
Edited by Zbigniew Darzynkiewicz, Mario Roederer, and Hans Tanke

Volume 76 (2004)
The Zebrafish: Cellular and Developmental Biology
Edited by H. William Detrich, III, Monte Westerfield, and Leonard I. Zon

Volume 77 (2004)
The Zebrafish: Genetics, Genomics, and Informatics
Edited by William H. Detrich, III, Monte Westerfield, and Leonard I. Zon

Volume 78 (2004)
Intermediate Filament Cytoskeleton
Edited by M. Bishr Omary and Pierre A. Coulombe

Volume 79 (2007)
Cellular Electron Microscopy
Edited by J. Richard McIntosh

Volume 80 (2007)
Mitochondria, 2nd Edition
Edited by Liza A. Pon and Eric A. Schon

Volume 81 (2007)
Digital Microscopy, 3rd Edition
Edited by Greenfield Sluder and David E. Wolf

Volume 82 (2007)
Laser Manipulation of Cells and Tissues
Edited by Michael W. Berns and Karl Otto Greulich

Volume 83 (2007) Cell Mechanics
Edited by Yu-Li Wang and Dennis E. Discher

Volume 84 (2007)
Biophysical Tools for Biologists, Volume One: *In Vitro* Techniques
Edited by John J. Correia and H. William Detrich, III

Volume 85 (2008)
Fluorescent Proteins
Edited by Kevin F. Sullivan

Volume 86 (2008)
Stem Cell Culture
Edited by Dr. Jennie P. Mather

Volume 87 (2008)
Avian Embryology, 2nd Edition
Edited by Dr. Marianne Bronner-Fraser

Volume 88 (2008)
Introduction to Electron Microscopy for Biologists
Edited by Prof. Terence D. Allen

Volume 89 (2008)
Biophysical Tools for Biologists, Volume Two: *In Vivo* Techniques
Edited by Dr. John J. Correia and Dr. H. William Detrich, III

Volume 90 (2008)
Methods in Nano Cell Biology
Edited by Bhanu P. Jena

Volume 91 (2009)
Cilia: Structure and Motility
Edited by Stephen M. King and Gregory J. Pazour